PALACKÝ UNIVERSITY OLOMOUC

FACULTY OF SCIENCE

DEPARTMENT OF PHYSICAL CHEMISTRY

Modeling of Biomembranes

Doctoral Thesis

Author:	Mgr. Martin Šrejber
Supervisor:	doc. RNDr. Karel Berka, Ph.D.
Consultant:	prof. RNDr. Michal Otyepka, Ph.D.

Study programme:	Chemistry
Study field:	Physical chemistry
Study form:	Daily

Olomouc 2023

Declaration of the author

I declare that this thesis and the work presented in it are my own and has been generated by me as a result of my own original research. I have duly acknowledged all the sources of information which have been used in this thesis.

Olomouc 2023

…….

Martin Šrejber

Bibliographical identification:

Authors first name and surname	Martin Šrejber
Title	Modeling of biomembranes
Type of thesis	Doctoral
Department	Department of Physical Chemistry
Supervisor	doc. RNDr. Karel Berka, Ph.D.
Consultant	prof. RNDr. Michal Otyepka, Ph.D.
The year of presentation	2023
Keywords	biomembrane, cytochrome P450, permeability, molecular dynamics, molecular mechanics
Number of pages	79
Number of appendices	3 publications
Language	English

Abstract

Biological membranes enable life as we know it. They constitute fundamental components of all living organisms and, with their unique physicochemical properties, diverse composition, and structure, play an integral role in regulating a wide range of biological processes. Biological membranes separate the cell's internal environment from the external one and contribute to the formation of intracellular compartments by serving as natural boundaries between different cellular components. One remarkable characteristic of biomembranes is their selective permeability, allowing the passage of various molecules through passive transport or indirectly through active transport regulated by membrane-embedded proteins. The processes of molecule transport across biological membranes, as well as the behavior of molecules and proteins within these unique "two-dimensional fluids," can be studied using a variety of computational chemistry tools, such as classical molecular dynamics (MD), enhanced sampling methods (metadynamics, umbrella sampling). However, these methods require experimental validation, which can be gathered from specialized databases (MolMeDB). In this thesis, I present the possibilities of employing these theoretical tools to investigate the behavior of substances – ranging from small molecules up to protein complexes – on biological membranes.

Bibliografická identifikace:

Jméno a příjmení autora	Martin Šrejber
Název práce	Modelování biologických membrán
Typ práce	Disertační
Pracoviště	Katedra fyzikální chemie
Vedoucí práce	doc. RNDr. Karel Berka, Ph.D.
Konzultant	prof. RNDr. Michal Otyepka, Ph.D.
Rok obhajoby práce	2023
Klíčová slova	biologická membrána, cytochrom P450, permeabilita, molekulová dynamika, molekulová mechanika
Počet stran	79
Počet příloh	3 publikace
Jazyk	Anglický

Abstrakt

Biologické membrány umožňují život tak jak jej známe. Tvoří základní komponenty všech živých organismů a díky svým unikátním fyzikálně-chemickým vlastnostem, rozmanitou kompozicí a strukturou plní nedílnou roli při regulaci celé řady biologických dějů. Biologické membrány oddělují vnitřní prostředí buňky od vnějšího a spoluvytvářejí intracelulární kompartmenty tím, že tvoří přirozené hranice mezi jednotlivými buněčnými komponenty. Unikátní vlastností biomembrán je jejich selektivní permeability pro průchod celé řady molekul pomocí pasivním transportu anebo nepřímo aktivním transportem, který je řízen proteiny kotvenými v membráně. Procesy transportu molekul přes biologické membrány tak i chování molekul a proteinů na těchto unikátních „dvojrozměrných kapalinách“ mohou být studovány celou řadou nástrojů výpočetních chemie např. metodami klasické molekulové dynamiky (MD), metodami efektivního vzorkování (metadynamika, umbrella sampling). Nicméně tyto metody vyžadují experimentální validaci, nebo využití referenčních dat ze specializovaných databází (MolMeDB). V této disertační práci prezentuji možnosti využití těchto teoretických nástrojů pří studiu chování látek – ať již malých molekul či proteinových komplexů – na biologických membránách.

Acknowledgement

First and foremost, I want to express my sincere appreciation to my supervisor, Karel Berka, for introducing me to the realm of scientific inquiry. Secondly, I am deeply grateful to my advisor, Michal Otyepka, for expanding the boundaries of my knowledge and pushing me to reach new heights. I would also like to extend my heartfelt thanks to my friends and colleagues from the Department of Physical Chemistry and CATRIN for their unwavering support, motivation, and those much-needed coffee breaks.

Lastly, I express my heartfelt gratitude to my wife, Jana, and daughter, Anežka, for their unwavering support and for enriching my life in countless ways. Their love and presence have played an instrumental role in shaping me into a better person throughout this journey.

Outline

Outline *- 1 -*

1. Motivation *- 3 -*

2. Biomembranes *- 4 -*

2.1 Lipids as building blocks **- 4 -**

2.2 Lipid composition of biomembranes **- 7 -**

2.3 Membrane structure and physical properties **- 9 -**

3. Interactions of drugs with membranes *- 12 -*

3.1 Effect of membrane composition **- 14 -**

4. Membrane proteins *- 16 -*

4.1 Cytochrome P450 enzymes **- 16 -**

4.2 Cytochrome P450 reductase **- 19 -**

5. Theoretical approach *- 21 -*

5.1 Molecular Mechanics **- 21 -**

5.2 Molecular Dynamics **- 24 -**

5.3 Enhanced sampling techniques **- 25 -**

5.3.1 Umbrella sampling - 25 -

5.3.2 Metadynamics - 26 -

5.4 COSMO calculations **- 27 -**

5.5 Calculations of Drug Permeabilities **- 28 -**

6. Results *- 32 -*

6.1 MolMeDB project **- 33 -**

6.1.1. MolMeDB user interface - 35 -

6.1.2. Case study - 36 -

6.2 Permeation of cyclosporin A through biomembranes **- 38 -**

6.2.1 Cyclosporin A behavior on membrane models - 41 -

6.2.2 Conclusions on cyclosporin A - 42 -

6.2.3 Methodology - 43 -

6.3 *In silico* screening of drug candidates for temperature-responsive liposome formulation - 44 -

6.3.1. MD simulation of bilayer phase transition - 45 -

6.3.2. COSMO-based partitioning and permeability calculations fort fluorescent dyes - 45 -

6.3.3. Selection criteria encapsulation/thermoresponsive release and DrugBank screening - 46 -

6.4 Behavior of Mitochondrial Cytochrome P450 11A1 on DOPC and Mitochondrial Membrane Models - 49 -

6.4.1 Behavior of CYP11A1 on DOPC - 50 -

6.4.2. Interaction of CYP11A1 with mitochondrial membrane - 52 -

6.4.3. CYP11A1 channels dynamics - 56 -

6.4.4. Interaction of CYP11A1 with Adrenodoxin - 57 -

6.4.5 Methodology - 57 -

6.5 Membrane-attached Model of Cytochrome P450 Reductase: Simulations of naturally occurring states and of the complex by cytochrome P450 3A4 - 59 -

6.5.1 Models of CPR in closed and open conformations - 59 -

6.5.2 Model of membrane-attached CPR-CYP 3A4 complex - 62 -

***7. Summary* - 64 -**

***8. Shrnutí* - 66 -**

***9. List of Abbreviations* - 68 -**

***10. References* - 70 -**

***11. List of Publications* - 78 -**

***12. Appendices* - 79 -**

1. Motivation

Computational chemistry is dynamically developing field of chemistry allowing us to understand the atomistic nature underlying all variety of naturally occurring phenomena. Especially nowadays with the exponential increase of computational power resources it allows us to tackle myriad of issues yet unreachable until today. The scope of computational chemistry ranges from studies related to solving of electronic states of systems by means of quantum mechanics (QM) usually limited by the size of studied systems up to dynamical studies by means of molecular dynamics simulations (MD) that are directly matching the sizes (nanometers) and time scales (microseconds) of experimental techniques. Molecular dynamics plays especially significant role in *in silico* study of biological processes and rationalizing the atomistic principles originating from them.

This thesis is focused on employment of theoretical tools (MD simulations, enhances sampling techniques, database data utilization) in study interactions of biological membranes with another naturally occurring species. The theoretical part of this thesis is focused on biomembranes itself i. e. their composition diversity, function and how they interact with drugs. It also briefly describes some essential proteins (cytochromes P450s (CYPs) and its redox partner cytochrome P450 reductase (CPR)) for which the interaction with biological membrane is vital and that are later discussed in result sections. The methodology section is focused on theoretical approaches and strategies used to study either biomembranes itself or their interaction with another chemical species. Finally, the Results chapter summarizes:

i. the development and usage of MolMeDB database. This database was design to systematically collect, validate and visualize data related to molecule-membrane interaction
ii. the permeation of widely used immunosuppressant – cyclosporin A – through several biological membrane models
iii. the development and validation of systematic computational methodology for prediction of suitable liposomal encapsulation and thermally induced release of bio-active compounds
iv. the effect of membrane composition on behavior of microsomal cytochrome P450 CYP11A1
v. the behavior of membrane-attached cytochrome P450 reductase and its interactions of its redox partner – cytochrome P450 CYP3A4.

2. Biomembranes

Biological membranes allow life as we know it. They are essential components of all biological cells, living systems and organisms. Biomembranes' key role originates from their structure, complexity of composition, physical-chemical properties, and irreplaceability in multiple biological processes. We define them as two-dimensional liquid composed of lipids and protein arrange primarily into the form of a lipid bilayer. This highly dynamical complex functions as a natural barrier between subcellular compartments and cell segregation from the external environment. In skin cells, membranes protect the human body from the intrusion of noxious substances. Due to their selective permeability, they control the flux of substances going through them. Biomembranes also serve as a matrix to anchor proteins involved in a variety of biological processes. They mediate the communication between individual compartments via protein capable of conformation changes or control chemical and electrical signals.

2.1 Lipids as building blocks

Lipids are a diverse group of macromolecules soluble in nonpolar solvents and insoluble in polar solvents, such as water. Lipids themselves are generally composed of "building blocks" such as alcohols, phosphates, glycerol, sphingosines, and fatty acids that characterize final lipid molecules' unique properties. In mammalian cells, the most abundant lipids components are glycerophospholipids, sphingolipids and sterols.[1]

Glycerophospholipids (GPLs) are the main building blocks of biomembranes, including plasma or organelle membranes. These constitute of *sn*-glycerol-3-phosphate backbone esterified by free fatty acids in positions *sn*-1 and *sn*-2. Subsequently, the phosphate is bound to a variety of alcohol groups. The chemical diversity of GPLs is determined by the interplay between various fatty acids, *sn*-1 linkage to glycerol and the head group. The polar head groups consist of negatively charged phosphate moiety bound to alcohol substituent (Figure 1).

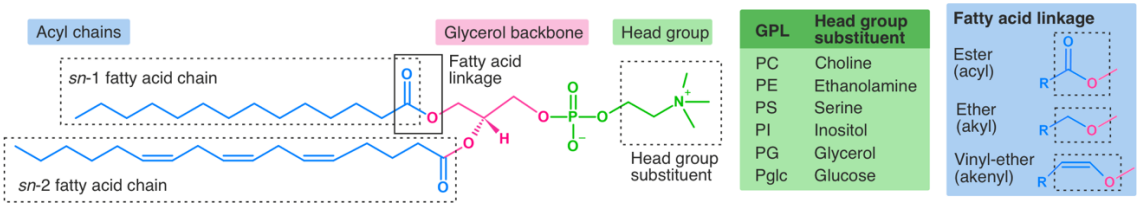

Figure 1. The structural diversity of glycerophospholipids. The structural diversity of individual lipids originates from a variety of acyl chains (blue), glycerol linkage (pink) and the choice of head group substituents (green).

The alcohols are bound to the phosphoryl group via -OH group and can be classified based on their charge as positively charged (choline, ethanolamine), neutral (glycerol, inositol) or neutral zwitterions (serine) (Figure 2). This interplay between negatively charged phosphates and variable charges of alcohol substituents determine the overall charge of lipids, e.g., phosphatidylcholines (PCs), phosphatidylethanolamines (PEs) and phosphatidylinositols (PIs) are neutral (zwitterionic) lipids due to the compensation of opposite charges. Similarly, phosphatidylserines (PSs) and phosphatidylglycerols (PGs) bear an overall negative charge. The chemical structure of alcohols affects their ability to intermolecular interactions through the hydrogen bonds network.[2] Lipids with more polar alcohol substituent (ethanolamine, glycerol and serine) serve as proton donors and acceptors for hydrogen bonds, while more minor polar alcohol groups (choline) cannot form hydrogen bonds. Head group electrostatics, shape and the hydrogen bond acceptor/donor capacity significantly affect the interaction between individual lipids and molecules' permeation through membranes or membrane-protein interaction.

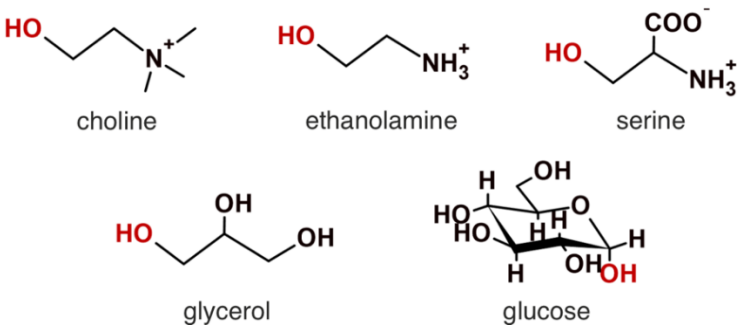

Figure 2. Example of head group substituents in glycerophospholipids.

Another aspect contributing to lipid structural diversity is the linkage between free fatty acids and the phosphoryl group. The linkage can be mediated either by ester, ether or vinyl-ethers (Figure 1). The vast majority of GPLs are acyl ester lipids. Alkyl ether (and alkenyl vinyl-ether) lipids, such as plasmalogens, constitute up to 20% of the total phospholipid mass in humans and are primarily localized in brain and heart tissue.[3]

The most important and structurally diverse constituents of lipids are fatty acids. Their variance originates from the variability of carbon chains length and the degree of saturation (Table 1). The typical length of free fatty acids varies between 14 to 20 carbon atoms. More than half of naturally occurring fatty acids is unsaturated. The *sn*-2 fatty acid chain is usually mono- or polyunsaturated, whereas the *sn*-1 fatty acid chain is usually fully saturated. The first saturations generally occur at C3 (ω-3) and C6 (ω-6) carbon atoms (numbered from terminal methyl group). Most fatty acids have a double bond in *cis* configuration resulting in ~30° bend in the hydrocarbon chain, whereas the *trans* configuration leads to a straight hydrocarbon chain. The presence of *cis* double bond configuration decreases the ordering of lipid tails hence increases the fluidity membrane.[4] The occurrence of triple bond and conjugated double bonds is rare.

Table 1. Common fatty acids found in biomembranes.

C:D*	Common name	Chemical formula
Saturated fatty acids		
12:0	Lauric acid	$CH_3(CH_2)_{10}COOH$
14:0	Myristic acid	$CH_3(CH_2)_{12}COOH$
16:0	Palmitic acid	$CH_3(CH_2)_{14}COOH$
18:0	Stearic acid	$CH_3(CH_2)_{16}COOH$
20:0	Arachidic acid	$CH_3(CH_2)_{18}COOH$
Unsaturated fatty acids		
14:1	Myristoleic acid	$CH_3(CH_2)_3CH{=}CH(CH_2)_7COOH$
16:1	Palmitoleic acid	$CH_3(CH_2)_5CH{=}CH(CH_2)_7COOH$
18:1	Oleic acid	$CH_3(CH_2)_7CH{=}CH(CH_2)_7COOH$
18:2	Linoleic acid	$CH_3(CH_2)_4CH{=}CHCH_2CH{=}CH(CH_2)_7COOH$
18:3	α-Linolenic acid	$CH_3CH_2CH{=}CHCH_2CH{=}CHCH_2CH{=}CH(CH_2)_7COOH$
20:4	Arachidonic acid	$CH_3(CH_2)_4(CH{=}CHCH_2)_4(CH_2)_2COOH$

* C corresponds to the number of carbon atoms; D corresponds to the number of double bonds

Another important lipid component of biomembranes is **sterols**. In plants and yeasts, the most abundant type is ergosterol, whereas plants' membrane composition is more complex and contains a mixture of sterol, e.g., cholesterol, campesterol, stigmasterol or sitosterol.[5] Cholesterol (CHOL) is the most abundant sterol in the mammal. Although the ratio of cholesterol varies in individual membranes. From a structural point of view, the cholesterol consists of semi-rigid fused rings with -OH group and aliphatic chain bound opposite sides of ring structure (Figure 3). Cholesterol plays a crucial role in maintaining membrane rigidity and ordering. The increasing amount of cholesterol in the liquid-disordered (L_d) phase results in membrane transition into a stiffer and thicker liquid-ordered (L_o) phase.[6] It is hypothesized that cholesterol is also involved in the formation of L_d/L_o phase-separated microdomains, so-called lipid "rafts".

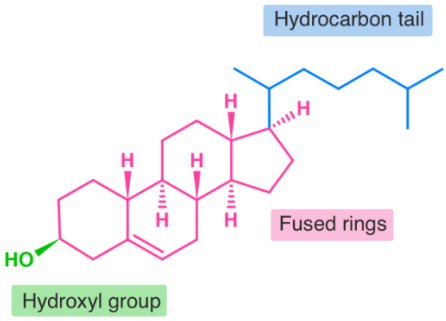

Figure 3. The structure of cholesterol.

Sphingolipids are composed of sphingoid base backbone, acyl chain and head group substituents (Figure 4). The sphingolipids' diversity arises from various lengths, degrees of saturation, and hydroxylation of the sphingoid base backbone. The N-acyl chains of sphingolipids are usually more saturated and longer when compared to acyl chains in GPLs. Similarly to GPLs, the head

group substituents are diverse and vary in shape and charge. The small hydroxyl group's connection to the serine moiety will lay the structural foundation for ceramide lipids (CERs), whereas phosphocholine's linkage will form sphingomyelins (SMs). Furthermore, the addition of saccharide group form **glycolipids**, e.g., glycosphingolipids (sphingoid base backbone bound to one or multiple sugars via ether bond) or glycophosphatidylinositol (sphingoid base backbone bound to PI moiety).

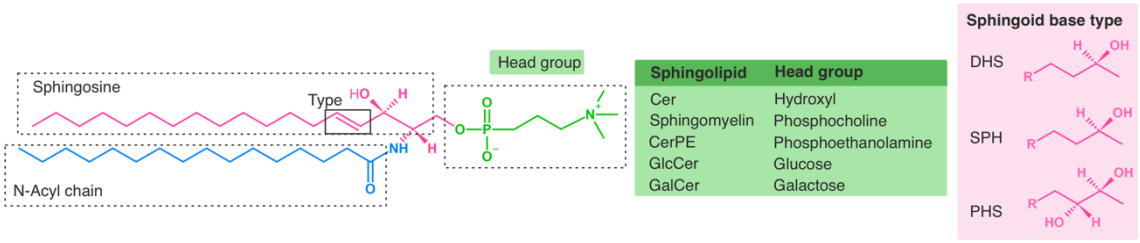

Figure 4. Structural bases of sphingolipids.

A particular group of lipids found in biomembranes are **glycerolipids**. Glycolipids can be found in three forms: mono- di- and trisubstituted glycerols (Figure 5). The best known are triacylglycerols (TAGs), fatty acid esters of glycerol. TAGs serve mainly as a caloric repository for mammals, with more than 90% TAGs stored in adipose tissue.[7,8]

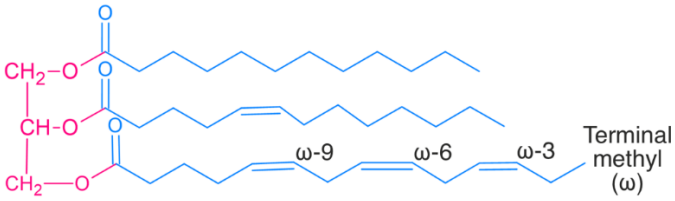

Figure 5. Structural representation of TAG.

2.2 Lipid composition of biomembranes

The distribution of lipids among individual organelle membranes and plasma membrane is heterogeneous. It differs in head group representation as well as in fatty acid length and degree of saturation. Even more, individual membrane leaflets are unique in their composition, and spatially, lipids are distributed asymmetrically across the bilayer.[9] The lipid composition is explicitly tailored for individual organelle function.[6]

The biosynthesis of lipids starts in the endoplasmic reticulum (ER), where the majority of phospholipids, sterols or ceramides is being produced.[10] Those later serve as precursors for the synthesis of specific lipids, e.g., ceramides for sphingolipids. Among the most abundant lipids synthesized in the ER are PCs, PEs, PIs, cholesterol and triacylglycerols. The precursors are transported to other organelles, where the biosynthesis continues. In the Golgi apparatus, further synthesis of sphingolipids from ceramides occurs, followed by their transport into the plasma membrane.[11] From the Golgi apparatus, lipids are sorted and transferred by endosomes.

Synthesized sphingolipids and cholesterol are predominantly accumulated in the plasma membrane. Here the tight packing of sphingolipids and cholesterol-enriched phospholipids (PCs, PEs and PSs) preserves the barrier between intracellular and extracellular compartments. Plasma membrane lipids (mainly PI derivatives) participate in the transduction of extracellular signals and regulation of integral proteins bound at PM, including voltage-gated potassium channels, calcium channels and transient receptor potential channels.[12,13] In mitochondria, unique and complex cardiolipin (CL) phospholipid is synthesized from its phosphatidylglycerol precursor. Unlike the other lipids, the synthesis of CL is placed exclusively in the inner mitochondrial membrane (IMM).[14] The CL plays a vital role in regulating an optimal activity for proteins bond in IMM, such as electron transport chain complexes[15], substrate carrier proteins[16] or mitochondrial cytochromes P450 (CYP11A1) responsible for steroid synthesis.[17]

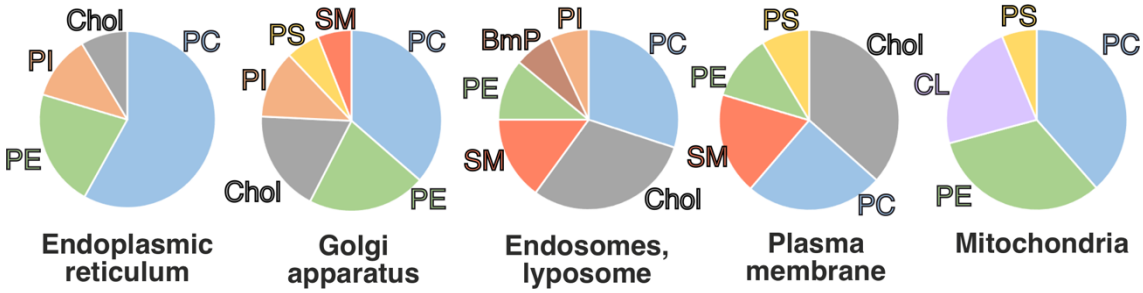

Figure 6. The lipid composition of biological membranes expressed as percentages of the total amount of individual lipids in the whole-cell compartment. Lipids abbreviated as follows: phosphatidylcholine (PC), phosphatidylethanolamine (PE), phosphatidylinositol (PI), cholesterol (Chol), phosphatidylserine (PS), sphingomyelin (SM), bis(monoacylglycerol)phosphate (BmP), cardiolipin (CL). Adapted from reference [18].

A special type of biomembrane in its lipid composition and function is the outermost layer of skin (epidermis), the so-called *stratum corneum* (SC). Skin biomembrane acts as a natural barrier that protects the human body from intrusion of noxious substances and prevents transdermal water loss. Structurally it can be described in the "brick and mortar" model where bricks represent corneocytes – dead cells mostly made up of creatine – and mortar stands for lipidic matrix. In contrary to a typical cellular membrane, the *stratum corneum* does not consist of phospholipids. Individual bilayers are roughly equimolar mixtures of ceramides, cholesterol, and free fatty acids.[19] Even though the exact organization of lipids in the SC membrane is unknown, a simplified three-component model (forming classical bilayer) is often used for transdermal permeation studies.[20,21]

2.3 Membrane structure and physical properties

The membrane is composed of lipid molecules separated into two distinguishable leaflets that act as a two-dimensional fluid. The formation of lipid bilayers originates from the amphipathic nature of lipid molecules, having the hydrophilic head region exposed to the aqueous environment and the hydrophobic tail region tightly packed core of the membrane. The amphipathic character causes the self-assembly of lipids in water into various shapes, starting from simple lipid bilayers into more complex vesicles and liposomes, depending on lipid structural parameters (head group substituent, length and saturation of acyl chains) and external factors such as temperature and pressure. The bilayer arrangement of membranes is driven to maximize the membrane surface and minimize the internal volume.

In eukaryotes, more than 50% of all GPLs found in membranes are phosphatidylcholines (PC). The head group's proportional size and the aliphatic tail make the overall molecular shape of PCs cylindrical. Structurally, they arrange into lamellar bilayers with no curvature strain. Lipids with proportionally smaller lipid head groups (PEs) and the asymmetrical truncated cone shape tend to form nonlamellar inverted hexagonal structures due to the negative curvature stress. The unsaturation of acyl chains further increases this behavior. In contrast, lipids with bulkier head groups (PIs, single acyl chain lipids, detergents) opposite to tail region and inverted conical lipid shape that induces positive curvature strain forms hexagonal structures.[22]

Apart from the membrane shape, lipid composition also strongly affects the lipid membrane phase. Membrane phase behavior originates from specific lipid-lipid interaction, and it is described by lipid parameters such as lipid order parameters (S_{CD}) or lateral diffusion coefficient (D_L) (Figure 7). At room temperature, most abundant mixtures of GPLs with longer and unsaturated carbohydrates are found in the L_d phase defined by low ordering acyl chains and high lipid mobility. Decrease of temperature or change of composition towards more saturated (sphingolipids) or longer acyls (e.g., stearic acid) lipids induce the phase transition into rigid solid gel (S_o) phase. Tight packing of lipids causes higher ordering of lipids and slow lateral diffusion. The addition of sterol molecules into the lipid mixture (binary or tertiary) forms a liquid-ordered phase that is highly ordered but highly fluid.

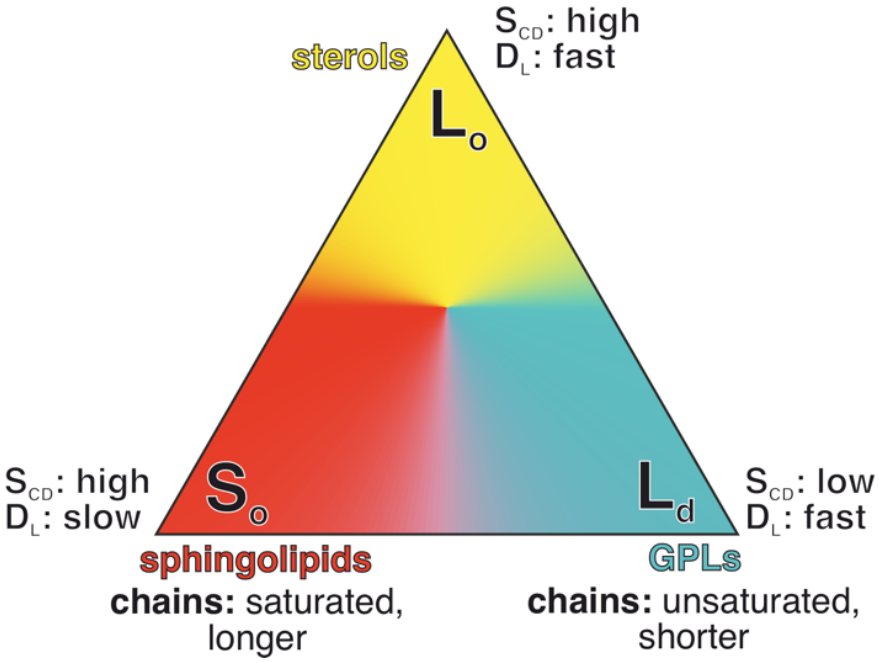

Figure 7. Lipid phase diagram. Cholesterol enriched membranes are found in the L_o phase defined by low order parameters and fast lipid diffusion. At a human body temperature, the L_d is the predominant membrane phase with the low ordering of acyl chains and fast lipid diffusion. The solid gel S_o phase is the preferential phase for sphingolipids.

It is not easy to describe all the membranes' physical properties only on account of lipid composition diversity. For this purpose, a set of fundamental parameters describing membrane structure and dynamics is defined. Both experimental and theoretical techniques can obtain those qualitative parameters, and the combination of those approaches helps to understand the structural nature of membranes.

Area/volume per lipid (A_L, V_L) are defined by the area/volume occupied by one lipid component in-plane membrane surface. Generally, A_L decreases with the increasing length of the hydrocarbon chain for fully saturated lipids.[23] In contrast to that, the acyl chain's unsaturation introduces disorder in membrane core, resulting in AL's non-linear response. The increase of A_L with respect to chain length reaches maxima for DOPC. After that area per lipid of monosaturated PCs again decreases.[24] Both A_L and V_L increase with increasing temperature.[25] Changes of V_L of chemically different lipids (PC, PG, PS and PE) tend to exhibit alike response changes in temperature.[26]

Membrane thickness determines the width of the lipid bilayer along its normal (z-axis). Its definition of this parameter varies based on used experimental techniques. The X-ray scattering data can be resolved as the distance between maxima in electron density profiles located in head groups (D_{HH} – "head-to-head"). Similarly, this information can be assessed from density profiles of individual lipid constituents (usually phosphates) from molecular dynamics simulations. In neutron scattering measurements, the thickness is defined by the contrast between protiated

lipids and deuterated water surrounding them (denoted as Luzzati thickness – D_B). Moreover, the width of hydrocarbon chains ($2D_C$) is often studied since it directly depicts the bilayer's structural feature. Those latter two mentioned can be directly derived from other structural parameters as follows:

$$A_L = \frac{2V_L}{D_B} = \frac{(V_L - V_{HL})}{D_C} \quad (1)$$

where V_L and V_{HL} are the total lipid volume and the volume of the lipid head group, respectively. This parameter directly reflects the length of acyl chains as well as the level of saturation. A linear increase of membrane thickness is observed in saturated and monounsaturated PC lipids with an increasing hydrocarbon chain.[27] This linear trend was also seen in PGs[28] and PEs[29], suggesting that membrane width is independent of head group composition and is a primary function of acyl chains.[26]

Order parameters (S_{CD}) describe the organization of membranes and are defined as:

$$S_{CD} = < \frac{3cos^2\theta - 1}{2} > \quad (2)$$

here θ denotes the time average of the angle between C – D bond vector (C – carbon atom; D – deuterium) and membrane normal. Those parameters depend on the ordering as well as the orientation of the system itself. S_{CD} can take on values between -0.5 and 1, where the first one corresponds to perfectly ordered chains with respect to the *z*-axis, whereas the latter describes a fully ordered system perpendicular membrane normal. The value of 0 is measured in a completely disordered system or order system at the "magic angle" of 54.7°. Generally, S_{CD} decreases from lipid headgroup towards terminal methyl. Also, the presence of double bond introduces further disordering and therefore decrease in S_{CD}.[30] In contrast, the presence of cholesterol increases membrane ordering.[31]

Lateral diffusion (D_L) describes the fluidity of the membrane. It is defined as a lateral displacement of lipids within the membrane as a function of time. Those movements occur in orders of nanoseconds and are related to external factors like temperature. The increase of temperature results in the loosening of membrane structure and, therefore, increasing lipid diffusion.[32] Lateral diffusion also increases with the level of unsaturation but decreases with the presence of cholesterol.[32,33] It can be measured by various experimental techniques such as fluorescence recovery after photobleaching (FRAP) or single-particle tracking (SPT).[34]

3. Interactions of drugs with membranes

The interaction of small molecules (drugs, xenobiotics, endobiotics, ligands, etc.) with membranes plays a crucial role in multiple physiological processes, and therefore a thorough understanding of the mechanism of drug-membrane interaction and consequential permeation is needed. The drug uptake (oral, intravenous, transdermal, intramuscular) passes through various biomembranes before reaching its target. Hence, the drug's ability to permeate those natural barriers may be the limiting step in drug absorption, distribution, metabolism and excretion (ADME).

The drug-membrane crossing can occur by many routes depending on the drug's chemical nature and external factors. Small and moderately polar and uncharged compounds can passively **diffuse across** the membrane without any energetical penalty. Here the process is driven simply by concentration gradients. This is especially noticeable for nonpolar small gasses like O_2, N_2, CO_2. In case of small polar solvents such as ethanol or water the passive diffusion is slower (by approximately three orders of magnitude) yet present.[35,36] Also small but less polar (more hydrophobic) compounds like benzene can diffuse passively through membranes. It is worth mentioning that even some larger and more polar molecules like Cyclosporin A (CsA) – an orally active immunosuppressant – are known to permeate passively even though their permeability is relatively low compared to typical smaller permeants.

Molecules that are not permeable using simple diffusion can be transferred across the cell membrane either by **facilitated diffusion** or **active transport**. The first of the mentioned utilizes the drug transport by transmembrane protein pores. This includes, for example, the aquaporin protein channels family (AQP) or the glucose transporters family (GLUT) responsible for glucose uptake. The latter governs drug influx and efflux via transmembrane carriers against a substrate concentration gradient. Active transport usually requires significant conformational changes of protein structure and energy use in the form of adenosine triphosphate (ATP). Here belongs the ATP-binding cassette (ABC) transporters or the solute carrier (SLC) transporters' family.

The last route of transmembrane transport is **endocytosis**. In this process, part of the plasma membrane surrounds and "devours" the permeant. The pocket with its cargo consequently detaches and is transported in the form of vesicles. In this way, even large macromolecular objects like viruses or whole bacteria can be transferred to cells.[37]

In assessing the permeability, Lipinski's rule of five[38] criteria generally defines the basic set of physicochemical descriptors for orally active compounds. It predicts that the molecule is potent after oral administration when:

i. the molecular weight is below 500 Da,

ii. there are less than five hydrogen bond donors,

iii. there are less than ten hydrogen bond acceptors,

iv. an octanol/water partition coefficient (log$K_{o/w}$) is lower than 5.

Those simple descriptors can be extended by other parameters to improve permeability predictions of small molecules. Alike molecular weight, the increase of molecular volume decreases the permeability of the permeant. The polarity of the molecule, another key property in assessing the molecule permeability, can be implemented by adding a polar surface area (PSA) descriptor. Generally, the increase of molecular polarity decreases the ability to permeate passively.[39] The capability of compounds (usually cyclic peptides) to form intramolecular hydrogen bonds also increases their permeability.[40,41] Usually, a combination of multiple descriptors is used to achieve a better permeability prediction score, e.g. Potts and Guy model for skin permeability based on molecular weight/volume and log$K_{o/w}$ [42]

$$log\ K_P = \log\left(\frac{D^0}{\delta}\right) + f \times \log K_{o/w} - \beta'' \times MW \qquad (3)$$

where D^0 is the diffusivity of a hypothetical molecule with zero volume, f coefficient accounts for the difference between the partitioning domain presented by octanol and that presented by the stratum corneum lipids, MW stands for molecular weight, β'' is constant (0.0061) and δ is diffusion path length.

The description of drug-membrane interaction is focused mainly on drug partitioning, permeability, diffusion, and its position in the membrane. **Partitioning** depicts the number of molecules dissolved in membrane and is described by lipid(membrane)/water partition coefficient log$K_{m/w}$:

$$K_{m/w} = \frac{c_{lipid}}{c_{water}} \qquad (4)$$

where c_{lipid} and c_{water} are concentrations of drug in lipid and water environment, respectively. The partition coefficient defines the ratio of concentrations of molecule distributed between lipid and water phases. Partitioning is sometimes used to describe the lipophilicity (i.e., affinity toward the lipid phase) of molecules.

In passive permeation, the drug is subjected to resistance from the membrane while being transferred. This solute resistance is proportional to the concentration of the drug being transferred and is therefore indirectly related to the solute's permeability. The **permeability** is defined in Fick's first law of diffusion as the steady-state flux of solute across the membrane and can be calculated as follows:

$$P = \frac{1}{R} = \frac{J}{\Delta c} \tag{5}$$

where R is resistance, J is the flux of the solute, and Δc is its concentration gradient.

Membrane permeation can be described by a simple model (*homogeneous solubility-diffusion model*) in which the solute permeates between two aqueous compartments separated by a homogeneous oil slab (mimicking the membrane). Thus, the permeability coefficient is directly connected to the membrane thickness and **diffusion of the solute** by the following equation:

$$P = \frac{K_{m/w} D}{h} \tag{6}$$

where D is the diffusion coefficient of solvent and h is the thickness of the oil phase. It also shows how permeability is directly connected to the lipophilicity of the molecule. The less lipophilic molecule will permeate slowly than more lipophilic ones for two molecules with the same diffusion coefficient with similar size.

3.1 Effect of membrane composition

The aforementioned varieties in biomembrane compositions cause differences in the physical properties of membranes. Those also affect the nature of interactions of the drug with biomembranes.

One of the key structural features that define membranes' properties – and consequently the drug-membrane interactions – is their lipid head group constituent. The effect of the head group region is rationalized mostly by theoretical studies. Permeation study of curcumin (therapeutic agent in cancer treatment) shows a higher affinity towards negatively charged DOPG lipid bilayer than DOPC membrane due to DOPG capacity to form hydrogen bonds.[43] Another theoretical prediction of water permeation showed that the translocation process is driven by the membrane phase (liquid disordered and solid gel phases studied) rather than by the lipid head group composition.[44] The permeation study of cytochrome P450 (CYPs) substrates/metabolites revealed slightly preferential partitioning into DOPC than into POPG membrane.[45] Comparative study on single-component lipid membrane permeability by Mathai et al. concluded that permeability is related strongly to the area occupied by lipid rather than bilayer thickness.[46]

As state above, cholesterol, as a major lipid component in many membranes, plays a crucial role in maintaining membrane phase and rigidity. The increase of cholesterol content in phospholipid membranes decreases the molecular motion of lipid tails and increases molecular packing, consequently observed as an increase in membrane ordering.[47] Cholesterol was shown to reduce water permeability, and this decrease is proportional to its concentration in the membrane.[48] Furthermore, it reduces the permeability of both cations (Na^+, K^+) and anions (Cl^-) as well as sugars (glucose) through various prototypical membranes (PCs, PSs, PGs).[49] In general, this shows that the decrease of permeability after the addition of cholesterol is independent of the surface charge of membranes.[49] Cholesterol also reduces the permeability of quinine-based photodynamic drugs (hypericin and its derivates) in mixtures with DPPC. The reduction of permeability was different for individual derivates and cholesterol content (9 and 25 mol%).[50] The partitioning of small drugs (ammonia, ethanol, nitric oxide, benzene, propane and neopentane) into the lipid tails region also decreases with cholesterol.[51] The effect of cholesterol-induced decrease of permeability is more profound in the presence of saturated lipids and membranes with smaller lipid head groups (PE as compared to PC).[51]

4. Membrane proteins

Membrane proteins (MPs) represent about a third of the proteins in living organisms and constitute about half of the total mass of biomembranes. They are responsible for processes occurring near the membrane interface or directly within the membrane based on the nature of protein-membrane interaction. Integral (intrinsic) membrane proteins are tightly bound to membrane structure by one (usually α-helical anchor) or more membrane-spanning domains or attached via lipids. Those transmembrane segments are composed of conserved hydrophobic motives that interact directly with hydrophobic space within the membrane core. These types of proteins mediate the transport of molecules (membrane channels and transporters), energy transduction (charge translocating MPs) or catalytical processes (membrane-bound enzymes). On the other hand, peripheral (extrinsic) proteins are loosely bound to the membrane surface, and the dynamics between bound and unbound state can be shifted by changing the natural conditions, for example, by the concertation of the salt. Those proteins are usually water-soluble enzymes (like phospholipases), and the contact with biomembranes is omitted to interactions with lipid head groups.

Many membrane proteins are, by some means, associated with drugs – either by the mediation of membrane translocation or by their biotransformation – since processes involving drugs closely related to biomembranes. Among those, an important class of cytochrome P450 enzymes play special role in metabolism of many endobiotics and xenobiotics.

4.1 Cytochrome P450 enzymes

Cytochrome P450 enzymes are a large superfamily of proteins found in animals, plants, fungi, protozoa, bacteria and even among viruses. Up to this day, more than 50,000 CYPs have been identified from which only 57 CYP genes from 17 families belong to humans. The pivotal role of this hemoprotein is the biotransformation of drugs and other xenobiotics.[52] They generally catalyze the biotransformation of hydrophobic substrate into more hydrophilic metabolite, that is rather easily eliminated from the organism. The mechanism of monooxygenase reaction underlying the catalytical activity of CYPs resides in the reduction of molecular oxygen into two atomic oxygens, with one atomic oxygen is then bound to aliphatic position of substrate molecule and the second oxygen atom is reduced to water by following scheme:

$$RH + O_2 + NADPH + H^+ \rightarrow ROH + H_2O + NADP^+ \quad (7)$$

where NADPH is the reduce form of nicotinamide adenine dinucleotide phosphate cofactor, RH is the aliphatic substrate and ROH the polar metabolite. The hydroxylation reaction itself is mediate by the heme cofactor buried within the center of the active site of CYP. The heme

cofactor is composed of the porphyrin ring with iron atom in its center. The heme-containing cavity of CYP is connected to protein surface via network of access and egress channels facilitating the transport of drug and its metabolite in and out the active site.

Despite relatively low sequential similarities (around 40%) among CYP families, the common fold of CYPs is highly conserved with predominantly α-helical motives with small fraction of β-sheets. CYPs secondary structural features are denoted in alphabetical order starting from the N-terminal part of protein. The most important structural motives are the I-helix, contain threonine amino acid involved in catalytic cycle of heme, the F/G-loop connecting the F and G helices and the B/C loop connecting the B and C-helices. Those highly flexible loops are (together with F and F-helices) important in drug trafficking as they gate the path in and out of the active site of CYPs. (Figure 8 panel A)

In contrary to water soluble prokaryotic CYPs, eukaryotic CYPs are usually attached to membranes. Most of the mammalian CYPs are bound to the cytosolic side of the endoplasmic reticulum membrane or to the inner mitochondria membrane. This provides them the matrix for to mediation of substrate and product channeling in and out of the active site of the protein. Moreover, biomembranes facilitate the interactions of CYPs with redox partners and also the with another CYPs. In general motive of CYP-membrane association, the hydrophobic N-terminal anchor is incorporated within the membrane while the catalytical domain of CYP flows on the membrane surface. Here the proximal side of catalytical domain (defined by orientation of heme cofactor) faces the aqueous environment, while the distal side is partially immersed in membrane by F/G and B/C-loops, parts of F and G-helices and partially by β4, β5-sheets and β4-β5 sheet (so called β-finger) (Figure 8 panel B). In this arrangement, the orientation of the distal side enables the interaction with redox partners.

The main distinguishing feature between microsomal and mitochondrial CYPs is the character of membrane interaction. Microsomal CYPs are synthesized by ribosomes directly bound to membranes rough ER and after translation are incorporated into the ER membrane. In contrary to that, mitochondrial CYPs are synthesized freely into cytoplasm and are post-translationally targeted to mitochondria via small leader sequence cleaved upon import. Compared to microsomal CYPs, cytochromes P450 found in mitochondria (like CYP11A1) are loosely associated with the inner mitochondrial membrane (IMM) since they lack the N-terminal anchor, and the interaction is omitted to specific segments of catalytical domain.

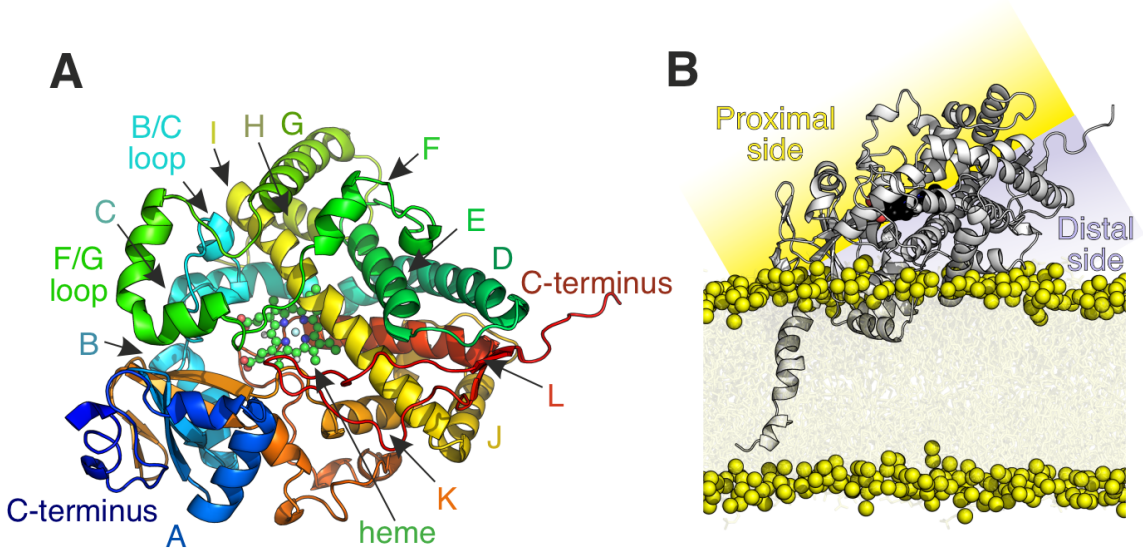

Figure 8. Structural features and membrane position of CYPs. The secondary structure of CYP with underlying individual protein segments denoted in alphabetical order starting from the N-terminal part of protein to C-terminal part (**A**). The orientation of CYPs on membrane surface (**B**). The N-terminal anchors the catalytical domain in membrane. The orientation of heme cofactors defines the proximal side (water facing) and the distal side (membrane facing) of the protein.

The immersion and overall orientation of CYP on the membrane depends on composition of membrane in which the protein is bound. The orientation of the catalytical domain can be determined from experimental measurements of the heme tilt angle (HTA). The heme tilt angle which is characterizes as the angle between plane of the heme cofactor and the membrane normal is widely used as benchmark for evaluation of MD simulations of membrane bound CYPs in comparison to spectroscopic measurements. The orientation of the CYP on the membrane is significantly affected by the lipid composition especially by the presence of charged lipid species originated from its head group substituent. For negatively charged lipid (like DOPG) CYPs show high inclination toward the membrane when compared to the neutral DOPC lipid. Also, the level of cholesterol content modulates the mutual CYP-membrane orientation as the HTA ranges from 52° to 68° (from pure membrane up to 50 wt% of cholesterol). The HTA values range from ~35° to 80° between different CYP isoforms.[53]

4.2 Cytochrome P450 reductase

All mammalian CYPs rely on a supply of redox equivalents in form of electrons from its redox partners. To catalyze the monooxygenase reaction, CYP needs to obtain consequently two electrons, each at given step of the catalytic cycle. The electron transport chain is facilitated by cytochrome P450 reductases and cytochrome b_5 enzymes in microsomes and by ferredoxin redox systems in mitochondria. In microsomes both redox partners are located at cytosolic side of the ER with the CPR:CYP ratio of approximately 3-15:1.[54] Even small disruption of CPR function may lead to a major disruption of various CYP catalytic reactions. Such examples of close connection between CPR function and CYP activity decrease are found in cases of patients suffering Antley-Bixler syndrome. The deleterious mutations in CPR gene are responsible for lanosterol 14α-demethylase (CYP51) activity decrease previously observed in ABS patients.[55]

Human cytochrome P450 reductase is coded by a single gene located at chromosome 7qll.2 and contains 680 amino acids in its sequence.[56] CPR is diflavin reductase – contains both flavin adenine dinucleotide (FAD) and flavin mononucleotide (FMN) cofactors – attached to the ER membrane by N-terminal anchor while its flavin domains are facing the cytosol. CPR also bears NADPH cofactor that subsequently reduces flavin cofactors. The catalytical domain of CPR comprises of four subunits – two flavine binding domains coupled by the connecting linker domain and the NADPH binding domain at C-terminus. The FMN binding domain is connected to the linker by so called hinge. This highly flexible loop (unresolved in crystal structures) seems to be responsible for domain movement as it enables the pivoting of individual flavodomains. (Figure 9)

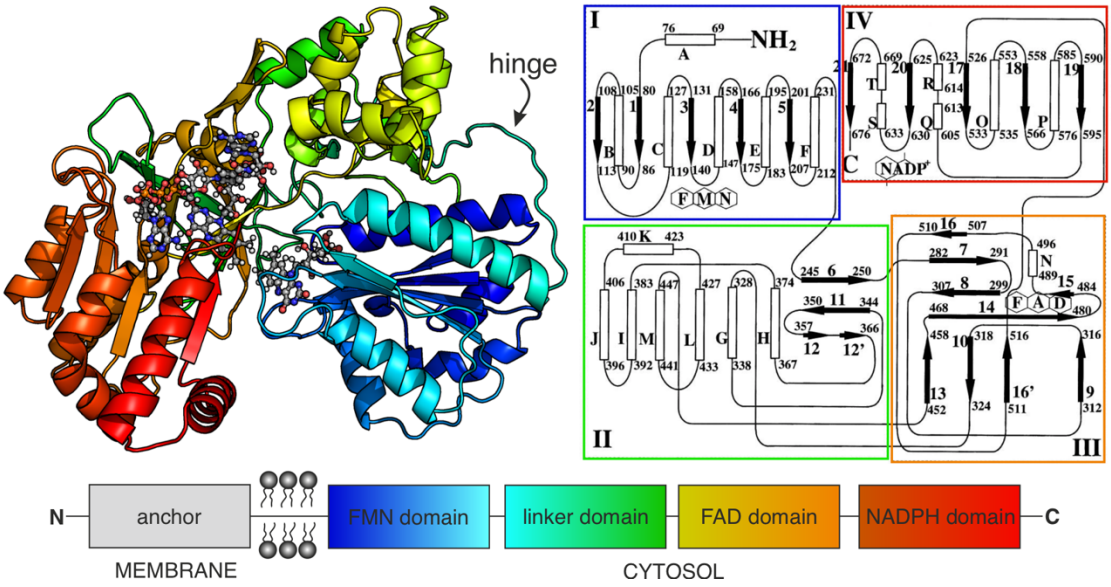

Figure 9. Basic structural features and topology diagram of CPR. Diflavin reductase is composed of 4 subdomains (cytosol facing) and N-terminal anchored (transmembrane part).

Based on the phase of the redox cycle, CPR can adopt two distinguishable conformations i.e., a closed or an open conformation. Multiple crystal structures of mammalian CPR in closed form are known, suggesting a compact and stable form, with flavin cofactors at close proximity (4 Å). At this conformation, all three cofactors are internally bound in a position allowing a cascade of intra-protein electron shuttling from NADPH to FAD and thereupon to FMN cofactor. The reduction of flavine cofactors then induces the CPR opening. Contrary to closed conformation, the open form is less compact with FMN and FAD cofactors being separated up to 86 Å apart (in case of yeast-human chimeric CPR). This leaves the FMN domain exposed to water environment clearly revealing the FMN cofactor. At this arrangement, CPR is compatible for the docking to its redox partner and for mediating the inter-protein electron transfer (Figure 10).

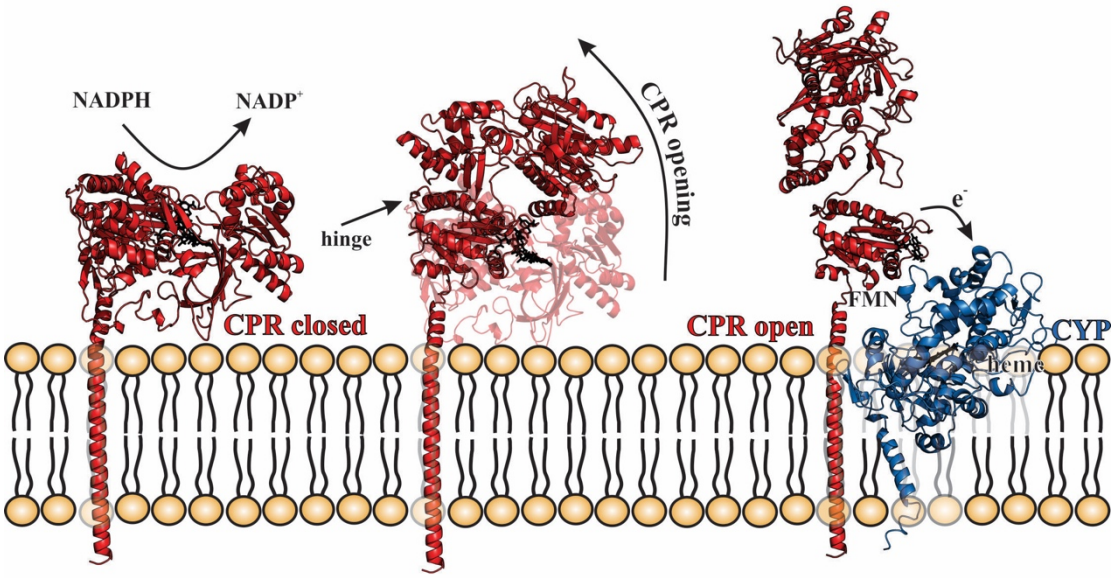

Figure 10. General scheme of CPR function. CPR is reduced by intra-cofactor electron cascade from NADPH cofactor. Upon CPR reduction, protein adopts more open conformation capable of enter-protein electron transfer towards its redox partner (CYP).

5. Theoretical approach

The first practical foundations of molecular simulations as we know them were laid in the late 1950s by Alder and Wainwright in calculations of state of hard spheres. Later on, calculations on correlation in the motion of liquid argon and thermodynamic properties of water showed promising potential of this new field. Not even 20 years after the first simulations of simple gasses were carried out, biological relevant processes like simulations of protein had been extensively studied starting with the work of McCammon on dynamics of bovine trypsin inhibitor. Those contributions in the field of theoretical calculations and simulations have been awarded by Nobel Prize in Chemistry 2013 for "the development of multiscale models for complex chemical reactions". Nowadays, with the increase of computational power resources, molecular modeling and especially molecular dynamics simulations of biological processes are widely used techniques in rationalization of natural phenomenon and in drug discovery.

This chapter briefly summarizes some fundamental principles of computational techniques – mostly molecular mechanics (MM) and molecular dynamics (MD) – used in study of membranes and protein dynamics. Special focus will be taken on calculations of drug permeabilities.

5.1 Molecular Mechanics

In contrary to quantum mechanics (QM) approach molecular mechanics completely neglects the presence of electrons and the potential energy of the system relies entirely on positions of atomis, $E_p = f(\boldsymbol{R})$. Therefore, it does not allow the study processes involving electrons, such chemical reactions. In molecular mechanics system is fully described as set of "balls and springs" representing atomic nuclei and bonds connecting them. In order to calculate the potential energy between individual atoms, MM uses so called **force field** (FF) i.e., set of simple algebraic equations and empirical parameters. Those parameters include complete data about individual atoms (atomic radii, mass or charge) as well as the information necessary for describing their interaction (bond length, angles or dihedral angles). Contributions to the overall potential energy of the system is then calculated as the sum of individual bonded and nonbond terms of force field as following:

$$
\begin{aligned}
E_p = \; & E_B + E_{NB} \\
& = \sum_{bond} E_{bond} + \sum_{angle} E_{angle} \\
& + \sum_{dihedral} E_{dihedral} \sum_{im.\ dihedral} E_{im.\ dihedral} \\
& + \sum_{Coulomb} E_{Coulomb} + \sum_{LJ} E_{LJ}
\end{aligned}
\tag{8}
$$

where E_B is the bonded term related to covalently bound atoms and E_{NB} is the nonbonded term describing the long-range electrostatic and van der Walls interactions.

In most force fields, **bonded interactions** are described as set of four contributions labeled as covalent bond stretching, angle bending, proper and improper dihedrals. Bond stretching of two covalently bound atoms is described by simple harmonic oscillation where the energy varies with the square of the displacement from the reference bond length

$$E_{bond}(r_{ij}) = \frac{1}{2} k_{ij}^{bond} (r_{ij} - r_{ij}^{id})^2 \tag{9}$$

where is k_{ij}^{bond} represents the force constant of the bond stretching derived from Hooks law, r_{ij} is the current distance between atoms *i* and *j* and r_{ij}^{id} is the reference bond length. Both constants are specific for individual pair of bound atoms and can be derived from quantum mechanical calculations or from experimental data. Harmonical potential describes well the bond stretching near its equilibrium length but for better description of anharmonicity of bond oscillation Morse potential is preferred.

The angle bending term between atoms *i*, *j* and *k* is also represented as harmonic potential as

$$E_{angle}(\theta_{ijk}) = \frac{1}{2} k_{ijk}^{angle} (\theta_{ijk} - \theta_{ijk}^{id})^2 \tag{10}$$

where k_{ijk}^{angle} is the force constant of angle bending, θ_{ijk} the actual angle and θ_{ijk}^{id} is the ideal angle. The force constants for angle bending are smaller compared to bond stretching since less energy is required to distort angle from its equilibrium.

Another force field term describes the changes in torsion. Here we can distinguish the torsion of proper and improper dihedral angles. In case of proper dihedrals, the barrier of rotation of two planes defined by angles between atoms *i*,*j*,*k* and *j*,*k*,*l* is represented as

$$E_{dihedral}(\phi_{ijkl}) = k_{\phi}^{dihedral} (1 + \cos(n\phi_{ijkl} - \phi_{ijkl}^{id})) \tag{11}$$

where $k_{\phi}^{dihedral}$ is torsion the force constant, ϕ_{ijkl} is the dihedral the actual dihedral, ϕ_{ijkl}^{id} is the reference dihedral angle and *n* is the multiplicity. The multiplicity (*n* = 1,2,3 ...) defines the number of minima while angle rotates through 360°. It is worth mentioning that most of the

variations in conformation of biological systems is driven by the interplay between torsions and nonbonded interactions.

In order to maintain the planarity of molecules the improper dihedral term (also known as out-of-plane bending term) defined by a harmonic potential is used:

$$E_{im.dihedral}(\xi_{ijkl}) = \frac{1}{2} k_{\xi}^{im.dihedral} (\xi_{ijkl} - \xi_{ijkl}^{id})^2 \quad (12)$$

where $k_{\xi}^{im.dihedral}$ is the force constant of improper dihedral, whereas ξ_{ijkl} and ξ_{ijkl}^{id} represent the current and reference values of dihedral angle.

In most force fields, **nonbonded interactions** are handled in two terms denoting the electrostatics and van der Waals interactions. The electrostatic interactions are described by classical Coulomb's law of interaction of charged particles as:

$$E_{Coulomb}(r_{ij}) = \frac{1}{4\pi\varepsilon_0\varepsilon_r} \frac{q_i q_j}{r_{ij}} \quad (13)$$

where ε_0 is the vacuum permittivity, ε_r is the relative dielectric constant, q_i and q_j are atomic point charges and r_{ij} distance between atoms *i* and *j*. Here simplified model of point charges (i.e., partial atomic charges or net atomic charges) located at the centers of each atom is used. Those charges are constant; thus they do not reflect polarization effects of surrounding. Calculations of electrostatic interactions are carried out through multipole expansion and are related to interactions of two charged particles, charged particle-dipole, dipole-dipole, and higher-order terms of multipole interaction.

Interactions of uncharged molecules are usually described by the Lennard-Jones potential:

$$E_{LJ}(r_{ij}) = 4\epsilon_{ij}[(\frac{\sigma_{ij}}{r_{ij}})^{12} - (\frac{\sigma_{ij}}{r_{ij}})^{6}] \quad (14)$$

where r_{ij} is distance of interacting atoms *i* and *j*, ϵ_{ij} is the depth of potential well and σ_{ij} is collision diameter i.e., separation for which the potential of interacting uncharged particles equals zero. The Lennard-Jones potential (also called "12-6" potential) is characterized by attractive part (r^{-6}) and repulsive part (r^{-12}). The attractive part is related to London dispersion and describes the attraction at long distances whereas the repulsion part approximates the Pauli electron repulsion and is more pronounced at short distances.

5.2 Molecular Dynamics

Concept on molecular dynamics is based on solving numerically classical mechanical equations of motion based on Newton's second law. The time propagation of coordinates (positions of atoms) is described by changes of forces acting on particles based on displacement in their positions. The force (F_i) acting on individual atom *i* (and on every atom described in system) is calculated from the gradient of the potential energy from molecular mechanics as following:

$$F_i = -\nabla_i E_p \tag{15}$$

where the acceleration is calculated from the force F_i as the second derivative of current atomic positions (x_i) with respect to time

$$\frac{d^2 x_i}{dt^2} = \frac{F_i}{m_i} \tag{16}$$

where m_i is the mass of atom *i*. To solve this many-body problem of time propagation of the coordinates finite difference techniques are used. Here the integration of the of equations of motion is divided into series of small finite number of iterations with defined time step (δt). The force on each atom is, at given time *t,* calculated from the vector sum of interactions of this atom with other particles. Thus, derived force is than used to calculate the acceleration of particles at current positions and velocities and consequently to generate new set of coordinates and velocities at time $t + \delta t$. Using this procedure, and with the assumption than the force is constant during those elemental steps, one can calculate the time propagation of atomic positions in time i.e., the trajectory. The final length of molecular dynamics trajectory is defined by number of those finite time steps and the size of one elementary step. Many numerical integration schemes were design using finite difference techniques e.g., Verlet and Leap-frog algorithms.

The initial coordinates are given by configuration of system and initial coordinates are determined from Maxwell-Boltzmann distribution at desired temperature:

$$p(v_i) = \left(\frac{m_i}{2\pi k_B T}\right)^{1/2} \exp\left(-\frac{1}{2}\frac{m_i v_i^2}{k_B T}\right) \tag{17}$$

where $p(v_i)$ is the probability of atom *i* moving with certain velocity v_i at given thermodynamical temperature *T* and k_B is the Boltzmann constant.

MD enables us to study time-dependent properties of biological systems, like conformational changes in proteins or nucleic acids, protein-protein or protein-membrane interactions or time-resolved behavior of drug membrane permeation.

5.3 Enhanced sampling techniques

Molecular dynamics simulations are useful tool in study of biomolecular systems and are usually the method of choice in computational exploration of behavior of proteins and membranes. Nevertheless, the method itself is not perfect and is limited by the accuracy of force field and computational cost. The later mentioned may result in inadequate sampling of conformational space. Biological processes like conformational changes of membrane transporters during drug translocation or signal transduction via protein receptors are processes that involve exploring the of large free-energy landscapes. Those "rare events" are often unreachable by means of simple molecular dynamics because of limited simulation time scale resulting in insufficient sampling of just local energetical minima. To address this problem many enhanced sampling techniques have been employed to effectively accelerate those calculations and to help examine the conformational dynamics of complex biological phenomenon. Those enhanced methods originate in modifying of free energy landscape by adding bias potential along reaction coordinate - collective variable (CV) - and therefore decreasing the energy barrier of monitored reaction.

In this chapter basic principles behind umbrella sampling (US) and metadynamics (MTD) – two most used enhanced sampling techniques – are described. Those techniques were also used in presented theses.

5.3.1 Umbrella sampling

Umbrella sampling was one of the first CV-based enhance sampling technique used to study biological processes out of its equilibria. The method is based on exploring free energy along predefined collective variables (CV). The reaction path is defined as a function of atomic coordinates describing the bottleneck path of studied phenomenon. In case of membrane permeability studies, CVs are usually defined as a distance of the drug from the center of the membrane. By adding series of harmonic potentials $h_i(q)$ along single reaction coordinate (q) the system can overcome the energy barriers. The potential energy of biased system is modified as

$$E_p(\boldsymbol{R}) \rightarrow E_p(\boldsymbol{R}) + h_i(q) \tag{18}$$

where $\boldsymbol{R}$ is a vector of all coordinates and $h_i(q)$ is a quadratic potential defined as

$$h_i(q) = \frac{k}{2}(q - q_i)^2 \ . \tag{19}$$

Here k is the harmonic force constant and q_i is the position along reaction coordinate. Series of independent biased simulations (N) for individual $q_{i,j,..,N}$ is then performed to attain the efficient sampling of monitored CV. The probability distribution function $\rho_i(q)$ for individual coordinate along represented CV is obtained as set of overlapping histograms. Those probability distribution functions are affected by the presence of biasing potentials thus not reflecting the natural unbiased

state. The unbiased probability distribution function $\rho^u(q)$ is than reconstructed using direct iteration algorithms like the Weighted Histogram Analysis Method (WHAM). The free energy along monitored reaction coordinate q can be calculated as

$$G(q) = G(q_0) - k_B T \ln \frac{\rho^u(q)}{\rho_0^u(q_0)} \tag{20}$$

where q_0 is reference point. Sufficient sampling of reaction path usually depends (apart from correctly chosen CV) on having large enough number of frames equidistantly located along CV so the overleaping of neighbor histograms is adequate. Also, the time set for individual biased simulation is a key factor for reaching the convergence of the US calculation.

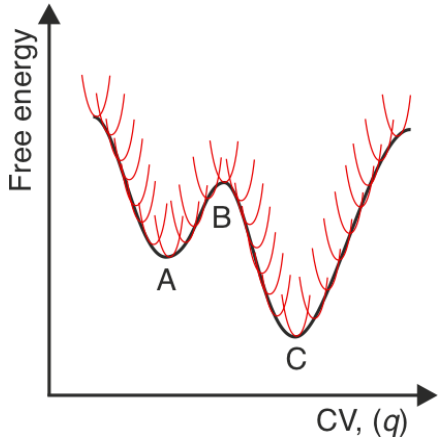

Figure 11. Illustration of the US procedure. Series of harmonic potentials along single reaction path is added. The free energy is reconstructed from the probability distribution function along monitored CV. Here A denotes the local minima, B the transition state and C the global energetical minima for given path.

5.3.2 Metadynamics

Contrary to US, in metadynamics method a single biased simulation is carried out to reconstruct the free energy profile. During this MTD run, a set of bias potentials (in form of Gaussian functions) is systematically imposed along the monitored CV (Figure 12). By applying history-dependent Gaussians at every time step, the system is encouraged to visit yet unsampled configuration space. In MTD run with single reaction coordinate q, the Gaussians are defined as following

$$V_G(q,t) = \sum_{\substack{t' = \tau_G, 2\tau_G, \ldots \\ t' < t}} w \, exp\left(-\frac{(q - q(t'))^2}{2\sigma^2}\right) \tag{21}$$

where w is the height of the Gaussian function, σ is its width, and τ_G is the Gaussian deposition frequency. These parameters are specifically adjusted based on knowledge of studied system and may influence the precision and efficiency of MTD calculation. For instance, if the height of the Gaussians is too large the free energy surface will be sampled hastily, and reconstructed energies

will be inaccurate. On the other hand, the lower the height of the Gaussians the slower the simulation is. Moreover, inappropriately high deposition frequencies of the Gaussians can also slower MTD run.

An unbiased estimate of free energy is determined by positions of history-dependent potentials deposited up to time *t*. The system is fully converged, when the sum of added potentials equals the negative free energy, and the system diffuses freely along CV.

$$V_G(q, t \longrightarrow \infty) = -G(q) \tag{22}$$

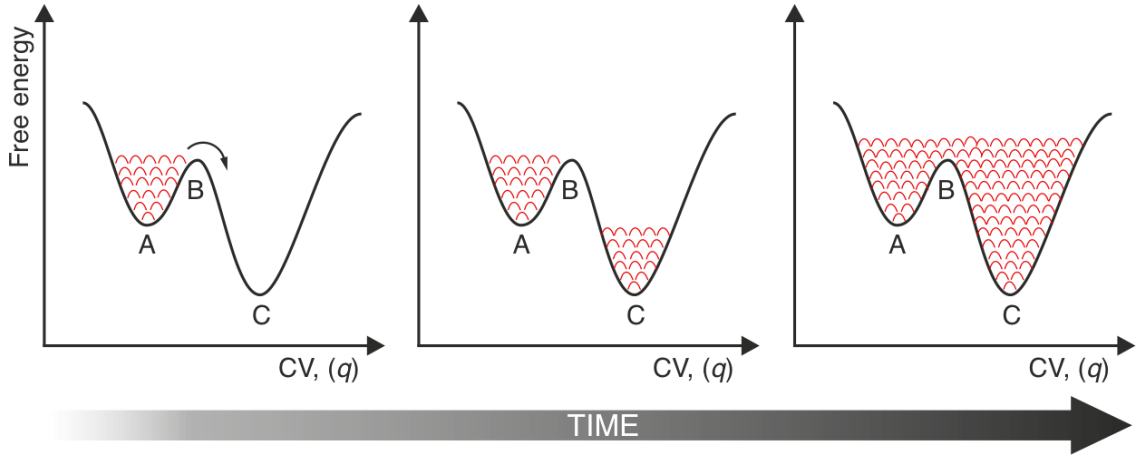

Figure 12. Schematic illustration of metadynamics approach. Series of history-dependent potential is added along the monitored CV. The calculated free energy is assessed from positions of imposed potentials. Here A denotes the local minima, B the transition state and C the global energetical minima for given path.

5.4 COSMO calculations

An alternative to molecular dynamics simulations in the investigation of the permeation through micellar systems is so called COSMO procedure. It is based on COSMO-RS (Conductor-like Screening Model for Real Solvents) approach where solvent (in our case membrane) is described by dielectric continuum of given dielectric constant. For each molecule, the van der Waals-like molecular surface based on molecule geometry is generated. Upon this surface, the dielectric screening charge densities (σ) induced by surrounding solvent are calculated. Consequently, density distributions of polarization charge density (σ-profiles) are generated, and intermolecular interactions are described as local pairwise interactions of those segments. The corresponding affinities of those molecular surface segments are denoted as σ-potentials.

Prior to membrane permeability prediction, COSMO surfaces are calculated on both solutes and solvent molecules by means of density field theory (DFT) method – usually by B-P functional and def2-TZVPD basis set. This includes COSMO surfaces of individual lipid molecules presented in membrane. In COSMOmic calculations, the inhomogeneous solvent representation

is defined by the membrane structure. Lipid bilayer (usually obtained from MD) is divided into layers perpendicular to membrane normal, each differing in the atomic composition. Individual layers are described as two-dimensional fluids with specific distribution of polarization charge densities, e.g., σ-profiles. The chemical potential $\mu_M^X(r, \boldsymbol{d})$ of solute *X* in solvent (membrane) *M* is calculated as function of its orientation and position for individual layer. For bilayer having *n* layers and solute with *m* possible orientations, the partitioning function of solute *X* is calculated from chemical potentials as following:

$$Z_M^X = \sum_{i=1}^{n}\sum_{j=1}^{m} exp\,\{-\frac{\mu_M^X(r_i, \boldsymbol{d_j})}{k_B T}\} \tag{23}$$

where r_i is solute position and $\boldsymbol{d}_j$ is its orientation. The probability of finding solute *X* in layer *i* is denoted as

$$p_M^X(r_i) = \frac{Z_M^X(r_i)}{Z_M^X} \tag{24}$$

and the free energy profile of solute *X* permeating though membrane *M* is given as

$$G_M^X(r_i) = -k_B T\, ln\, p_M^X(r_i) \tag{25}$$

Various tools from COSMO family have been developed based on COSMO-RS method allowing mechanistic predictions of permeabilities of micellar systems. For example, COSMOperm[57] method is based on COSMOmic[58] approach and extends the calculations of permeabilities for charged molecules. The requirement of single DFT calculation per molecule is advantageous compared to extensive sampling in MD simulations. Along with good precision, it makes COSMO approach suitable for high throughput permeability studies.

5.5 Calculations of Drug Permeabilities

The first step in prediction of drug-membrane permeabilities is the calculation of free energy profile with respect to the membrane normal (described above). Generally, the free energy profile can denote the energetical information of membrane crossing event along defined pathway (Figure 13). It defines the height of the penetration barriers (ΔG_{PEN}) which are the time-limiting steps of crossing events. The affinity of drugs towards the membrane is also captured as the height of the membrane/water barrier, ΔG_{WAT}, which usually correlates well with the partitioning coefficient $\log K_m$. It also determines the depths of the permeation as the position of the free energy minima (Z_{MIN}).

Once the permeability calculations are performed and the free energy across given path is enumerated the task is to predict properties characterizing the membrane permeability itself e.g., the **permeability** and **diffusion coefficients** and drug **partitioning into membrane**.

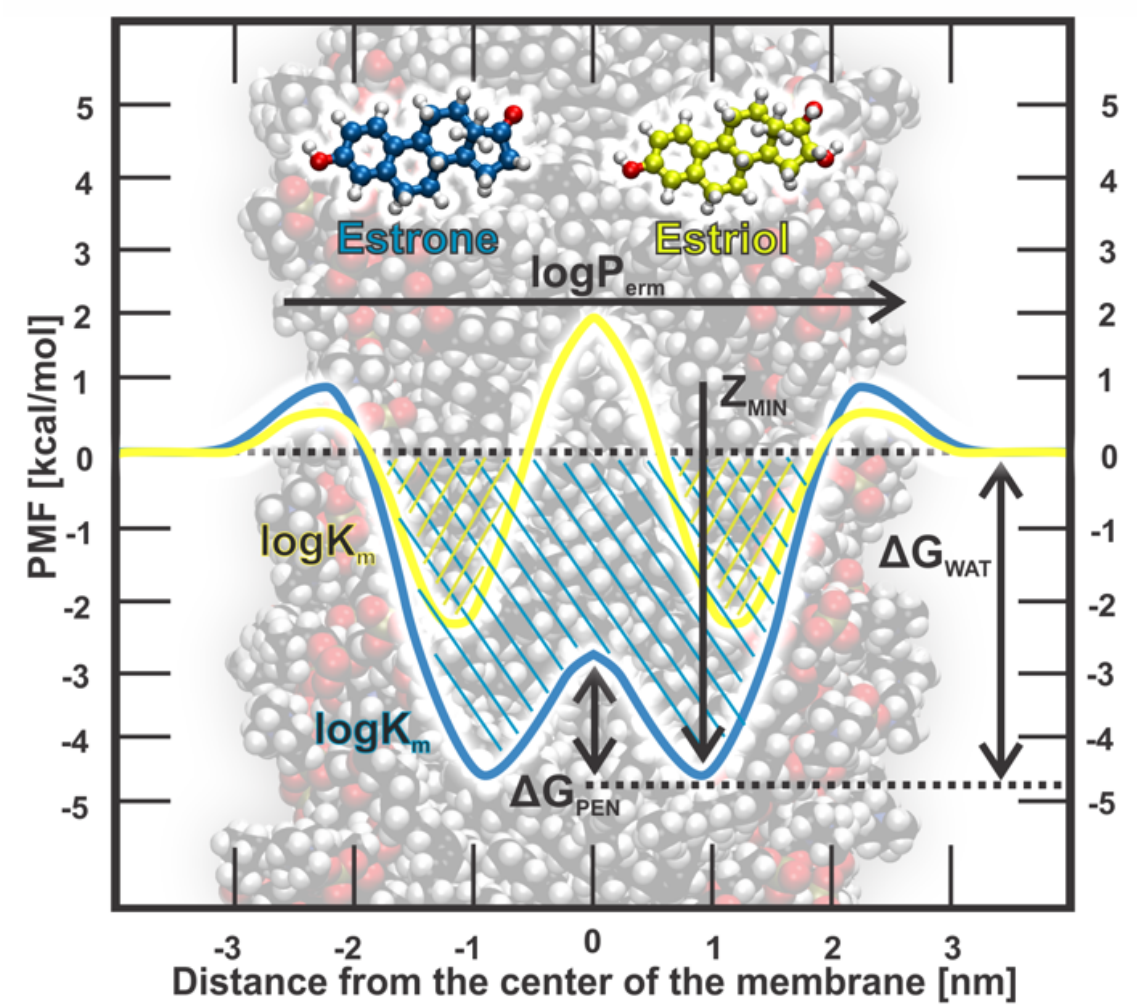

Figure 13. Overall schematic representation of the permeation process on example of two steroid molecules. The height of the penetration barriers (ΔG_{PEN}) and the affinity towards the membrane (ΔG_{WAT}) are calculated directly from the corresponding the energetical profile. The Z_{MIN} defines energetically preferential position along followed pathway.

Early concepts of cell permeabilities were proposed by Overton, simplifying the membrane permeability as transport through homogeneous oil slab where permeability coefficients correlate with oil/water partition coefficients. Here the permeation process depends only on the thickness of bulk solvent (oil) and the ability of solute to passively diffuse. In contrary to isotropic hydrophobic oil medium, membranes are highly heterogenous and anisotropic systems. Their heterogeneity arises from its varying lipid composition and can be characterized by density distributions, order parameters or lipid diffusion. Besides, lipids consist of highly polar moieties, like glycerol/ester containing head groups, that could not be represented by simple oil phase. Overton's model was therefore not sufficient in depicting the structural and dynamic properties of membranes as transport medium.

More sophisticated model, so called *inhomogeneous solubility-diffusion model* was proposed encompassing the membrane heterogeneity. Here properties underlying the transport phenomenon depend on the depth of permeation and vary locally during molecule translocation. The overall **permeability coefficient** is than calculated as if the membrane was divided into finite number of layers in an integral form

$$P = \frac{1}{R} = 1/\int_{z_1}^{z_2} R(z)\, dz = 1/\int_{z_1}^{z_2} \frac{exp\,(^{\Delta G(z)}/_{k_B T})}{D(z)}\, dz \tag{26}$$

where $R(z)$, $D(z)$ and $\Delta G(z)$ are solute resistance, diffusion coefficient and free energy of transfer, respectively, at given position z along the membrane normal. Due to the exponential character of $\Delta G(z)$ in the denominator, more appreciable changes of the permeability coefficient are found for systems with positive free energy values, while the partitioning into the membrane is neglected.

The overall **partitioning coefficient** in the membrane/water environment, integrated over membrane and water regions, can be calculated from free energy profile as

$$K = \int_{z_1}^{z_2} exp\ \left(\frac{-\Delta G(z)}{k_B T}\right) dz \tag{27}$$

Since the partitioning defines the ration of concentrations of molecules between the membrane and the water phase it is necessary to define the boundaries between those two phases. Defining the exact borders is not trivial task, since biological membranes are predominantly found in disordered phase which is highly flexible and with inclinations to undulations. An elegant way around it was proposed by Klamt et al., by weighting the free energy based on the ratio of density of water in each layer $\rho_{(z)}^{water}$ and bulk water density ρ_{bulk}^{water}. The partitioning coefficient than independent on the size of the system and can be calculated by following

$$K = \int_{z_1}^{z_2} exp\ \left(\frac{-\Delta G(z)}{k_B T} - \frac{\rho_{(z)}^{water}}{\rho_{bulk}^{water}}\right) dz \times \frac{APL}{M_{lip} m_u} \tag{28}$$

where *APL* stand for the area per lipid, M_{lip} is the molecular weight of lipids and m_u the atomic mass constant. The multiplication factor converts values of the partition coefficient into values directly comparable with experiments kg(lipid)/L(water). In contrary to permeability coefficient, the partitioning depends strongly on the negative values of the free energy.

In order to enumerate the permeability coefficients, the inhomogeneous solubility-diffusion model requires the calculation of local **diffusion coefficients** $D(z)$. In enhanced sampling simulations, such as the umbrella sampling or the *z*-constraint method, molecules are constrained at given position along membrane normal, therefore their diffusion is restricted to the *xy* - plane.

The local diffusion coefficients are calculated by integrating the autocorrelation function (ACF) of the average constrained force acting on molecules as

$$D(z) = \frac{(k_B T)^2}{\int_0^\infty < ACF(F(z)) > dt} \tag{29}$$

where $ACF(F(z))$ is the autocorrelation function of the force on solute when constrained at position z along the axis. Similarly, the diffusion coefficient can be calculated from the velocity ACF or from the mean square displacement of the drug.

It is worth mentioning, that obtaining experimentally values for free energy of transfer $\Delta G(z)$ or diffusion coefficients $D(z)$ is not possible since there are no techniques capable of grasping such fine properties. In contrary, the partition coefficients are relatively easy to resolve by numerous experimental techniques, such as solid phase microextraction or equilibrium dialysis and are directly comparable to calculated ones. As for experimental permeabilities, the most straightforward approach is to measure diffusion (and consequently concentration) of drug between compartments (donor and acceptor) separated by thin film (skin graft), for example by Franz diffusion cell. Another *in vitro* approach is to use biological cell assays, like Parallel artificial membrane permeability assay (PAMPA[59,60]), or colorectal adenocarcinoma cells (Caco-2[61]) line cells. Unlike to simple partitioning, the permeability coefficients vary based on technique used and therefore are not suitable for a direct comparison with calculated permeabilities. Nevertheless, cautious comparison of calculated permeabilities based on the same methodology is generally acceptable.

6. Results

Following chapter summarizes our contributions to understanding and rationalization of how biomembranes interact with other biological species using different theoretical approaches.

The Results chapter is divided into five subchapters each dedicated to individual project and contains both, results published in peer-reviewed articles and not yet published papers and data. First subchapter describes the development and usage of MolMeDB database. Second subchapter is dedicated to an unpublished study on how cyclosporin A permeates through various of biological membrane models. Third subchapter refers to the development and validation of systematic computational methodology for prediction of suitable liposomal encapsulation for thermally induced release of bio-active compounds. Finally, two last subchapters describe the effect of membrane on behavior of the membrane-interacting proteins from superfamily of heme-containing enzymes i.e. cytochromes P450s and its mutual interaction with redox partner CPR.

6.1 MolMeDB project

Biomembranes are complex systems that serve as natural barriers for many compounds. They act on multiple levels within the human body – on cellular and sub-cellular level as well as on macroscopic scale, like skin barrier. At all those levels, the molecule-membrane interactions are important for the course of action of individual molecules in the organism and for their pharmacokinetics and pharmacodynamics. Multiple experimental techniques for assessing drugs partitioning (like SPME[62,63]) or permeabilities (Caco-2[64], PAMPA[65]) were derived, providing us with large amount of data on how molecules interact with membranes. Furthermore, various databases like EDETOX[66] focused on *in vitro* and *in vivo* percutaneous permeabilities or PerMM database[67] using thermodynamics-based computational method to predict permeabilities through artificial and natural systems have been developed. Moreover, molecular dynamics simulations can provide complex information on both partitioning and permeability and on general behavior like orientation and favorable positions within membrane. MD-based methods generally focus on the effect of specific drug class or membranes. Finally, COSMO-based calculations represent and an accurate and relatively fast prediction of drug-membrane behavior suitable for high-throughput screening. All those data are not interlinked and scattered across multiple platforms and in literature, thus lacking thorough benchmark comparison among individual method/membrane systems.

To fill this gap, we have developed Molecules on Membrane database (MolMeDB) – an open chemistry database about interaction of molecules with membranes. Up to this day, MolMeDB contains more than 931,000 specific drug-membrane interactions for more than 456,000 unique molecules. Interaction data are linked directly to specific membrane system and technique – up to now database contains 41 membrane systems and 54 methods. (Figure 14) The membrane systems are further divided based on its localization within organism such brain, cell, eye, intestine, or skin membranes and based on the used approach e.g., theoretical models (like simple bilayers) or experimental systems (complex cell lines like Calu-3 or Caco-2). Similarly, methods are divided based on the source of interaction data e.g., experimentally obtained, computed/calculated (QSARs, COSMO-based calculations) or simulated (MD-based techniques at different level of approximation).

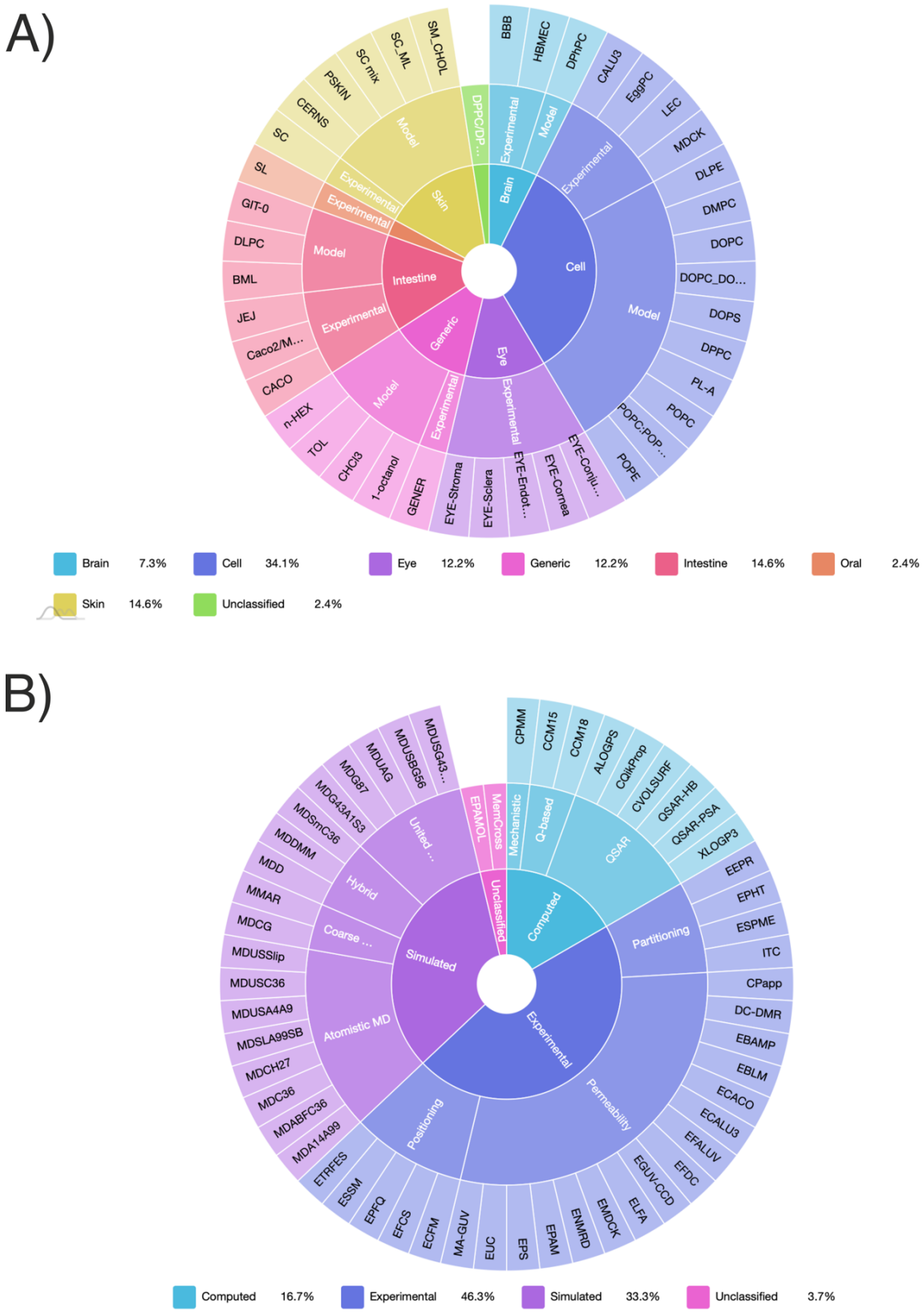

Figure 14. Distribution of total membranes (**A**) techniques (**B**) found in MolMeDB database.

It is worth mentioning that the latest version of MolMeDB also includes new information on membrane transporters and its interaction with small molecules. Especially on their relations to compound in terms of substrate or inhibitory/non-inhibitory effect.

6.1.1. MolMeDB user interface

Web version of MolMeDB database is accessible (https://molmedb.upol.cz/) and provides a user-friendly interface. Interaction data are accessible via Browse or Search mode, where user can either browse through lists of compounds that appertain to specific membranes and techniques or to directly search for desired compound by its name or SMILES notation. Upon choosing the entry a page for individual compound contains four sections:

1. **General info** – provides a description of basic molecular properties like molecular weight, octanol/water partition coefficient predicted from RDkit software[68] or standard chemical identifiers and notations (InChiKey, SMILES). Moreover, it directly visualizes 2D and 3D structure of molecule. This section contains links to other databases like PubChem[69], DrugBank[70], ChEBI[71], ChEMBL[72] or Protein Data Bank[73].

2. **Interactions** – displays an interactive table of all interactions available for a selected compound. For a given membrane-method combination is lists interactions such as membrane/water partition coefficient ($\log K_m$), permeability coefficient ($\log P_{erm}$), the height of the penetration barriers (ΔG_{PEN}), the affinity of drugs towards the membrane (ΔG_{WAT}) or the position of the interaction minima (ΔZ_{MIN}). It also contains the charge of the molecule (Q), temperature and link to reference publication from which data were obtained.

3. **Transporters** – provides information about transporters and its interactions with compounds found on the database. It shows a targeted transporter with a link to UniProt database as well as characteristic constants such as half maximal effective concentration (pEC_{50}), half maximal inhibitory concentration (pIC_{50}), inhibition constant (pK_i) an Michaelis constant (pK_m). It also classifies the nature of interaction towards transporter as substrate, inhibitor, or non-inhibitor.

4. **Free energy graph** – demonstrates free energy profiles of molecule-membrane crossing with respect to membrane normal between the membrane center (0 nm) and water environment (3.5 nm). At any given membrane depth (blocks separated by 0.1 nm) the free energy value can be interactively visualized.

6.1.2. Case study

Multiple free energy profiles can be visualized together allowing the user to denote the effect of specific membrane/method on permeation of specific molecule or to compare multiple compounds on one specific membrane/method system setup. Both, interaction data and free energy profiles can be directly export in .csv format. The following case studies demonstrate the usage of the MolMeDB database.

Caffeine and its metabolites

Here the example of comparison of free energy profiles for caffeine and its derivatives shows the effect of different type of metabolizing reaction on metabolites permeation with respect to unmetabolized substrate (Figure 15). Caffeine is metabolized by various of metabolizing enzymes into following metabolites – theobromine (CYP1A2, CYP2E1), theophylline (CYP1A2, CYP2E1), 1,3,7-trimethyluric acid (xanthine oxidase), 6-amino-5(N-formylmethylamino)-1,3-dimethyluracil (CYP1A2) and paraxanthine (CYP1A2). The type of metabolizing reaction (demethylation, oxidation or decyclization) defines the chemical modification of resulting products. Free energy profiles showed distinguishable differences for individual metabolites with respect to caffeine substrate molecule. Demethylation reaction showed increase of the penetration barrier by ~3.4 kcal/mol for theobromine, theophylline and paraxanthine. Products of oxidation and oxidation/decyclization reactions displayed additional increase of penetration barriers with respect to caffeine by 5.4 and 5.9 kcal/mol, respectively. The most discernible increase of the penetration barrier was observed in the aliphatic tail region membrane while the affinity towards the membrane (ΔG_{WAT}) defined as the height of the membrane/water barrier remained almost unchanged for all molecules.

Comparison of methods

This case study shows bigger datasets (101 compounds) that allows the comparison of multiple membrane/method entries. Here we demonstrated the evaluation of theoretical methods against experimentally obtained data (Figure 16). Permeability coefficients obtained from two different theoretical approaches COSMOmic/COSMOperm18 calculations and PerMM predictions were evaluated against black lipid membrane (BLM) experimental setup. In COSMO-based calculations model of DOPC lipid bilayer was used while in BLM setup and PerMM predictions the permeabilities were determined on generic phosphatidylcholine membrane. Linear regression fit was employed to identify the level of correlation between the combination of two methods. The resulted coefficient of determination (R^2) of 0.76 and 0.77 for COM18/BLM and PerMM/BLM, respectively presented good agreement of both theoretical approaches compared to experiment.

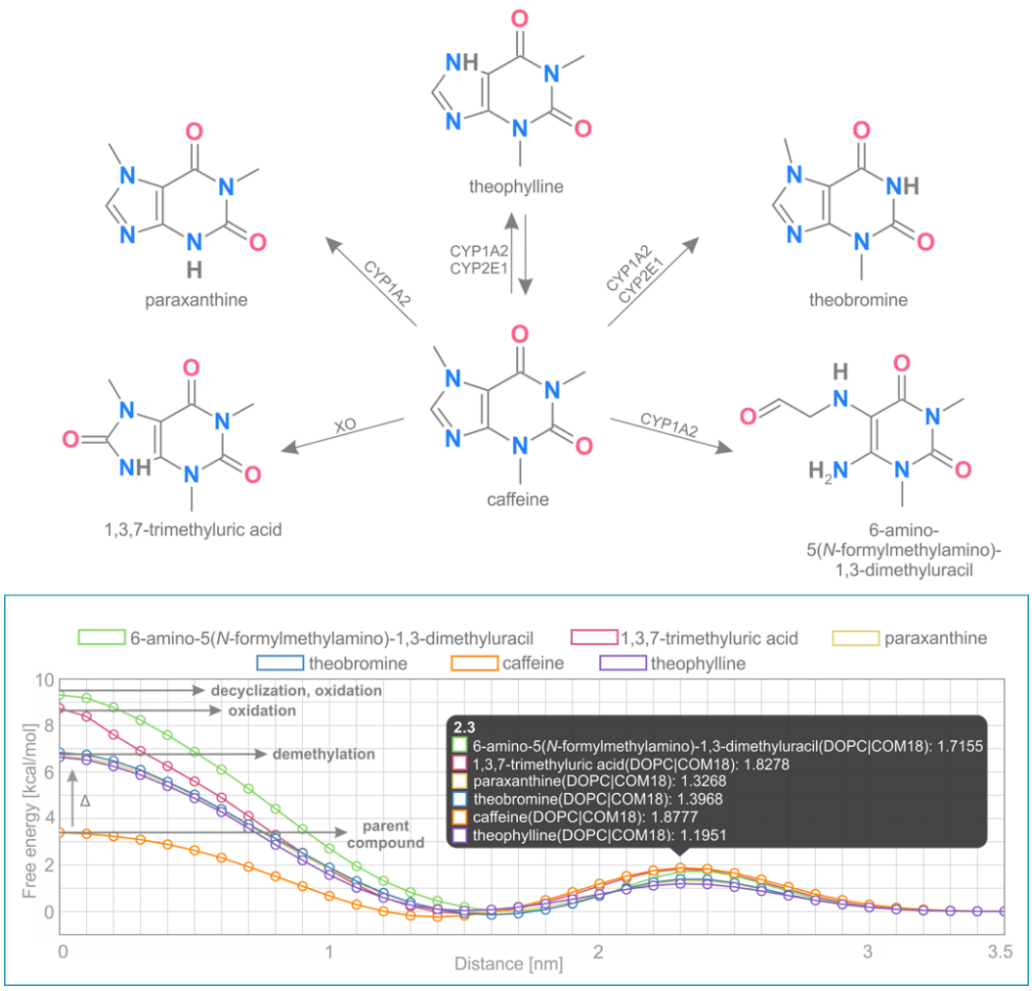

Figure 15. Free energy profiles of caffeine and caffeine metabolites permeation through DOPC membrane calculated with COSMOmic18 as example of MolMeDB usage. Structures of individual molecules are depicted along with enzymes responsible for caffeine metabolism. Figure taken from reference[74].

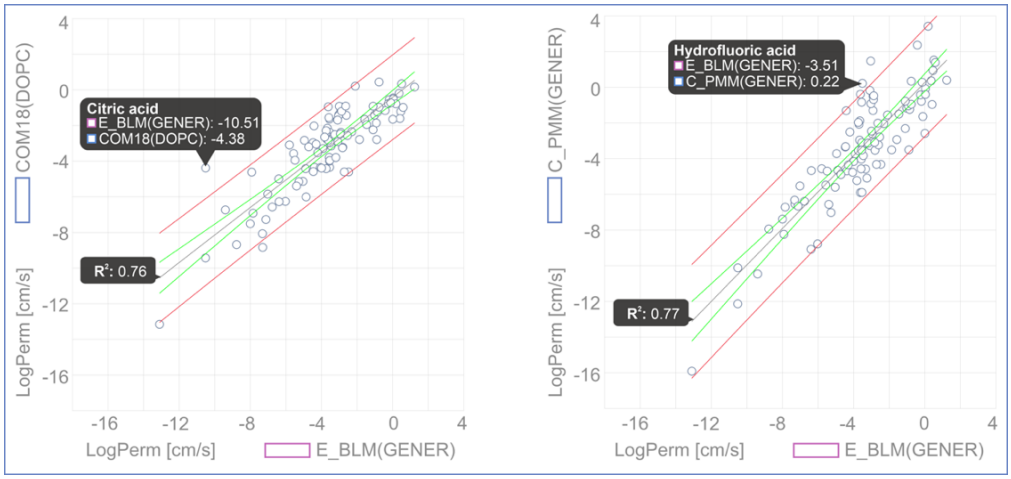

Figure 16. Comparison of permeability coefficients obtained from theoretical PerMM model, COSMO-based calculations against experimental BLM setup. The coefficients of determination and for COM18/BLM (0.76) and PerMM/BLM (0.77) along with almost identical slope to experimental data showed good correlation of between individual techniques. Prediction interval shown in green and confidence interval set to 95% shown in red. Figure taken from reference[74].

6.2 Permeation of cyclosporin A through biomembranes

Many naturally occurring cyclopeptides have been promising alternatives to traditional small drug exceeding beyond the rule of five (bRo5) space. Exceptional biological activity and the possibility of engineering their chemical structure to alter specific target response made them highly anticipated candidates in novel drug research.[75] Contrary to traditional small molecules, peptides are biodegradable back to simple amino acid making them less toxic and fast removal upon proteolytic degradation restricts their accumulation in organs. On the other hand, the low oral bioavailability of cyclic peptides is limiting step in drug administration. One of the most prominent members of cyclopeptide family is cyclosporin A, widely used immunosuppressant, that possesses both membrane permeability and good oral bioavailability properties.

Cyclosporin A is an important immunosuppressant drug. In complex with cyclophilin A, CsA is bounds to calcineurin, calcium/calmodulin-dependent serine/threonine protein phosphatase responsible for dephosphorylation T-cells transcription factors. This ternary complex then specifically targets T-cells signaling pathways restricting the transcription and proliferation of T-lymphocytes (e.g. T-lymphocytes activation).[76]

From the structural point of view cyclosporin A is a homodetic cyclopeptide composed of 11 amino acids, where 7 nitrogen atoms are N-methylated (Figure 17). Cyclosporin A exhibits structural polymorphism, with two predominant conformations based on surrounding environments e.g. free form of CsA in non-polar solution and bound form in cyclophilin complex. In non-polar medium CsA adopts more “closed” conformation resulting four intramolecular hydrogen bonds and formation of antiparallel β-sheet.[77,78] In contrary to that, while bound in complex with cyclophilin A in water, polar moieties of CsA are more exposed to maximize possible hydrogen bonding to protein and polar environment.[79] This structural flexibility is crucial for membrane permeability of CsA.[80]

After oral administration up to the point of reaching side of action, CsA permeates through various biomembranes differing in lipid composition and phase state. Specific interactions of CsA with individual inhomogeneous environment along with specific CsA physicochemical and structural properties (high hydrophobicity, low aqueous solubility, or N-methylated peptide backbone) underline the nature of distinct permeation process. Due to the hydrophobic character and limited water solubility suggested CsA is located primary in aliphatic membrane interior.[81] In fully saturated phospholipids (namely DPPC) the presence of CsA affects the ordering of acyl chains according to phase state e.g. increase in ordering above phase temperature and decrease of lipid ordering bellow transition temperature as well as decreases the enthalpy of transition from gel to

liquid crystalline phase.[81,82] The partitioning of between both gell and liquid crystalline phase is governed by the amount of CsA present in mixture.[82] Furthermore, the topology of membrane is changed by CsA partitioning into regions separating gel and liquid phases in cholesterol enriched membrane mixtures.[83]

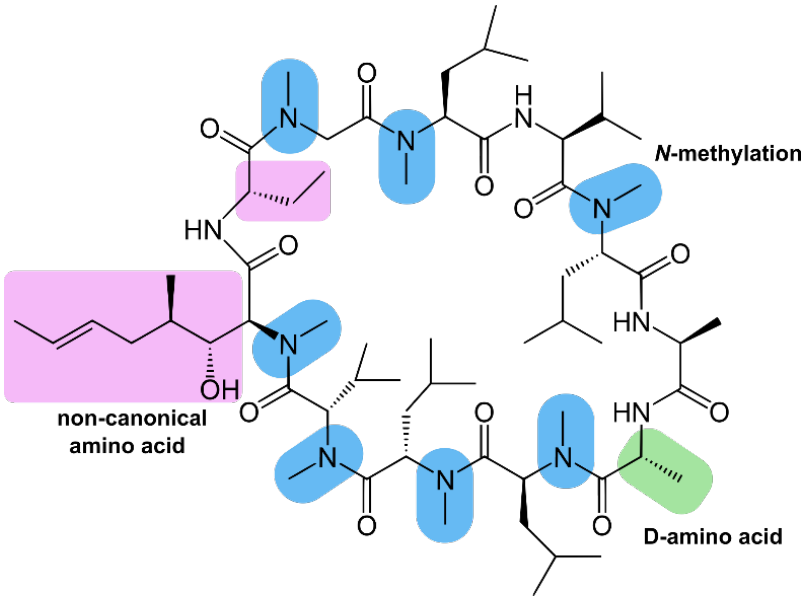

Figure 17. Structure of cyclosporin A. *N*-methylation sides highlighted in blue, two non-proteigeneric amino acids highlighted in pink, D-alanine highlighted in green. Adopted from reference.[84]

In present study, we describe the effect of different membrane composition of CsA permeation. We used enhanced umbrella sampling technique to investigate energetical profiles of CsA passage along membrane normal. In order to investigate the structural behaviour of CsA, we first carried out simulations in water and hexane.

In simulations of CsA in water and hexane the drug adopts two different conformational states as structural response to different environments. Measured "hydrophobic distances" – distances between COM of hydrophobic side chain residues and COM of whole CsA - (Figure 18. left) showed tighter packing of hydrophobic residues of CsA in hexane. In contrast to that, while CsA was in water, the hydrophobic moieties had greater conformation freedom, maximizing the interactions with surrounding water molecules. Furthermore, the native contacts between hydrophobic side chain residues and the rest of the molecule were measured (Figure 18. middle). The total amount of contacts was greater in simulation of hexane suggesting the effort to maximize the intramolecular contacts within CsA. This led to structural changes in CsA and exposing the more polar backbone of peptide while shielding the hydrophobic moieties within. Moreover, solvent accessible surface area (SASA) showed smaller area occupied by CsA in

presence of hexane (Figure 18. right) as solvent also suggesting tighter packing in CsA molecule structure.

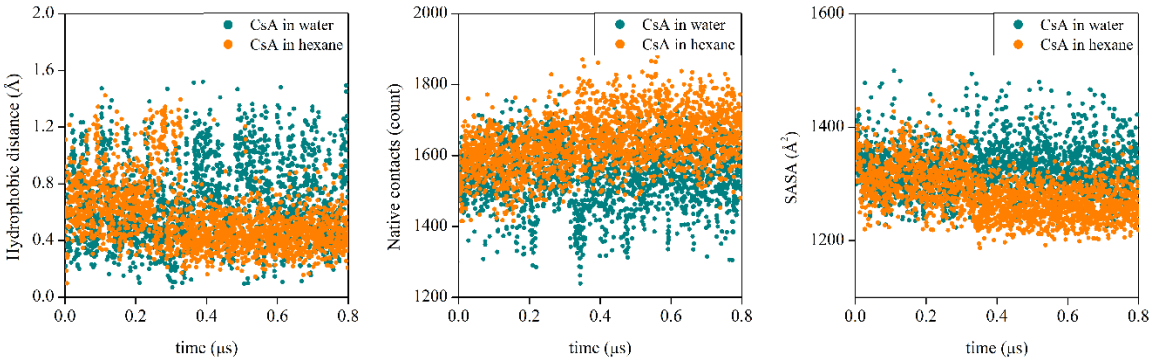

Figure 18. Different behavior of CsA in simple conditions e.g., in water and in hexane. In hexane CsA exhibited "closed" conformation while maximizing the intramolecular interactions. In contrary to that, the overall molecular surface was greater for CsA placed in water suggesting preferential interaction with water environment upon adopting "open" conformation.

Table 2. Energetical properties of cyclosporin A permeation in various membrane models

Membrane composition	**z_{min} [Å]**	**ΔG_{WAT} [kcal/mol]**	**ΔG_{PEN} [kcal/mol]**
DOPC	12.55	-8.15	4.00
DPPC	0	-30.44	0
DMPC	6.45	-10.00	3.05
POPE	9.55	-6.42	3.80
POPC	9.35	-11.75	4.14
POPC:CHOL (1:1)	3.25	-16.37	0.40
POPC:CHOL (4:1)	10.35	-8.06	5.20
POPC:POPE (1:1)	6.75	-9.36	3.62
POPC:POPE:CHOL (2:1:1)	11.05	-7.51	4.14

As the strongly hydrophobic character and limited water solubility suggested CsA is located primary in aliphatic membrane interior.

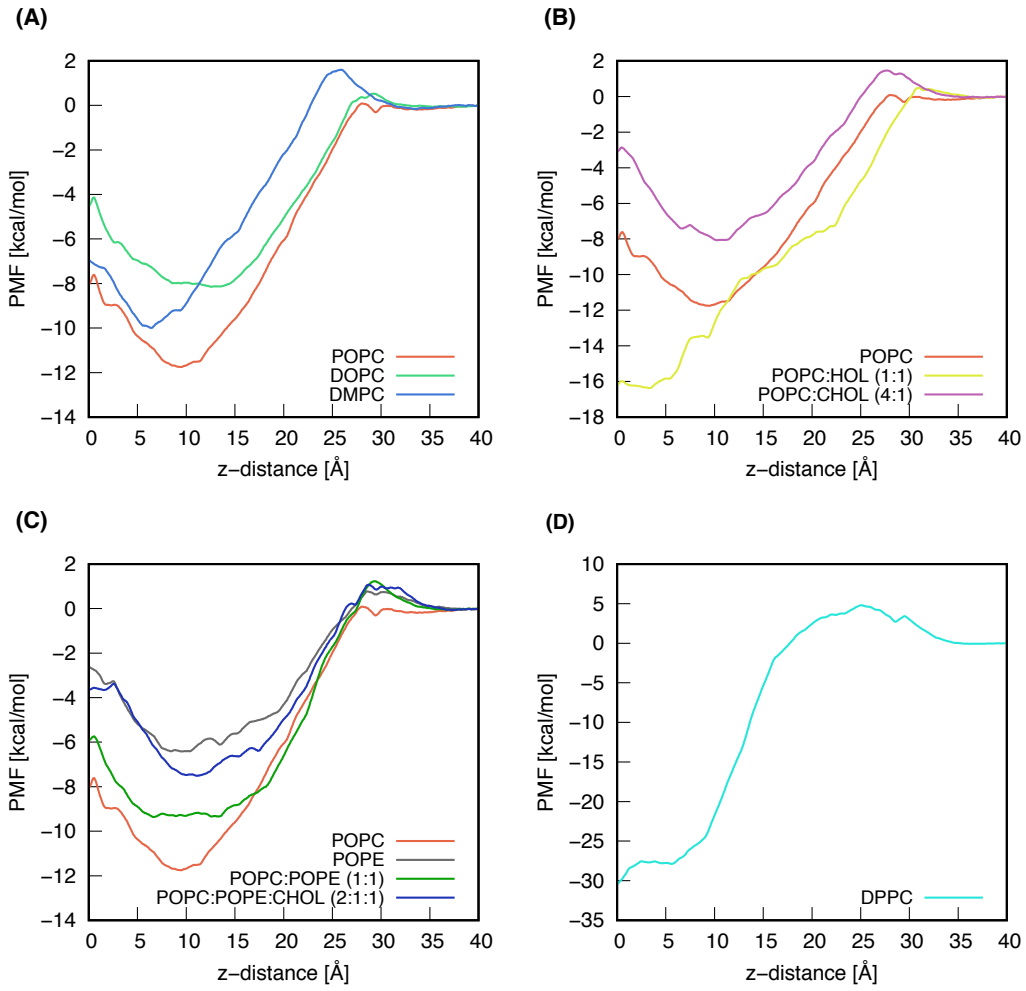

Figure 19. Calculated free energy profiles of CsA membrane permeation divided into four groups based on membrane composition. CsA passing through membrane starting at bilayer center (z=0) to water (z=40). **(A)** PMF profiles of CsA permeation through pure phosphatidylcholines membranes. **(B)** PMF profiles of pure POPC and analogues with different cholesterol amount. **(C)** PMF profiles of pure POPC, POPE membranes and its cholesterol enriched content. **(D)** PMF profile of CsA passing through DPPC bilayer found in gel ordered phase.

6.2.1 Cyclosporin A behavior on membrane models

Phosphatidylcholines (PC) are one of the most abundant phospholipids in mammalian cell membranes most likely to be involved in passage of small molecules. Three prominent member of PC lipids were selected (POPC, DOPC and DMPC) differing in length and saturation of acyl chains. In case of POPC and DOPC, where the only differentiating factor is saturation in Δ9-cis bond, the PMF profiles show different position of energetical minima slightly shifted towards region of double bonds in case of DOPC (12.55 Å). The energy minima decreased by ~3.5 kcal/mol in case of POPC. Nevertheless, the energy required for CsA to cross those membranes (ΔG_{WAT}) was almost the same. In case of DMPC the position of minima and the initial barrier for entering the membrane was shifted towards core due to the shorter length of acyl chains (Figure 19 A).

Second group considers case of pure POPC and its analogues with increasing amount of cholesterol content (POPC:CHOL (4:1; 1:1)). In case of pure POPC bilayer and system with lower saturation of cholesterol the energetical minima reside within same the position (~10 Å) from membrane center. In equimolar amount of POPC and cholesterol higher membrane ordering resulted into displacement of bilayer leaflets and shift of CsA energetical minima directly to the center of membrane which is the only disordered region. Once in the middle of membrane it is unlikely for CsA to overcome barrier of 16.37 kcal/mol (Figure 19 B).

In the third group the effect of changes in the polar headgroups was studied in prototypical types of lipids e.g. POPC, POPE. The most apparent difference of CsA permeation was the deepening of energetical minima by ~5.33 kcal/mol while changing from PE to PC headgroup (ΔG_{WAT} -6.42 and -11.75 for POPE and POPC respectively) while the position of energetical minima was almost the same. Subsequently, while in equimolar composition of POPC and POPE lipids the energetical barrier of crossing showed average between POPC and POPE (ΔG_{WAT} -9.36) the PMF profile showed significant bordering of energetical minima oscillating from 6 to 14 Å. As showed in previous case, additional increase of cholesterol content affected negatively the partitioning of CsA into membrane (Figure 19 C).

Extreme case of CsA crossing DPPC membrane found in gel ordered phase. In contrary to other systems PMF profile shows significant barrier for entering membrane from water environment ~5 kcal/mol. Once penetration beyond headgroup region CsA finds its minima in the center of the membrane with ΔG_{WAT} of -30.44 kcal/mol where it will reside (Figure 19 D).

6.2.2 Conclusions on cyclosporin A

In simplified phosphatidylcholine membrane models, the energetical profiles for CsA passage were relatively similar. However, the presence of cholesterol induced changes in the membrane's ordering, leading to a shift of the energetical minima directly towards the center of the lipid bilayer when equimolar concentrations of cholesterol and phosphatidylcholine were present. The borderline case of DPPC also revealed that CsA was unable to permeate through membranes in the gel-ordered phase. In all cases, the strongly hydrophobic nature of CsA and its limited water solubility indicated that CsA primarily resides within the aliphatic interior of the membrane. These findings shed light on the importance of membrane composition in influencing the permeation behavior of CsA and highlight the preferential localization of CsA within the lipid bilayer.

6.2.3 Methodology

MD setup

All simulations were carried out using Amber16 software packages. Lipid14 was used for all lipid parameters. Parameters for CsA were derived from AMBER ff14SB. Bonds involving hydrogens were restrained with SHAKE algorithm allowing 2 fs time step. Temperature was kept constant at 310 K with Langevin dynamics with collision frequency of γ = 1 ps. Pressure of 1 atm was maintained using Berendsen barostat at semiisotropic conditions with pressure relaxation time of 1 ps. Real space electrostatic and van der Waals interactions were calculated within distance of 10 Å. Long range interactions were treated with PME algorithm. Periodic boundary conditions were applied at all directions.

US simulations

To generate starting structures of CsA in distinct positions in lipid bilayers pulling procedure was performed. CsA was slowly pulled from membrane interior (z=0 Å) to water environment (z = 40 Å) with frequency of 1 Å/ns and force constant of 1.1 kcal/mol for 40 ns. Then, series of 40 structures with equidistant CsA distances of 1 Å in membrane z-axis were generated to serve as starting coordinates for umbrella sampling windows. Each window was then subjected to 100 ns production run restraining drug at given position with harmonic potential with force constant of 5 kcal/mol. Final potential of the mean force (PMF) profiles of CsA-membranes crossing were established using weight histogram analysis (WHAM[85]) with 1 x 10^{-8} tolerance.

Permeability calculation

Inhomogeneous solubility diffusion model (ISDM) describing drug-membrane crossing through inhomogeneous-like medium was used in order to obtain key permeation properties such as permeation coefficients from PMF. Permeation coefficients are obtained as reciprocal value of integration of individual resistances R(z) at given position along z-normal from Equation 26.

6.3 *In silico* screening of drug candidates for temperature-responsive liposome formulation

Liposomes are spherical vesicles which comprises of aqueous core surrounded by a lipidic shell arranged in form of bilayer. The lipidic part of liposomes usually contains various of phospholipids and cholesterol. Upon initial encapsulation into internal cavity, liposomes as are used as carriers for large numerous active substances such active pharmaceutical ingredients (APIs), fluorescent dyes or genes. The properties of liposomal vehicles such as size, stability, and composition can be specifically altered for the purpose of desired delivery and release mechanism. The precise tailoring of the composition of lipid species may also affect the one of the key properties for successful payload release e. g. the permeability of encapsulated compounds. At lower temperatures lipid bilayers tend to reside in order phase which is non-permeable for trapped species and is desired for sufficient transport of encapsulated compounds towards their side of the action. On the other hand, when heated, the phase transition of lipid bilayers into disordered state must assure the controlled release of encapsulated species. The phase properties of lipid bilayers are to the greatest extent govern by the composition of lipidic part of the liposomes.

Up to this day, liposomal formulation and the encapsulation-release mechanism faces many drawbacks originating from the non-systematic ways of determining the correct formulation approaches or the appropriate identification pharmaceutical ingredients suitable for encapsulation. The goal of the present work was to develop and validate a systematic computational methodology for prediction of suitable encapsulation and thermally induced release of bio-active compounds. The proposed strategy combined classical molecular dynamics simulations and quantum chemistry-based calculations to determine selection criteria for identification of compounds capable of stable in encapsulation and temperature-induced release from liposomes on well-established membrane model (membrane composed of DPPC:DPPG:CHOL at molar ratio of 75:10:15). Those criteria were validated against series of experiments confirming the methodology precision using an identical set of fluorescent dyes. Furthermore, we screened the DrugBank database against those criteria and successfully identified potent drug – cycloserine – capable of liposomal loading ant thermal release.

6.3.1. MD simulation of bilayer phase transition

Molecular dynamics simulations of mixed membrane (DPPC:DPPG:CHOL at molar ration of 75:10:15) were carried out at scale of temperatures mimicking different stages of liposomal formation a subsequent cargo release – the liposome storage temperature (293 K), slightly elevated body temperature (313 K) and the temperature desired for the controlled release of trapped payload (323 K and 333 K). At the temperature corresponding to liposomal storage (293 K) and body temperature (313 K) the bilayers were found at highly ordered state. Sharp changes in bilayer structural features (A_L increase by approximately 1 nm^2 and lower order parameters marked the phase shift into disordered state between 323 K and 333 K. At the temperature of 333 K, required for the cargo release, lipid bilayer was found in completely disordered state. Structures from abovementioned MD simulations served as templates for following COSMOmic/COSMOperm calculations.

6.3.2. COSMO-based partitioning and permeability calculations fort fluorescent dyes

Set of five fluorescent dyes was used as starting set for derivation of encapsulation/release selection criteria – namely 5-carboxyflourescein (5-CF), 6-carboxyflourescein (6-CF), fluorescein (F), fluorescein-5-isothiocyanate (FITC) and calcein (Cal). For each fluorescent dye/bilayer system partitioning and permeability coefficients were calculated at given temperature range (Figure 20). The temperature dependent calculations showed no significant changes in partitioning of fluorescent dyes into mixed membrane (Figure 20 panel A). Only at elevated temperature (333 K) slight inclination to increase of partitioning was manifested. From the partitioning coefficients the lipophilicity of individual compounds could be assessed as follows Cal < 6-CF < 5-CF < F < FITC. On the contrary, the permeabilities of studied dyes increased almost linearly with increasing temperature (Figure 20 panel B). Those differences varied widely also between individual compounds. The further analysis of partitioning and permeability coefficient at limited temperatures (293 K and 333 K) suggested the 5-carboxyflourescein and 6-carboxyflourescein as the best candidates for thermoresponsive release as they would prefer aqueous cavity ($logK_{lip/wat}^{293K} = 0.72 \pm 0.43$ and 0.35 ± 0.36 for 5-CF and 6-CF, respectively) and would not escape from the liposome core rapidly ($logP_{erm}^{293K} = -5.64 \pm 0.06$ and -5.78 ± 0.06 for 5-CF and 6-CF, respectively) In contrary to that, higher permeability coefficients for fluorescein ($logP_{erm}^{293K}$ = -2.59 ± 0.09) and fluorescein-5-isothiocyanate ($logP_{erm}^{293K}$ = -2.26 ± 0.52) would suggest higher than optimal permeability even at lower temperatures. Moreover, the lowest permeability even at higher temperatures for calcein ($logP_{erm}^{333K}$ = -9.05) denotes its inability to escape from aqueous core of liposome.

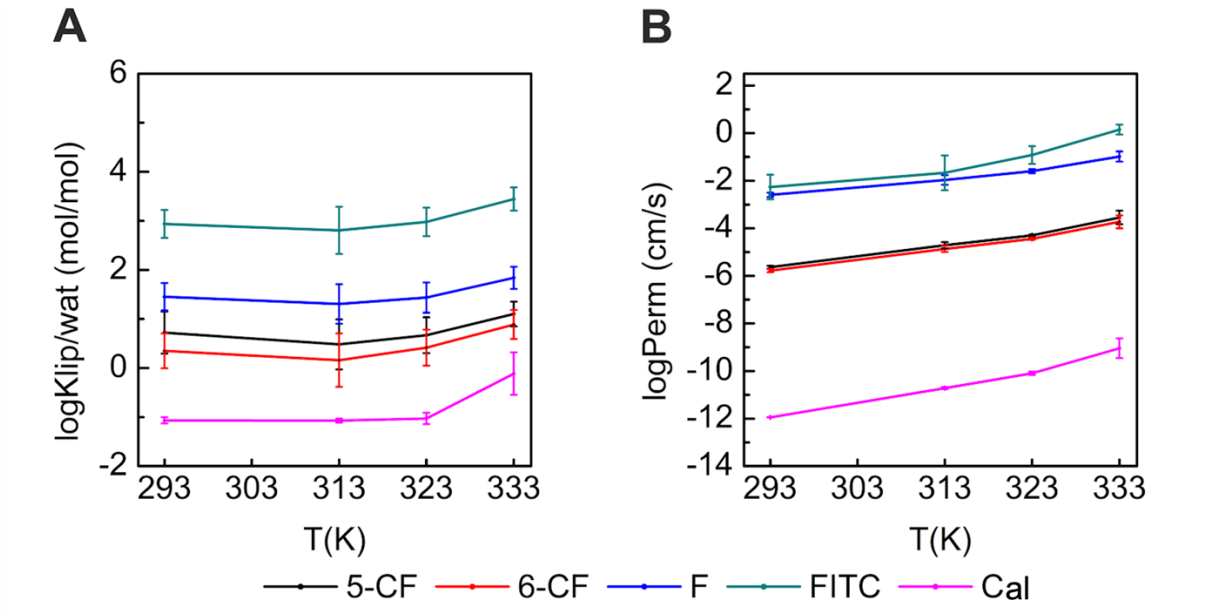

Figure 20. Calculated partitioning (**A**) and permeability (**B**) coefficients for the set of fluorescent dyes through mixed membrane (DPPC:DPPG:CHOL at molar ratio of 75:10:15).

6.3.3. Selection criteria encapsulation/thermoresponsive release and DrugBank screening

Based on theoretically calculated partitioning and permeability coefficient and encapsulation and released experiments with fluorescent dyes we derived set of ground criteria for prediction of successful liposomal encapsulation/thermoresponsive release (Figure 21) for DPPC:DPPG:CHOL (75:10:15) membrane mixture. From the experimental point of view, adjustments were made to reflect real experimental conditions. For example, the boundary of partitioning coefficients was shifted to reflect the equal contribution of volumes of lipidic part/aqueous phase of liposomes (lipids tend to occupy 100 – 10,000x less volume compared to aqueous core) which resulted at the rule $\log K_{lip/wat} < 2$ (rather than 0) for optimal encapsulation into aqueous cavity. The border values for permeability coefficients were recalculated into apparent permeabilities to reflect the fraction of unionized species and correction to unstirred water layer. The apparent permeabilities at given temperatures of 293 K and 333 K ($\log P_{app}^{293K}$) outlined boundaries for optimal temperature controlled released as $\log P_{erm} < -9.1$ at lower temperatures (273 K) and $\log P_{erm} > -8.1$ at release trigger temperature (333 K). Based on these rules (Figure 21), neutral molecules can be sorted into following categories:

i/ compound are not suitable for liposomal encapsulation

ii/ compound are suitable for liposomal encapsulation but are not suitable for the thermally controlled release

iii/ compound are suitable for liposomal encapsulation and for the thermally controlled release.

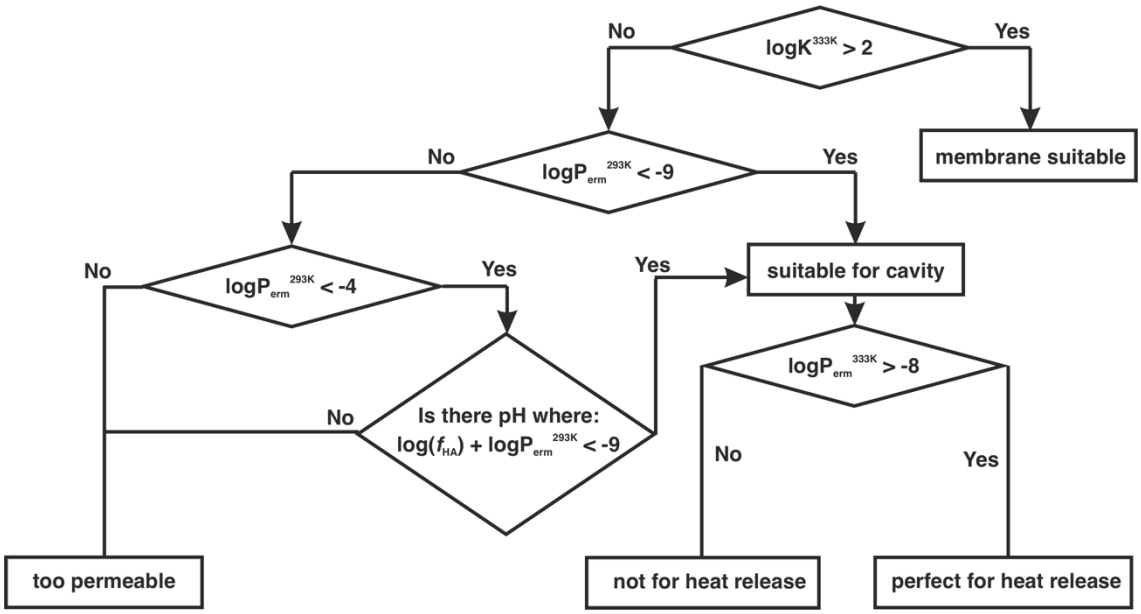

Figure 21. Selection criteria defining the optimal molecule candidates for successful liposomal encapsulation and subsequent release at trigger temperature.

To further validate those selection criteria, we performed rapid *in silico* screening of compounds found in DrugBank database. In total of 56 bioactive (mostly toxic) compounds were selected for which their $\log K_{lip/wat}$ and $\log P_{erm}$ values were calculated. From abovementioned selection criteria those 56 compounds were high divided into three categories:

i/ 27 compounds would encapsulate rapidly into membrane phase of the liposomes due to their high partitioning coefficients (Figure 22. yellow dots) and 4 compounds were not acceptable for liposomal formulation using the Bangham approach (low permeability even at higher temperature of 333 K; Figure 22. red dots)

ii/ 16 compounds were not acceptable for liposomal formulation as they were classified as too permeable (Figure 22. black dots).

iii/ 9 compounds were classified as potential candidates for both suitable liposomal encapsulation and thermally controlled release (Figure 22. blue dots).

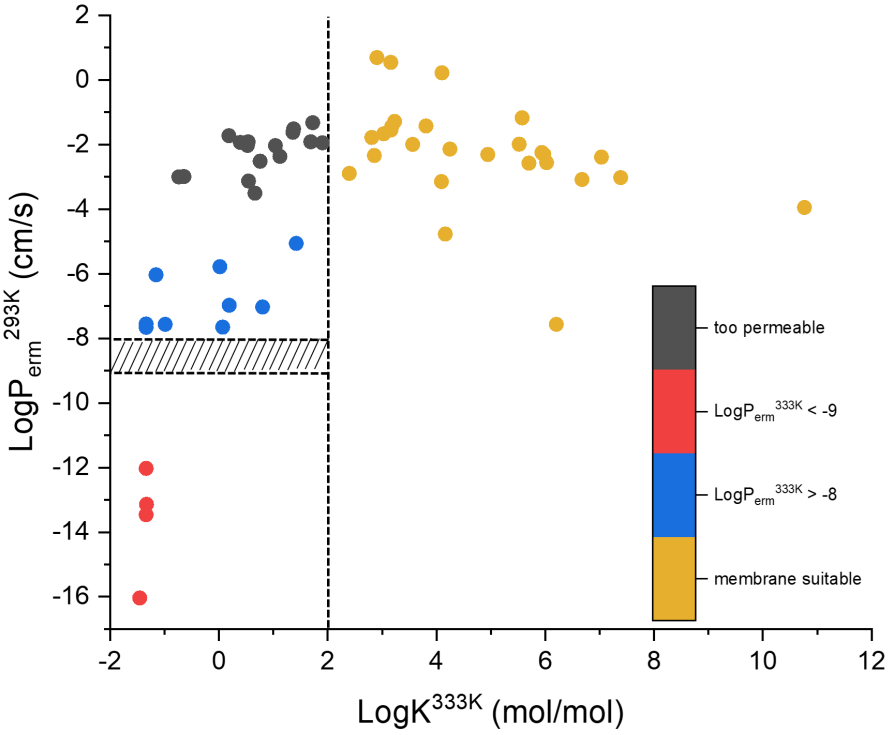

Figure 22. Classification of 56 toxic compounds into categories database based on selection criteria. Almost half of selected drugs would reside predominantly in the membrane phase rather than in the aqueous environment (yellow dots). Another 20 compounds were classified as either too permeable (black dots) or as almost not permeable even at higher temperatures (red dots) and therefore not suitable for controlled release. The remaining 9 compound met both selection criteria for feasible entrapment into aqueous phase and consequent release at desired temperature (blue dots).

Furthermore, out of those 9 possible candidates cycloserine (bioactive compound with antibacterial properties) was chosen for liposomal formulation experiment. After liposomal encapsulation the stability of originated liposomes at both storage and release temperatures was tested on measuring the proliferation of *E.coli* bacteria on the resazurin assay. Estimated apparent permeabilities confirmed the ability of cycloserine to permeate at elevated temperatures ($logP_{app}^{333K}$ = -8.66) while not being prematurely released from liposome at lower temperatures ($logP_{app}^{273K}$ = -10.1).

6.4 Behavior of Mitochondrial Cytochrome P450 11A1 on DOPC and Mitochondrial Membrane Models

The mitochondrial cytochrome P450s are enzymes involved in the biotransformation of many compounds predominantly secreted from the adrenals and gonads.[86] One of the most important processes mediated by mitochondrial CYPs is steroidogenesis that leads to the production of steroid hormones responsible for the regulation of metabolism, balance of energy or responses to stress.[87] The steroidogenesis in mitochondrion is mediated by cytochromes P450 from family 11 – CYP11A1, CY11B1 and CYP11B2 which all contain mitochondrial targeting sequence affecting their cellular specificity.[87] Cytochrome P450 11A1 (CYP11A1), also known as P450scc (side-chain cleavage enzyme), is located in the inner mitochondrial membrane of the adrenal cortex and the other steroidogenic tissues.[88] CYP11A1 converts cholesterol to pregnenolone, precursor for all steroid hormones, that represents the first and also rate-limiting step of the biosynthesis of steroid hormones.[89–91]

Even though CYP11A1 is membrane attached, it lacks the N-terminal transmembrane anchor as is typical for microsomal CYPs.[92] CYP11A1-membrane interaction is represented by membrane-faced amino acids on the distal side of the enzyme mainly by F/G loop.[93,94] This was also confirmed by cysteine side chain mutagenesis studies in combination with fluorescent labelling of mutated residues suggested association of F/G loop of 11A1 with phospholipid vesicles.[95] Replacements of N210S/V211M and L218R/F219Y in putative F/G loop of *E. Coli* CYP11A1 lead almost to 2-fold increase of the turnover i.e. increase of P450 presence in the cytosol after protein expression.[94] A' helix and F/G loop were also identified as a membrane contact region deduced from hydrophobicity profiles of CYP11A1. Moreover, deletion within putative A helix caused protein expression instabilities indicating importance of this region on membrane binding.[95] Although the absence of the transmembrane anchor is the main distinguishing feature between microsomal and mitochondrial CYPs, the character of the interaction with membrane lipids thus remains similar.

The composition of lipid bilayers significantly affects the behavior of membrane attached CYPs, as well as their catalytic activities. It has been shown that the presence of overall neutral phosphatidylcholine and phosphatidylethanolamine lipids increased the catalytic activity of CYP2B4.[96] In addition, the presence of negatively charged phosphatidic acid (PA) and phosphatidylserine increased catalytic activity by 2-3-fold and 6-fold for CYP1A2 and CYP3A4 respectively.[97,98] The mitochondrial membranes are heterogeneous systems composed of both neutral and anionic lipids components roughly in ratio PC:PE:cardiolipin 2:2:1.[99]

The presence of cardiolipin in mitochondrial membranes significantly alters CYP11A1 behavior. According to the rotational diffusion experiments mobility of the protein depends on the cardiolipin concentration.[100] Cardiolipin has significant effect to the anchoring and embedding of CYP11A1 to the membrane bilayer caused probably by specific interaction with the negatively charged cardiolipin headgroups.[100] Moreover, the presence of phosphatidylcholines with branched fatty acyl chains elevates the activity of CYP11A1 and enhances the cholesterol binding.[101]

In this work, we studied the behavior of mitochondrial CYP11A1 on mitochondrial membrane model (POPC:POPE:cardiolipin in 2:2:1 molar ratio) in comparison to simple pure DOPC bilayer that was previously used as simplified membrane model for microsomal membranes.[53,92] We focused on the atomistic description of interactions of protein with individual lipids as well as on protein immersion, mutual membrane-protein orientation and their contact regions. We observed significant differences in terms of immersion and orientation of CYP11A1 in comparison to microsomal CYPs that is also reflected by the selection of the redox partners.

6.4.1 Behavior of CYP11A1 on DOPC

Up to this date both experimental and theoretical studies rationalized the role of lipid bilayer on mutual CYPs-membrane interaction, orientation, and the ability of CYPs to uptake drugs and release of its metabolites via the network of access and egress channels mainly on simple membrane models such as single component liquid disordered DOPC lipid bilayer as a baseline for membrane-protein interactions. As was shown previously for example in our studies of CYP3A4 on the membrane with various ratios of cholesterol[102] or on membranes containing lipids with different head groups[103], the membrane composition is, however, important for overall behavior of membrane-attached CYP proteins.

To investigate the behavior of CYP11A1 on DOPC membrane, three separate MD simulations of 500 ns each were carried out. The structural fold of CYP11A1 was preserved with the root mean square deviation (RMSD) not exceeding 0.4 nm with respect to original crystal structure. Despite the conservation of protein secondary structure, the CYP11A1-DOPC membrane interaction changed significantly over time. The number of hydrogen bonds between protein and DOPC membrane decreased to the half from original pose from 34 counts to an average of ~16 hydrogen bonds depicting a weak interaction with protein surface (Figure 23 panel A). Moreover, the HTA showed significant differences between individual 500-ns long replica MD simulations (Figure 23 panel B). The individual three replicas with averaged HTA at 76.0 ± 8.7 deg, 57.0 ± 8.8 deg and 62.2 ± 7.7 deg.

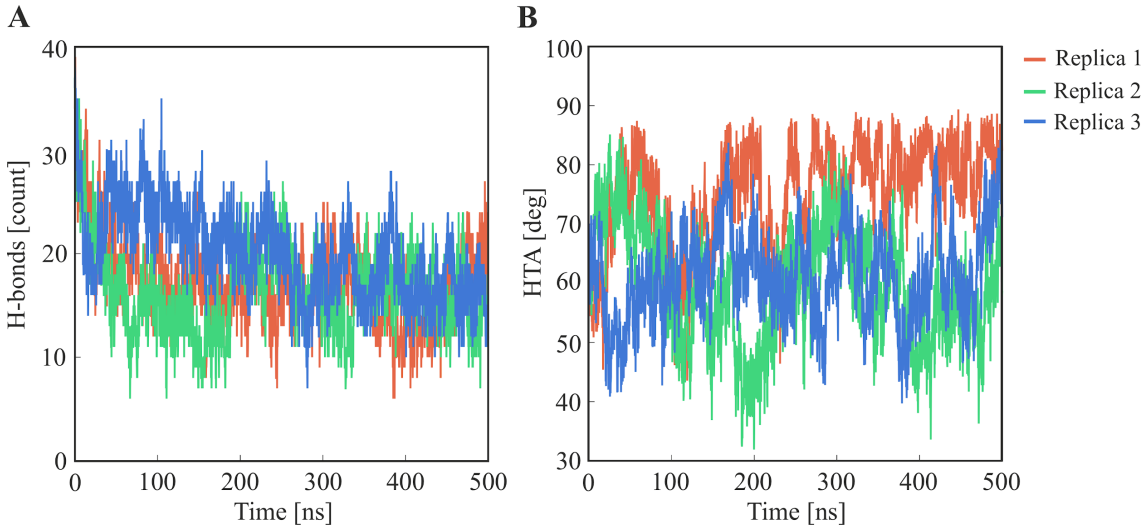

Figure 23. The number of calculated hydrogen bonds (panel A) and heme tilt angle (panel B) over the course of 500 ns simulation for three separate replicas. The diminishing of CYP11A1-DOPC membrane interactions is portrayed by the decrease of calculated hydrogen bonds between CYP11A1 and DOPC membrane and changes of HTAs.

Weak mutual CYP11A1 DOPC membrane interactions resulted in completely dissimilar final structures and different interactional patterns between individual replicas (Figure 24). Such behavior is quite dissimilar to the common structure of CYP3A4 or other microsomal CYPs which show strong and experimentally measurable unique HTA.[53,104]

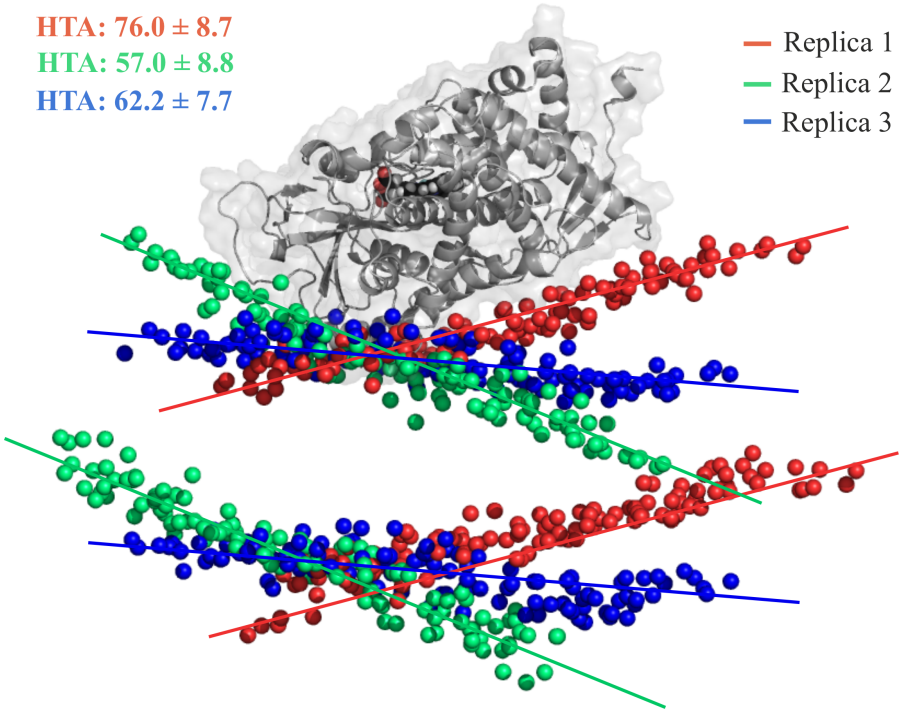

Figure 24. Snapshots of final structures from three separate replicas aligned by the catalytic sites of CYP11A1. Each replica shows significant changes in calculated HTAs. The loss of most CYP11A1-membrane interactions leads to completely different orientations of protein on DOPC membrane surface. CYP11A1 represented as cartoon with transparent surface. Phosphate atoms of DOPC headgroups depicting membrane surface showed as spheres.

6.4.2. Interaction of CYP11A1 with mitochondrial membrane

The composition of lipid bilayers significantly affects the behavior and stability of membrane-integrated proteins. The simple DOPC lipid though widely acknowledged and used in as membrane model, showed great instability in case of CY11A1 simulations. Those discrepancies manifested in unstable CYP11A1-DOPC interactions, orientation and tilt may be caused by the lack of electrostatic interactions governing the process of protein-membrane binding. Following those findings, we employed simulation of CYP11A1 of membrane mimicking the composition of inner mitochondrial (MIT) membrane. Three replica of systems containing CYP11A1 embedded into mitochondrial mimicking memebrne (POPC:POPE:cardiolipin in 2:2:1 molar ratio) were simulated for total of 500 ns production run in order to investigate protein stability and protein-membrane interactions. CYP11A1 was stable during three 500 ns-long MD simulations with the RMSD not exceeding 0.4 nm (with respect to crystal structure) converging into the same CYP11A1-MIT orientations and tilt. Moreover, the CYP11A1-MIT interaction pattern corresponds closely to previously obtained results from both, theoretical models and experimental measurements.

The initial interaction of the CYPs with MIT membrane followed the general contact region localized on the distal side of the enzyme. During the first ~40 ns of 500 ns simulations the mutual protein-membrane orientation shifted leaving the distance of catalytic domain of CYP11A1 and MIT membrane at ~4.5 nm from original value of 3.9 nm. This led to omitting most interactions from its original pose and change of the tilt of the protein to (HTA of 22.11-26.43 deg with respect to individual replicas) on membrane surface adopting more vertical orientation of CYP11A1.

While the soluble protein did not keep its original immersion within the membrane core the interaction remained stable during the whole production run. The tight association is important for CYP11A1 uptake of water insoluble cholesterol molecules from hydrophobic membrane environment via the net of access channels. Analysis of minimal distances between CYP11A1 and MIT membrane showed interaction patterns on distal side of namely on A′ helix, F/G loop, and part of protein secondary structure motifs corresponding to G helix, B′helix, β1 sheet and β2 sheet (Figure 25). The tightest membrane association was observed for A′ helix and F/G loop. It was previously shown that deletion of A′ helix decreases the amount of expressed CYP11A1 protein association with bacterial *E. coli* membrane.[95,105] Our models revealed stable monotopic association of A′ helix with MIT membrane. Previous theoretical model also pointed out hydrophobic patches involving tryptophan residues in F/G loop region as potential membrane binding domain.[95] Moreover, the enhance of fluorescence signal for cysteine mutants in this region showed the association of F/G loop and most likely of C-terminal part of G helix with lipid

vesicles.[95] Side chain mutations of F/G loop also affects the subcellular distribution of enzyme associated with bacterial membrane.[94] The terminal part of G helix following the F/G loop segment was also in close contact with MIT membrane in our models (Figure 25).

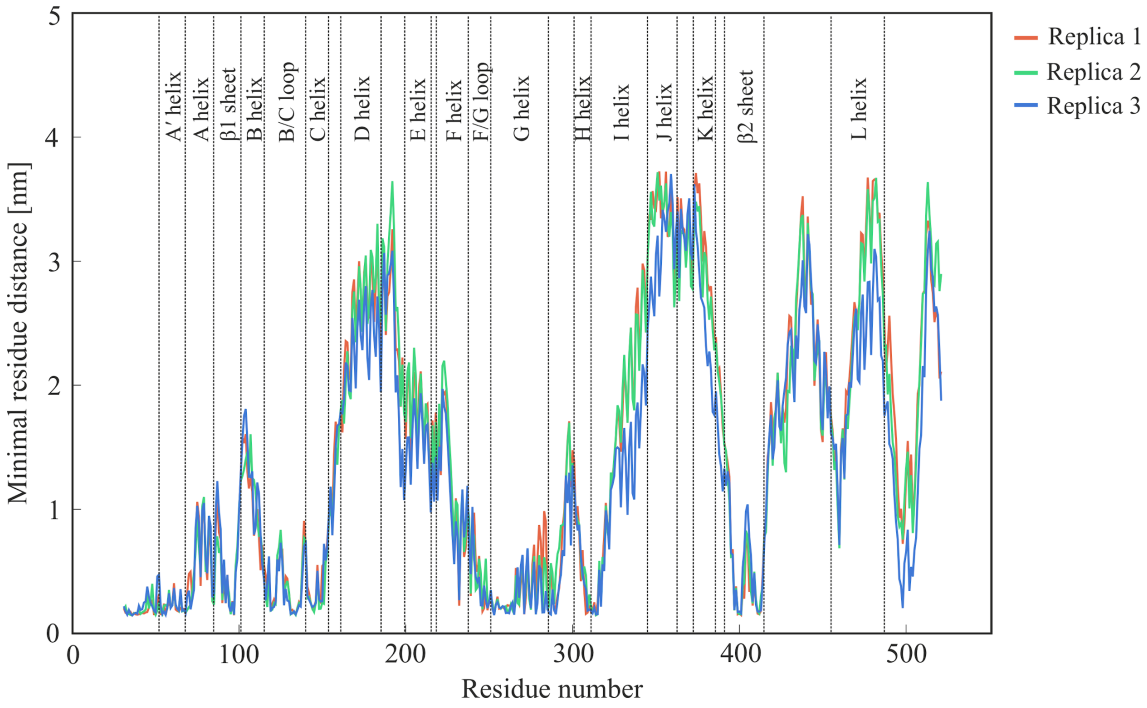

Figure 25. Minimal distances of individual amino acid CYP11A1 residues from MIT membrane. Secondary structure motifs of CYP11A1 depicted in the upper panel. Interaction with MIT membrane can be seen via A′ helix, B/C loop, C helix, F/G loop, G helix and β2 sheet.

Table 3. Measured averages and standard deviations for CYP11A/MIT simulations in 3 replicas.

CYP11A10-MIT*	REP1	REP2	REP3
distance/height [nm]	4.50 ± 0.12	4.48 ± 0.13	4.51 ± 0.16
num. of H-bonds [count]	32.47 ± 4.47	31.43 ± 6.13	23.99 ± 4.22
HTA [deg]	22.11 ± 8.21	21.85 ± 6.43	26.43 ± 6.85
A′ helix [nm]	2.42 ± 0.20	2.33 ± 0.16	2.57 ± 0.19
F/G loop [nm]	2.31 ± 0.14	2.40 ± 0.14	2.43 ± 0.12
R90-Y100 (β1 sheet) [nm]	2.71 ± 0.14	2.46 ± 0.12	2.81 ± 0.14
H130-G138 (B′helix) [nm]	2.61 ± 0.19	2.76 ± 0.24	2.61 ± 0.27
T260-W270 (G helix) [nm]	2.67 ± 0.21	2.88 ± 0.18	2.48 ± 0.16
L398-L402 (β2 sheet) [nm]	2.75 ± 0.19	2.70 ± 0.19	3.00 ± 0.17
P410-V415 (β2 sheet) [nm]	2.70 ± 0.14	2.54 ± 0.15	2.83 ± 0.14

* distances measured as the COMs between CYP11A1 or individual protein segments and MIT membrane in z-axis

The composition of mixed lipid bilayer mimicking the inner mitochondrial membrane played crucial role on overall CYP11A1-membrane interaction pattern. Even though, the interaction of CYP11A1 and MIT membrane was omitted to the fraction of interactions from the initial immersed model (initial structure) their pattern was stable across all replicas (see above). The radial distribution function (Figure 26) of CYP11A1 surface with the center of masses of closest lipid headgroup atoms showed that all lipid components interact at approximately same distance with sharp overlapping peaks of distribution distances at ~0.4 nm. The predominant interaction was observed in case of zwitterionic POPE lipid. For POPC lipid the interaction was reduced to almost half of POPE interactions with the same amount of lipid molecules taking into calculation. The least significant interaction pattern was observed in case of cardiolipin with negligible peak at closest distribution distances.

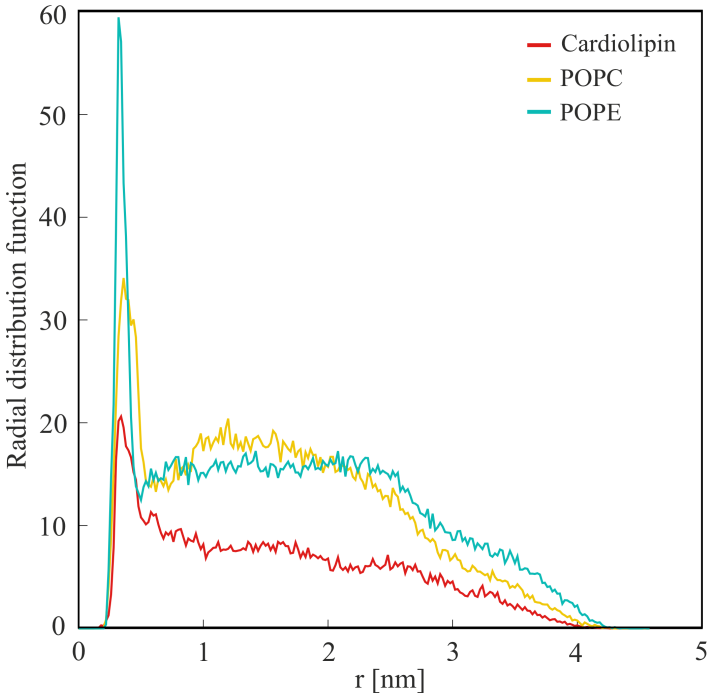

Figure 26. The radial distribution function measured between the surface of CYP11A1 and the center of masses of closest atoms in lipid headgroup in upper headgroup leaflet.

Even though the RDF showed less favorable interaction pattern for cardiolipin the presence of this highly negatively charged molecule was previously found crucial for mitochondrial CYP-membrane interaction. More detail analysis of CYP11A1-cardiolipin interaction revealed significant amount positively charged amino acids on CYP1A1 surface to be directly interacting or in close contact with anionic cardiolipin molecules. In total, 13 positively charged amino acids (8 arginines - R31, R43, R46, R67, R90, R135, R256 and R259; 5 lysines - K92, K143, K261, K264 and K412) located at proximity to cardiolipin headgroup surface (Figure 27). From those amino acids, arginines - R67 is locate in A′ helix, R256 and R259 in F/G loop; lysines K261 and

K264 in G helix matching segments of CYP11A1 previously reported to interact with membrane. This may conclude, that even though the overall anchorless CYP11A1-MIT membrane interactions are looser in comparison to membrane-anchored CYPs, those electrostatically driven interaction may contribute to overall stability and preferable orientation of CYP11A1 on inner mitochondrial membrane.

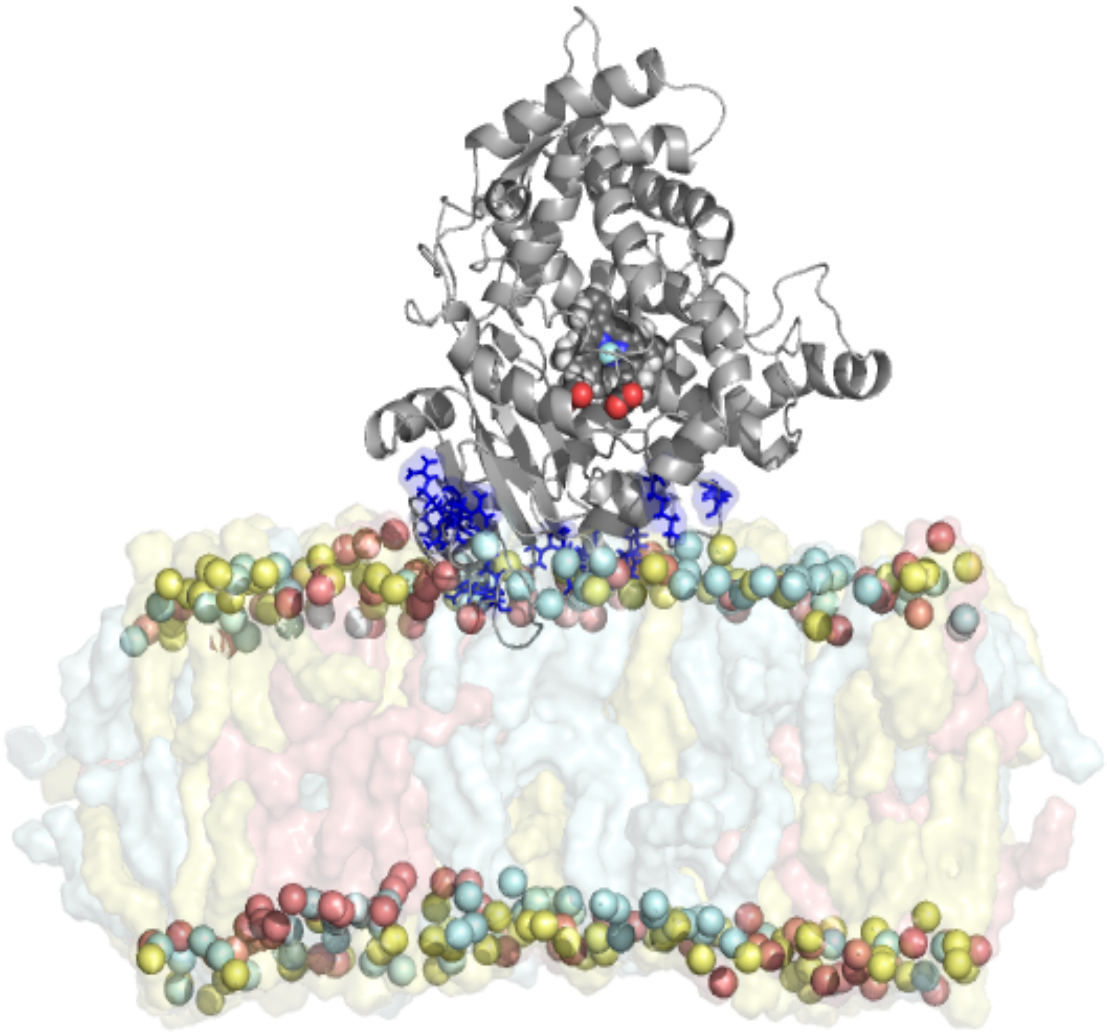

Figure 27. Final snapshot (500 ns) of CYP11A1 on mitochondrial membrane. Positively charged amino acids (presented as blue sticks) in close contact with cardiolipin headgroups showed as sticks. Phosphate atoms shown as spheres with rest of membrane in transparent representation (POPE in cyan, POPC in yellow, cardiolipin in pale red).

6.4.3. CYP11A1 channels dynamics

The active pocket of CYP11A1 is buried within the enzyme structure in the close proximity to the heme-binding region where the substrate - cholesterol - is metabolized. The CYP11A1 uptake of water-insoluble molecules (such as cholesterol) from the hydrophobic membrane environment is mediated via the net of access channels. Here, we characterized potential channels and their position and opening/closing during a 500-ns long simulation.

During the 500-ns long simulation, 5 main channels – S, 2e, 2a/x, 2e, 3 – were detected connecting the heme-binding cavity with the protein surface allowing the substrate/metabolite entrance/excess (Figure 28). Those channels are located on distal side of CYP11A1. One channel was recognized as channel solvent channel (S) egress from the heme-binding region and passes between E, F and I helices and β3-4 sheets. Moreover, two channels from channels 2 subclass characterized as 2e passing through B/C loop and channel 2b egressing between B and B′ helices and β1 sheet. One additional channel, here denoted as channel 2ax, that was not described before and bears the most similarities to 2a channel. Channels 2b and 2e end within the membrane while the channels 2, 3, S or 2ax end above the membrane. Given that the CYP11A1 transforms cholesterol to slightly more polar pregnenolone, it can be hypothesized that cholesterol enters the CYP11A1 via channel 2e or 2b, while pregnenolone egress through channel S, 3 or channel 2ax.

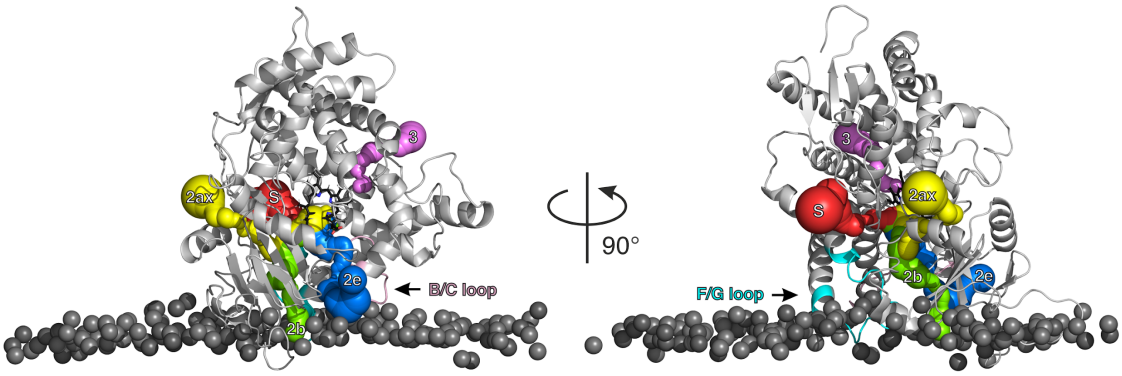

Figure 28. Characterization of access/egress channels of CYP11A1 on mitochondrial membrane. Left panel show final snapshot of CYP11A1 structure from proximal side of heme while the later one shows the side view rotated by 90° of the same structure. The phosphate atoms of lipid headgroups of upper lipid bilayer are shown as grey spheres. The access/egress channels radius is visualized by their radius. The channels here are characterized by standard nomenclature by Cojocaru et al.[106] and show as channel S (red), channel 2b (green), channel 2e (blue), channel 2ax (yellow) and channel 3 (violet).

6.4.4. Interaction of CYP11A1 with Adrenodoxin

CYP11A1 is essential for synthesis of various steroid hormones such as cholesterol, where it catalyzes the cholesterol side-chain cleavage to pregnenolone. Prior to the biotransformation reactions the supply of electrons from its redox partner is needed. The primary electron carrier for mitochondrial CYP11A1 is adrenodoxin (Adx), which mediates electron transfer between adrenodoxin reductase (AdR) and CYP11A1 itself. In order to successfully mediate the electrons, the direct contact between Adx and CYP11A1 needs to occur resulting in stable Adx-CYP11A1 complex. Therefore, the appropriate mutual orientation of both redox partner is crucial. Here we rationalize the possible intra-protein interaction scenario based on our simulation of CYP11A1 on lipid bilayer mimicking the inner mitochondrial membrane where the second part of electron transfer chain takes place.

As shown above, the loose yet preserved interaction of CYP11A1-MIT membrane with monotopic orientation above membrane surface resulted in more vertical orientation of CYP11A1. This orientation exposes to water the proximal side of CYP11A1 where the binding of redox partner occurs. As reported previously, the interaction is driven by strong electrostatic attraction between negatively charged amino acid residues of Adx and positively charged CYP11A1 surface near heme containing region. Those basic residues located of protein surface are conserved among all mitochondrial CYP family. Since Adx is cleaved from terminal part of transit peptide it might approach its redox partner directly from mitochondrial matrix or from site of inner mitochondrial membrane to which it is loosely bound. Our model shows that either of those is scenarios is possible since the loose membrane association allows the CYP11A1 to orient its proximal face to approaching partner. Moreover, the K helix with conserved positive amino acid residues (K378, K382 and R386) facing the space above MIT membrane allows approach of Adx. Furthermore, C- and L- helices as well as the heme binding loop, previously reported as potential interaction regions, are also sterically oriented for potential intra-protein binding.

6.4.5 Methodology

Full-length structure of CYP11A1 without transmembrane anchor was provided by following homology modelling procedure. The template structure of CYP11A1 was taken from the Protein Data Bank (PDB ID: 3N9Y; R = 2.1 Å)[107]. Missing parts were remodelled based on the known amino acid sequence of human CYP11A1 from UNIPROT (UniProt ID: P05108) using Modeller 9.13[108] within Chimera visualization software. Final model was then embedded into preequilibrated pure DOPC and POPC:POPE:cardiolipin (further as MIT membrane, molar ratio 2:2:1) membrane mixture mimicking inner mitochondrial membrane using g_membed tool.[109] All systems were solvated with TIP3P water model[110] in 0.15 mol/L physiological concentration of Na^+ and Cl^- ions.

All MD simulations were performed via GROMACS 4.5.4.[111] simulation package using single precision. AMBER ff99SB force field[112] was used for CYP11A1 along with Cheatham parameters for heme cofactor.[113] Slipids force field[114] was used for description of lipids. Lipid parameters were obtained from CHARMM-GUI Membrane builder repository.[115] Three separate replicas of CYP11A1 in pure DOPC membrane and in MIT membrane mixture were subjected to 500 ns simulation. All bonds were constrained with LINCS algorithm with time steps of 2 fs. Electrostatic interactions were treated by Particle Mesh Ewald[116] method with 1.0 nm cutoff. Van der Waals interactions were calculated at cutoff of 1.0 nm with function decreasing to zero at 0.9 nm. Temperature was kept at constant 310 K using Nose-Hoover thermostat[117] with coupling constant of 0.5 ps and pressure was set to 1.013 bar with Parrinello-Rahman barostat[118] with semi-isotropic conditions and same coupling constant. Periodic boundary conditions were used in all directions.

6.5 Membrane-attached Model of Cytochrome P450 Reductase: Simulations of naturally occurring states and of the complex by cytochrome P450 3A4

The biotransformation processes catalyzed by all mammalian CYPs depends on a supply of electrons from various of redox partners. In the microsomal electron transfer cascade redox equivalents are provided by cytochrome P540 reductase (CPR) and cytochrome b_5. In microsomes, proteins involved in electron transport chain are membrane-attached proteins located on the cytosolic side of the endoplasmic reticulum.

This chapter summarizes a comprehensive study of membrane-attached CPR in various biologically relevant states. We conducted molecular dynamics simulations of CPR in both closed and open conformations investigating the stability of both conformations and its interactions with membrane model composed of DOPC. Furthermore, we conducted metadynamics simulations revealing the mechanism of CPR transition from open to closed state. Resulting models further served as a necessary step to establish fully atomistic model of stable CYP-CPR complex on membrane depicting mutual interaction sides of microsomal redox partners.

6.5.1 Models of CPR in closed and open conformations

Model of membrane-attached CPR in closed conformation was very stable during 700 ns simulations. There were no structural changes suggesting spontaneous transition into open conformation. Orientation of CPR domains remained unchanged leaving them (as well as all containing cofactors) in direct contact necessary for intra-protein electron transfer. Also hinge region, often found to be responsible for structural changes between open and closed form, showed no significant changes which could lead to conformation transformation. We measured the height of globular part of CPR above the membrane as 5.6 ± 0.4 nm which is in a great agreement with experimental value of 5.6 ± 2.2 nm provided by AFM measurement.[119]

We also investigated our model in terms of interaction amino acid residues of catalytic domain which are in contact with DOPC membrane. We identified those residues E270-P275, I307-R313 and N464 from the FAD domain, W549-G554 in NADPH binding domain as point of contacts with the membrane. Those interactions stabilized the position of CPR on membrane and restricted additional free reorientation of protein upon membrane surface.

In contrast to stable and compact closed conformation, in an open crystal conformation, both domains are in great distance from each other leaving flavin cofactors 86 Å apart. In this condition

CPR binds CYP and reduces its iron atom in heme since the FMN binding domain is exposed and the FMN cofactor is reveled enabling the possible interaction to its redox partners. As our model shows, CPR in open conformation is in principle able to interact with its redox partner (e.g., the favorable orientation and FMN cofactor exposure) but it is not (as opposite to closed CPR) supported by contact with membrane and the mobility of catalytic domains is therefore unrestricted. Moreover, FAD, linker and NADPH binding domains are connected freely with FMN domain via hinge region and are exposed to the solvent environment. Three independent replica simulations revealed instability of opened form resulting into different scenarios (Figure 29). Resulted structures deviated greatly from its crystal structure mostly with the most noticeable difference in mutual orientations of flavine domains especially at hinge region. While the internal structures of each catalytic domain remained intact, mutual mobility of catalytic domains was observed. In all simulations, however, the FMN domain is turned toward membrane inaccessible for interaction with redox partner.

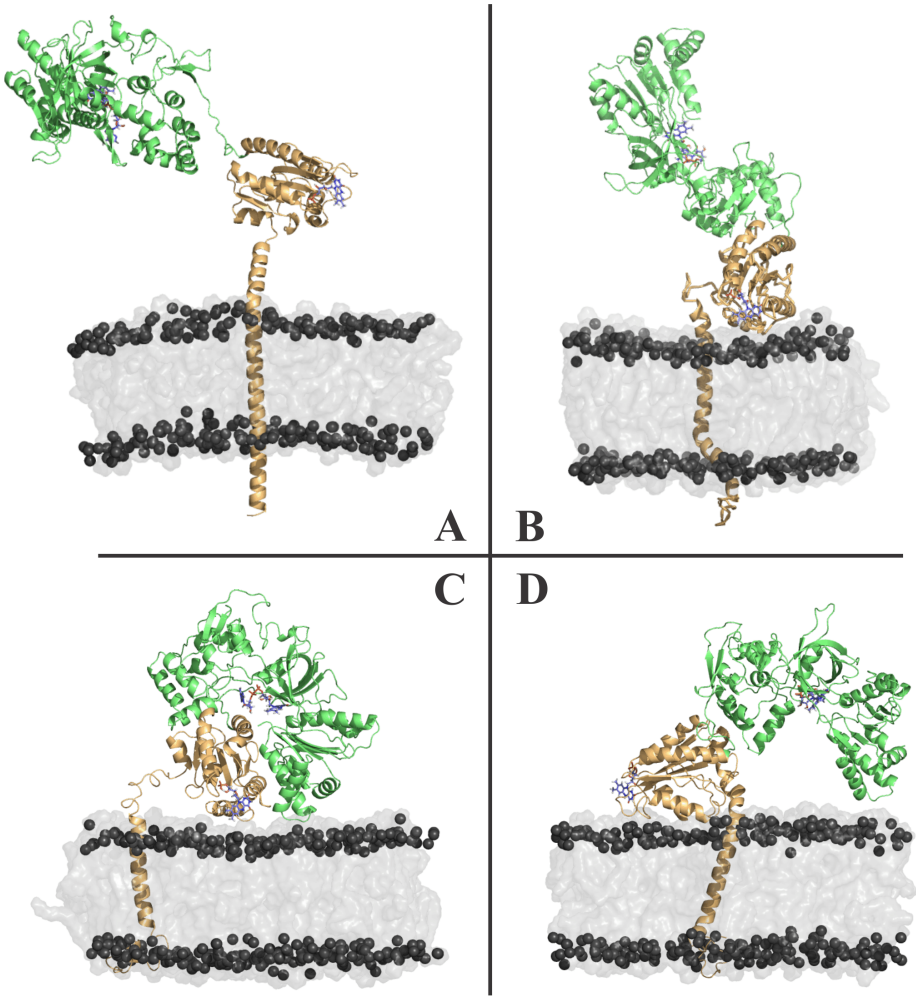

Figure 29. Snapshots of open structures of CPR in different conditions. Panel A represents starting structure for simulations of CPR in open conformation embedded in DOPC bilayer. Panels B, C and D represent different structural changes after 100 ns simulations. In all three scenarios FMN domains are in direct contact with membrane surface disallowing electron transfer to CYPs to occur.

Because no spontaneous closing was observed during classical MD simulations of CPR in open conformation additional metadynamics simulations were employed. An external bias potential was applied on distance root mean square deviation (DRMSD) of protein backbone of amino acid residues F201-V345 (including the hinge region) as collective variable during conformation transition from open to closed conformation. During ~20 ns MTD simulation protein adopted compact conformation comparable with crystal structure of CPR in closed conformation. The process of conformation transition can be described as following. At first, mutual reorientation between FMN domain and the rest of catalytic domain occurred (Figure 30 at time of 5 ns). The rotation movement was conducted by flexible hinge region. Then catalytic domains approached closer. FAD, linker and NADPH domains are approaching FMN domain from (Figure 30 at times of 10 and 15 ns) its upper part where helixes A183-L192 and E213 and E229 are located. At last, the front part of FMN domain, where FMN cofactor molecule is located was covered by the rest of catalytic domain leaving flavin cofactors at distance of ~5 Å in positions corresponding with crystal structure of closed CPR (Figure 30 at time of 20 ns). After complete closure, CPR was inappropriately oriented on membrane surface resulting in no successive opening.

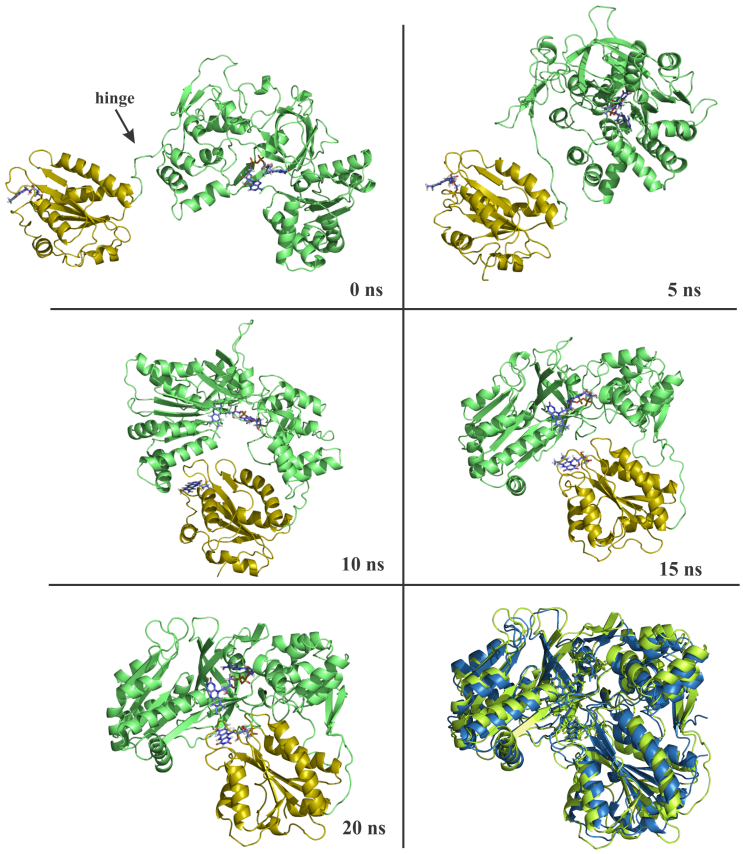

Figure 30. Conformation changes of CPR from open to closed conformation. that occurred during 20 ns of metadynamics simulations. After 20 ns, protein adopts as well as cofactors adopted structure identical with crystal structure of CPR in closed conformation. The last images represent aligned structures after 20 ns of MTD simulation (green) with crystal structure of CPR (blue). Protein shown in cartoon representation (FMN domain gold; the rest of catalytic domains green) with cofactors as sticks (blue).

6.5.2 Model of membrane-attached CPR-CYP 3A4 complex

Since the main role of cytochrome P450 reductase is electron supply to its redox partners from cytochrome P450 family, we studied model of inter-protein complex of CPR and cytochrome P450 3A4, both embedded in membrane. The model was created using CPR in open conformation as an electron donor protein. In the starting position, proteins were oriented, so CYP faced with proximal site of heme molecule to exposed FMN cofactor. In course of 400 ns simulation $FMNH_2$ – heme molecule distance dropped from original value of 29.6 Å to constant value of 21.7 ± 0.5 Å (at the closest approach at 18.3 Å) resulting in a very stable protein complex in contrast with open CPR conformation itself. Strong interaction between those redox partners was mainly driven by electrostatic forces due to oppositely charged amino acid residues at interaction sites of proteins. Strong interaction of proteins as well as sufficient distance between cofactors made our purposed model valid for study of possible protein-protein interaction and electron transfer pathways. In CPR-CYP3A4 complex (Figure 31), nitrogen N5 atom of $FMNH_2$ molecule is oriented towards heme cofactor molecule allowing electron transfer to occur. On redox partners, loops that may be important for electron transport were defined as Y140-D144 (Y140, G141, E142, G143 and D144) in CPR structure and Asn441-Arg446 (N441, C442, I443, G444, M445, R446) in CYP3A4 structure. Those residues are located directly between $FMNH_2$ and heme cofactors at the side of interaction. Amino acid residues of C442, M445 and R446 of CYP 3A4 were previously proposed to be involved in interaction with redox partners.[120] Moreover, side chain mutation R446A of CYP 2B4, located at same region as R446 at CYP 3A4, lead to decrease of interaction with CPR.[121] In addition, recent solution NMR study clarified interaction sites of CPR with redox partners, namely cytochrome P450 17A1 as Loop 1 of CPR (^{87}QTGT^{90}).[122] Our model of membrane bound CYP-CPR complex meets those experimental data for binding site of CPR as the Loop 1 located at close proximity to $FMNH_2$ cofactor was found in direct contact with CYP 3A4 in our simulation.

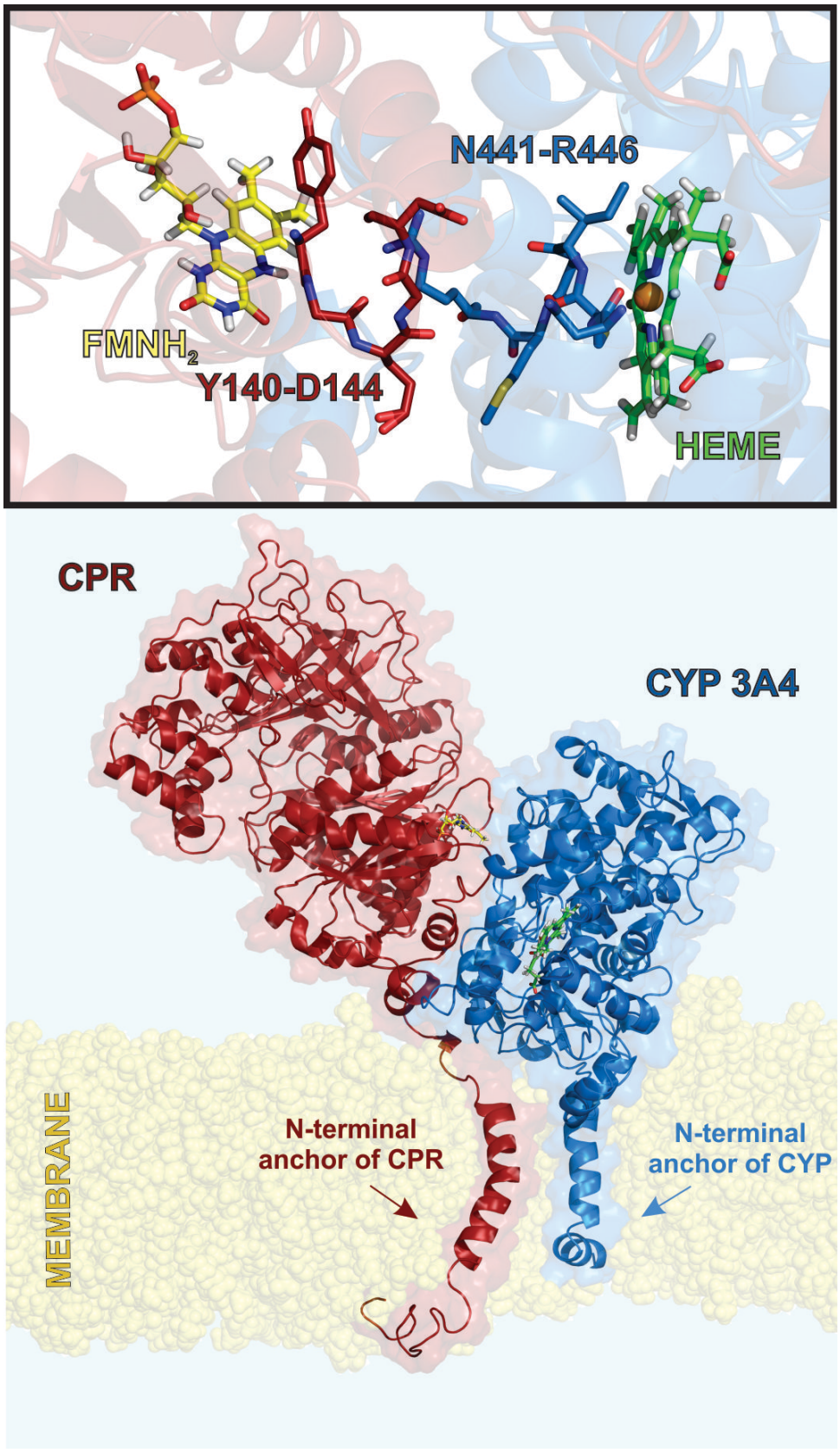

Figure 31. Final structure of human CPR-CYP3A4 complex embedded in DOPC membrane. The $FMNH_2$ and heme cofactors were located at proximity with residues including the Y140-D144 loop of CPR and N441-R446 of CYP3A4 as possible electron transfer mediators.

7. Summary

This dissertation thesis focuses on exploring the significance of biological membranes through a range of computational techniques, encompassing the utilization of scientific databases, precise quantum mechanical calculations, and investigating their dynamic behaviour using molecular dynamics simulations.

Initially, our focus was on the development of a scientific database aimed at curating and rationalizing the interactions between molecules and membranes. These interactions play a crucial role in the actions of individual molecules within an organism, as well as in their pharmacokinetics and pharmacodynamics. However, currently, these valuable data are not interconnected and are scattered across various platforms and literature sources, resulting in a lack of comprehensive benchmark comparisons among different experimental and theoretical methods for studying membrane systems. To address this issue, we created the Molecules on Membrane database (MolMeDB). Here, I present the process of developing and utilizing this database, along with highlighting its significant advantages. These advantages include facilitating direct comparisons of results from various entries, showcasing examples of membrane interactions involving caffeine and its metabolites, as well as enabling the comparison of large datasets obtained from different theoretical methods.

Subsequently, our focus shifted towards investigating the permeation of cyclosporin A, a widely used immunosuppressant, across various models of biological membranes. Through enhanced molecular dynamics (MD) simulations, we discovered that the composition of the membrane significantly influences the mechanism of CsA permeation. In simplified phosphatidylcholine membrane models, the energetical profiles for CsA passage were relatively similar. However, the presence of cholesterol induced changes in the membrane's ordering, leading to a shift of the energetical minima directly towards the centre of the lipid bilayer when equimolar concentrations of cholesterol and phosphatidylcholine were present. The borderline case of DPPC also revealed that CsA was unable to permeate through membranes in the gel-ordered phase. In all cases, the strongly hydrophobic nature of CsA and its limited water solubility indicated that CsA primarily resides within the aliphatic interior of the membrane. These findings shed light on the importance of membrane composition on the permeation of CsA and highlight the preferential localization of CsA within the lipid bilayer.

Then, our research focused on the development and validation of a systematic computational methodology for predicting suitable liposomal encapsulation and thermally induced release of bio-active compounds. By combining classical molecular dynamics (MD) simulations with

quantum chemistry-based calculations, we were able to establish selection criteria for identifying compounds capable of stable encapsulation and temperature-induced release from liposomes. To explore a wide range of potential candidates, we performed an *in silico* screening of the DrugBank database against these selection criteria. This analysis led us to identify a new drug, cycloserine, as a promising candidate for tailored liposomal loading and thermal release. Through our computational/experimental approach, we have paved the way for more efficient and targeted encapsulation and release of bio-active compounds using liposomes. Our methodology allows *in silico* design and optimization of liposomal drug delivery systems.

In a subsequent study on the effect of membrane composition role, our aim was to elucidate the influence of membrane lipid composition on the behaviour of mitochondrial cytochrome P450 CYP11A1 enzyme. To achieve this, we investigated the enzyme's behaviour on two distinct membrane models: a simple DOPC bilayer and a more complex membrane mixture with cardiolipin mimicking mitochondrial lipid composition. Our findings revealed that using a simple pure DOPC membrane model inadequately captures the interactions between the membrane and CYP11A1 enzyme. Specifically, the simulation results showed different interaction patterns when employing a multiple-replica simulation setup. In contrast, employing a more complex model mimicking the composition of the mitochondrial membrane more accurately described the mutual orientation and immersion of CYP11A1 in relation to experimental data. Our investigation concluded that while the overall interactions between anchorless CYP11A1 and the mitochondrial membrane are less tight compared to membrane-anchored CYPs, these interactions, which are primarily driven by electrostatic forces, may contribute to the overall stability and preferred orientation of CYP11A1 on the inner mitochondrial membrane. These findings shed light on the intricate interplay between membrane lipid composition and the behaviour of CYP11A1.

The final project of this thesis focuses on studying the behaviour of membrane-attached cytochrome P450 reductase (CPR) and its interactions with its redox partner, cytochrome P450 CYP3A4. Our investigation revealed that in the closed conformation, CPR adopts a highly compact structure reminiscent of its crystal form. This structural stability is facilitated by its close association with the membrane. On the other hand, when bound in a DOPC membrane model, the open form of CPR was found to be unstable, and the resulting structures were unable to interact effectively with its redox partner CYP3A4. However, we observed significant mutual stabilization between the interacting CPR and CYP3A4 proteins. Through this model, we identified several amino acids located in the proximal site of CYP3A4 and the FMN binding site of CPR that are involved in protein-protein electron transport. These findings provide valuable insights into the dynamic behaviour and interplay between CPR and CYP3A4 in a membrane context.

8. Shrnutí

Tato disertační práce je zaměřena na význam biologických membrán z hlediska různých výpočetních technik, zahrnující využití vědeckých databází, přesných kvantově-mechanických výpočtů a zkoumání jejich dynamického chování pomocí molekulárně dynamických simulací.

Nejdříve jsme se zaměřili na vývoj vědecké databáze, která má za cíl klasifikovat a uspořádat informace o interakcích mezi molekulami a membránami. Tyto interakce hrají klíčovou roli v působení jednotlivých molekul v organismu a v jejich farmakokinetice a farmakodynamice. Avšak v současnosti jsou tyto cenné informace nesouvislé a roztříštěné v různých platformách a literatuře, což vede k nemožnosti srovnání mezi různými experimentálními a teoretickými metodami pro studium membránových systémů. Abychom toto omezení překonali, vytvořili jsme databázi Molecules on Membrane database (MolMeDB). V této práci prezentuji proces vývoje a využití této databáze. Mezi její přednosti patří možnost přímého srovnání výsledků z rozličných datových vstupů na příkladech interakcí molekul s membránami, jako je kofein a jeho metabolity, nebo porovnání rozsáhlých souborů dat z různých teoretických metod.

Následně jsme se zaměřili na průchod imunosupresiva cyklosporinu A (CsA) přes různé modely biologických membrán. Molekulárně dynamické metody efektivního vzorkování odhalily, že složení membrány výrazně ovlivňuje mechanismus průchodu CsA. V jednoduchých modelech fosfatidylcholinových membrán byly energetické profily průchodu CsA téměř identické, ale přítomnost cholesterolu měnila uspořádání membrány a energetická minima se posunula přímo do středu lipidové dvojvrstvy při ekvimolárních koncentracích cholesterolu a fosfatidylcholinu. Mezní případ DPPC dále ukázal, že CsA nedokáže proniknout přes membrány nacházející se v gelové fázi. Ve všech případech naznačoval silně hydrofobní charakter CsA jeho výskyt převážně v alifatickém prostředí membrány. Tato zjištění objasňují důležitost složení membrány pro průchod CsA a poukazují na preferenční lokalizaci CsA v lipidové dvojvrstvě.

Poté jsme se zaměřili na vývoj a ověření systematické výpočetní metodiky pro predikci optimálních podmínek pro liposomální enkapsulaci a tepelně řízeného uvolňování bioaktivních látek. Kombinací klasických molekulárně dynamických simulací a kvantově-chemických výpočtů jsme určili kritéria pro výběr látek schopných stabilní enkapsulace a teplotně řízeného uvolňování z liposomů. Následný screening databáze DrugBank proti těmto kritériím nám umožnil identifikovat cykloserin jako perspektivního kandidáta pro možnou liposomální enkapsulaci a následné teplotně řízené vylučování z liposomu. Díky našemu kombinovanému výpočetnímu/experimentálnímu přístupu jsme navrhli cestu k efektivnější a cílené liposomální

enkapsulaci a uvolňování bioaktivních látek. Naše metodologie umožňuje *in silico* návrh a optimalizaci doručování léčiv pomocí liposomálních systémů.

V následujícím studii jsme se zaměřili na vliv složení membrány na chování mitochondriálního enzymu cytochromu P450 CYP11A1. Pro dosažení tohoto cíle jsme zkoumali chování enzymu na dvou různých modelech membrán, a to na zjednodušeném modelu DOPC membrány a komplexnějším membránovém systému odpovídajícího složením mitochondriální membráně. Naše zjištění ukázala, že použití zjednodušeného DOPC modelu nedostatečně popisuje interakce mezi membránou a enzymem CYP11A1. Naopak použití komplexnějšího modelu, který svým složením více odpovídá mitochondriální membráně, umožnilo přesnější popis vzájemné orientaci CYP11A1 na membráně ve srovnání s experimentálními daty. Naše zjištění naznačují, že i když jsou celkové interakce mezi CYP11A1 a mitochondriální membránou slabší ve srovnání s membránově kotvenými cytochromy, tak tyto interakce, které jsou převážně elektrostatického charakteru, mohou přispívat k celkové stabilitě a preferované orientaci CYP11A1 na vnitřní mitochondriální membráně. Tato zjištění přináší nové poznatky o vztahu mezi lipidovým složením biologických membrán a jejich vlivu na chováním enzymu CYP11A1.

Poslední projekt této disertační práce se zabývá studiem chování membránově kotveného enzymu cytochromu P450 reduktázy (CPR) a jeho interakcemi s redoxním partnerem cytochromem P450 CYP3A4. Náš výzkum odhalil, že uzavřená konformace CPR je velmi kompaktní, podobná krystalové struktuře. Tato strukturní stabilita je umožněna právě díky interakci s membránou. Na druhou stranu, otevřená forma CPR je i při ukotvení v membránovém modelu DOPC nestabilní a výsledné struktury nedokážou efektivně interagovat s redoxním partnerem CYP3A4. Dále jsme pozorovali významnou vzájemnou stabilizaci mezi interagujícími proteiny CPR a CYP3A4. Na základě tohoto modelu jsme identifikovali několik aminokyselin umístěných v blízkosti proximální strany CYP3A4 a vazebného místa FMN kofaktoru u CPR, které se mohou podílet na elektronovém přenosu mezi těmito proteiny. Tato zjištění poskytují cenné poznatky o dynamickém chování a vzájemném mechanismu interakce mezi redoxními partnery CPR a CYP3A4 kotvenými na biologické membráně.

9. List of Abbreviations

ABC	ATP-binding cassette transporter
ADME	absorption, distribution, metabolism and excretion
AdR	adrenodoxin reductase
Adx	adrenodoxin
A_L	area per lipid
API	active pharmaceutical ingredient
AQP	aquaporin channels
ATP	adenosine triphosphate
BLM	black lipid membrane
bRo5	beyond the Rule of five
CER	ceramide
CHOL	cholesterol
COSMO	conductor-like screening model
CPR	cytochrome P450 reductase
CsA	cyclosporin A
CYP	cytochrome P450
CV	collective variable
D_L	lateral diffusion coefficient
$D_{(z)}$	transversal diffusion coefficient
ER	endoplasmic reticulum
FRAP	fluorescence recovery after photobleaching
GLUT	glucose transporters
GPL	glycerophospholipids
HTA	heme tilt angle
IMM	inner mitochondrial membrane
$K_{m/w}$	lipid(membrane)/water partition coefficient
$K_{o/w}$	octanol/water partition coefficient
MD	molecular dynamics
MM	molecular mechanics
MIT	mitochondrial
MP	membrane proteins
MTD	metadynamics
P	permeability coefficient
PA	phosphatidic acid

PC	phosphatidylcholines
PE	phosphatidylethanolamines
PG	phosphatidylglycerol
PI	phosphatidylinositol
PM	plasma membrane
PS	phosphatidylserines
PSA	polar surface area
RMSD	root mean square deviation
DRMSD	distance root mean square deviation
SASA	solvent accessible surface area
S_{CD}	order parameters
SC	stratum corneum
SM	sphingomyelin
SLC	solute carrier transporters
SPT	single-particle tracking
TAG	triacylglycerol
US	umbrella sampling
V_L	volume per lipid

10. References

1. Harayama, T. & Riezman, H. Understanding the diversity of membrane lipid composition. Nat. Rev. Mol. Cell Biol. 19, 281–296 (2018).
2. Fong, T. M. & Mcnamee, M. G. Stabilization of Acetylcholine Receptor Secondary Structure by Cholesterol and Negatively Charged Phospholipids in Membranes. Biochemistry 26, 3871–3880 (1987).
3. Braverman, N. E. & Moser, A. B. Functions of plasmalogen lipids in health and disease. Biochim. Biophys. Acta - Mol. Basis Dis. 1822, 1442–1452 (2012).
4. Koynova, R. & Caffrey, M. Phases and phase transitions of the phosphatidylcholines. Biochim. Biophys. Acta - Rev. Biomembr. 1376, 91–145 (1998).
5. Dufourc, E. J. Sterols and membrane dynamics. J. Chem. Biol. 1, 63–77 (2008).
6. van Meer, G., Voelker, D. R. & Feigenson, G. W. Membrane lipids: where they are and how they behave. Nat. Rev. Mol. Cell Biol. 9, 112–124 (2008).
7. Ahmadian, M., Duncan, R. E., Jaworski, K., Sarkadi-Nagy, E. & Sul, H. S. Triacylglycerol metabolism in adipose tissue. Future Lipidol. 2, 229–237 (2007).
8. Coleman, R. A. & Mashek, D. G. Mammalian triacylglycerol metabolism: Synthesis, lipolysis, and signaling. Chem. Rev. 111, 6359–6386 (2011).
9. Devaux, P. F. Static and dynamic lipid asymmetry in cell membranes. Biochemistry 30, 1163–1173 (1991).
10. Bell, R. M., Ballas, L. M. & Coleman, R. A. Lipid topogenesis. J. Lipid Res. 22, 391–403 (1981).
11. Holthuis, J. C. M., Pomorski, T., Raggers, R. J., Sprong, H. & Van Meer, G. The organizing potential of sphingolipids in intracellular membrane transport. Physiol. Rev. 81, 1689–1723 (2001).
12. Di Paolo, G. & De Camilli, P. Phosphoinositides in cell regulation and membrane dynamics. Nature 443, 651–657 (2006).
13. Hilgemann, D. W., Feng, S. & Nasuhoglu, C. The Complex and Intriguing Lives of PIP2 with Ion Channels and Transporters. Sci. Signal. 2001, re19 (2001).
14. Paradies, G., Paradies, V., Ruggiero, F. M. & Petrosillo, G. Role of Cardiolipin in Mitochondrial Function and Dynamics in Health and Disease: Molecular and Pharmacological Aspects. Cells 8, 728 (2019).
15. Vos, M. et al. Cardiolipin promotes electron transport between ubiquinone and complex I to rescue PINK1 deficiency. J. Cell Biol. 216, 1–14 (2017).
16. Malhotra, K. et al. Cardiolipin mediates membrane and channel interactions of the mitochondrial TIM23 protein import complex receptor Tim50. Sci. Adv. 3, 26–28 (2017).
17. Lambeth, J. D. Cytochrome P-450scc. Cardiolipin as an effector of activity of a

mitochondrial cytochrome P-450. J. Biol. Chem. 256, 4757–4762 (1981).

18. Escribá, P. V. et al. Membrane lipid therapy: Modulation of the cell membrane composition and structure as a molecular base for drug discovery and new disease treatment. Prog. Lipid Res. 59, 38–53 (2015).
19. Pappas, A. Epidermal surface lipids. Dermatoendocrinol. 1, 72–76 (2009).
20. Das, C., Noro, M. G. & Olmsted, P. D. Simulation studies of stratum corneum lipid mixtures. Biophys. J. 97, 1941–51 (2009).
21. Gupta, R., Sridhar, D. B. & Rai, B. Molecular Dynamics Simulation Study of Permeation of Molecules through Skin Lipid Bilayer. J. Phys. Chem. B 120, 8987–8996 (2016).
22. Casares, D., Escribá, P. V. & Rosselló, C. A. Membrane lipid composition: Effect on membrane and organelle structure, function and compartmentalization and therapeutic avenues. Int. J. Mol. Sci. 20, 1–30 (2019).
23. Petrache, H. I., Dodd, S. W. & Brown, M. F. Area per Lipid and Acyl Length Distributions in FluidPhosphatidylcholines Determined by2H NMR Spectroscopy. Biophys. J. 79, 3172–3192 (2000).
24. Kucerka, N. et al. Areas of monounsaturated diacylphosphatidylcholines. Biophys. J. 97, 1926–32 (2009).
25. Pan, J., Tristram-Nagle, S., Kucerka, N. & Nagle, J. F. Temperature dependence of structure, bending rigidity, and bilayer interactions of dioleoylphosphatidylcholine bilayers. Biophys. J. 94, 117–24 (2008).
26. Kučerka, N., Heberle, F. A., Pan, J. & Katsaras, J. Structural Significance of Lipid Diversity as Studied by Small Angle Neutron and X-ray Scattering. Membranes (Basel). 5, 454–472 (2015).
27. Lewis, B. A. & Engelman, D. M. Lipid Bilayer Thickness Varies Linearly with Acyl Chain Length in Fluid Phosphatidylcholine Vesicles. J. Mol. Biol. 166, 211–217 (1983).
28. Pan, J., Marquardt, D., Heberle, F. A., Ku, N. & Katsaras, J. Revisiting the bilayer structures of fl uid phase phosphatidylglycerol lipids : Accounting for exchangeable hydrogens. Biochim. Biophys. Acta 1838, 2966–2969 (2014).
29. Kučerka, N. et al. Molecular Structures of Fluid Phosphatidylethanolamine Bilayers Obtained from Simulation-to-Experiment Comparisons and Experimental Scattering Density Profiles. J. Phys. Chem. B 119, 1947–1956 (2015).
30. Vermeer, L. S., de Groot, B. L., Réat, V., Milon, A. & Czaplicki, J. Acyl chain order parameter profiles in phospholipid bilayers: computation from molecular dynamics simulations and comparison with 2H NMR experiments. Eur. Biophys. J. 36, 919–31 (2007).
31. Kučerka, N. et al. The Effect of Cholesterol on Short- and Long-Chain Monounsaturated Lipid Bilayers as Determined by Molecular Dynamics Simulations and X-Ray Scattering.

Biophys. J. 95, 2792–2805 (2008).

32. Bag, N., Yap, H. X. D. & Wohland, T. Temperature dependence of diffusion in model and live cell membranes characterized by imaging fluorescence correlation spectroscopy. BBA - Biomembr. 1838, 802–813 (2014).
33. Filippov, A., Orädd, G. & Lindblom, G. Domain Formation in Model Membranes Studied by Pulsed-Field Gradient-NMR: The Role of Lipid Polyunsaturation. Biophys. J. 93, 3182–3190 (2007).
34. Saxton, M. J. & Jacobson, K. Single-particle tracking: applications to membrane dynamics. Annu. Rev. Biophys. Biomol. Struct. 26, 373–399 (1997).
35. Yang, N. J. & Hinner, M. J. Getting Across the Cell Membrane: An Overview for Small Molecules, Peptides, and Proteins. Methods Mol. Biol. 1266, 29–53 (2015).
36. Walter, A. & Gutknecht, J. Permeability of small nonelectrolytes through lipid bilayer membranes. J. Membr. Biol. 90, 207–217 (1986).
37. Cossart, P. & Helenius, A. Endocytosis of Viruses and Bacteria. Cold Spring Harb. Perspect. Biol. 6, a016972–a016972 (2014).
38. Lipinski, C. A., Lombardo, F., Dominy, B. W. & Feeney, P. J. Experimental and computational approaches to estimate solubility and permeability in drug discovery and development settings. Adv. Drug Deliv. Rev. 46, 3–26 (2001).
39. Palm, K., Stenberg, P., Luthman, K. & Artursson, P. Polar molecular surface properties predict the intestinal absorption of drugs in humans. Pharmaceutical Research vol. 14 568–571 (1997).
40. Rezai, T., Yu, B., Millhauser, G. L., Jacobson, M. P. & Lokey, R. S. Testing the conformational hypothesis of passive membrane permeability using synthetic cyclic peptide diastereomers. J. Am. Chem. Soc. 128, 2510–2511 (2006).
41. White, T. R. et al. On-resin N-methylation of cyclic peptides for discovery of orally bioavailable scaffolds. Nat. Chem. Biol. 7, 810–817 (2011).
42. Potts, R. O. & Guy, R. H. Predicting Skin Permeability. Pharm. Res. An Off. J. Am. Assoc. Pharm. Sci. 9, 663–669 (1992).
43. Jalili, S. & Saeedi, M. Study of curcumin behavior in two different lipid bilayer models of liposomal curcumin using molecular dynamics simulation. J. Biomol. Struct. Dyn. 34, 327–340 (2016).
44. Qiao, B. & de la Cruz, M. O. Driving Force for Water Permeation Across Lipid Membranes. J. Phys. Chem. Lett. 4, 3233–3237 (2013).
45. Paloncýová, M., Berka, K. & Otyepka, M. Molecular insight into affinities of drugs and their metabolites to lipid bilayers. J. Phys. Chem. B 117, 2403–2410 (2013).
46. Mathai, J. C., Tristram-Nagle, S., Nagle, J. F. & Zeidel, M. L. Structural determinants of water permeability through the lipid membrane. J. Gen. Physiol. 131, 69–76 (2008).

47. Chapman, D. Penkett, S. A. Nuclear Magnetic Resonance Spectroscopic Studies of the Interaction of Phospholipids with Cholesterol. Nature 211, 1304–1305 (1966).
48. Finkelstein, A. Cass, A. Effect of cholesterol on the water permeability of thin lipid membranes. Nature 216, 717–718 (1967).
49. Papahadjopoulos, D. Nir, S. Oki, S. Permeability properties of phospholipid membranes: effect of cholesterol and temperature. Biochim. Biophys. Acta 226, 561–583 (1972).
50. Eriksson, E. S. E. & Eriksson, L. A. The Influence of Cholesterol on the Properties and Permeability of Hypericin Derivatives in Lipid Membranes. J. Chem. Theory Comput. 7, 560–574 (2011).
51. Wennberg, C. L., van der Spoel, D. & Hub, J. S. Large influence of cholesterol on solute partitioning into lipid membranes. J. Am. Chem. Soc. 134, 5351–5361 (2012).
52. McDonell, A. M. & Dang, C. H. Basic Review of the Cytochrome P450 System. J. Adv. Pract. Oncol. 4, 263–268 (2013).
53. Šrejber, M. et al. Membrane-attached mammalian cytochromes P450: An overview of the membrane's effects on structure, drug binding, and interactions with redox partners. J. Inorg. Biochem. 183, 117–136 (2018).
54. Shephard, E. A., Phillips, I. R., Bayney, R. M., Pike, S. F. & Rabin, B. R. Quantification of NADPH: cytochrome P -450 reductase in liver microsomes by a specific radioimmunoassay technique. Biochem. J. 211, 333–340 (1983).
55. Flück, C. E. et al. Mutant P450 oxidoreductase causes disordered steroidogenesis with and without Antley-Bixler syndrome. Nat. Genet. 36, 228–230 (2004).
56. Shephard, E. A. et al. Isolation of a Human Cytochrome P-450 Reductase cDNA Clone and Localization of the Corresponding Gene to Chromosome 7q11.2. Ann.Hum.Genet. 53, 291–301 (1989).
57. Schwöbel, J. A. H. et al. COSMO perm: Mechanistic Prediction of Passive Membrane Permeability for Neutral Compounds and Ions and Its pH Dependence. J. Phys. Chem. B 124, 3343–3354 (2020).
58. Klamt, A., Huniar, U., Spycher, S. & Keldenich, J. COSMOmic: a mechanistic approach to the calculation of membrane−water partition coefficients and internal distributions within membranes and micelles. J. Phys. Chem. B 112, 12148–12157 (2008).
59. Ottaviani, G., Martel, S. & Carrupt, P.-A. Parallel Artificial Membrane Permeability Assay: A New Membrane for the Fast Prediction of Passive Human Skin Permeability. J. Med. Chem 49, 3948–3954 (2006).
60. Kansy, M., Senner, F. & Gubernator, K. Physicochemical High Throughput Screening: Parallel Artificial Membrane Permeation Assay in the Description of Passive Absorption Processes. J. Med. Chem. 41, 1007–1010 (1998).
61. Hidalgo, I. J., Raub, T. J. & Borchardt, R. T. Characterization of the human colon

carcinoma cell line (Caco-2) as a model system for intestinal epithelial permeability. Gastroenterology 96, 736–49 (1989).

62. Difilippo, E. L. & Eganhouse, R. P. Assessment of PDMS-Water Partition Coefficients : Implications for Passive Environmental Sampling of Hydrophobic Organic Compounds. Environ. Sci. Technol. 44, 6917–6925 (2010).
63. Endo, S., Escher, B. I. & Goss, K.-U. Capacities of membrane lipids to accumulate neutral organic chemicals. Environ. Sci. Technol. 45, 5912–5921 (2011).
64. van Breemen, R. B. & Li, Y. Caco-2 cell permeability assays to measure drug absorption. Expert Opin. Drug Metab. Toxicol. 1, 175–185 (2005).
65. Avdeef, A. et al. Caco-2 permeability of weakly basic drugs predicted with the double-sink PAMPA method. Eur. J. Pharm. Sci. 24, 333–349 (2005).
66. Williams, F. M. EDETOX. Evaluations and predictions of dermal absorption of toxic chemicals. Int. Arch. Occup. Environ. Health 77, 150–151 (2004).
67. Lomize, M. A. et al. PerMM: A Web Tool and Database for Analysis of Passive Membrane Permeability and Translocation Pathways of Bioactive Molecules. J Chem Inf Model 59, 3094–3099 (2019).
68. RDKit: Open-source cheminformatics. Available 11/6/2023 at https://www.rdkit.org.
69. Kim, S. et al. PubChem 2023 update. Nucleic Acids Res. 51, D1373–D1380 (2023).
70. Wishart, D. S. DrugBank: a comprehensive resource for in silico drug discovery and exploration. Nucleic Acids Res. 34, D668–D672 (2006).
71. Hastings, J. et al. ChEBI in 2016: Improved services and an expanding collection of metabolites. Nucleic Acids Res. 44, D1214–D1219 (2016).
72. Davies, M. et al. ChEMBL web services: streamlining access to drug discovery data and utilities. Nucleic Acids Res. 43, W612–W620 (2015).
73. Berman, H. M. et al. The Protein Data Bank. Nucleic Acids Res. 28, 235–42 (2000).
74. Juračka, J., Šrejber, M., Melíková, M., Bazgier, V. & Berka, K. MolMeDB: Molecules on Membranes Database. Database 2019, (2019).
75. Abdalla, M. & McGaw, L. Natural Cyclic Peptides as an Attractive Modality for Therapeutics: A Mini Review. Molecules 23, 1–19 (2018).
76. Ho, S. et al. The Mechanism of Action of Cyclosporin A and FK506. Clin. Immunol. Immunopathol. 80, S40–S45 (1996).
77. Loosli, H.-R. et al. Peptide conformations. Part 31. The conformation of cyclosporin a in the crystal and in solution. Helv. Chim. Acta 68, 682–704 (1985).
78. Kessler, H., Köck, M., Wein, T. & Gehrke, M. Reinvestigation of the Conformation of Cyclosporin A in Chloroform. Helv. Chim. Acta 73, 1818–1832 (1990).
79. Jin, L. & Harrison, S. C. Crystal structure of human calcineurin complexed with cyclosporin A and human cyclophilin. Proc. Natl. Acad. Sci. 99, 13522–13526 (2002).

80. Wang, C. K., Swedberg, J. E., Harvey, P. J., Kaas, Q. & Craik, D. J. Conformational Flexibility Is a Determinant of Permeability for Cyclosporin. J. Phys. Chem. B 122, 2261–2276 (2018).
81. Wiedmann, T. S., Trouard, T., Shekar, S. C., Polikandritou, M. & Rahman, Y.-E. Interaction of cyclosporin A with dipalmitoylphosphatidylcholine. Biochim. Biophys. Acta - Biomembr. 1023, 12–18 (1990).
82. O'Leary, T. J., Ross, P. D., Lieber, M. R. & Levin, I. W. Effects of cyclosporine A on biomembranes. Vibrational spectroscopic, calorimetric and hemolysis studies. Biophys. J. 49, 795–801 (1986).
83. Söderlund, T., Lehtonen, J. Y. A. & Kinnunen, P. K. J. Interactions of Cyclosporin A with Phospholipid Membranes: Effect of Cholesterol. Mol. Pharmacol. 55, 32–38 (1999).
84. Ito, K., Passioura, T. & Suga, H. Technologies for the Synthesis of mRNA-Encoding Libraries and Discovery of Bioactive Natural Product-Inspired Non-Traditional Macrocyclic Peptides. Molecules 18, 3502–3528 (2013).
85. Grossfield, A. WHAM: the weighted histogram analysis method, available 11/6/2023 at http://membrane.urmc.rochester.edu/wordpress/?page_id=126.
86. Omura, T. Mitochondrial P450s. Chem. Biol. Interact. 163, 86–93 (2006).
87. Chien, Y., Rosal, K. & Chung, B. Function of CYP11A1 in the mitochondria. Mol. Cell. Endocrinol. 441, 55–61 (2017).
88. Schwarz, D. et al. Direct visualization of a cardiolipin-dependent cytochrome P450scc-induced vesicle aggregation. J. Struct. Biol. 113, 207–215 (1994).
89. Waterman, M. R. & Simpson, E. R. Regulation of the biosynthesis of cytochromes P-450 involved in steroid hormone synthesis. Mol. Cell. Endocrinol. 39, 81–89 (1985).
90. Miller, W. L. Steroid hormone synthesis in mitochondria. Mol. Cell. Endocrinol. 379, 62–73 (2013).
91. Spinello, A., Ritacco, I. & Magistrato, A. The Catalytic Mechanism of Steroidogenic Cytochromes P450 from All-Atom Simulations: Entwinement with Membrane Environment, Redox Partners, and Post-Transcriptional Regulation. Catalysts 9, 1–22 (2019).
92. Berka, K., Paloncýová, M., Anzenbacher, P. & Otyepka, M. Behavior of human cytochromes P450 on lipid membranes. J. Phys. Chem. B 117, 11556–11564 (2013).
93. Edwards, R. J., Murray, B. P., Boobis, A. R. & Davies, D. S. Identification and location of alpha-helices in mammalian cytochromes P450. Biochemistry 28, 3762–3770 (1989).
94. Pikuleva, I. A. Putative F–G loop is involved in association with the membrane in P450scc (P450 11A1). Mol. Cell. Endocrinol. 215, 161–164 (2004).
95. Headlam, M. J., Wilce, M. C. J. & Tuckey, R. C. The F–G loop region of cytochrome P450scc (CYP11A1) interacts with the phospholipid membrane. Biochim. Biophys. Acta

- Biomembr. 1617, 96–108 (2003).
96. Ingelman-Sundberg, M., Haaparanta, T. & Rydstroem, J. Membrane charge as effector of cytochrome P-450LM2 catalyzed reactions in reconstituted liposomes. Biochemistry 20, 4100–4106 (1981).
97. Ahn, T., Guengerich, F. P. & Yun, C.-H. Membrane insertion of cytochrome P450 1A2 promoted by anionic phospholipids. Biochemistry 37, 12860–12866 (1998).
98. Ingelman-Sundberg, M., Hagbjörk, A.-L., Ueng, Y.-F., Yamazaki, H. & Guengerich, F. P. High rates of substrate hydroxylation by human cytochrome P450 3A4 in reconstituted membranous vesicles: Influence of membrane charge. Biochem. Biophys. Res. Commun. 221, 318–322 (1996).
99. Fleischer, S., Rouser, G., Fleischer, B., Casu, A. & Kritchevsky, G. Lipid composition of mitochondria from bovine heart, liver, and kidney. J. Lipid Res. 8, 170–180 (1967).
100. Schwarz, D., Kruger, V., Chernogolov, A. A., Usanov, S. A. & Stier, A. Rotation of Cytochrome P450SCC (CYP11A1) in Proteoliposomes Studied by Delayed Fluorescence Depolarization. Biochem. Biophys. Res. Commun. 195, 889–896 (1993).
101. Kisselev, P. et al. Branched Phosphatidylcholines Stimulate Activity of Cytochrome P450SCC (CYP11A1) in Phospholipid Vesicles by Enhancing Cholesterol Binding, Membrane Incorporation, and Protein Exchange. J. Biol. Chem. 273, 1380–1386 (1998).
102. Navrátilová, V., Paloncýová, M., Kajšová, M., Berka, K. & Otyepka, M. Effect of cholesterol on the structure of membrane-attached cytochrome P450 3A4. J. Chem. Inf. Model. 55, 628–635 (2015).
103. Navrátilová, V., Paloncýová, M., Berka, K. & Otyepka, M. Effect of lipid charge on membrane immersion of cytochrome P450 3A4. J. Phys. Chem. B 120, 11205–11213 (2016).
104. Baylon, J. L., Lenov, I. L., Sligar, S. G. & Tajkhorshid, E. Characterizing the membrane-bound state of cytochrome P450 3A4: Structure, depth of insertion, and orientation. J. Am. Chem. Soc. 135, 8542–8551 (2013).
105. Murtazina, D. et al. Membrane-Protein Interactions Contribute to Efficient 27-Hydroxylation of Cholesterol by Mitochondrial Cytochrome P450 27A1. J. Biol. Chem. 277, 37582–37589 (2002).
106. Cojocaru, V., Winn, P. J. & Wade, R. C. The ins and outs of cytochrome P450s. Biochim. Biophys. Acta - Gen. Subj. 1770, 390–401 (2007).
107. Strushkevich, N. et al. Structural basis for pregnenolone biosynthesis by the mitochondrial monooxygenase system. Proc. Natl. Acad. Sci. 108, 10139–10143 (2011).
108. Eswar, N. et al. Comparative Protein Structure Modeling Using Modeller. Curr. Protoc. Bioinforma. 15, chapter 5 (2006).
109. Wolf, M. G., Hoefling, M., Aponte-SantamaríA, C., Grubmüller, H. & Groenhof, G.

g_membed: Efficient insertion of a membrane protein into an equilibrated lipid bilayer with minimal perturbation. J. Comput. Chem. 31, 2169–2174 (2010).

110. Jorgensen, W. L., Chandrasekhar, J., Madura, J. D., Impey, R. W. & Klein, M. L. Comparison of simple potential functions for simulating liquid water. J. Chem. Phys. 79, 926–935 (1983).
111. Pronk, S. et al. GROMACS 4.5: A high-throughput and highly parallel open source molecular simulation toolkit. Bioinformatics 29, 845–854 (2013).
112. Hornak, V. et al. Comparison of multiple Amber force fields and development of improved protein backbone parameters. Proteins Struct. Funct. Bioinforma. 65, 712–725 (2006).
113. Shahrokh, K., Orendt, A., Yost, G. & Cheatham, T. Quantum Mechanically Derived AMBER-Compatible Heme Parameters for Various States of the Cytochrome P450 Catalytic Cycle. J. Comput. Chem. 33, 191–133 (2011).
114. Jämbeck, J. P. M. & Lyubartsev, A. P. Another piece of the membrane puzzle: Extending slipids further. J. Chem. Theory Comput. 9, 774–784 (2013).
115. Jo, S., Kim, T., Iyer, V. G. & Im, W. CHARMM-GUI: A web-based graphical user interface for CHARMM. J. Comput. Chem. 29, 1859–1865 (2008).
116. Darden, T., York, D. & Pedersen, L. Particle mesh Ewald: An N ·log(N) method for Ewald sums in large systems. J. Chem. Phys. 98, 10089–10092 (1993).
117. Nosé, S. A unified formulation of the constant temperature molecular dynamics methods. J. Chem. Phys. 81, 511–519 (1984).
118. Parrinello, M. & Rahman, A. Polymorphic transitions in single crystals: A new molecular dynamics method. J. Appl. Phys. 52, 7182–7190 (1981).
119. Bayburt, T. H., Carlson, J. W. & Sligar, S. G. Single molecule height measurements on a membrane protein in nanometer-scale phospholipid bilayer disks. Langmuir 16, 5993–5997 (2000).
120. Liu, J., Tawa, G. J. & Wallqvist, A. Identifying cytochrome P450 functional networks and their allosteric regulatory elements. PLoS One 8, e81980 (2013).
121. Bridges, A. et al. Identification of the binding site on cytochrome P450 2B4 for cytochrome b 5 and cytochrome P450 reductase. J. Biol. Chem. 273, 17036–17049 (1998).
122. Estrada, D. F., Laurence, J. S. & Scott, E. E. Cytochrome P450 17A1 interactions with the FMN domain of its reductase as characterized by NMR. J. Biol. Chem. 291, 3990–4003 (2016).

11. List of Publications

1. **Šrejber M.**, Navrátilová V., Paloncýová M., Bazgier V., Berka K., Anzenbacher P., Otyepka M. Membrane-attached mammalian cytochromes P450: An overview of the membrane's effects on structure, drug binding, and interactions with redox partners. (2018) *J. Inorg. Biochem.* 183. 117-136. (https://doi.org/10.1016/j.jinorgbio.2018.03.002)
- IF in 2018: 3.224

2. Juračka J.[†], **Šrejber M.**[†], Melíková M., Bazgier V., Berka K. MolMeDB: Molecules on Membranes Database. (2019) *Database.* 2019. baz078 (https://doi.org/10.1093/database/baz078)
- IF in 2019: 2.331
[†]Authors contributed equally.

3. Balouch M., **Šrejber M.**, Šoltys M., Jánská P., Štěpánek F., Berka K. In silico screening of drug candidates for thermoresponsive liposome formulations. (2021) *Mol. Syst. Des. Eng. 6. 368-380* (https://doi.org/10.1039/D0ME00160K)
- IF in 2021: 3.323

List of other publications not involved in this thesis:
Paloncýová M., **Šrejber M.**, Čechová P., Kührová P., Zaoral F., Otyepka M. Atomistic Insights into Organization of RNA-Loaded Lipid Nanoparticles. (2023) *J. Phys. Chem. B.* 127 (5) 1158-1166

Paloncýová M., Čechová P., **Šrejber M.**, Kührová P., Otyepka M. Role of Ionizable Lipids in SARS-CoV-2 Vaccines As Revealed by Molecular Dynamics Simulations: From Membrane Structure to Interaction with mRNA Fragments. (2021) *J. Phys. Chem. Lett.* 12 (45) 11199-11205

Pykal M., Vondrák M., **Šrejber M**., Tantis I., Mahammadi E., Bakandritsos A., Medveď M., Otyepka M. Accessibility of grafted functional groups limits reactivity of covalent graphene derivatives. (2022) *Appl. Surf. Sci.* 598. 153792

Annadurai N., Malina L., Salmona M., Diomede L., Bastone A., Cagnotto A., Romeo M., **Šrejber M.**, Berka K., Otyepka M., Hajdúch M., Das W. Antitumour drugs targeting tau R3 VQIVYK and Cys322 prevent seeding of endogenous tau aggregates by exogenous seeds. (2021) FEBS J. 289. 1929-1949

12. Appendices

DATABASE
The Journal of Biological Databases and Curation

Database, 2019, 1–9
doi: 10.1093/database/baz078
Original article

Original article

MolMeDB: Molecules on Membranes Database

Jakub Juračka†, Martin Šrejber†, Michaela Melíková, Václav Bazgier and Karel Berka*

Regional Centre of Advanced Technologies and Materials, Department of Physical Chemistry, Faculty of Science, Palacký University Olomouc, Tř. 17, listopadu 12, 771 46 Olomouc, Czech Republic

*Corresponding author: Tel: +420 585 634 769; Fax: +420 585 63 4761; Email: karel.berka@upol.cz

†Authors contributed equally.

Citation details: Juračka,J., Šrejber,M., Melíková,M., *et al.* MolMeDB: Molecules on Membranes Database. *Database* (2019) Vol. 2019: article ID baz078; doi:10.1093/database/baz078

Received 16 November 2018; Revised 22 May 2019; Accepted 23 May 2019

Abstract

Biological membranes act as barriers or reservoirs for many compounds within the human body. As such, they play an important role in pharmacokinetics and pharmacodynamics of drugs and other molecular species. Until now, most membrane/drug interactions have been inferred from simple partitioning between octanol and water phases. However, the observed variability in membrane composition and among compounds themselves stretches beyond such simplification as there are multiple drug–membrane interactions. Numerous experimental and theoretical approaches are used to determine the molecule–membrane interactions with variable accuracy, but there is no open resource for their critical comparison. For this reason, we have built Molecules on Membranes Database (MolMeDB), which gathers data about over 3600 compound–membrane interactions including partitioning, penetration and positioning. The data have been collected from scientific articles published in peer-reviewed journals and complemented by in-house calculations from high-throughput COSMOmic approach to set up a baseline for further comparison. The data in MolMeDB are fully searchable and browsable by means of name, SMILES, membrane, method or dataset and we offer the collected data openly for further reuse and we are open to further additions. MolMeDB can be a powerful tool that could help researchers better understand the role of membranes and to compare individual approaches used for the study of molecule/membrane interactions.

Database URL: http://molmedb.upol.cz

Introduction

Biological membranes consist of complex lipid and protein mixtures that play a crucial role in molecular transport into/out of cells. Apart from passive or active permeation, molecules can also accumulate in the membranes at specific functional positions or they can disrupt the membrane altogether. All those molecule–membrane interactions are important for the actions of individual molecules in the organism and their pharmacokinetics.

And yet, most chemical databases use octanol/water partition coefficient (logP) as the only measure of small molecule interactions with lipid membranes, but the membrane compositions of individual cells and organelles can widely vary as it is being currently unraveled by findings from lipidomics (1). The membrane protein structural databases provide additional information not only about the position and the topology of the membrane proteins but also about the membrane-type localization (e.g. OPM (2), PDBTM (3), MemProtDB (4), TPML (5) or EncoMPASS (6)); however, the data about various molecule/membrane interactions are scattered among different sources. For example, DrugBank (7) covers logP and information about membrane transporters and carriers for many drug molecules, but it does not provide a measure for the assessment of penetration nor does it involve partitioning through individual membranes. Permeability of compounds through skin membranes is either present in EDETOX database (8) or scattered throughout literature, e.g. sources cited in supplemental information of reference (9). Similarly, the recently established PerMM database (10) covers only cellular permeability together with permeability prediction using an implicit membrane model with rigid compounds. Finally, molecular dynamics simulations are often used for predictions of membrane partitioning (11) or permeability even on a large scale (12,13). However, current theoretical predictions of molecule/membrane interactions vary by method as well as in comparison with data from experiments, lacking community benchmark comparison between individual methods.

To fill this gap, we have developed Molecules on Membranes Database (MolMeDB) as an open and up-to-date online manually curated depository of molecule/membrane interactions. MolMeDB contains over 3600 interactions described in the literature or obtained by our COSMOmic-based high-throughput calculations (14). In addition to listing the individual molecule/membrane interactions, we provide a simple tool for comparison of interactions between multiple methods and/or membranes. Using this information, it is possible to analyze the membrane behavior of the selected subsets of molecules. Examples of these analyses are provided as case studies to better illustrate efficient ways to extract useful knowledge from the MolMeDB database.

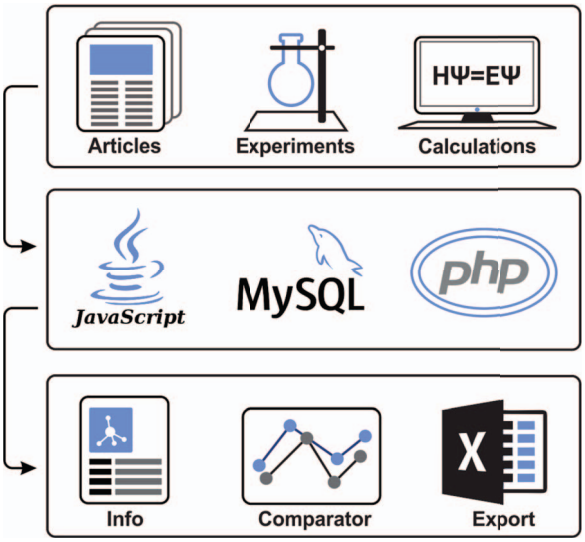

Figure 1. Illustrative scheme of MolMeDB workflow. Input data collected from experimental/theoretic studies are curated and introduced into the MySQL database with a web interface in HTML5/CSS + PHP7. Data for individual molecule/membrane interactions are visualized either as data tables or in interactive JavaScript graphs, and they can be directly compared and downloaded.

Materials and Methods

Data collection

To collect datasets of molecule–membrane interactions, a manual inspection of articles (15–23) and already existing databases (e.g. PerMM database (10)) with the focus on expressions like 'membrane partition coefficient', 'membrane permeability' or 'permeability coefficient' was performed (Figure 1). Primarily, we focused on high-throughput experimental setups like black lipid membrane (BLM) (24), parallel artificial membrane permeability assay (17,25), Caco-2 permeability assay (22), liposomal fluorescence assay (20), *n*-hexane passive dosing (26) and polydimethylsiloxane-based permeabilities (19,27) that provide partition coefficients of compounds on a variety of natural and artificial membranes. Moreover, we have also collected resources from a broad variety of computational methods, e.g. molecular dynamics-based umbrella sampling approach, COnductor like Screening MOdel for Real Solvents (COSMO-RS) theory-based COSMOmic calculations, or implicit solvent-based Permeability of Molecules across Membranes (PerMM) model. Those methods also differ in the level of approximation or force fields used to predict the compounds properties. This diversity within individual methods provides additional verification, especially in comparison to experimental data.

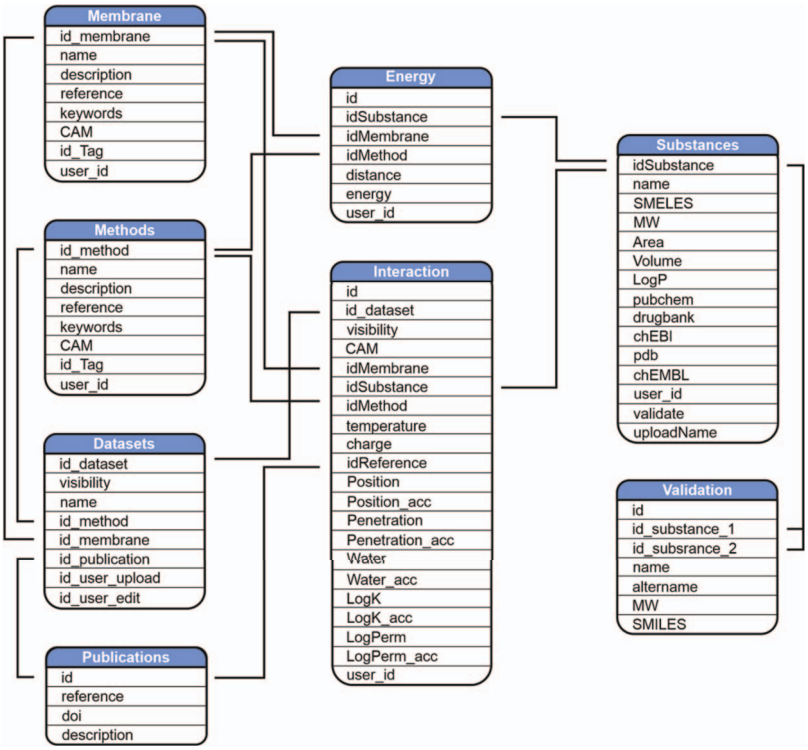

Figure 2. Scheme of MolMeDB database.

In-house COSMOmic calculations

Apart from the already published data, we have added our original dataset of XY compounds on various membranes mimicking either cell-like membranes (1,2-dimyristoyl-sn-glycero-3-phosphocholine (DMPC) or 1,2-dioleoyl-sn-glycero-3-phosphocholine (DOPC) bilayers) or skin-like membranes (ceramide NS or *stratum corneum* mixture bilayers consisting of an equimolar mixture of ceramide NS:cholesterol:lignoceric acid).

Neutral conformers of compounds were generated from SMILES with the LigPrep and MacroModel modules (Small-Molecule Drug Discovery Suite 2015–4, Schrödinger, LLC, New York, NY, 2016, https://www.schrodinger.com). Individual conformers of each compound were generated using the OPLS_2005 force field (28) in vacuum. Mixed MCMM/LMC2 conformational searches were performed to enable low-mode conformation searching with Monte Carlo structure selection. A maximum of 10 conformers were selected for further analysis if they were within 5 kcal/mol of the lowest energy conformer and, to reduce the number of similar conformers, had an atom-positional RMSD of at least 2 Å relative to all other selected conformers. Each selected conformer was subjected to a series of DFT/B-P/cc-TZVP vacuum and COSMO optimizations using Turbomole 6.3 (Turbomole V6.3 2011, http://www.turbomole.com) within the cuby4 framework (29). After each optimization step, single-point energy calculations at the DFT/B-P/cc-TZVPD level with a fine grid (30) were performed to obtain COSMO files for each conformer. The structures of COSMO.mic files describing bilayers were then obtained from fitting COSMO files of individual lipids to the bilayer structures obtained from free 200 ns + long molecular simulations from refs for DMPC (11), for DOPC and ceramide NS (31) and for *stratum corneum* mixture bilayers (32).

For each conformer/lipid sets we calculated free energy profiles using COSMOmic 15 (14) or COSMOmic/COSMOperm 18 to obtain averaged free energy profiles. From those, information about membrane partitioning, permeability and affinity, central energy barrier and the position of drug at its energetical minima was extracted.

Database architecture

MolMeDB webpage is built with the combination of HTML5/CSS and PHP7 layouts running on Apache server. The database runs on MySQL (Figure 2). The AJAX search engine allows search over names of compounds, datasets or SMILES. 2D structures are generated from SMILES using CDK Depict (33). 3D structure visualization is provided by LiteMol (34) over MOL files generated via RDkit (RDKit: Cheminformatics and Machine Learning Software. 2018, http://www.rdkit.org), or downloaded from PubChem (35), or DrugBank (7) databases, or uploaded by the user. DrugBank is used also for interconnection links

to other databases. Free energy profiles of individual molecule/method/membrane sets, where available, are visualized using Chart.js JavaScript application (https://chartjs.org). The potential of mean force (PMF) profiles data are stored as equidistant values spaced 1 Å for possible comparison between individual PMF profiles and they are interpolated from the uploaded data by Neville's algorithm of iterated interpolation.

Results

User interface and database usage

To provide a user-friendly interface for the molecule-membrane interaction data, we developed a web version of MolMeDB database, freely accessible at http://molmedb.upol.cz. Interaction data can be accessed via browse or search functions. 'Browse' section (Figure 3A) allows the user to scroll through the list of available compounds, membranes and methods used to describe the molecule-membrane interactions. 'Search' section (Figure 3B) enables the user to search for a desired compound by its name or SMILES notation and to look up compounds measured/-computed by individual methods and membranes. Dataset search allows the user to browse within a list of publications by title or authors' names. All data can be added into the Comparator tool (described below). MolMeDB web also includes 'Documentation' section (Figure 3C) explaining the methodology, giving several examples and a tutorial for using the database. Finally, 'Statistics' section (Figure 3D) keeps track of the number of entries and of interactions in subsets of individual methods or membranes.

The user can use the 'Search' section (Figure 3A) to list all compounds matching the entry name. As example of 'xanthine' entry, six compounds were listed partially matching the given expression (Figure 3). Among the listed entries, the user gets a quick overview of the compounds' properties, 2D structure and links to other chemical databases containing information about the molecule (e.g. Protein Data Bank (36), PubChem (35), ChEBI (37), ChEMBL (38), DrugBank (7)). Desired molecules can be added into the Comparator tool (see below). After selecting a compound, in our case 'xanthine', a purine-based molecule that serves as a parent compound for caffeine and its derivatives, the page is divided into the following three sections (Figure 4):

1. General info (Figure 4A)—provides a description of compound properties like molecular weight along with links to other databases via the molecule's identifiers. The first section also shows a 2D image generated from SMILES via CDK Depict and a 3D structure generated by RDKit or downloaded from PubChem or DrugBank databases visualized with LiteMol.
2. Interactions table (Figure 4B)—displays an interactive table with molecule-membrane interactions such as membrane/water partitioning ($\log K_m$), permeability coefficient ($\log P_{erm}$), free energy barrier in the membrane center (ΔG_{pen}), affinity toward the membrane measured by the energetical minimum (ΔG_{wat}) or the position of the interaction minimum for the molecule on membrane (Z_{min}) available for a combination of membranes and methods with variation where available. Charge of compound (Q) and temperature are specified for each molecule–membrane interaction. The user can then switch among individual methods to compare the measured/calculated properties. Source references are also listed in the Publication field. The desired data can be directly downloaded as a .csv table.
3. Free energy profile graph (Figure 4C)—demonstrates the course of the free energy profile along the membrane normal with energetical barriers and minima between membrane center (0 nm) and water environment (3.5 nm). For an individual method, the user can switch among available membranes and directly visualize given energetical profiles.

Use cases—Comparator tool

Although interaction data for individual compounds are valuable as such, their comparison allows the use of the data for research within multiple scientific fields. For this purpose, we have embedded the Comparator tool that allows to gather molecule–membrane interaction data for multiple compounds from one or more methods and to compare them in order to visualize patterns within the data or to assess the validity of predictive methods.

Caffeine and its metabolites Caffeine is a purine-based molecule, which is metabolized in a set of multiple-step reactions into a series of chemically modified compounds. In the first step, caffeine is metabolized to the following metabolites: theobromine (by enzymes CYP1A2, CYP2E1), theophylline (CYP1A2, CYP2E1), 1,3,7-trimethyluric acid (XO), 6-amino-5(*N*-formylmethylamino)-1,3-dimethyluracil (CYP 1A2) and paraxanthine (CYP1A2) (Figure 5) (39,40).

Free energy profiles on DOPC membrane for this set of caffeine derivatives were calculated using COSMOmic 18. The nature of the chemical modification of the parent molecule caused different interactions of the metabolites with the membrane. Caffeine derivatives are metabolized in three distinct types of reactions: demethylation (theobromine, theophylline, paraxanthine), oxidation (6-

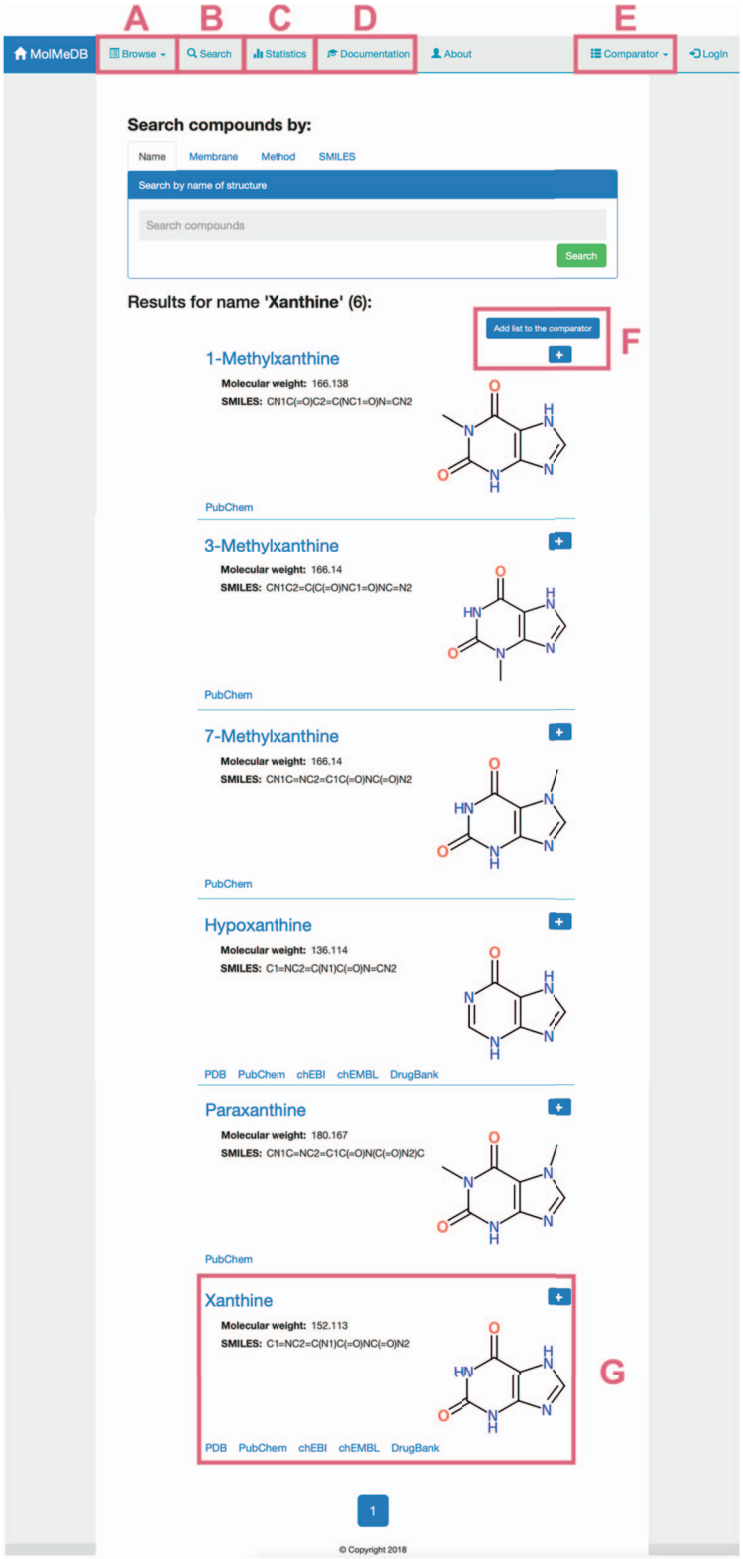

Figure 3. Layout of a page showing the toolbar of Browse/Search (**A**, **B**) utility along with menu items for Statistics (**C**), Documentation (**D**) and Comparator tool (**E**). Example of search utility for 'xanthine' molecule. Compounds with corresponding pattern of name are selected and displayed along with 2D structure (**G**). Target molecules can be directly added into molecule Comparator (**F**) by clicking on '+' sign.

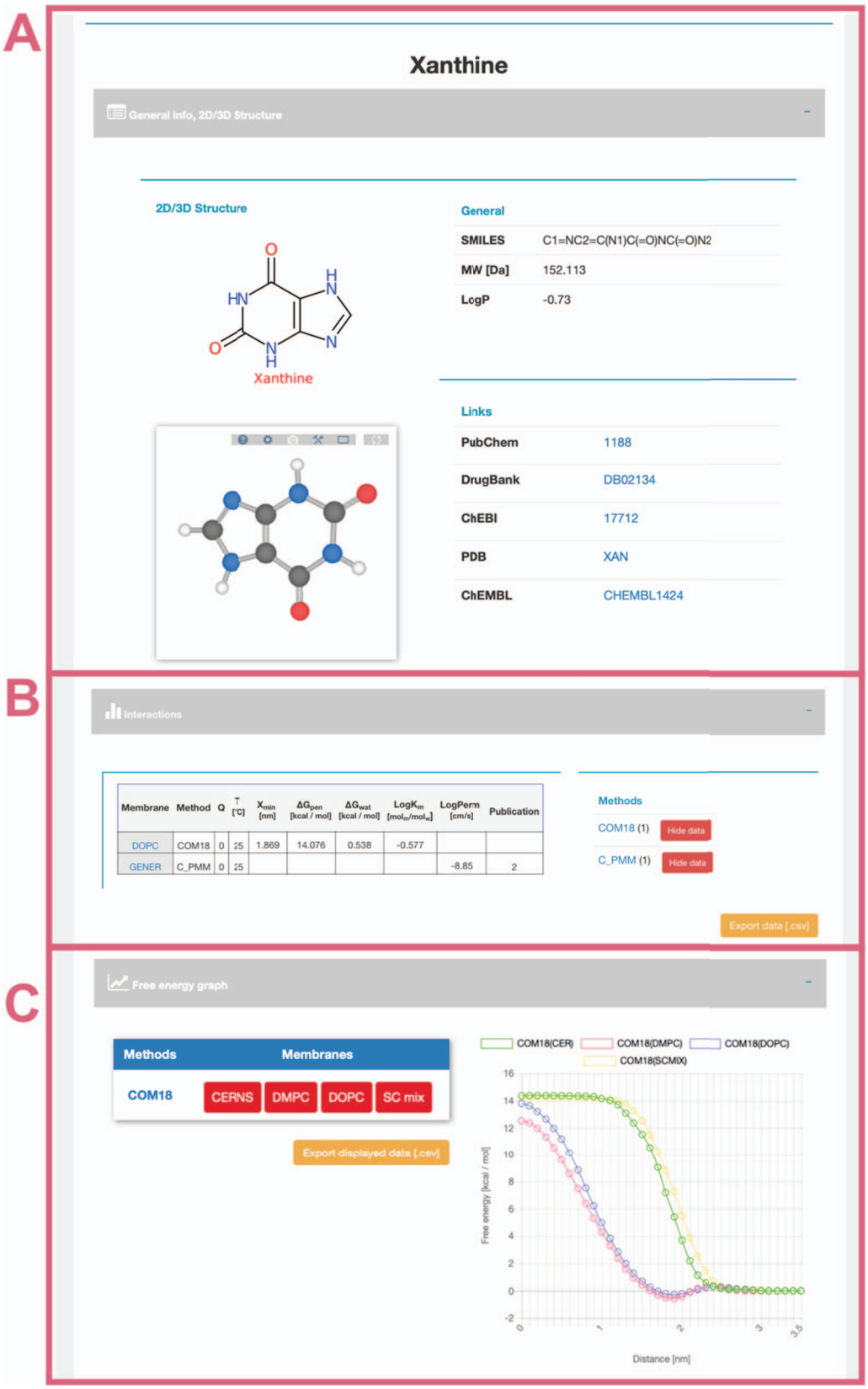

Figure 4. Interface of selected 'xanthine' molecule divided into separate panels for general information (**A**) about the molecule with its 2D and 3D structure and links to other databases; interactive table showing available data about molecule–membrane interactions (**B**) on position, partitioning, energy barrier and permeability coefficient for a given pair of method/membrane and charge; and interactive graph with available free energy profiles (**C**).

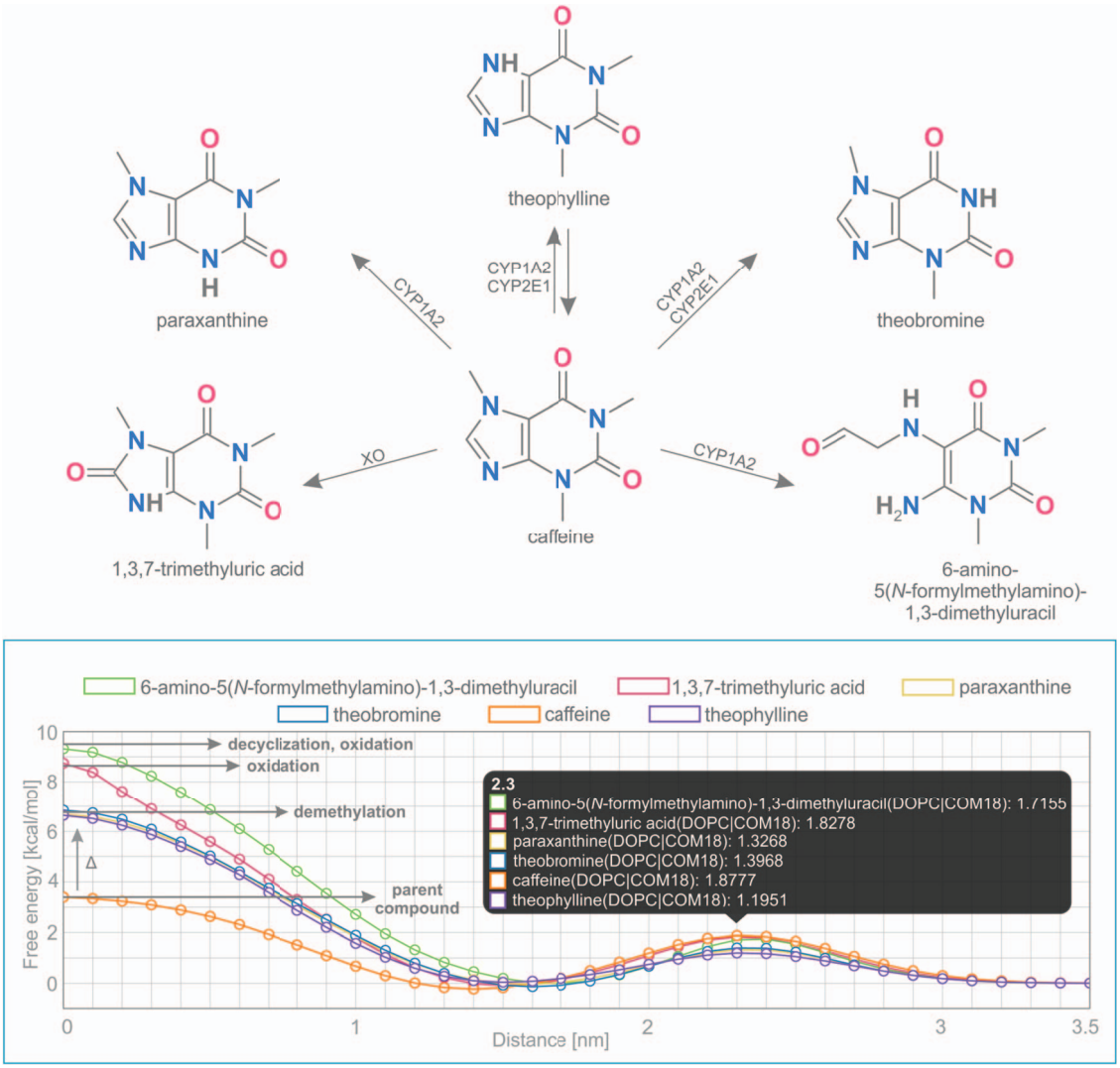

Figure 5. Comparison of free energy profiles of caffeine and its metabolites showing an increase of penetration barrier according to the type of metabolizing reaction and to the nature of chemical modification.

amino-5(*N*-formylmethylamino)-1,3-dimethyluracil, 1,3,7-trimethyluric acid) and decyclization (6-amino-5(*N*-formylmethylamino)-1,3-dimethyluracil). Here we show that individual types of caffeine metabolites exhibit distinguishable changes in free energy profiles (Figure 5). The lowest energetic barrier (ΔG_{pen}) is shown for caffeine as the parent compound, followed by all demethylated metabolites with an identical increase of penetration barrier by ~3.4 kcal/mol. Oxidized and oxidized/decyclized products experienced an even greater increase of penetration barrier compared with the original caffeine molecule by 5.4 and 5.9 kcal/mol, respectively.

Overall, all products of caffeine metabolism show a hindered passage through the membrane core as evidenced by the increase in the penetration barrier energy (ΔG_{pen}). On the other hand, the affinity of all molecules toward the membrane (ΔG_{wat}) remained almost the same, which is in concord with their very similar logP values. Finally, all metabolites shifted their energetic minima (Z_{min}) toward the membrane/water interface by 2 Å.

Comparison of methods The Comparator tool also allows a comparison of multiple methods/membranes with each other over selected compounds. Such type of comparison can be used to evaluate different theoretical approaches (e.g. PerMM, COM18) versus experimental data (e.g. BLM).

In this example, we show a comparison of permeability coefficient datasets obtained from theoretical PerMM and COSMOmic/COSMOperm 18 predictions and experimental BLM method for 101 neutral/unionized compounds on DOPC/generic phosphatidylcholine membrane. The user can reach the whole dataset for an individual Method-/Membrane via the Search tool and add it directly into the Comparator tool. Upon choosing the desired combination

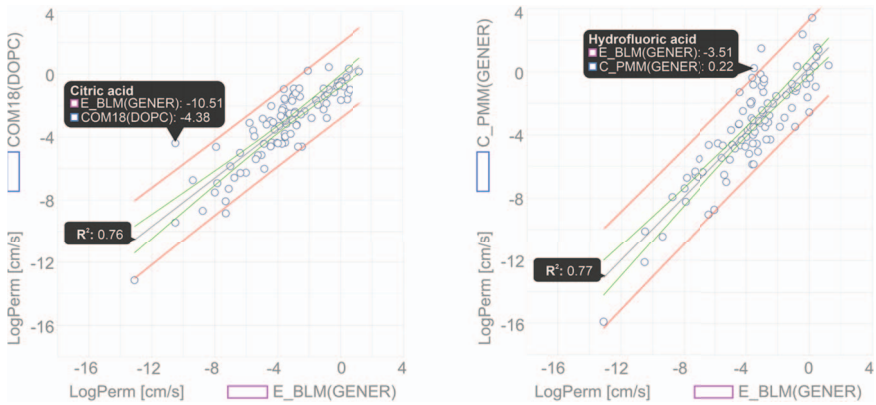

Figure 6. Comparison of permeability coefficients obtained from experimental BLM method and theoretical PerMM model. The figure was manipulated externally from downloaded data to add linear regression line shown in gray with confidence interval shown in red and prediction interval in green. Confidence interval was set to 95%.

of multiple Method/Membrane options and charge of molecules, the data can be plotted in an interactive window (Figure 6). Hovering a cursor over a data point shows the name of the compound and its plotted property. Figure 6 shows examples of permeability coefficients for Citric acid and Hydrofluoric acid. Linear regression fit was used here to determine the level of correlation between the two methods, obtaining the coefficient of determination (R^2) of 0.76 and 0.77 for COM18/BLM and PerMM/BLM respectively, while PerMM data show almost identical slope to the experimental data.

Discussion

MolMeDB is a unique, manually curated database on interactions of compounds with membranes. To date it contains more than 1200 compounds and 3600 molecule-membrane interactions obtained both theoretically and experimentally. MolMeDB stores multiple descriptors of molecule/membrane interactions and provides the tools for searching and browsing these data and their comparison. MolMeDB can prove to be a valuable resource for many research groups to benchmark the key data on molecule–membrane interactions, which are important in the fields of pharmacology, toxicology and molecular simulations. In the future, we plan to add further datasets and implement also the involvement of transporters and carriers. More complex statistical analysis within the selected datasets and further FAIRification of the data is anticipated in following versions of MolMeDB. We believe that MolMeDB can be a useful starting point, which can facilitate future studies devoted to a deeper understanding of biological roles of molecules on membranes and that it will attract the biological membrane community to establish a common ground for sharing open data in this field.

Availability and requirements

MolMeDB database is freely available at http://molmedb.upol.cz. The visualization of 3D structures with the LiteMol molecular viewer requires the browser to have WebGL enabled.

Funding

Czech Science Foundation [17-21122S]; ELIXIR CZ Research Infrastructure Project (MEYS) [LM2015047]; ERDF/ESF Project "Nanotechnologies for Future" [project CZ.02.1.01/0.0/0.0/16_019/0000754 to K.B.]; Palacký University Olomouc [IGA_PrF_2019_031 to M.Š. and M.M.]. Funding for the open access charge: Czech Science Foundation [17-21122S].

Conflict of interest. None declared.

References

1. Shevchenko,A. and Simons,K. (2010) Lipidomics: coming to grips with lipid diversity. *Nat. Rev. Mol. Cell Biol.*, **11**, 593–598.
2. Lomize,M.A., Pogozheva,I.D., Joo,H. *et al.* (2012) OPM database and PPM web server: resources for positioning of proteins in membranes. *Nucleic Acids Res.*, **40**, D370–D376.
3. Kozma,D., Simon,I. and Tusnády,E.E. (2012) PDBTM: protein data Bank of transmembrane proteins after 8 years. *Nucleic Acids Res.*, **41**, D524–D529.
4. Stansfeld,P.J., Goose,J.E., Caffrey,M. *et al.* (2015) MemProtMD: automated insertion of membrane protein structures into explicit lipid membranes. *Structure*, **23**, 1350–1361.
5. Postic,G., Ghouzam,Y., Etchebest,C. *et al.* (2017) TMPL: a database of experimental and theoretical transmembrane protein models positioned in the lipid bilayer. *Database*, **2017**, 1–7.
6. Sarti,E., Aleksandrova,A.A., Ganta,S.K. *et al.* (2019) EncoMPASS: an online database for analyzing structure and symmetry in membrane proteins. *Nucleic Acids Res.*, **47**, D315–D321.

7. Wishart,D.S., Feunang,Y.D., Guo,A.C. *et al.* (2018) DrugBank 5.0: a major update to the DrugBank database for 2018. *Nucleic Acids Res.*, **46**, D1074–D1082.
8. Williams,F.M. (2004) EDETOX. Evaluations and predictions of dermal absorption of toxic chemicals. *Int. Arch. Occup. Environ. Health*, **77**, 150–151.
9. Chen,L., Lian,G. and Han,L. (2010) Modeling transdermal permeation. Part I. predicting skin permeability of both hydrophobic and hydrophilic solutes. *AIChE J.*, **56**, 1136–1146.
10. Lomize,A.L. and Pogozheva,I.D. (2017) Prediction of passive membrane permeability and translocation pathways of biologically active molecules. *Biophys. J.*, **112**, 525a.
11. Paloncýová,M., Fabre,G., DeVane,R.H. *et al.* (2014) Benchmarking of force fields for molecule–membrane interactions. *J. Chem. Theory Comput.*, **10**, 4143–4151.
12. Tse,C.H., Comer,J., Wang,Y. *et al.* (2018) Link between membrane composition and permeability to drugs. *J. Chem. Theory Comput.*, **14**, 2895–2909.
13. Menichetti,R., Kanekal,K.H., Kremer,K. *et al.* (2017) In silico screening of drug-membrane thermodynamics reveals linear relations between bulk partitioning and the potential of mean force. *J. Chem. Phys.*, **147**, 125101.
14. Klamt,A., Huniar,U., Spycher,S. *et al.* (2008) COSMOmic: a mechanistic approach to the calculation of membrane−water partition coefficients and internal distributions within membranes and micelles. *J. Phys. Chem. B*, **112**, 12148–12157.
15. Bennion,B.J., Be,N.A., McNerney,M.W. *et al.* (2017) Predicting a drug's membrane permeability: a computational model validated with in vitro permeability assay data. *J. Phys. Chem. B*, **121**, 5228–5237.
16. Carpenter,T.S., Kirshner,D.A., Lau,E.Y. *et al.* (2014) A method to predict blood-brain barrier permeability of drug-like compounds using molecular dynamics simulations. *Biophys. J.*, **107**, 630–641.
17. Di,L., Kerns,E.H., Fan,K. *et al.* (2003) High throughput artificial membrane permeability assay for blood–brain barrier. *Eur. J. Med. Chem.*, **38**, 223–232.
18. Dickson,C.J., Hornak,V., Pearlstein,R.A. *et al.* (2017) Structure–kinetic relationships of passive membrane permeation from multiscale modeling. *J. Am. Chem. Soc.*, **139**, 442–452.
19. Endo,S., Escher,B.I. and Goss,K.-U. (2011) Capacities of membrane lipids to accumulate neutral organic chemicals. *Environ. Sci. Technol.*, **45**, 5912–5921.
20. Eyer,K., Paech,F., Schuler,F. *et al.* (2014) A liposomal fluorescence assay to study permeation kinetics of drug-like weak bases across the lipid bilayer. *J. Control. Release*, **173**, 102–109.
21. Lundborg,M., Wennberg,C.L., Narangifard,A. *et al.* (2018) Predicting drug permeability through skin using molecular dynamics simulation. *J. Control. Release*, **283**, 269–279.
22. Yazdanian,M., Glynn,S.L., Wright,J.L. *et al.* (1998) Correlating partitioning and caco-2 cell permeability of structurally diverse small molecular weight compounds. *Pharm. Res.*, **15**, 1490–1494.
23. Swift,R.V. and Amaro,R.E. (2013) Back to the future: can physical models of passive membrane permeability help reduce drug candidate attrition and move us beyond QSPR? *Chem. Biol. Drug Des.*, **81**, 61–71.
24. White,S.H. (1972) Analysis of the torus surrounding planar lipid bilayer membranes. *Biophys. J.*, **12**, 432–445.
25. Avdeef,A., Artursson,P., Neuhoff,S. *et al.* (2005) Caco-2 permeability of weakly basic drugs predicted with the double-sink PAMPA method. *Eur. J. Pharm. Sci.*, **24**, 333–349.
26. Gobas,F.A., Lahittete,J.M., Garofalo,G. *et al.* (1988) A novel method for measuring membrane-water partition coefficients of hydrophobic organic chemicals: comparison with 1-octanol-water partitioning. *J. Pharm. Sci.*, **77**, 265–272.
27. Kwon,J.-H., Wuethrich,T., Mayer,P. *et al.* (2009) Development of a dynamic delivery method for in vitro bioassays. *Chemosphere*, **76**, 83–90.
28. Banks,J.L., Beard,H.S., Cao,Y. *et al.* (2005) Integrated modeling program, applied chemical theory (IMPACT). *J. Comput. Chem.*, **26**, 1752–1780.
29. Řezáč,J. (2016) Cuby: an integrative framework for computational chemistry. *J. Comput. Chem.*, **37**, 1230–1237.
30. Klamt,A. and Diedenhofen,M. (2018) A refined cavity construction algorithm for the conductor-like screening model. *J. Comput. Chem.*, **39**, 1648–1655.
31. Paloncýová,M., DeVane,R.H., Murch,B.P. *et al.* (2014) Rationalization of reduced penetration of drugs through ceramide gel phase membrane. *Langmuir*, **30**, 13942–13948.
32. Paloncýová,M., Vávrová,K., Sovová,Ž. *et al.* (2015) Structural changes in ceramide bilayers rationalize increased permeation through stratum corneum models with shorter acyl tails. *J. Phys. Chem. B*, **119**, 9811–9819.
33. Steinbeck,C., Han,Y., Kuhn,S. *et al.* (2003) The chemistry development kit (CDK): an open-source java library for chemo- and bioinformatics. *J. Chem. Inf. Comput. Sci.*, **43**, 493–500.
34. Sehnal,D., Deshpande,M., Vařeková,R.S. *et al.* (2017) LiteMol suite: interactive web-based visualization of large-scale macromolecular structure data. *Nat. Methods*, **14**, 1121–1122.
35. Kim,S., Thiessen,P.A., Bolton,E.E. *et al.* (2016) PubChem substance and compound databases. *Nucleic Acids Res.*, **44**, D1202–D1213.
36. Berman,H.M., Westbrook,J., Feng,Z. *et al.* (2000) The protein data Bank. *Nucleic Acids Res.*, **28**, 235–242.
37. Hastings,J., Owen,G., Dekker,A. *et al.* (2016) ChEBI in 2016: improved services and an expanding collection of metabolites. *Nucleic Acids Res.*, **44**, D1214–D1219.
38. Gaulton,A., Hersey,A., Nowotka,M. *et al.* (2017) The ChEMBL database in 2017. *Nucleic Acids Res.*, **45**, D945–D954.
39. Arnaud,M.J. (2011) Pharmacokinetics and metabolism of natural methylxanthines in animal and man. *Handb. Exp. Pharmacol.*, 33–91.
40. Paloncýová,M., Berka,K. and Otyepka,M. (2013) Molecular insight into affinities of drugs and their metabolites to lipid bilayers. *J. Phys. Chem. B*, **117**, 2403–2410.

Volume 6
Number 5
1 May 2021
Pages 329–400

MSDE

Molecular Systems Design & Engineering

rsc.li/molecular-engineering

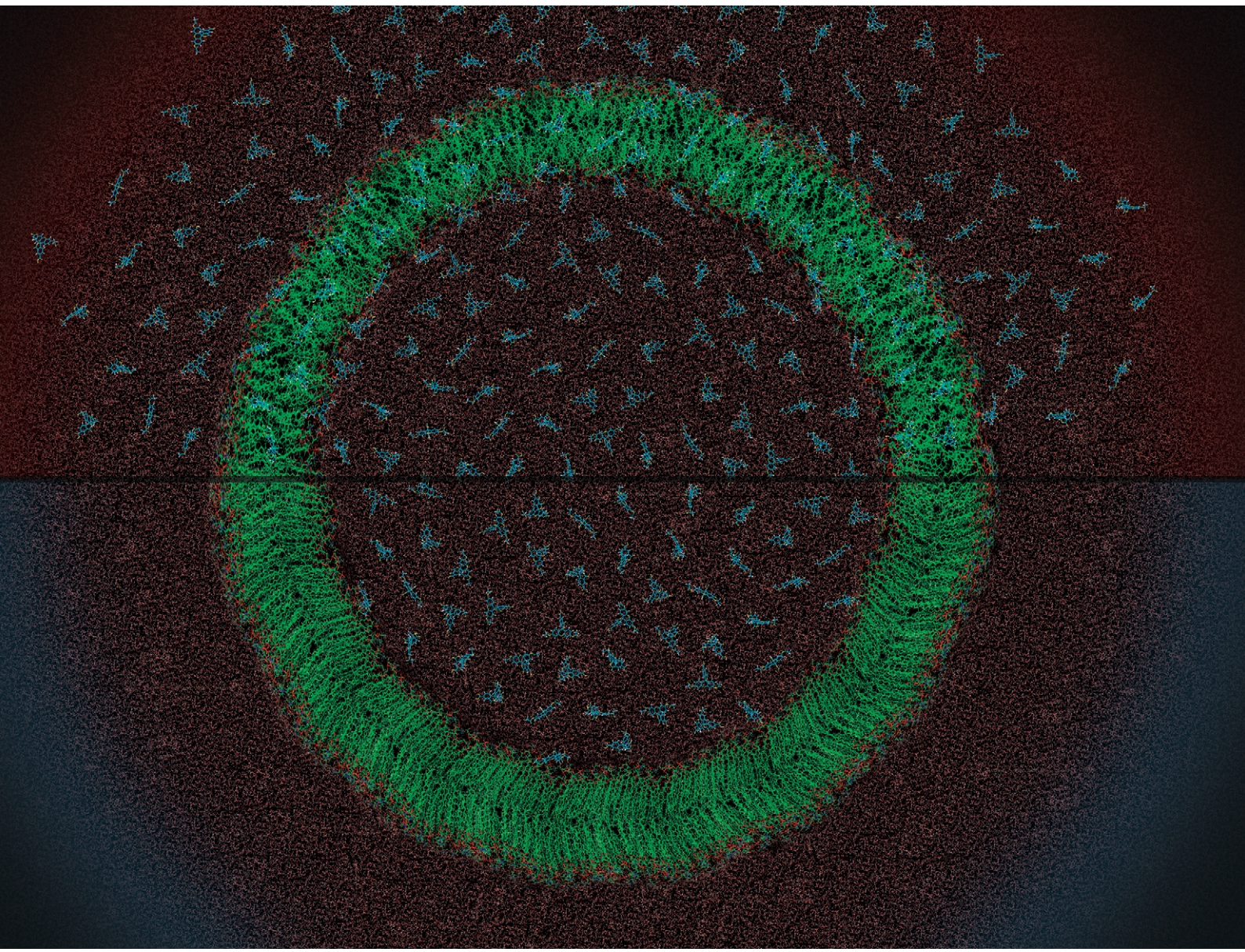

ISSN 2058-9689

ROYAL SOCIETY OF CHEMISTRY

PAPER

František Štěpánek, Karel Berka *et al.*
In silico screening of drug candidates for thermoresponsive liposome formulations

IChemE ADVANCING CHEMICAL ENGINEERING WORLDWIDE

MSDE

ROYAL SOCIETY OF CHEMISTRY

PAPER

View Article Online
View Journal | View Issue

Cite this: *Mol. Syst. Des. Eng.*, 2021, **6**, 368

In silico screening of drug candidates for thermoresponsive liposome formulations†

Martin Balouch, [a] Martin Šrejber, [bc] Marek Šoltys, [a] Petra Janská, [a] František Štěpánek *[a] and Karel Berka *[c]

Received 26th November 2020,
Accepted 8th February 2021

DOI: 10.1039/d0me00160k

rsc.li/molecular-engineering

Liposomal formulations can be advantageous in many scenarios such as targeted delivery to reduce the systemic toxicity of highly potent active pharmaceutical ingredients (APIs), to increase drug bioavailability by prolonging systemic circulation, to protect labile APIs from degradation in the gastrointestinal tract, or to improve skin permeation in dermal delivery. However, not all APIs are suitable for encapsulation in liposomes. Some of the issues are too high permeability of the API across the lipid bilayer, which may lead to premature leakage, too low permeability, which may hinder the drug release process, or too strong membrane affinity, which may reduce the overall efficacy of drug release from liposomes. Since the most reliable way to test API encapsulation and release from liposomes so far has been experimental, an *in silico* model capable of predicting API transport across the lipid bilayer might accelerate formulation development. In this work, we demonstrate a new *in silico* approach to compute the temperature-dependent permeability of a set of compounds across the bilayer of virtual liposomes constructed by molecular dynamics simulation. To validate this approach, we have conducted a series of experiments confirming the model predictions using a homologous series of fluorescent dyes. Based on the performance of individual molecules, we have defined a set of selection criteria for identifying compatible APIs for stable encapsulation and thermally controlled release from liposomes. To further demonstrate the *in silico*-based methodology, we have screened the DrugBank database, identified potent drugs suitable for liposome encapsulation and successfully carried out the loading and thermal release of one of them – the antimicrobial compound cycloserine.

Design, System, Application

Liposomes are spherical vesicles consisting of an aqueous core and a lipidic shell. They have been proven to be efficient as drug delivery carriers that enable the encapsulation, targeted delivery and controlled release of bio-active substances in the human body. However, the number of approved liposome-based pharmaceutical products has been limited by a lack of systematic formulation approaches: not all active pharmaceutical ingredients are suitable for liposome encapsulation, and the identification of suitable compounds has been purely empirical so far. The present work describes a systematic computational methodology that makes it possible to determine the suitability of bio-active compounds for liposomal formulation. By the combination of molecular dynamics simulation to construct a digital twin phospholipid membrane, and quantum chemistry based calculations to determine the permeation rate of a given molecule through the membrane as function of temperature, it is possible to screen a large number of candidate compounds from the DrugBank database and identify those that can be encapsulated into, and released from liposomes. The computational methodology has been validated experimentally and its applicability has been demonstrated using the antibiotic cycloserine.

1 Introduction

Liposomes are spherical vesicles containing an internal aqueous cavity enclosed by a bilayer usually made of phospholipids, often with sterols. At low temperatures, the lipid bilayer exists in an ordered state and is non-permeable for hydrophilic payloads; the content of the internal cavity is trapped inside and protected from the outside environment.[1] Therefore, liposomes can be used as carriers for the encapsulation and controlled release of active substances including small-molecule drugs,[2] biomolecules[3] and genes,[4,5] or as building blocks for more complex drug delivery

[a] *Department of Chemical Engineering, University of Chemistry and Technology, Technická 3, 166 28 Prague 6, Prague, Czech Republic.*
E-mail: frantisek.stepanek@vscht.cz
[b] *Czech Advanced Technology and Research Institute, Palacký University Olomouc, Křížkovského 511/8, 779 00 Olomouc, Czech Republic*
[c] *Department of Physical Chemistry, Faculty of Science, Palacký University Olomouc, 17. listopadu 12, 771 46 Olomouc, Czech Republic.*
E-mail: karel.berka@upol.cz

† Electronic supplementary information (ESI) available: Analysis of MD simulations, COSMOmic calculation workflow, calculation of permeability coefficients with COSMOperm, rationalization of time of permeation, calculated permeability and partition coefficients, explanation of cycloserine protonation pattern. See DOI: 10.1039/d0me00160k

systems.[6] Beyond pharmaceutics, liposomes find applications in cosmetic[7] or nutraceutical[8] formulations. To this day, liposomes were successfully used in several FDA approved products available on the market.[9]

The properties of liposomes can be tailored to specific delivery and release mechanisms.[8,10–12] Among the most critical parameters affecting the storage stability and the final application properties of liposomes are the bilayer composition, lamellarity and size.[1,13,14] These parameters can be influenced by the liposome preparation method, which typically involves the dissolution of lipids in an organic solvent and subsequent dispersion into aqueous media[15] with or without relying on membrane permeation of the encapsulated solute.[16] The solute permeation mechanism at the point of use can include spontaneous loss of lipid bilayer integrity upon interaction with living cells[17] or an externally triggered event such as local hyperthermia.[10] Depending on its composition, the lipid bilayer has a phase transition temperature at which it changes from a highly ordered into a disordered state where it becomes significantly more permeable for the encapsulated solutes.[18] This transition between states is usually reversible,[19] and can be triggered by incorporated magnetic nanoparticles[20] stimulated by an external magnetic field. This offers interesting possibilities for customised controlled release scenarios, *e.g.* in theranostics.

However, the actual permeability through the lipid bilayer is specific to the encapsulated compound and strongly depends on the liposome composition. The encapsulated compound needs to permeate through the bilayer to escape the liposome when heated, but it should not permeate when the lipidic bilayer is in the ordered state. The occurrence of the following cases makes a compound incompatible with a given liposome composition: (i) it is permeable not only in the disordered state but also in the ordered state, resulting in premature leakage; (ii) a strong repulsion between the bilayer and the compound will prevent permeation even in the disordered state; (iii) a strong attraction towards the bilayer will not permit the compound to be released. Predicting these behaviours for specific compounds in combination with a particular lipid bilayer composition and its physical state is a non-trivial task and exploring all the possible compositions experimentally would require an extensive parametric study. Formulation optimisation by trial-and-error is therefore extremely time-consuming and often leads to the rejection of the entire liposome formulation route for a given compound simply because a limited number of experiments performed within a random sub-region of the parametric design space did not result in a "hit".

Recently, *in silico* molecular modelling became increasingly feasible as an accurate predictive tool, reducing the need for extensive experimental parametric studies during formulation development.[21,22] The availability of computational power in combination with efficient algorithms made it possible to construct atomistic models of lipid bilayers based on molecular dynamics simulations,[23,24] making *in silico* models a realistic alternative to physical experiments. Hence, the aim of the present work was to develop and validate an *in silico* tool specifically for the case of encapsulation and thermally induced release of small-molecule payloads from liposomes. The proposed strategy was to utilise a computational model[25,26] to construct a virtual three-component phospholipid bilayer in different conditions and states (*i.e.* below and above its phase transition temperature) using molecular dynamics, and then to predict the permeability of a set of compounds through the bilayer using quantum chemistry based statistical thermodynamic computation. The calculated predictions were then validated by conducting physical experiments using liposomes loaded with the same compounds – a homologous series of fluoresceins. Once the model was experimentally validated, a series of potent drug molecules from the DrugBank database[27] were analysed by the computational model to predict which of them might be suitable for liposome encapsulation and temperature-responsive release. Based on the *in silico* selection, antimicrobial compound cycloserine was successfully formulated in liposomes, and its thermo-responsive release was demonstrated experimentally.

2 Methods

2.1 Computational methods

2.1.1 Molecular dynamics simulations of lipid bilayers. All molecular dynamic (MD) simulations were performed using the GROMACS 4.5.4 software package.[28] Model of a membrane mixture containing premixed 1,2-dipalmitoyl-sn-glycero-3-phosphocholine (DPPC) : 1,2-dipalmitoyl-sn-glycero-3-phosphoglycerol (DPPG) : cholesterol (Chol) at a molar ratio of 75 : 10 : 15 was created using an in-house script with a total number of 128 lipids (64 lipids per leaflet). For simulations of the lipid bilayer, the Slipids parameters[29] were used along with TIP3P water model.[30] Na^+ and Cl^- counterions were added to maintain electroneutrality of the system and to reach physiological concentration. Each bilayer system without solute was simulated for 250+ ns until equilibrium was reached (see time evolution of the area of lipid at ESI† Fig. S1.1). The temperature was kept constant using the Nosé–Hoover thermostat with a coupling constant of 0.5 ps.[31,32] The pressure was kept constant at 1 atm by Parrinello–Rahman barostat and semi-isotropic coupling with a coupling constant of 10 ps and isothermal compressibility of 4.5×10^{-5} bar^{-1}.[33] The long-range electrostatic interactions were calculated using the particle-mesh Ewald scheme with a 1.6 nm cutoff.[34] The cutoff for Lennard-Jones interactions was set to 1.0 nm with switching the function to zero at 1.5 nm. The LINCS algorithm was used to constrain all bonds.[35] Periodic boundary conditions were applied in all directions. The temperature dependence of membrane model was simulated in the range between 293 K and 333 K (Fig. 1).

2.1.2 COSMOmic/COSMOperm calculations of solute permeation. The LigPrep and MacroModel packages[36,37] were used to generate neutral conformers of compounds in vacuum using the OPLS_2005 force field.[38] For each compound, a maximum of 10 conformers (within 5 kcal mol^{-1} of conformer with the lowest energy and RMSD at least

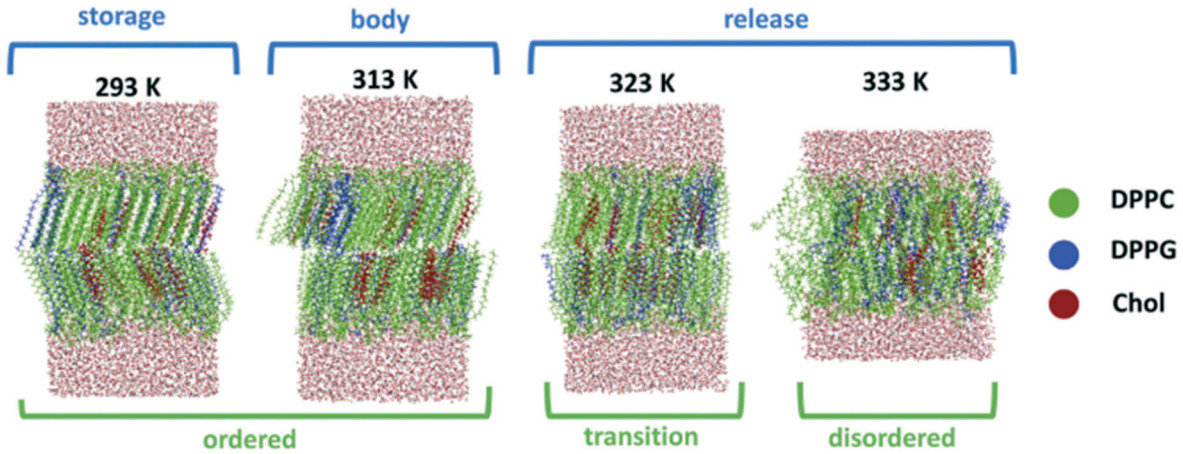

Fig. 1 Structures of mixed DPPC : DPPG : Chol (75 : 10 : 15) membranes obtained by MD simulations at various temperatures corresponding to liposome storage, human body temperature and release of compounds from liposomes.

0.2 nm between individual conformers) were selected based on MCMM/LMC2 conformation searching algorithm with Monte Carlo structure selection. For each conformer, a subsequent DFT/B-P/cc-TZVP vacuum and COSMO optimisation were carried out using Turbomole 6.3 (ref. 39) implemented in cuby4 framework[40] followed by a single-point energy DFT/B-P/cc-TZVP calculation with fine grid option to obtain the COSMO files.

The overall .mic files for lipid bilayers were obtained by fitting individual lipid COSMO files to an average of 10 bilayer structures from the MD simulations. For each compound, conformer/lipid bilayer system COSMOmic/COSMOperm X18 calculations[41,42] were performed to obtain averaged free energy profiles and hence the partition ($\log K_{lip/wat}$) and permeability ($\log P_{erm}$) coefficients. The procedure of these calculations is described in ESI.† Initially, a set of 5 fluorescent chemical compounds was used for validation purposes: fluorescein, 5-carboxyfluorescein, 6-carboxyfluorescein, fluorescein-5-isothiocyanate, and calcein. Once the computational model was validated experimentally (section 2.2), the permeation of a further 56 compounds selected from the DrugBank database was computed and used as a basis for proposing criteria for drug selection with respect to their suitability for liposome encapsulation and release. These 56 compounds were selected based on their high toxicity on living organisms accompanying their biological activity (*e.g.* antimicrobial) and potential benefits of a liposomal formulation. A full list of the compounds is provided in section 3.4. Calculations of all molecules were performed ten times. The most promising drug candidate was then selected based on its $\log K_{lip/wat}$, and $\log P_{erm}$ values and its liposomal formulation and thermoresponsive release were demonstrated experimentally (section 2.3).

2.2 Experimental validation of model predictions

2.2.1 Materials. Cholesterol (Chol, >99%), ammonium hydroxide solution (28–30%), phosphate-buffered saline (PBS) tablets, 5-(6)-carboxyfluorescein (5(6)-CF, 95%), calcein (C, >95%), D-cycloserine, fluorescein (F, 95%), fluorescein-5-isothiocyanate (FITC, 90%) and TRITON® X-100 were purchased from Sigma-Aldrich. Ethanol (for UV spectroscopy, 99.8%), chloroform (p.a.), sodium chloride (>99%), sodium hydroxide (p.a.), methanol (p.a.) and hydrochloric acid (HCl, 35%, p.a.) were purchased from penta. Dipalmitoylphosphatidyl-choline (DPPC) and sodium dipalmitoyl-phosphoglycerol (DPPG) were purchased from Corden Pharma. All chemicals were used as received. Deionised water (Aqual 25, 0.07 μS cm^{-1}) was used for all reactions and treatment processes.

2.2.2 Preparation of liposomes. Liposomes were prepared using the Bangham method. Briefly: 10 mg of lipid and cholesterol mixture was dissolved in 2 mL of chloroform : methanol mixture (2 : 1) in a 25 mL round flask. The mixture was evaporated in a rotary evaporator at a constant temperature of 55 °C and gradually lowering pressure from atmospheric to 150 mbar. The dried lipids formed a film around the flask. The sample was then kept under vacuum for at least 12 hours. For further rehydration, 2 mL of a hydration phosphate buffer solution containing the substance to be encapsulated was added to the flask (the compounds and their concentrations are listed in Table 1). The flask's content was then heated and stirred using a vortex shaker until no visible lipid film pieces were present on the flask walls. 1 mL of the obtained lipid suspension was then transferred to a liposome extrusion device (Avanti Polar Lipids), heated to 69 °C and extruded through a porous membrane with 800 nm pores 21 times to decrease and unify

Table 1 Solutions used for the lipid film hydration

Fluorescent dye	Abbreviation	Concentration [mg mL^{-1}]	pH
Calcein	Cal	5.0	7.4
5(6)-Carboxyfluorescein	5(6)-CF	7.5	7.4
Fluorescein	F	2.5	7.4
Fluorescein-5-isothiocyanate	FITC	0.1	7.4

the size of the formed liposomes. The size distribution of the prepared liposomes was measured using the Malvern Zetasizer. The liposomes were also visualised using transmission electron microscopy (TEM, Jeol JEM-1010, acceleration voltage 80 kV).

2.2.3 Measurement of thermo-responsive release. For experimental validation of the computational model, fluorescein derivatives with systematically varying chemical properties have been chosen (Table 1). Since the release measurement is based on the dye's fluorescence emission dissolved in an aqueous supernatant, only water-soluble fluorescent dyes were used. Four fluorescein derivatives were found to be sufficiently soluble for this purpose. From these four compounds, near-saturated water solutions were made and used for hydration of the lipid film to form liposomes. The actual concentrations and pH values used for liposome encapsulation are summarised in Table 1.

The measurement of the thermally induced release of these substances from the liposomes was based on repeated liposome separation by centrifugation and fluorescence emission intensity measurement of the supernatant (Cary Eclipse Fluorescent Spectrophotometer, Agilent). First, four cycles of centrifugation, supernatant removal, dilution and redispersion were conducted to remove any non-encapsulated dye present in the samples after liposome preparation. After liposome extrusion, approximately 1 mL of the liposome dispersion was transferred to several 2 mL Eppendorf vials and cooled to room temperature. The samples were then filled up to the to 2 mL mark with a buffer solution of the same ionic strength as the hydration solution. Then, centrifugation at 5000 RCF (Minispin, Eppendorf AG Hamburg) for 15 minutes was performed. The supernatant was removed and replaced with a fresh buffer solution, and the liposomes were redispersed and again centrifuged. After the last centrifugation, the supernatant's fluorescence emission intensity was measured to verify the completion of the purification. The excitation wavelength was set to 490 nm, and the emission spectra were measured at the maximum intensity for each dye (between 515 nm and 525 nm). Based on the calibration using the same settings, the concentration of dye was calculated. The amount of released dye was calculated from the difference in measured dye quantities before and after release.

To determine the total quantity of the encapsulated dye inside the liposomes, 2 μL of TRITON® X-100 was added to the sample, which resulted in membrane destabilisation and release of all the dye that was present either in the liposomal cavity or in the membrane. In order to measure thermally induced release from liposomes, the purified samples were heated to 65 °C for 1 hour to bring the liposome membranes into the disordered state and make them more permeable. In both measurements (membrane destruction using TRITON® and thermal release), the samples were centrifuged once more, and the fluorescence emission intensity of the supernatant was measured. From the difference in the fluorescence emission before and after TRITON® addition or heating, the fluorescent dye's released quantity was calculated.

Since each of the four fluorescent dyes was used at different concentrations (due to difference in their aqueous solubility), a theoretical loading capacity for each dye was calculated to allow effective comparison of the samples. For simplicity, it was considered that all phospholipids used in the experiment were DPPC, and the liposome size was uniform at 800 nm in diameter. The area occupied by a single DPPC lipid was considered to be 0.6 nm^2.[43] From the known area of one lipid and the known surface area of one liposome, the quantity of DPPC molecules forming one liposome was calculated. With the known mass of lipids in one experiment (10 mg), the molar mass of DPPC (734 g mol^{-1}) and the concentration of fluorescent dye in the hydration solution, the theoretical loading capacity could then be obtained from eqn (1):

$$m_F/m_{DPPC} = 1000cA_1N_Ad/(12M_{DPPC}) \quad (1)$$

where m_F/m_{DPPC} is the theoretical capacity in μg of solute per 1 mg of lipids, c is the fluorescent dye concentration in mg mL^{-1}, A_1 is the area of one DPPC molecule, d is the mean liposome diameter, N_A is the Avogadro constant and M_{DPPC} is the molar mass of DPPC (734 g mol^{-1}). In this theoretical calculation, it was assumed that the hydration solution was encapsulated inside all liposome cavities. Upon release, the entire volume of the encapsulated solution and the dissolved dye's corresponding quantity was considered the theoretical maximum capacity of the liposomes prepared.

For the possibility of comparison between experiments and calculations made for unionised species, the fraction of unionised species was calculated using MarvinSketch 20.16.[44]

2.2.4 Visualisation of membrane partition and release. Laser scanning confocal microscopy (Olympus Fluoview FV1000 with Canon EOS 100D camera) was used to visualise the liposomes and their surrounding medium both before and after the thermally induced release of the encapsulated dyes. Furthermore, liposomes loaded with all four used dyes, centrifuged and redispersed were also visualised. The prepared liposomes were not extruded through the 800 nm membrane after keeping their size large (for easier observation). For the confocal images Olympus UPLSAPO Objective 40×, excitation wavelength 405 nm and fluorescence detection 505–540 nm were used.

2.3 Liposomal formulation of drug identified by *in silico* model

The most promising substance identified by the *in silico* model from a sample of 56 entries in the DrugBank database (cycloserine) was encapsulated into liposomes as described in section 2.2. The stability of liposomes at storage temperature and the ability to release the substance above the lipid bilayer's phase transition temperature was demonstrated by measuring the proliferation of bacteria *E.coli* using the

resazurin assay.[45] The bacteria suspension was grown overnight in LB media at 37 °C, shaken at 200 rpm. The inoculate was diluted to the appropriate cell density (OD = 0.06) and seeded on 96-well plates. The assay composed of a row of samples exposed to liposomes before release, liposomes after heat release (60 °C for 30 minutes), liposomes after membrane disruption by TRITON® as a positive control, and a row of bacteria with an added antibiotic (50 μg mL^{-1} kanamycin) as a further positive control. Each well was filled with 100 μl of the sample (liposomes loaded with 10 mg mL^{-1} cycloserine, repeatedly diluted and centrifugated). Then, 20 μl of diluted bacterial suspension was added into all wells and mixed thoroughly. Samples after release and antibiotics were performed in triplicates. Sample before the release in duplicates of both samples, which were later used for release. After overnight incubation at 37 °C, 20 μL resazurin was added to all wells and incubated at 37 °C for another 4 h. Colour changes were observed. Fluorescence measurements were performed in a spectrofluorometer (Infinite 200 PRO, Tecan Austria) at 560 nm excitation and 590 nm emission wavelength. Bacteria without any antibiotics were used as a negative control.

3 Results

3.1 Computational studies

3.1.1 MD simulations of bilayer state at various temperatures. Molecular dynamics simulations of the mixed DPPC : DPPG : Chol (75 : 10 : 15 molar ratio – chosen from previous experimental experiences as ideal composition for encapsulation of 5(6)-CF[10]) membrane model were carried out at temperatures corresponding to the liposome storage temperature (293 K), the approximate body temperature in the side of inflammation (313 K) and the temperatures presumed to be required for the release of encapsulated solute (323 K and 333 K). At lower temperatures for the liposome storage, the membranes were found to be in a highly ordered phase (Fig. 1). An increase of temperature by 20 K to the body temperature did not result in any phase ordering changes, and the membrane remained in an ordered phase. The dependent simulations showed a sharp change in the membrane structure between 323 K and 333 K, where a phase shift into the disordered phase was observed. This shift is located slightly higher than the experimentally observed phase transition temperature of this membrane mixture[10] (315 K). Above 323 K the lipid bilayer formed a disordered structure preferable for the release of the encapsulated compounds from the internal liposomal cavity.

3.1.2 COSMO-based partitioning and permeability calculations for fluorescent dyes. The values of temperature-dependent partition coefficients $\log K_{lip/wat}$ obtained from the COSMOmic calculations compared in Fig. 2A showed no significant changes with increasing temperature for the given fluorescent compounds. The compounds' lipophilic character increased in the order of Cal < 6-CF < 5-CF < F < FITC but the drug partitioning between water and the lipidic membrane was not found to be much sensitive to temperature changes while all the compounds became only slightly more hydrophobic at elevated temperatures.[46] In contrast, the permeability coefficients $\log P_{erm}$ obtained from COSMOperm calculations have shown a significant increase with the temperature of about two orders of magnitude within 40 K difference and varied widely between the compounds (Fig. 2B). Therefore, we have analysed each dye's performance in both partitioning and permeability at the lowest (293 K) and the highest (333 K) temperature in more detail.

Each fluorescent derivative has shown different behaviour in terms of the partitioning coefficient and permeability. The

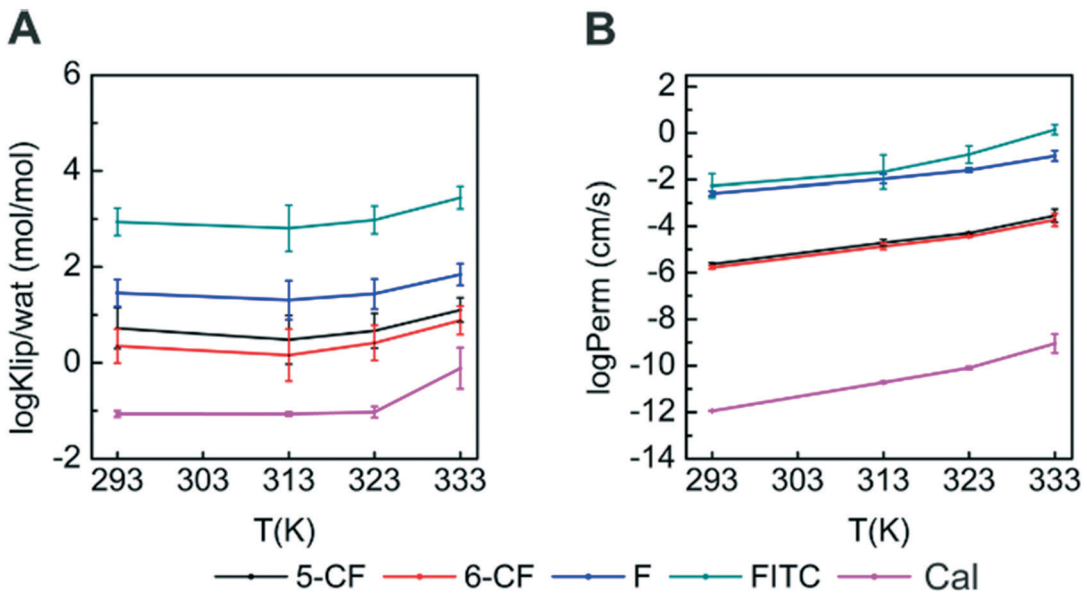

Fig. 2 Computed temperature dependence of membrane/water partition coefficients $\log K_{lip/wat}$ [mol mol^{-1}] (panel A) and permeability coefficients $\log P_{erm}$ [cm s^{-1}] (panel B) for a series of five fluorescent dyes on the DPPPC : DPPG : Chol mixed membrane.

dye with the highest partition coefficient is fluorescein-5-isothiocyanate (FITC), having a $\log K_{lip/wat}^{293K} = 2.94 \pm 0.28$. This would suggest a strong presence of the dye within the membrane while only a small amount of FITC would remain encapsulated in the internal aqueous cavity of the liposome. At the same time, FITC would easily permeate through the membrane due to its high permeability coefficient ($\log P_{erm}^{293K} = -2.26 \pm 0.52$) even at low temperature. As such, FITC does seem suitable for encapsulation in the membrane cavity but not for temperature-controlled release in the used lipid mixture. For fluorescein (F), a slightly lower partition coefficient $\log K_{lip/wat}^{293K} = 1.45 \pm 0.28$ would suggest a shift of equilibrium towards the aqueous phase. Therefore, it is likely that fluorescein would prefer equivalent partitioning into the aqueous core and the lipidic membrane. However, the high permeability at all temperatures ($\log P_{erm} = -2.59 \pm 0.09$, -1.60 ± 0.09 and -0.98 ± 0.22 at 273 K, 323 K and 333 K, respectively) again does not make it a promising candidate for liposome encapsulation.

Relatively low partition coefficients were observed for 5-carboxyfluorescein (5-CF) and 6-carboxyfluorescein (6-CF), namely $\log K_{lip/wat}^{293K} = 0.72 \pm 0.43$ and 0.35 ± 0.36, respectively. Therefore, these compounds should prefer the aqueous phase within the liposomal cavity. Moreover, their permeability is nicely temperature-dependent since they have a low permeability at low temperatures ($\log P_{erm}^{293K} = -5.64 \pm 0.06$ and -5.78 ± 0.06, respectively) and two orders of magnitude higher permeability at high temperatures ($\log P_{erm}^{333K} = -3.55 \pm 0.28$ and -3.73 ± 0.27, respectively). As a result, these two compounds appear to be suitable candidates that could provide stable liposomal encapsulation during storage, followed by temperature triggered release.

Finally, calcein (Cal) shows the lowest values for both partitioning and permeation coefficients. The lowest partitioning $\log K_{lip/wat}^{293K} = -1.07 \pm 0.07$ at all temperatures among all dyes suggests predominant encapsulation of the drug in the water phase within the liposomal cavity, which seems like a great property to block drug release from the storage liposome. However, calcein also shows an extremely low ability to permeate through the bilayer and leave the liposome even at elevated temperatures ($\log P_{erm}^{333K} = -9.05 \pm 0.41$). Therefore, calcein is probably a wrong candidate for thermally controlled drug release, although it might be suitable for other release mechanisms.

These *in silico* predictions suggest that out of the tested set of fluorescent dyes, the most promising candidates for encapsulation and temperature-controlled release from DPPC : DPPG : Chol (75 : 10 : 15 molar ratio) liposomes are 5-CF and 6-CF, while FITC and F seem to be too permeable and Cal will not be able to permeate even at higher temperatures.

3.2 Experimental verification

3.2.1 Liposome properties. To validate our theoretical predictions, we have prepared dye-loaded liposomes as described in section 2.2. The prepared liposomes' size was centred at 800 nm irrespective of the loaded dye (Fig. 3A). However, a fraction of liposomes with a size around 100 nm was present in all samples and confirmed by TEM analysis (Fig. 3B). We suggest that the smaller liposomes (100 nm) do not settle during the centrifugation steps and are disposed of together with the supernatant during the purification process. This can be a possible source of losses of the encapsulated substance and thus somewhat lower measured quantities of the released dye, as discussed below.

3.2.2 Encapsulation and release experiments with fluorescent dyes. The loading of 5(6)-carboxyfluorescein into liposomes was relatively efficient, achieving 73 ± 35 μg_{dye} mg_{lipid}^{-1}, representing approximately 30% of the theoretical capacity (Table 2). The dye remained stable inside the liposomes when kept at the storage temperature (Fig. 4A), but it was readily released upon heating to 333 K (62 ± 8 μg_{dye} mg_{lipid}^{-1}). This shows that 5(6)-CF is an excellent example of a molecule for encapsulation in liposomes with thermally controlled release, confirming the theoretical calculations. From the comparison between theoretical and experimental results, we can conclude that $\log P_{erm} = -5.6$ at 293 K is not high enough to allow premature membrane permeation. On the other hand, $\log P_{erm} = -3.6$ at 333 K seems to be sufficient for release – this opens a window for applicability.

On the other hand, fluorescein was visibly washed out from the liposomes during the purification procedure, which consisted of repeated centrifugation and dilution steps performed at 293 K. Ultimately, only a tiny fraction of the theoretical loading capacity was retained in the liposomes (0.3 ± 0.1 μg_{dye} mg_{lipid}^{-1}), and there was no observable thermal release (Table 2). This is because the liposomal membrane is permeable for fluorescein even in 293 K and therefore all of F is washed out during dilution before heating. These results do not qualify fluorescein as a suitable compound for liposome formulation using the chosen lipid membrane composition due to too high permeability even at the storage temperature ($\log P_{erm}^{293K} = -2.6$). The small amount of fluorescein detected after TRITON® treatment must have resided in the membrane (Fig. 4B). Such membrane partitioning is consistent with the *in silico* model, which predicted a significantly higher membrane affinity for fluorescein ($\log K_{lip/wat}^{293K} = 1.45$) compared to 6-CF ($\log K_{lip/wat}^{293K} = 0.35$).

The effect of high membrane partitioning coefficient was even more pronounced in the case of FITC ($\log K_{lip/wat}^{293K} = 2.94$). Although FITC was visibly encapsulated into liposomes (Fig. 4C), no release upon heating was detected (Table 2). Despite high permeability prediction for FITC, on par with fluorescein as shown in Fig. 2B. Only when a more invasive method of membrane disruption with TRITON® was used, a significant release of FITC was observed (0.6 ± 0.2 μg_{dye} mg_{lipid}^{-1}, being 18% of the theoretical capacity). Similarly to fluorescein, FITC resided in the membrane rather than in the aqueous core. It can be concluded that solutes with a high partitioning coefficient toward the lipid membrane are not

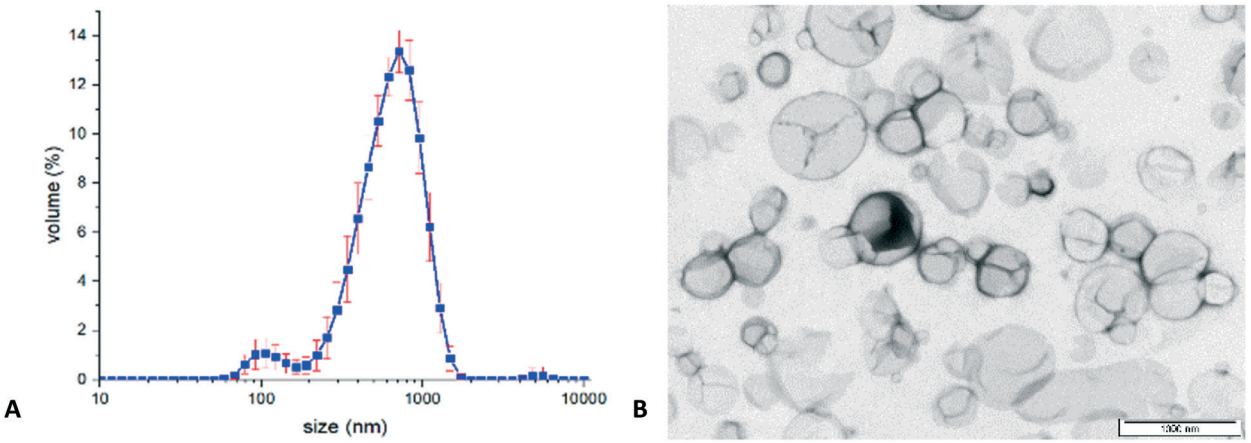

Fig. 3 Volume size distribution (panel A) and TEM micrograph (panel B) of the prepared liposomes. The scale bar represents 1000 nm.

Table 2 Measured release from liposomes after heating

Dye	pH[a]	Released after heating (μg_{dye} mg_{lipid}^{-1})	Released after membrane disruption (μg_{dye} mg_{lipid}^{-1})	Theoretical capacity (μg_{dye} mg_{lipid}^{-1})	Fraction of unionized species (%)
5(6)-CF	7.4	62 ± 8	73 ± 35	246	0.03%
F	7.4	0.0	0.3 ± 0.1	82	95.4%
FITC	7.4	0.0	0.6 ± 0.2	3.3	95.4%
Cal	7.4	0.03 ± 0.02	0.4 ± 0.1	164	<0.01%

[a] Hydrating solution: 10 mM PBS adjusted to pH 7.4.

suitable for thermally controlled release from liposomes. This does not necessarily make lipophilic molecules unsuitable for liposomal formulations in general, but it means they are not good candidates for temperature-controlled release.

Finally, let us consider calcein. In terms of permeability predicted by the *in silico* model, calcein was at the opposite end of the spectrum than fluorescein or FITC, with a very low value of permeability even at elevated temperatures ($\log P_{erm}^{333K} = -9.05$) and also the lowest membrane affinity from all the investigated fluorescent dyes ($\log K_{lip/wat}^{293K} = -1.07$). Consequently, only 0.02% of the theoretical capacity was released after heating, and this value did not substantially improve even after membrane disruption by TRITON® (Table 2). This implies that calcein was probably not present in most of the liposomes already when the liposomes were formed, a hypothesis confirmed by fluorescence microscopy of "raw" liposomes observed just after the lipid hydration step (Fig. 4D, inset). The clearly visible empty liposomes surrounded by concentrated calcein solution contrast with a similar view of 5(6)-CF liposomes (Fig. 4A, inset) where the fluorescence intensity inside and outside the raw liposomes was essentially identical.

The results of these visualisation experiments lead to a proposed mechanism of "solute rejection" during the liposome hydration step, shown schematically in Fig. 5. While well-permeating molecules such as 5(6)-CF can readily enter into the nascent liposome's cavity, poorly permeating substances such as calcein cannot. Therefore, the knowledge of temperature-dependent membrane permeability provided by the *in silico* model is very valuable not only for predicting the liposome behaviour during storage and temperature controlled release but also for assessing the chances that liposomes loaded by a given substance can be prepared at all.

3.3 Generalisation of rules for drug loading and thermal release from liposomes

The combination of *in silico* predictions and experimental findings discussed above makes it possible to define a set of rules for the suitability of compounds for incorporating temperature-controlled liposomal drug delivery systems. The *in silico* model provides two temperature-dependent coefficients for each candidate molecule: the partitioning towards the lipids ($\log K_{lip/wat}$) and the membrane permeability ($\log P_{erm}$). Given that in unilamellar liposomes, the lipidic shell volume is typically between 100× and 10 000× lower than the aqueous core, a $\log K_{lip/wat}$ value that ensures equal contribution of both phases to the drug loading capacity would be about 2–4 (rather than 0). This gives a limit for the encapsulation of the compound preferentially into the aqueous cavity to about $\log K_{lip/wat} < 2$. As discussed in section 3.2, compounds that preferentially partition into the membrane are difficult to be released thermally.

The permeability coefficient imposes two limits: (i) a lower limit for the storage conditions, where negligible or only very slow elution of the drug from the liposome at low temperatures is crucial to ensure stable encapsulation

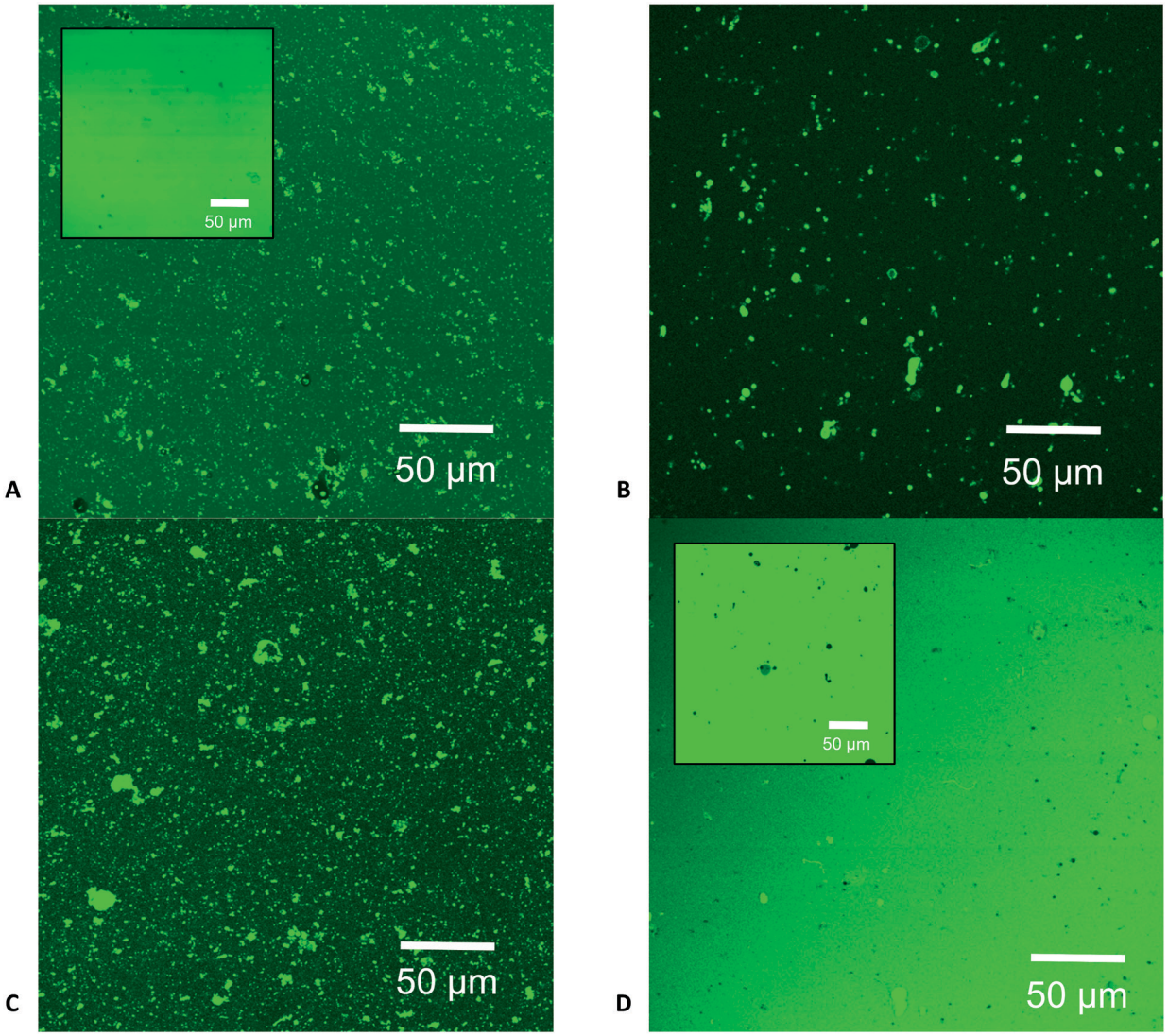

Fig. 4 Fluorescence microscopy images of liposomes hydrated by solutions of fluorescent dyes according to Table 1: A) 5(6)-carboxyfluorescein, B) fluorescein, C) FITC, D) calcein. The images show unextruded liposomes at room temperature, washed by repeated centrifugation and dilution. The insets in cases A) and D) show also "raw" liposomes before the washing steps.

without premature leakage from the liposome; and (ii) an upper limit for the thermal release at elevated temperatures when the membrane changes to the disordered state.

To set the border values for permeation, we have to take into consideration the highest $\log P_{\mathrm{erm}}$, where the compound did not permeate (5(6)-CF through the membrane at 273 K ≈ −5.6) and the lowest $\log P_{\mathrm{erm}}$, where the compound permeated (5(6)-CF through the membrane at 333 K ≈ −3.6). We have to also take into consideration that only non-ionic species can permeate the membrane. Also, the permeation through unstirred water should be taken into consideration as can be seen from eqn (2):[47]

$$\frac{1}{P_{\mathrm{app}}} = \frac{1}{P_{\mathrm{erm}} f_{\mathrm{HA}}} + \frac{1}{P_{\mathrm{aq}}} \qquad (2)$$

where P_{app} is an apparent permeation coefficient (which is proportional to permeation time), f_{HA} is a fraction of the unionised species (0.0003 for 5(6)-CF at pH 7.4) and P_{aq} is a permeation coefficient through unstirred water layer on the membrane. The P_{aq} is not directly dependent on a character of permeating molecule and therefore remains constant, the apparent permeability of a compound can be estimated from calculated P_{erm} and f_{HA}.

Based on the experiments and assumptions mentioned above, we propose that the ideal non-ionic compound for encapsulation and temperature-controlled release should have $\log P_{\mathrm{erm}} < -9.1$ at the low (ambient) temperature and $\log P_{\mathrm{erm}} > -7.1$ at the high (release trigger) temperature.

To set these rules more precisely, the whole procedure of liposome preparation, separation and heat release measurement was repeated with 1 mg ml^{-1} 5(6)-CF solution with PBS buffer at pH 5.4 and 6.4. The results (Table 3) show that at lower pH, the 5(6)-CF is released at room temperature

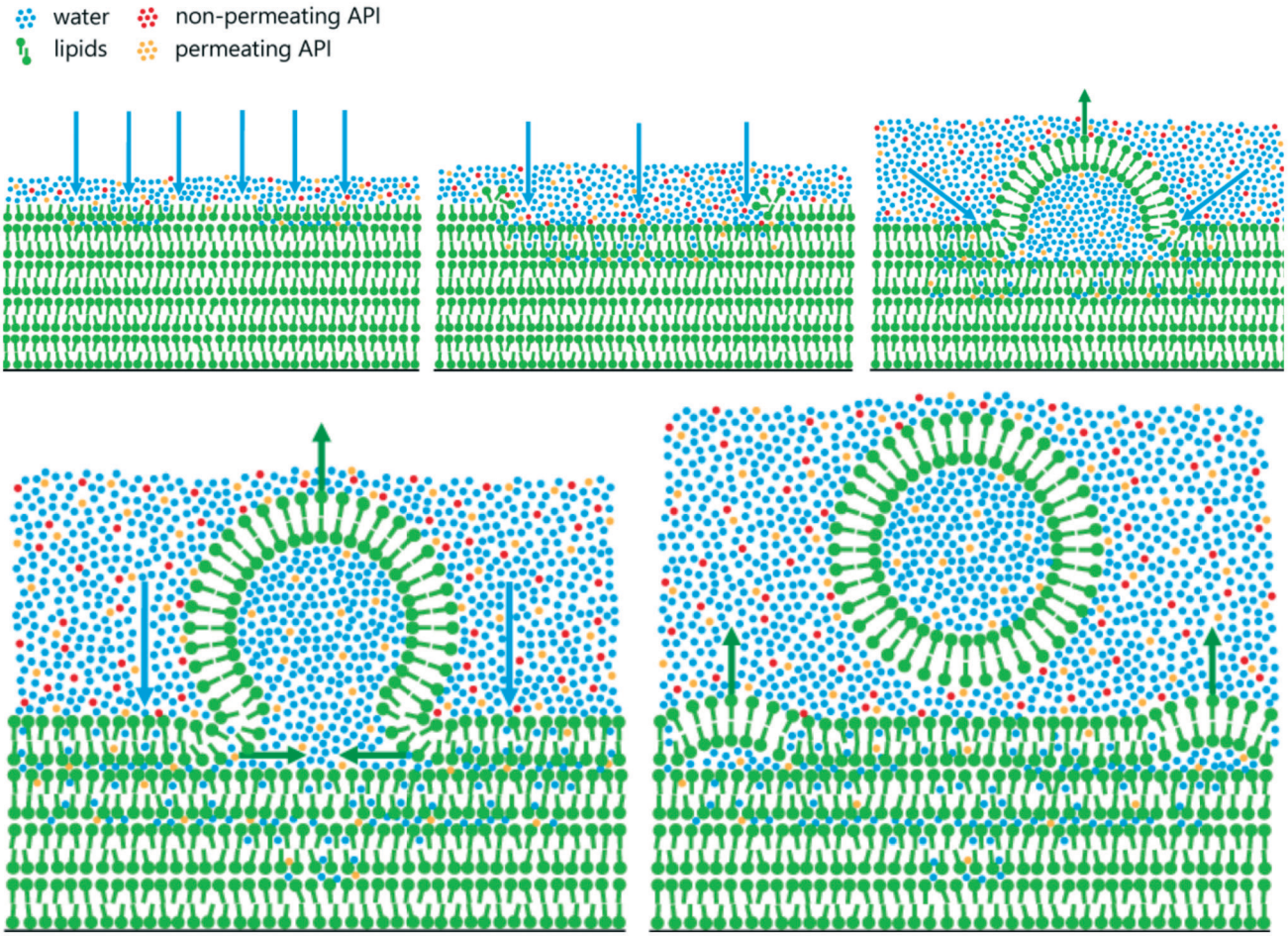

Fig. 5 Scheme of liposome formation by the hydration of a dried lipid film. It is proposed that non-permeating solutes are excluded from the liposome cavity during this process.

and only small amount of the dye is later released in a heat-induced experiment.

The results imply that for P_{app} = −8.1, the molecule still rapidly permeates. Since the COSMOperm method has an accuracy of 1 log value,[42] more precise determination of rules for heat induced release is unnecessary.

To rationalise these experiment-based rules, the calculation of time dependence of released quantity of 5(6)-CF can be made. Based on experimental approach[48] for measurement of permeation coefficient in two compartments separated by bilayer, half of the 5(6)-CF at 293 K should be released in 2.5 hours and at 333 K or pH 5.4 at 293 K in 10 seconds (derivation in ESI†). This is not in perfect agreement with the experiment, where not even 1% of 5(6)-CF was released at 293 K in 25 hours,[10] and therefore final rules were needed to be tuned experimentally.

According to these limits, the neutral drug molecules can be sorted into three categories:

1) Compounds not suitable for liposome encapsulation with the chosen membrane composition.

2) Compounds suitable for encapsulation but not suitable for the thermal release mechanism.

3) Compounds suitable for both encapsulation and thermal release.

Table 3 Measured quantities of 5(6)-CF upon heat release at different pH

5(6)-CF conc. (mg ml^{-1})	pH[a]	Release[b] at 293 K	Released after heating (μg_{dye} mg_{lipid}^{-1})	Theoretical capacity (μg_{dye} mg_{lipid}^{-1})	Fraction of unionized species (%)	log P_{app}^{293K}
7.5	7.4	None	62 ± 8	246	0.03%	−9.1
1	6.4	Visible	0.4 ± 0.2	32.8	0.26%	−8.1
1	5.4	Visible	0.3 ± 0.2	32.8	2.59%	−7.1

[a] Hydrating solution: 10 mM PBS adjusted to pH 7.4. [b] Qualitative only by visual inspection.

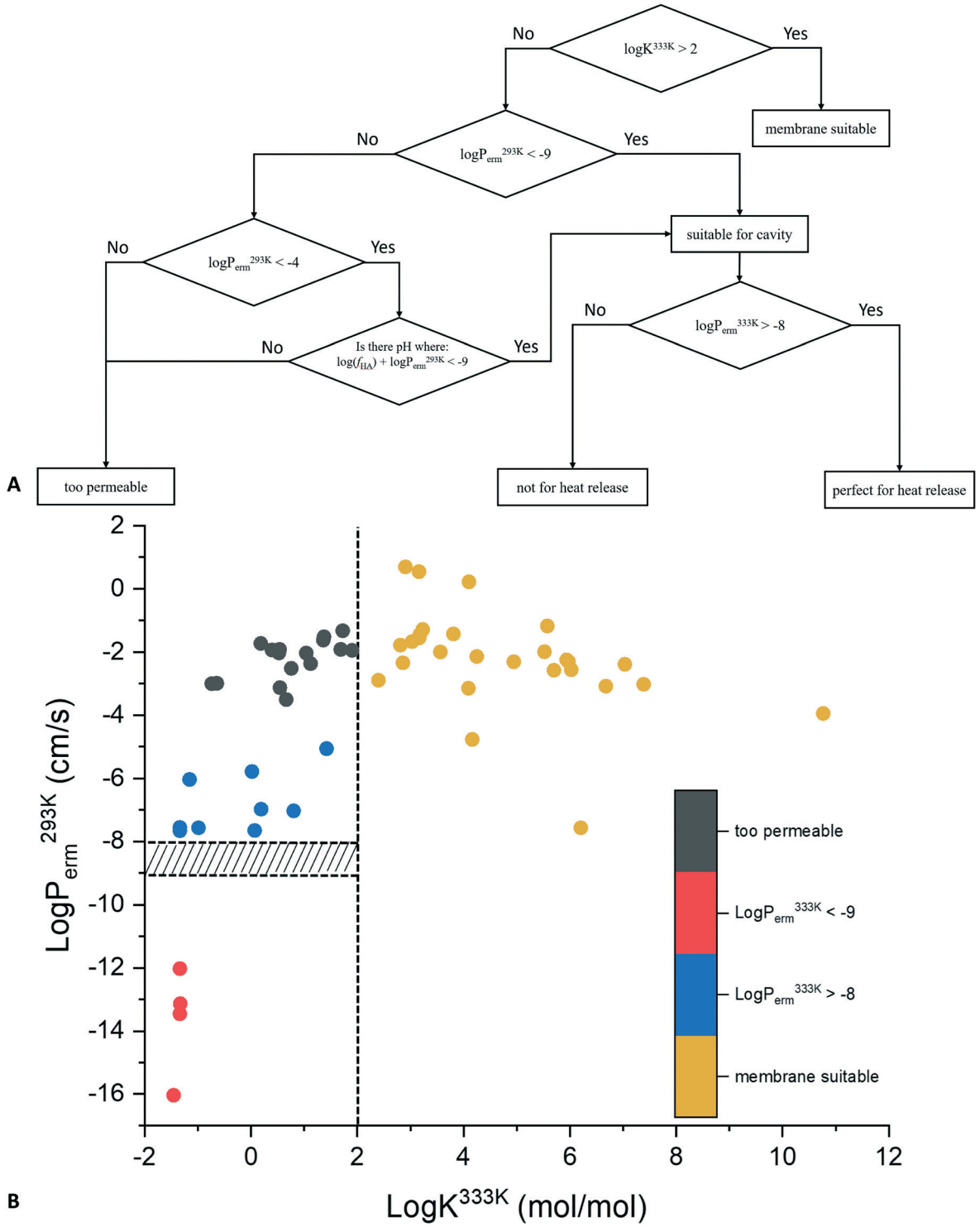

Fig. 6 A) Decision tree dividing molecules into liposome compatibility groups according to their partition and permeation coefficients. B) Calculated partition and permeation coefficients for 56 DrugBank molecules, color-coded according to their suitability for liposome formulation (DPPC : DPPG : Chol = 75 : 10 : 15 membrane). The dotted lines denote the cut-off criteria for membrane partitioning and permeability. Molecules that are more appropriate for lipid bilayer formulation are to the right (yellow), molecules that are too permeable are in the top left corner (black), and molecules suitable for aqueous cavity formulation are further distinguished according to the likelihood of thermal release: not possible (red) and possible (blue) for which the permeability can be lowered using sufficient pH.

A decision tree for substance classification based on their log $K_{\_lip/wat}$ and log P_{erm} values is summarised in Fig. 6A, and it can be used as a basis for assessing the suitability of a given substance for incorporation into a liposomal drug delivery system.

3.4 *In silico* screening of compounds from DrugBank

In order to test this set of rules, a total of 56 toxic compounds from the DrugBank database were chosen, and their $\log K_{\text{\_lip/wat}}$ and $\log P_{\text{erm}}$ values were computed. The substances had a broad category of chemical actions, including the potentially harmful or deadly effect on living organisms. Since toxicity means bioactivity, such substances – even though harmful on their own – are potential candidates for applications in human or veterinary medicine, disinfection, crop protection, *etc.* Encapsulation into liposomes followed by controlled release could be a way how to apply such substances safely at the appropriate dose.

After applying the classification criteria (Fig. 6A) to all 56 evaluated molecules, the following groups were obtained:

- 27 substances were suitable for membrane-bound liposome encapsulation due to their high partition coefficient (yellow dots in Fig. 6B): anacetrapib, amitraz, dalcetrapib, chlorotoxin I-131, calyculin A, deltamethrin, cyfluthrin, cypermethrin, altretamine, bempedoicacid, cerivastatin, benfluorex, coumaphos, atorvastatin, acifluorfen, bisphenol A, benzyl benzoate, clofibrate, 1,2-dichlorobenzene, ciprofibrate, crotamiton, bromoform, bezafibrate, 9*H*-carbazole, dantron and chlorambucil.

4 substances were not suitable for liposomal formulation using the Bangham method due to too low permeation even at 333 K. This could be potentially solved using a liposome loading method that does not require membrane permeation. These compounds (red dots in Fig. 6B) were: allosamidin, azacitidine, cytarabine, decitabine,

- 16 substances were not suitable for liposomal formulation due to high partitioning (black dots in Fig. 6B): buthionine sulfoximine, carboquone, 2-methoxyethanol, acipimox, benznidazole, carmustine, cerulenin, cyclophosphamide, carboxin, cantharidin, carbendazim, cythioate, busulfan, allicin, aminacrine, chlorine.
- 9 substances were identified as possible for encapsulation into the aqueous liposome cavity with a potential for thermally controlled release: clofarabine, 8-azaguanine, broxuridine, cordycepin, capecitabine, azathioprine, cycloserine, dacarbazine, PhIP.

The details of 9 compounds identified as potentially suitable for liposome encapsulation and thermal release are summarised in Table 4. The pH range for f_{HA} needed was calculated using Protonation Plugin Group in Marvin Sketch 20.16.[44] All nine compounds have a theoretical window of pH opportunity to be encapsulated into liposomes and later thermally released. On the other hand, some of the theoretically viable pH ranges are strongly acidic or basic, and therefore practical encapsulation would be very problematic.

3.5 Liposomal formulation of cycloserine delivery

As a final experimental validation of the *in silico* screening methodology, one of the most promising candidates was selected and encapsulated into liposomes. Since D-cycloserine is reasonably safe to work with and has well-documented antibiotic properties, this compound was chosen and tested in experiments with bacteria (*E. coli*) as described in section 2.3. The roughly estimated P_{app} (ESI† S5) at pH 7.4 is −10.1 at 293 K and −8.66 at 333 K. This means that cycloserine is clearly not permeating at low temperature but can be permeating at a higher temperature because the permeation coefficient is at the uncertain region between −9 and −8.

The results of the resazurin assay are summarised in Fig. 7. The liposomes' ability to retain the encapsulated bioactive compound cycloserine was evidenced by a control group exposed to the supernatant from intact liposomes, whose resazurin metabolic activity was almost the same as that of the negative control (pure bacteria).

On the other hand, bacteria groups exposed to cycloserine released from liposomes after heat or TRITON® treatment exhibited a substantially reduced metabolic activity. The antibacterial effect was not as strong as that of the control group exposed to 50 μg mL^{-1} kanamycin, but that is only a matter of the applied dose. Crucially, there was no statistical difference between the antibacterial effect of TRITON® release and heat release groups, which means that cycloserine is indeed a suitable compound for liposomal formulation and release by the heating mechanism.

As a result, our *in silico* methodology benchmarked on fluorescein derivatives was successful in selecting cycloserine

Table 4 Calculated $\log P_{\text{erm}}$ and $\log K$ values for 9 toxic compounds in neutral form that were identified as possible candidates for encapsulation and thermal release from DPPC : DPPG : Chol (75 : 10 : 15) liposomes

Compound	$\log K^{293\text{K}}$	$\log P_{\text{erm}}{}^{293\text{K}}$ (cm s^{-1})	$\log K^{333\text{K}}$	$\log P_{\text{erm}}{}^{333\text{K}}$ (cm s^{-1})	f_{HA} needed (%)	pH range
Clofarabine	−1.3	−7.66	−1.34	−5.44	4.6	0–0.8
8-Azaguanine	0.71	−7.65	0.07	−5.85	4.5	7.2–14
Broxuridine	−1.3	−7.57	−0.99	−5.54	3.7	9.8–14
Cordycepin	−1.31	−7.55	−1.34	−5.44	3.5	0–2.6
Capecitabine	0.02	−7.03	0.8	−4.71	1.1	10.8–14
Azathioprine	0.54	−6.98	0.19	−5.18	0.095	0–0.6, 10.8–14
Cycloserine	−0.83	−6.04	−1.15	−4.6	0.11	0–14[a]
Dacarbazine	0.4	−5.78	0.02	−4.15	0.058	12.2–14
PhIP	2.56	−5.06	1.42	−3.88	0.011	0–0.8

[a] Cycloserine is present mainly in zwitterionic and not neutral form.

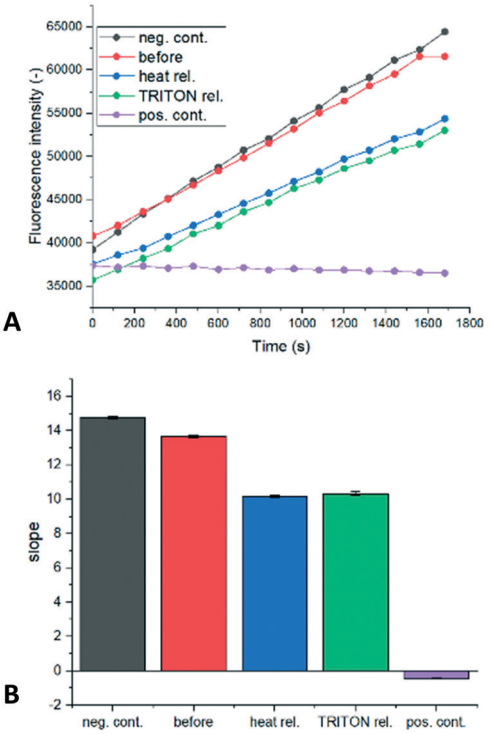

Fig. 7 Effect of cycloserine on *E. coli* tested by the Resazurin assay. A) Dependence of measured fluorescence intensity on time (each line was averaged from 3–6 wells). B) Calculated slopes from the fluorescence measurement for individual control groups. Neg. cont. – bacteria only; before – bacteria exposed to supernatant from cycloserine loaded liposomes kept at ambient temperature; heat. rel. – bacteria exposed to supernatant from cycloserine loaded liposomes after heat release; TRITON rel. – bacteria exposed to supernatant from cycloserine loaded liposomes after membrane disruption by TRITON®; pos. cont. – bacteria exposed to 50 μg mL^{-1} kanamycin.

as a valid candidate for liposomal formulation with heat release and selected lipid composition.

4 Conclusions

A new *in silico* methodology for selecting potent candidate substances suitable for the encapsulation and thermally controlled release from liposomes has been proposed and verified experimentally. The whole procedure comprises a molecular dynamic simulation of a small patch of a bilayer with defined composition used for liposome formulation, COSMOperm/COSMOmic calculations for candidate molecules in neutral form and their selection using a set of experimentally validated rules. In this work, we used bilayer composition DPPC : DPPG : Chol (75 : 10 : 15 molar ratio) and 56 drug candidates. Comparison between experimentally measured thermal release and COSMOperm/COSMOmic calculations of a set of fluorescent dyes enabled us to derive rules for selecting molecules that can be encapsulated in liposomal cavities and thermally released. These rules were then applied to predict the liposomal compatibility of 56 toxic compounds from the DrugBank database. From this set of compounds, 16 showed no suitability for liposome encapsulation, 27 showed suitability for encapsulation into the liposome membrane, 4 showed suitability for cavity encapsulation using methods that do not involve membrane permeation during liposomes loading, and finally, 9 compounds were deemed suitable for encapsulation into the liposome cavity. One of these compounds – cycloserine – was then selected for a successful experimental demonstration of liposome encapsulation and thermal release.

In the present work, the composition of the lipid bilayer was fixed. However, this represents additional potential degrees of freedom. For example, the *in silico* methodology developed in this work can be extended to find such a combination of lipids in the liposome membrane that will meet the $\log K$ and $\log P_{\mathrm{erm}}$ criteria for a specific molecule whose liposome encapsulation is highly desirable. Such computational formulation optimisation can save valuable experimental resources and lead to novel compositions that might not be found experimentally. Similarly, during the development of new pharmaceutically active compounds, the lead structure optimisation can be partially driven by criteria for $\log K$ and $\log P_{\mathrm{erm}}$ that were proposed and validated in the present work. In this way, new chemical entities can be optimised for their biological efficacy and formulation manufacturability.

Author contribution

M. B. – liposome loading/release experiments, TEM measurements, data analysis, manuscript writing. M. Šr. – computer simulations, data analysis. M. Šo. – liposome loading/release experiments, data analysis, confocal analysis. P. J. – bacterial assay experiments, data analysis. F. Š. – conceptualisation, data interpretation, manuscript writing, funding acquisition. K. B. – conceptualisation, computer simulations, data analysis, manuscript writing, funding acquisition.

Conflicts of interest

There are no conflicts to declare.

Acknowledgements

M. B., M. Šo. and P. J. acknowledge support by Specific University Research (project MŠMT no. 21-SVV/2020). M. Šr. acknowledges support by Palacký University Olomouc (project IGA_PrF_2021_031). F. Š. would like to thank the Czech Science Foundation (project no. 19-09600S) for financial support. K. B. and M. Šr. would like to thank the Czech Science Foundation (project no. 17-21122S).

Notes and references

1 M. Li, S. Li, C. Du, N. Guo, Y. Teng, X. Meng, H. Sun, P. Yu and H. Galons, *Eur. J. Med. Chem.*, 2019, **164**, 640–653.

2 S. K. Golombek, J.-N. May, B. Theek, L. Appold, N. Drude, F. Kiessling and T. Lammers, *Adv. Drug Delivery Rev.*, 2018, **130**, 17–38.
3 F. Sacchetti, G. Marverti, D. D'Arca, L. Severi, E. Maretti, V. Iannuccelli, S. Pacifico, G. Ponterini, M. Costi and E. Leo, *Pharm. Res.*, 2018, **35**, 206.
4 C. Bellefroid, A. Lechanteur, B. Evrard and G. Piel, *Eur. J. Pharm. Biopharm.*, 2019, **137**, 95–111.
5 Y. Xia, J. Tian and X. Chen, *Biomaterials*, 2015, **79**, 56–68.
6 M. Ullrich, J. Haša, J. Hanuš, M. Šoóš and F. Štěpánek, *Powder Technol.*, 2016, **295**, 115–121.
7 V. Van Tran, J.-Y. Moon and Y.-C. Lee, *J. Controlled Release*, 2019, **300**, 114–140.
8 M. R. Islam Shishir, N. Karim, V. Gowd, X. Zheng and W. Chen, *Trends Food Sci. Technol.*, 2019, **85**, 177–200.
9 U. Bulbake, S. Doppalapudi, N. Kommineni and W. Khan, *Pharmaceutics*, 2017, **9**, 12.
10 J. Haša, J. Hanuš and F. Štěpánek, *ACS Appl. Mater. Interfaces*, 2018, **10**, 20306–20314.
11 Y. Yoshizaki, E. Yuba, N. Sakaguchi, K. Koiwai, A. Harada and K. Kono, *Biomaterials*, 2014, **35**, 8186–8196.
12 S. Rawal and M. M. Patel, *J. Controlled Release*, 2019, **301**, 76–109.
13 A. H. Hassan, K. M. Hosny, Z. A. Murshid, A. Alhadlaq, A. Yamani, G. Naguib, H. M. Alkhalidi and A. R. Afify, *J. Liposome Res.*, 2016, **26**, 148–155.
14 C. Skyttner, K. Enander, C. Aronsson and D. Aili, *Langmuir*, 2018, **34**, 6529–6537.
15 Y. P. Patil and S. Jadhav, *Chem. Phys. Lipids*, 2014, **177**, 8–18.
16 L. D. Mayer, P. Tardi and A. C. Louie, *Int. J. Nanomed.*, 2019, **14**, 3819–3830.
17 V. P. Torchilin, *Nat. Rev. Drug Discovery*, 2005, **4**, 145–160.
18 M. C. Phillips, B. D. Ladbrooke and D. Chapman, *Biochim. Biophys. Acta, Biomembr.*, 1970, **196**, 35–44.
19 J. Hanuš, M. Ullrich, J. Dohnal, M. Singh and F. Štěpánek, *Langmuir*, 2013, **29**, 4381–4387.
20 E. Amstad, J. Kohlbrecher, E. Müller, T. Schweizer, M. Textor and E. Reimhult, *Nano Lett.*, 2011, **11**, 1664–1670.
21 F. Di Meo, G. Fabre, K. Berka, T. Ossman, B. Chantemargue, M. Paloncýová, P. Marquet, M. Otyepka and P. Trouillas, *Pharmacol. Res.*, 2016, **111**, 471–486.
22 C. H. Mehta, R. Narayan and U. Y. Nayak, *Drug Discovery Today*, 2019, **24**, 781–788.
23 D. Bassolino-Klimas, H. E. Alper and T. R. Stouch, *Biochemistry*, 1993, **32**, 12624–12637.
24 R. O. Dror, R. M. Dirks, J. P. Grossman, H. Xu and D. E. Shaw, *Annu. Rev. Biophys.*, 2012, **41**, 429–452.
25 M. Paloncýová, K. Vávrová, Ž. Sovová, R. DeVane, M. Otyepka and K. Berka, *J. Phys. Chem. B*, 2015, **119**, 9811–9819.
26 M. T. Paloncýová, R. H. DeVane, B. P. Murch, K. Berka and M. Otyepka, *Langmuir*, 2014, **30**, 13942–13948.
27 D. S. Wishart, Y. D. Feunang, A. C. Guo, E. J. Lo, A. Marcu, J. R. Grant, T. Sajed, D. Johnson, C. Li, Z. Sayeeda, N. Assempour, I. Iynkkaran, Y. Liu, A. MacIejewski, N. Gale, A. Wilson, L. Chin, R. Cummings, D. Le, A. Pon, C. Knox and M. Wilson, *Nucleic Acids Res.*, 2018, **46**, D1074–D1082.
28 B. Hess, C. Kutzner, D. van der Spoel and E. Lindahl, *J. Chem. Theory Comput.*, 2008, **4**, 435–447.
29 J. P. M. Jämbeck and A. P. Lyubartsev, *J. Phys. Chem. B*, 2012, **116**, 3164–3179.
30 H. W. Horn, W. C. Swope, J. W. Pitera, J. D. Madura, T. J. Dick, G. L. Hura and T. Head-Gordon, *J. Chem. Phys.*, 2004, **120**, 9665–9678.
31 S. Nosé, *J. Chem. Phys.*, 1984, **81**, 511–519.
32 W. G. Hoover, *Phys. Rev. A: At., Mol., Opt. Phys.*, 1985, **31**, 1695–1697.
33 M. Parrinello and A. Rahman, *J. Appl. Phys.*, 1981, **52**, 7182–7190.
34 T. Darden, D. York and L. Pedersen, *J. Chem. Phys.*, 1993, **98**, 10089–10092.
35 B. Hess, H. Bekker, H. J. C. Berendsen and J. G. E. M. Fraaije, *J. Comput. Chem.*, 1997, **18**, 1463–1472.
36 *Schrödinger Release 2017-2: LigPrep*, Schrödinger, LLC: New York, NY, 2017.
37 *Schrödinger Release 2017-2: MacroModel*, Schrödinger, LLC: New York, NY, 2017.
38 J. L. Banks, H. S. Beard, Y. Cao, A. E. Cho, W. Damm, R. Farid, A. K. Felts, T. A. Halgren, D. T. Mainz, J. R. Maple, R. Murphy, D. M. Philipp, M. P. Repasky, L. Y. Zhang, B. J. Berne, R. A. Friesner, E. Gallicchio and R. M. Levy, *J. Comput. Chem.*, 2005, **26**, 1752–1780.
39 *TURBOMOLE 6.3*, a development of University of Karlsruhe and Forschungszentrum Karlsruhe GmbH, 1989–2007, TURBOMOLE GmbH, since 2007: 2011.
40 J. Řezáč, *J. Comput. Chem.*, 2016, **37**, 1230–1237.
41 A. Klamt, U. Huniar, S. Spycher and J. Keldenich, *J. Phys. Chem. B*, 2008, **112**, 12148–12157.
42 J. A. H. Schwöbel, A. Ebert, K. Bittermann, U. Huniar, K.-U. Goss and A. Klamt, *J. Phys. Chem. B*, 2020, **124**, 3343–3354.
43 J. F. Nagle, *Biophys. J.*, 1993, **64**, 1476–1481.
44 *MarvinSketch 20.16*, ChemAxon Ltd., 2020.
45 T. L. Riss, R. A. Moravec, A. L. Niles, S. Duellman, H. A. Benink, T. J. Worzella and L. Minor, in *Assay Guidance Manual [Internet]*, ed. S. Markossian, G. S. Sittampalam, A. Grossman, K. Brimacombe, M. Arkin, D. Auld, C. P. Austin, J. Baell, J. M. M. Caaveiro, T. D. Y. Chung, N. P. Coussens, J. L. Dahlin, V. Devanaryan, T. L. Foley, M. Glicksman, M. D. Hall, J. V. Haas, S. R. J. Hoare, J. Inglese, P. W. Iversen, S. D. Kahl, S. C. Kales, S. Kirshner, M. Lal-Nag, Z. Li, J. McGee, O. McManus, T. Riss, P. Saradjian, O. J. Trask Jr, J. R. Weidner, M. J. Wildey, M. Xia and X. Xu, Eli Lilly & Company and the National Center for Advancing Translational Sciences, Bethesda (MD), 2004, PMID: 23805433.
46 A. Finizio and A. Di Guardo, *Chemosphere*, 2001, **45**, 1063–1070.
47 T. X. Xiang and B. D. Anderson, *J. Membr. Biol.*, 1994, **140**, 111–122.
48 T. X. Xiang, X. Chen and B. D. Anderson, *Biophys. J.*, 1992, **63**(1), 78–88.

Journal of Inorganic Biochemistry 183 (2018) 117–136

Contents lists available at ScienceDirect

Journal of Inorganic Biochemistry

journal homepage: www.elsevier.com/locate/jinorgbio

Review article

Membrane-attached mammalian cytochromes P450: An overview of the membrane's effects on structure, drug binding, and interactions with redox partners

Martin Šrejber[a], Veronika Navrátilová[a], Markéta Paloncýová[a], Václav Bazgier[a], Karel Berka[a], Pavel Anzenbacher[b,*], Michal Otyepka[a,*]

[a] Regional Centre of Advanced Technologies and Materials, Department of Physical Chemistry, Faculty of Science, Palacký University Olomouc, tř. 17, listopadu 12, 771 46 Olomouc, Czech Republic

[b] Department of Pharmacology, Faculty of Medicine and Dentistry, Palacký University Olomouc, Hněvotínská 3, 775 15 Olomouc, Czech Republic

ARTICLE INFO

Keywords:
CYP
Drug metabolism
Protein-membrane interactions
Ligand passage

ABSTRACT

Mammalian cytochromes P450 are an important class of enzymes involved in the biotransformation of many endo- and exogenous compounds. Cytochrome P450 isoforms are attached to the membrane of the endoplasmic reticulum or mitochondria, and their catalytic domains move along the membrane surface while being partially immersed in the membrane environment. Their active sites are connected to both the membrane and cytosolic environments via a complex network of access channels. Consequently, they can accept substrates from both environments. The membrane also supports the interactions of cytochromes P450 with their redox partners. In this review, we provide an overview of current knowledge of the structure, flexibility, and interactions with substrates and redox partners of cytochrome P450 on membranes, amalgamating information derived from both experiments and simulations.

1. Introduction

Cytochrome P450 (CYP) enzymes are large and important class of proteins involved in the biotransformation of many xenobiotic and endobiotic compounds [1,2]. So far, 57 human CYP genes from 17 families and 3753 mammalian CYP genes from 18 families have been described [3]. The prototypical biotransformation catalyzed by CYPs is the monooxygenase reaction, but they also catalyze many other chemical reactions [1,4]. These reactions take place over a heme cofactor housed in a deeply buried active site. Although CYPs are highly promiscuous enzymes capable of oxidizing many different substrates [5], their reactions display high stereo- and regioselectivity [6].

CYPs play a dominant role in phase I of drug biotransformation [7–9]. The products formed in this phase are usually more hydrophilic than the corresponding substrates [10,11] and are therefore more readily excreted. The major drug-metabolizing CYP is CYP3A4, which is involved in the biotransformation of 20% of all orally taken drugs, followed by the CYP2D6, CYP1A2, and CYP2C9 isoforms, each of which can metabolize about 10% of existing pharmaceutical compounds (Fig. 1) [12]. In general, phase I metabolism of xenobiotics mostly involves the CYP1, CYP2, and CYP3 families. Other families, i.e., CYP4 up to CYP51, accept endogenous substrates [13]. Unsurprisingly, CYPs are associated with many drug–drug interactions [14], and their activity can be influenced by interactions with food, genetic polymorphisms, and many other factors [7].

The first CYP was described by Klingenberg and Garfinkel [15,16] as an unknown pigment with a significant absorption maximum at 450 nm of reduced state with bound carbon monoxide, which has been found to be a new cytochrome by Omura and Sato [17,18]. They have been studied actively ever since, producing many important findings. This review focuses on the features and properties of membrane-attached CYPs. Many X-ray structures of different CYP isoforms have been resolved [19,20] and deposited in the PDB database (www.rcsb.org) [21]. Additional structural information has been obtained via experimental techniques including NMR [22–24], microscopy [25–27], epitope labeling [28,29], mass spectrometry [30–34], tryptophan fluorescence scanning [35], linear dichroism [36], and cross-linking [37]. In addition, in silico methods such as molecular dynamics (MD) simulations [10,38–40] and homology modeling [41–43] have revealed valuable information about CYPs' structure, dynamics, and interactions with substrates. This allows us to combine information obtained via a broad portfolio of complementary techniques, and to establish a rather

* Corresponding authors.
E-mail addresses: pavel.anzenbacher@upol.cz (P. Anzenbacher), michal.otyepka@upol.cz (M. Otyepka).

https://doi.org/10.1016/j.jinorgbio.2018.03.002
Received 1 December 2017; Received in revised form 16 February 2018; Accepted 1 March 2018
Available online 05 March 2018

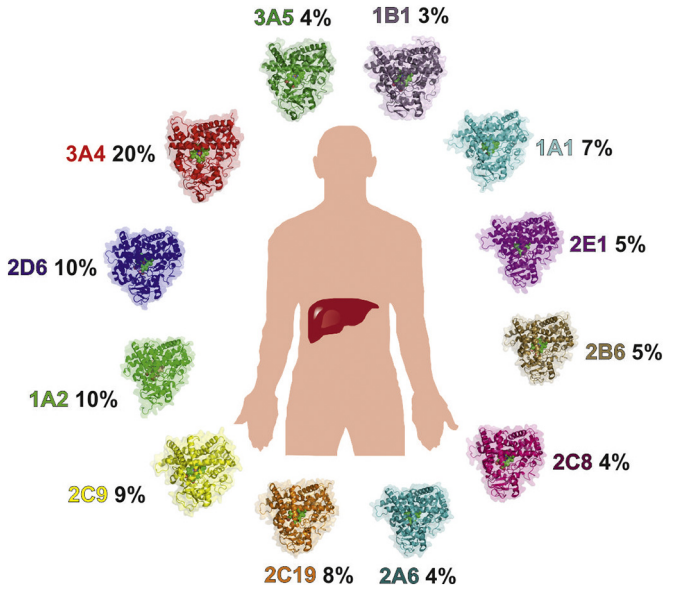

Fig. 1. CYP isoforms involved in metabolism of all chemicals according to Rendic et al. [12]. The percentages represent the participation of individual CYP isoforms in metabolism. CYP isoforms are represented as individual X-ray structures (a list of X-ray structures with PDB IDs is shown in Table S1 of Supplementary Information).

detailed and complex picture of CYPs' behavior on biomembranes.

Although the level of sequence similarity among CYP families is not very high (around 40% [44]), the common CYP fold is highly conserved [19] (cf. Fig. 1). This fold is predominantly α-helical, with a small proportion of β-sheets. Its twelve helices are designated A to L, and are named in alphabetical order starting from the N-terminus [45]. The most important structural regions of CYPs include the highly conserved I-helix bearing the threonine amino acid, which plays important role in the catalytic processes, the F/G-loop, and the F and G-helices together with the B/C-loop, which form a 'lid' over the active site cavity [19]. The active site is deeply buried within the structure and is connected to the exterior by a complex network of access and egress channels [46,47]. It houses a protoporphyrin IX (heme b) cofactor, which is connected to the CYP catalytic domain by an S—Fe bond to the thiolate group of a highly conserved cysteine [48].

Thanks to the wealth of mechanistic and structural experiments and computations, CYP structure and mechanism of its catalysis are known. However, many questions remain unanswered. This review focuses on the structural features of mammalian membrane-anchored CYPs and their interactions with drugs and redox partners, combining information from experimental and computational studies.

2. Biomembranes

2.1. Composition of biomembranes

Biomembranes form barriers between cells, organelles, and the intercellular environment. Their composition depends on their location and function in the cell [49]. Proteins account for around half the total mass of a typical biomembrane [50], with the rest being a bilayer-forming lipid mixture that serves as a support for embedded and interacting proteins, including CYPs. Human cell membranes contain many types of lipids but are dominated by phospholipids, sphingolipids, and cholesterol.

Phospholipids consist of two aliphatic nonpolar acyl tails that are connected to a phosphate-based head via a glycerol unit. The head may be zwitterionic with overall neutral charge (as in phosphatidylcholine, PC or phosphatidylethanolamine, PE; see Fig. 2) or charged (as in phosphatidylserine, PS or phosphatidylinositol, PI). The properties of

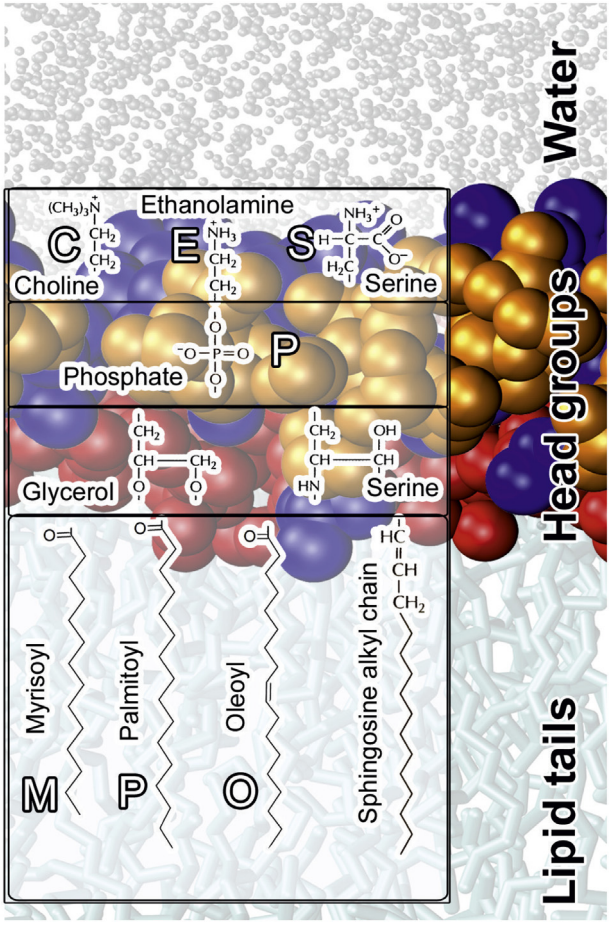

Fig. 2. A bilayer leaflet (background) with lipid tails shown in cyan, head groups represented as colored balls, and water molecules as grey dots. The inset shows the chemical structures of the most common lipids in the endoplasmic reticulum membrane. Glycerophospholipids have two acyl tails, a glycerol unit, a phosphate, and another head group. Sphingolipids are composed of a sphingosine acyl chain, another acyl tail connected by serine, and other head groups such as phosphate and choline in the case of sphingomyelin.

individual lipids are determined by the identity of the lipid head, the length of the acyl tails, and the number of double bonds in the acyl chains. Shorter and more unsaturated acyl chains decrease the membrane's order and increase its fluidity [49]. Sphingolipids are acylated sphingosine derivatives with acyl groups derived from long fatty acids and polar groups that are bound to additional polar groups (such as choline in the case of sphingomyelin). Their longer acyl tails make them predominantly ordered, and they tend to concentrate around cholesterol molecules in membranes [51,52].

Finally, cholesterol plays an important role in determining the properties of biological membranes [53] and can contribute to the regulation of membrane-embedded proteins [54,55]. It also significantly influences the membrane's biophysical properties, for instance, by increasing the ordering or thickness of disordered membranes, suppressing lipid diffusion [56], and reducing the membrane's permeability to substrates [57]. The amount of cholesterol in biological membranes varies from ~20 wt% in the plasma membrane to ~6 wt% in the endoplasmic reticulum (ER) membrane and 3–6 wt% in mitochondrial membranes [58]. In some specific cases, such as senile plaques known as one of the hallmark lesions of Alzheimer's disease, higher concentrations of cholesterol were observed [59], which indicates that the relationships between cholesterol concentration and CYP function and their implications for biological processes should be addressed in future studies.

Mammalian CYPs are mainly attached to the ER membrane. The

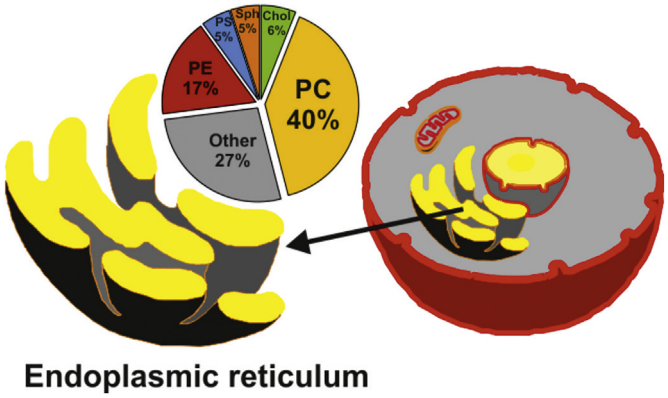

Fig. 3. Lipid composition of the endoplasmic reticulum (ER) membrane by mass: 40% PC (phosphatidylcholine), 17% PE (phosphatidylethanolamine), 6% Chol (cholesterol), 5% PS (phosphatidylserine), 5% Sph (sphingomyelin), and 27% other lipids such as cardiolipin and PI (phosphatidylinositol) [50].

most abundant membrane lipids in ER are neutral and charged phospholipids (PC, PE, PS, and PI; see Fig. 3), but it also contains cholesterol, sphingomyelin, and cardiolipin [60]. Due to the complexity of biological membranes, in vitro and in silico membrane experiments often use simpler model systems such as single lipid-containing bilayers or simplified lipid mixture bilayers.

2.2. Interactions of xenobiotics with biomembranes

Biomembranes form natural barriers to molecular traffic in living organisms and significantly affect the kinetics and disposition of chemicals in cells [61]. It should be noted that the interaction of xenobiotics with lipids can be as important as nonspecific interactions with proteins [62]. Chemicals can pass across a membrane actively [63], i.e., with the assistance of transporters and pores, passively by passive diffusion [64], or by some combination of active and passive means [65]. The membrane's lipid composition and phase affect the kinetics of the permeation process [65–68] and the affinity of various substances for the membrane [69]. Xenobiotics can partition into membranes: amphiphilic drug-like molecules concentrate in the membrane below the head groups region, staying in contact with both the hydrophobic lipid part and the hydrophilic head groups [70]. Xenobiotics of this type might be CYP substrates, and their accumulation in the membrane enables them to enter CYP active sites from the membrane environment [10,71]. The products of CYP biotransformation generally have lower affinities for membranes [71] so their preferred positions are closer to the membrane/water interface and they mostly leave to the bulk solvent. These findings together with the membrane's role in CYP anchoring (see below) indicate that the membrane can be an active player in the biotransformation of xenobiotics, causing pre-concentration of xenobiotics and their colocation with biotransformation enzymes, among other things.

3. Structure and dynamics of CYPs on biomembranes

3.1. Anchoring CYPs to lipid membranes

Mammalian CYPs are membrane-associated enzymes in contrast to prokaryotic CYPs, which are soluble. Most mammalian CYPs are attached to the ER and mitochondrial membranes [28,72] on cytosolic side and on plasma membrane on luminal side [73,74]. The knowledge about mode of CYPs binding to membranes drastically evolved in time. Originally CYP was proposed to be an integral membrane protein with at least eight transmembrane segments [75], the number of segments was then supposed to be lower [76]. Later CYPs were identified as membrane-associated proteins with short N-terminal membrane anchoring segment [77,78]. It was also shown that another sequence contributes to CYP anchoring by Cullin [79]. Current knowledge converged to a model, where the CYP catalytic domain lies on the cytosolic side of the ER [80], being anchored by the N-terminal transmembrane α-helix [28] with N-terminus on the luminal side of the ER [80]. The hydrophobic amino acids in the N-terminal anchor maintain its interaction with the hydrophobic ER membrane environment. The microsomal N-terminal anchor also contains a different signal peptides sequence [81] that governs CYP trafficking into the ER or mitochondria respectively [82]. The N-terminal anchor is also important for interactions with different phospholipids [83,84] and as the mediator of CYP heteromer formation [85]. There is significant variation in the amino acid composition of the N-terminal helix in various CYP families [86]. However, the mitochondrial CYPs do not need an N-terminal transmembrane anchor because they have a so-called topogenic sequence [87] localized at the beginning of the enzyme sequence that initially serves as a signal peptide but is sequestered once the recognition process is complete [88,89].

The first crystal structure of a mammalian CYP was published in 2000 and lacked the N-terminal transmembrane helix [90], which was deleted by enzyme engineering to facilitate crystallization. Most subsequent expression and crystallographic studies of mammalian CYPs have used truncated derivatives for the same reason [91–94]. It should be noted that these engineered structures are biochemically relevant because the deletions did not diminish the enzymes' catalytic activity [90] or eliminate their ability to attach to membrane surfaces [95]. The first (and to date, only) published structures of full-length CYP enzyme including the N-terminal anchor are crystal structures of lanosterol 14-α demethylase (PDB ID: 4LXJ, 4K0F both from *Saccharomyces cerevisiae*) co-soaked with various ligands [96–98]. These structures feature a resolved N-terminal anchor showing its attachment to the catalytic domain (Fig. 4), although it should be noted that the structural features of the enzyme, namely mutual position of the N-terminal anchor and the catalytic domain, in its native environment may be slightly different from those in the crystal structure because the latter is affected by crystal contacts in the lattice [99].

The need for structural data on full-length CYPs in their native environment has motivated many computational studies on these enzymes. The first atomistic models of full-length CYP2C9 attached to a PC bilayer were presented in 2011 [101,102]. These models were developed by two independent groups using different approaches but had many common features, suggesting that the results describe the protein's behavior reasonably well. The conformation of the catalytic domain of CYP2C9 was maintained during the simulations and resembled the structure resolved by X-ray crystallography. Later studies on other membrane-attached CYPs helped to identify common features of the CYP positioning on the membrane [10] (see Table S2 of Supplementary Information; for assignments of secondary structural features in 3D, see the Pymol session file in the same place).

The simulations indicate that the catalytic domain floats on the membrane surface, and is anchored by the membrane-crossing N-terminal helix. The distal side of the CYP faces the membrane and is partially immersed in its hydrophobic environment, while the proximal side remains exposed above the membrane ready to interact with redox partners (cf. 5. Interactions of CYPs with redox partners on membranes). The F/G-loop is the most deeply buried part of the CYP catalytic domain in the membrane, but the B/C-loop and β1, β2, β4–β5 sheets also form extensive membrane contacts. These features are in a good agreement with experimental observations [72,96,103,104], supporting the predictive power of molecular dynamics simulations.

Recent studies combining small-angle X-ray scattering (SAXS) experiments with molecular dynamics simulations of full-length CYP3A4 attached to a nanodisc membrane again confirmed that the N-terminal transmembrane anchor is embedded in the hydrophobic membrane core while the CYP-membrane contact area is immersed in the upper leaflet of the membrane and the catalytic domain is exposed to the

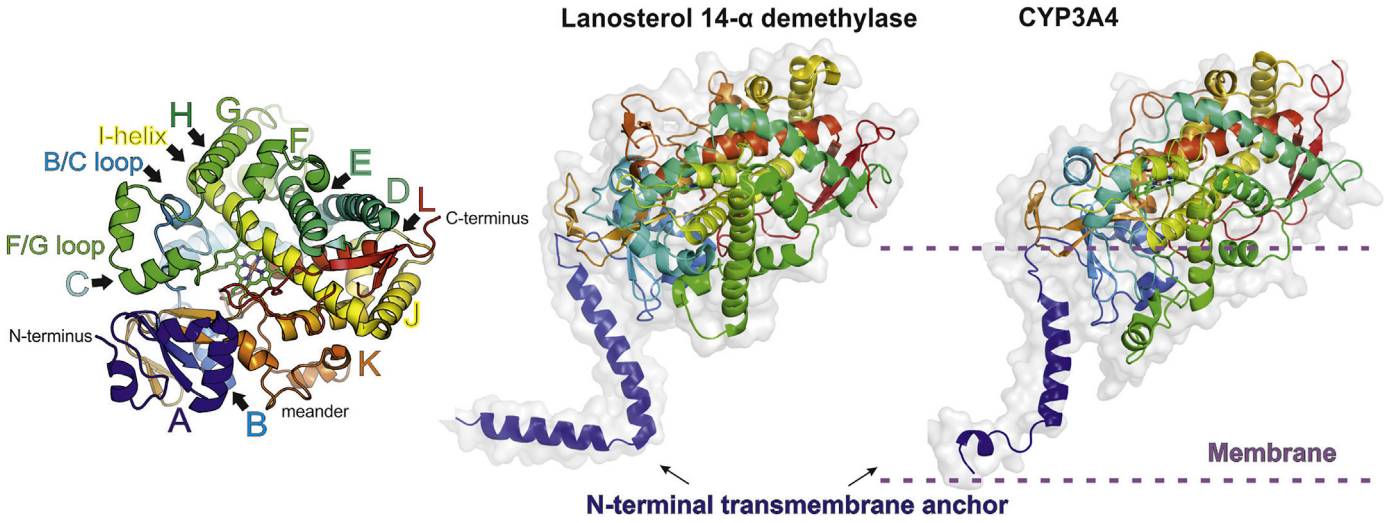

Fig. 4. Common fold of the CYP catalytic domain (without the N-terminal anchor) illustrated by the X-ray structures of CYP3A4 [100] (left panel), the full-length lanosterol 14-α demethylase [96] (middle panel), and CYP3A4 with the N-terminal anchor taken from a 100 ns MD simulation of the protein in a DOPC (1,2-dioleoyl-*sn*-glycero-3-phosphocholine) membrane [10] (right panel). The dashed lines represent the membrane surface.

surrounding solvent [105]. Another study based on SAXS in combination with MD observed certain flexibility of soluble form of prostacyclin synthase, but the CYP common fold remains unchanged [106]. It should be noted that the structural features of the connection between the N-terminal helix and the catalytic domain agreed well with the full-length structure of lanosterol 14-α demethylase [96], and multiple molecular dynamics simulations [10,36,40,101,102,107–110].

3.2. Orientation of CYP on membranes

The orientation of the CYP on the membrane has been determined from experimental measurements [36,111] of the heme tilt angle. The heme tilt angle is the angle between the plane of the heme cofactor and the membrane normal, and experimental measurements of this parameter are readily used as benchmarks for evaluation of MD simulations (Fig. 5). Early models of the heme cofactor position suggested that the heme is oriented parallel or perpendicular to the membrane plane [112]. However, experimental heme tilt angle measurements using the linear dichroism method revealed significant tilting of the heme relative to the membrane for CYP3A4 in POPC (2-oleoyl-1-palmitoyl-*sn*-glycero-3-phosphocholine) nanodiscs, which had a heme tilt angle of ~60° [36] (Table 1). MD simulations also suggested significant tilting of the heme relative to the membrane. Simulations of CYP3A4 in a highly mobile membrane mimetic (HMMM) bilayer predicted a heme tilt angle of about 70° [36]. Another model of CYP3A4 on a DOPC membrane yielded a heme tilt angle of ~56°, even closer to the experimental value [10]. The heme tilt angle is sensitive to the membrane composition: its value increased from 52° to 69° as the membrane's cholesterol content was increased [107]. The nature of the membrane lipid head group also affected the heme tilt angle, which varied between 64° for DOPC and 77° for DOPG (1,2-dioleoyl-*sn*-glycero-3-[phospho-*rac*-(3-lysyl(1-glycerol))]), with higher values in negatively charged membranes [108]. Individual CYP isoforms have different heme tilt angle values, ranging from 35° to 80° (Table 1). Increased computational power has enabled longer MD studies that revealed up to microsecond-scale dynamics of CYPs on the membrane. These simulations revealed floating motions of CYPs on the membranes, with significant fluctuations in their heme tilt angle values and immersion depths during the course of simulations [40,108] (Fig. 5). These floating movements may be responsible for the relatively high variation of reported experimental heme tilt angle values.

Both the position of a CYP on a membrane and its structure fluctuate dynamically [19,99,114], which may be essential for the enzyme's biological function. For instance, it may facilitate substrate/product channeling to the active site. Individual CYP isoforms differ in their tendencies to undergo such conformational changes, which is reflected in their plasticity. CYP plasticity can be evaluated by both experiment and simulation, as discussed in multiple literature reviews [115–117].

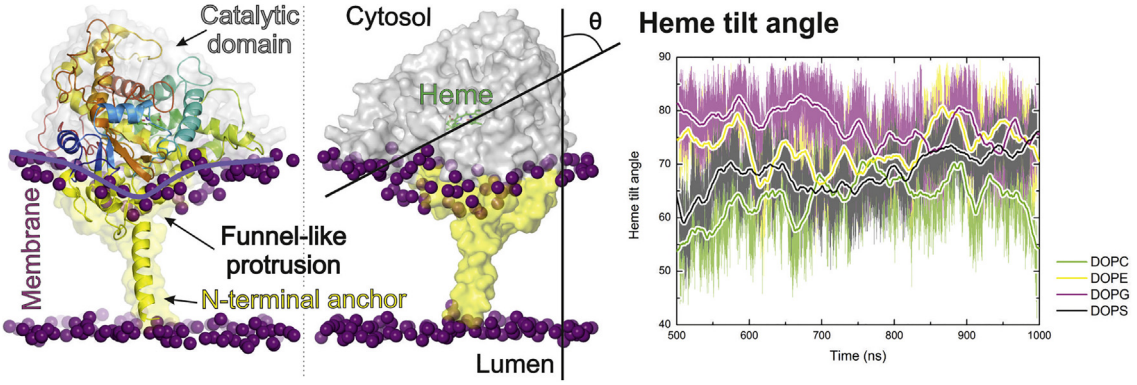

Fig. 5. Left: a structure of CYP2C9 anchored in a DOPC bilayer via a funnel-like protrusion, showing the typical orientation of a CYP on a membrane. Center: definition of the heme tilt angle (θ). Right: evidence of significant fluctuations in the heme tilt angle of CYP3A4 in DOPC, DOPE (1,2-dioleoyl-sn-glycero-3-phosphoethanolamine), DOPG, and DOPS (1,2-dioleoyl-sn-glycero-3-phosphoserine) membranes during the last 500 ns of MD simulations (data adapted from ref. [108]). The plot shows the raw data (background) and time averages over individual 1-ns-long sliding window intervals.

Table 1
Heme tilt angle values of CYP isoforms. Experimentally determined values are highlighted in bold.

CYP	Membrane	Heme tilt angle [°]	Method	Ref.
1A2	DOPC	67 ± 6	MD	[10]
19A1	POPC	31 ± 5[*], 34 ± 5[†]	MD	[40]
2A6	DOPC	69 ± 5	MD	[10]
2C9	DOPC	61 ± 4	MD	[10]
2C9	POPC	50 ± 9[a] or 35 ± 9[a]	MD	[102]
2C9	DOPC	35 ± 5	MD	[101]
2D6	DOPC	72 ± 6	MD	[10]
2E1	DOPC	60 ± 5	MD	[10]
3A4	**POPC**	**60 ± 4**	**LD[c]**	[36]
3A4	POPC	73 ± 5	MD	[36]
3A4	DOPC	56 ± 5	MD	[10]
3A4	DOPC/cholesterol	52 ± 8–69 ± 5[b]	MD	[107]
3A4	DOPS	69 ± 5	MD	[108]
3A4	DOPG	77 ± 5	MD	[108]
3A4	DOPE	73 ± 6	MD	[108]
$P450_{LM2}$ /CPR	**PC/PE/PS**	**55 ± 1**	**RDM[d]**	[113]
17A1	POPC	41 ± 3–66 ± 4	MD	[109]
21A1	**PC/PE/PS**	**38 ± 1 or 78 ± 1**	**RDM[d]**	[111]
CYP51	POPC	63 ± 5	MD	[110]

[*] Protonated at D309 [40].
[†] Deprotonated at D309 [40].
[a] Recalculated to the z-axis according to Baylon et al. [36].
[b] Varied with cholesterol content.
[c] Linear dichroism (LD).
[d] Rotational diffusion measurement (RDM).

It has been suggested that the flexibility of the active site correlates with substrate promiscuity; as the highly promiscuous CYP3A4 is very flexible, whereas the more selective CYP2A6 and CYP1A2 are relatively rigid in comparison to CYP2D6 and CYP2C9 that show intermediate levels of both flexibility and substrate promiscuity [117,118]. For the sake of completeness it should be noted that CYP plasticity depends on various factors; among other things, it can change dramatically upon ligand binding [119]. Since membranes are more viscous than typical aqueous environments, immersed parts of the catalytic domain (e.g., F/G-loop) show reduced flexibility in the membrane environment than in water. However, these parts still belong to the most flexible regions of CYPs [101,102]. However, the N-terminal helix anchor can undergo precession movements leading to relatively large fluctuations in its membrane position (Fig. 5).

CYPs also affect the membranes in which they are anchored. Their presence causes the formation of funnel-like protrusions in the area where they are inserted into the membrane interior (Fig. 6) [101]. The phosphate head groups are pushed away from this region, while glycerol and lipid tails remain, and the F/G-loop can thus interact directly with the lipids' hydrophobic tails. The addition of cholesterol enables CYPs to form some polar contacts in the funnel region, because the hydroxyl group of cholesterol is not pushed to the side of the funnel [107]. MD simulations have suggested that cholesterol may accumulate in the vicinity of the N-terminal helix and F/G-loop [107].

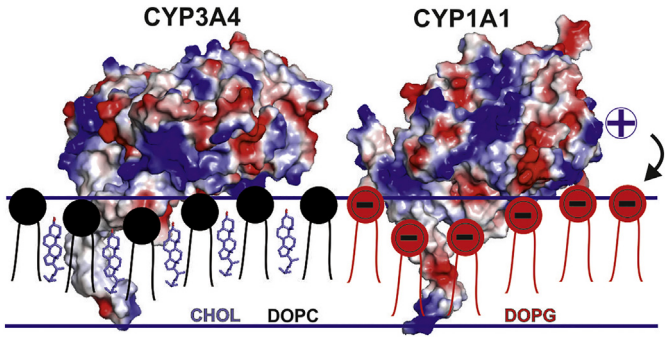

Fig. 6. Electrostatic interactions of CYPs with membrane lipids. The left panel shows CYP3A4 interacting with neutral DOPC lipids and cholesterol, which accumulates near the N-terminal transmembrane anchor and the immersed parts of the catalytic domain. The right panel shows enhanced CYP1A1 interaction with negatively charged membrane DOPS lipids via its positively charged amino acids (represented by blue regions) on the protein surface.

3.3. Similarities and differences among membrane-attached CYP isoforms

Individual CYP isoforms differ with respect to their membrane immersion depth and orientation on the membrane (Fig. 7). MD studies on several CYP isoforms have revealed several common features of CYP membrane binding as well as individual differences. In all CYP-membrane structures published to date, the F/G segment (comprising the F- and G-helices and the F/G-loop) and N-terminal anchor helix are always present in the membrane and interact with hydrophobic tails. There are also other membrane-interacting regions, which contact areas depending on the particular CYP isoform-membrane pair. β1-sheet has the largest contact for CYP2E1 and the smallest one for CYP2D6 [10]. B/C-loop has the smallest contact area for CYP1A2 and the largest one for CYP2D6. The contact regions are mostly determined by orientation of individual isoforms on the membrane (Table S1, Fig. 7) [10]. The 3D structures of membrane-embedded CYPs have been deposited in the CYP-membrane database accessible at http://cyp.upol.cz. MD simulations generally indicate that there are minor differences between the structural fluctuations of different CYP isoforms, but it would be premature to correlate these differences with the enzymes' biological functions given the inherent dynamics of CYP-membrane systems.

Published MD studies of CYP-membrane systems indicate that all-atom MD simulations typically reach convergence on a ~100 ns timescale, meaning that simulations of at least microseconds are needed to provide biologically relevant data. Unfortunately, such simulations currently have prohibitively high computational costs. Faster simulations can be performed using coarse-grained (CG) models, which unite individual atoms into “beads”—for example, the popular MARTINI CG scheme [120] combines groups of four heavy atoms into a single bead. Although CG simulations sacrifice some accuracy, they are becoming increasingly popular because they make it possible to study more complex systems on longer timescales. CG MD simulations of membrane-bound CYP3A4 have identified interacting regions and access/egress channels that closely resemble those seen in all-atom studies [121]. Similarly, a CG model of membrane-bound CYP1A2 exhibited rather small deviations from the all-atom model [122]. This CG model was used to study the interactions of CYP1A2 with its redox partner, cytochrome b_5 [123]. Although CG simulations have a “lower resolution” than all-atom simulations, they seem to provide relevant results at affordable costs and thus have many potential applications in studies on larger and more complex biological systems.

3.4. The composition of biomembranes affects CYP behavior

Membranes' biophysical properties depend on their composition, so changes in membrane composition can affect many physiologically important processes. The presence of lipid rafts can explain certain aspects of lipids' influence on the behavior of membranes and membrane enzymes [124–129]. Lipid rafts are proposed to be regions with enhanced lipid ordering resulting from elevated levels of cholesterol and saturated lipids [49]. Detergent dissolution experiments [130,131] have suggested that some CYPs prefer disordered lipid membranes, while others prefer more ordered ones [114,132]. For instance, CYP1A2 seemed to prefer ordered regions of ER membranes [114,132], CYP1A1 [84] and CYP2E1 [131] preferred disordered regions, and CYP2B4 partitioned into both [131]. Changes in cholesterol concentrations induced the relocation of CYP1A2, CYP2E1, and CYP2B4 isoforms to disordered regions [131]. In addition to that, in different lipid mixtures (e.g., POPC:DMPC - 1,2-dimyristoyl-*sn*-glycero-3-phosphocholine) the

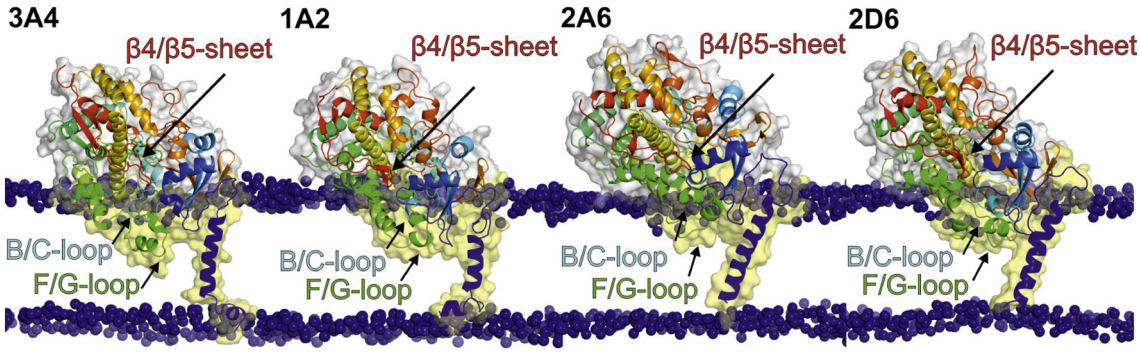

Fig. 7. Structures (adapted from ref. [10]) of various CYP isoforms on DOPC membranes (for clarity, the polar head groups are represented as blue spheres and the lipid tails are not shown). The isoforms differ slightly in their orientation, depth of immersion, and immersed parts. The secondary structures are displayed using the colors of the labels.

CYPs are sensitive to membrane fluidity, which is related to acyl-chain composition [133].

Cholesterol can also function as both substrate and inhibitor of CYPs. It is hydroxylated by CYP3A4 at the 4β-position [134]. However, at higher concentrations, it acts as a non-competitive inhibitor of another substrate than itself, preventing other substrates from accessing the CYP active site [135]. MD simulations of CYP3A4 embedded in a cholesterol-containing DOPC membrane suggested that the common CYP fold and the enzyme's interactions with the membrane were preserved under the simulated conditions. However, raising the membrane's cholesterol concentration caused the catalytic domain to sink deeper into the membrane, with the formation of new interactions between cholesterol molecules and the F/G-loop. Higher membrane cholesterol levels caused changes in the interior of the CYP, leading to the closure of channels with mouths inside the membrane and the opening of channels having mouths in the water phase [107]. These structural changes may negatively affect ligand access from the membrane and could explain the inhibition of CYP34A by cholesterol [135].

While most experimental membrane models consist only of PC lipids, the effect of individual lipid types has also been studied. The insertion of CYP1A2 in PE membranes was not different from that in PC membranes [136]. However, the presence of anionic lipids enhanced CYP membrane attachment, and its insertion depth depended on the identity of the anionic lipid; phosphatidic acid (PA) promoted penetration especially strongly. Greater membrane insertion correlated with increased O-deethylation activity towards 7-ethoxycoumarin, which was lowest in zwitterionic PE vesicles and highest in PA-enriched vesicles [136]. Additionally, CYP1B1 derivatives lacking the N-terminal anchor (due to the deletion of residues 2–4 and 2–26) exhibited increased activity in the presence of PA and cardiolipin [83], but not in the presence of PS. Conversely, the activity of CYP3A4 initially increased with the PS content, but very high levels of PS (above 50%) caused rapid decline in its enzymatic activity [137].

MD simulations have supported these experimental observations by showing that electrostatic interactions between individual CYPs and membrane lipids cause significant changes in the CYPs' properties [108]. In contrast to CYP1A2, the behavior of CYP3A4 on a pure DOPC membrane was shown to differ significantly from that on membranes made of DOPE (which has a zwitterionic ethanolamine-phosphate head group) or of the anionic lipids DOPG and DOPS. PE, PG, and PS head groups can form hydrogen bonds with CYP, like cholesterol. But in the anionic PG and PS membranes, CYP3A4 was immersed more deeply and oriented differently. The behavior of CYPs on membranes appears to be sensitive to electrostatic interactions, especially with negatively charged lipids, which may affect the enzymes' catalytic activity [108,138]. In general, anionic membrane lipids may interact with positively charged amino acids on the CYP surface, increasing the number of the amino acids immersed in the membrane and thereby increasing the proportion of the catalytic domain that is membrane-immersed [108]. The negative membrane charge may also [139] enhance electron transfer between CYPs and their redox partners (cytochrome P450 reductase (CPR) and cytochrome b_5) via a currently unknown mechanism [139–141].

CYP–membrane interactions therefore depend on both the charge of the membrane and the charge distribution on the CYP surface, and that the more positively charged distal sides of CYP proteins will be more strongly attracted to anionic membranes than to neutral ones. This attraction is mirrored by changes in CYP orientation and membrane immersion depth, and both the cholesterol content and the content of charged lipids could be related to the differences in the localization of individual CYPs in the (dis)ordered membrane domains [108] (Fig. 6).

It should be noted that a more complex membrane model composed of a lipid-rich mixture was used in 250-ns-long MD simulations of human aromatase (CYP19A1) [40]. The model mimicked the composition of rat liver endoplasmic reticulum and contained nine lipid types with different lipid tail lengths: cholesterol (10.0%), DPPE (9.0%, 1,2-dipalmitoyl-*sn*-glycero-3-phosphoethanolamine), DOPE (11.0%), DSPC (8.4%, 1,2-distearoyl-*sn*-glycero-3-phosphocholine), DAPC (8.1%, 1,2-diarachidonoyl-*sn*-glycero-3-phosphocholine), SOPC (13.2%, 1-stearoyl-2-oleoyl-*sn*-glycero-3-phosphocholine), DPPC (6.3%, 1,2-dipalmitoyl-*sn*-glycero-3-phosphocholine), DOPC (16.4%), and POPS (17.6%, 1-palmitoyl-2-oleoyl-*sn*-glycero-3-phospho-L-serine). However, the authors focused mainly on the behavior of CYP19A1, and the membrane's properties were not discussed. This work has undoubtedly paved the way to MD simulations of CYPs on more complex membranes. However, simulations of such systems require substantial computational resources to achieve equilibrated MD trajectories that can be meaningfully interpreted.

4. CYP active site and active site channels

4.1. CYP active site

The CYP active site is a deeply buried cavity inside the enzyme structure housing the heme cofactor, where drug biotransformation occurs. The active site can accommodate diverse substrates with a wide range of different sizes and shapes because of its malleability [142–146]. However, it also exhibits high regio- and stereo-selectivity. It should be noted that the CYP active site can also catalyze other reactions besides the prototypical monooxygenase reaction, as beautifully reviewed by Guengerich [147].

The mechanism of ligand binding to the CYP buried active site is complex. Two major theories have been proposed to describe this mechanism: i) the classical induced fit model [148–151], in which the active site easily adapts to the size and shape of the inserted drug; and ii) the currently preferred theory that compounds are selectively bound to the most suitable conformation of the active site [152–154]. In addition, multiple occupancy of the CYP active site has been observed [155], which can lead to positive cooperativity as occurs in the binding of aflatoxin B1 to CYP3A4 [156], or negative cooperativity as in the

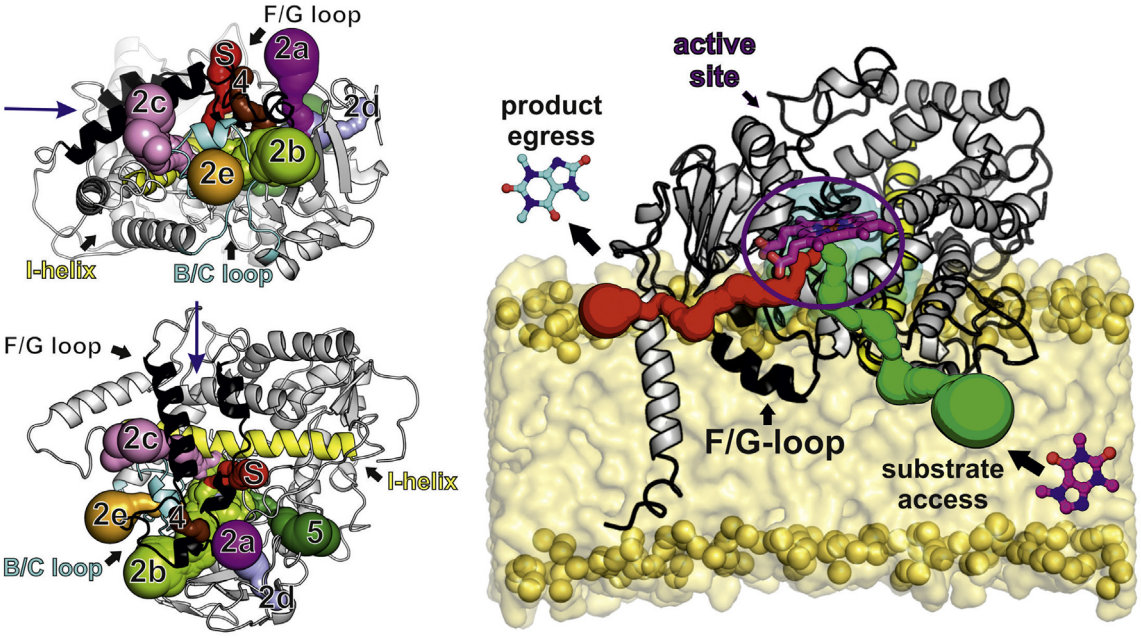

Fig. 8. Localization of selected channels in the structure of CYP3A4 (top and side views are shown in the left-hand panels). The F/G-loop is highlighted in black, and the arrow shows the direction towards its tip (the F′/G′-loop). The right panel shows the suggested metabolic pathway for amphiphilic compounds; such substrates enter the CYP active site from the membrane interior via a family 2 channel (shown in green). In the active site housing the heme cofactor (violet), they are transformed and the corresponding products leave the CYP via, e.g., the solvent channel (shown in red).

binding of acetaminophen to CYP3A4 [157]. Ligand-binding cooperativity can also be either homotropic or heterotropic, and can influence drug–drug interactions or inhibition effects [148].

Many experimental studies concerning CYP–ligand interactions have been reported, and are reviewed in detail elsewhere [24,149,155]. We discuss some of them here as examples of selected methods. Absorption spectroscopy provides information on properties such as differences in substrate binding between CYP isoforms (shifts the Soret peak maximum) [158,159], changes in active site flexibility caused by high pressure [160] (experiments of this sort showed that CYP1A2 is less malleable than CYP2C9, 2D6, which in turn are less malleable than CYP3A4 [118]), and changes in cooperativity [161]. Electron paramagnetic resonance (EPR) spectroscopy provides information on local rearrangements caused by point mutations of the CYP or the binding of substrates [162,163], or heterotropic cooperativity [164]. Both absorption spectroscopy and EPR detect transitions of the heme iron between low- and high-spin states in response to changes in substrate binding [165]. Nuclear magnetic resonance (NMR) spectroscopy can be used to detect multiple binding of substrates to a CYP [166,167] and changes in ligand conformation [168]. Fluorescence methods (notably fluorescence resonance energy transfer (FRET)) can shed light on allosteric mechanisms, their consistency with substrate binding, and the stoichiometry of interactions of multiple substrates with CYP [161,169,170]. Finally, as discussed at length in the preceding sections, X-ray crystallography provides direct evidence of CYP–ligand binding interactions [171–176], and many structures of various CYPs with bound ligands or inhibitors can be found in the PDB database [21,177].

In addition to these experimental techniques, several theoretical approaches have been used to study the active sites and binding mechanisms of CYPs. Molecular docking uses a scoring function to find the most favorable binding pose of a molecule inside an active site. Docking was used to predict metabolism by CYPs such as CYP2C9 [178], and it has also been used in combination with MD to study active site plasticity in CYP2D6 [143,179]. Classical MD simulations can identify regions of CYPs that are responsible for their wide substrate specificity, such as amino acids 211–218 in CYP3A4 [180] and the key residue F304 in the same enzyme, which is important in the homotropic cooperative binding of diazepam as both an effector and an active substrate [181]. Simulations of CYP2C19 derivatives with point mutations were used to calculate binding free energies and locate enzymes' channel openings [182]. Finally, umbrella sampling using the weighted histogram analysis method (WHAM) [183], which is an advanced MD technique, can provide thermodynamic information about the conformations of ligands bound to the CYP active site [184].

4.2. Access/egress channels

The deeply buried CYP active site is connected to the protein surface and exterior via a network of interconnected access/egress channels [46,47] that enable substrate/product traffic. These channels can be identified in the structures of CYPs using specialized channel detection software tools such as MOLE [185], MOLE*online* [186], or CAVER [187]. Channels are annotated using the nomenclature established by Wade and coworkers [46], and can be searched for as either single structures or structure ensembles [188]. The channel-searching programs are mostly based on the construction of Voronoi diagrams and finding the shortest path connecting the buried active site to the protein surface. They provide geometrical key characteristics of the computed channels, such as their length and profile. MOLE and MOLE*online* can also estimate the physicochemical properties of individual channels [185]. The recently introduced ChannelsDB database contains information about known channels in available structures, and stores structures of CYPs with annotated channels [189]. This information can be used to rationalize CYPs' substrate specificity, among other things.

The openings of channels belonging to family 2 (i.e., channels 2a, 2b, 2c, 2 ac, 2d, 2e, 2f) lie on the F/G-loop and/or nearby parts of the F- and G-helices that face towards the membrane. Channels 4 and 3 go through the tip of the F/G-loop and between the F- and G-helices, respectively (Fig. 8), and both have their openings pointing towards the membrane. The solvent channel connects the active site to the surrounding solvent and may be involved in transporting water molecules and metabolized products [190]. The water channel (under the B/C-loop), channel 1 (between the C- and H-helices), and channel 5 lying near the K′-helix and meander (see Fig. 8) are localized on the proximal

side of the CYP catalytic domain.

The channels with openings on the distal side of the catalytic domain are proposed to be substrate access/egress channels, while channels leading to the opposite (i.e., proximal) side of the CYP could transport oxygen or water molecules. In contrast to prokaryotic CYPs that showed one main channel for access and egress [191–193], the membrane-bound mammalian CYPs have access (substrate passage) and egress (metabolite output) channels according to channels membrane localization [10,101,194]. As mentioned in 3.2. Orientation of CYP on membranes, CYP substrates may accumulate in membranes and at the membrane/water interface. Molecules accumulated inside the membrane may be drawn to the active site via membrane-access channels, i.e., channels of family 2 and channel 4, which have mouth openings located in the hydrophobic membrane environment [10,71,101,195]. Channels 4 and 2f are particularly likely to serve as trafficking paths for lipophilic substrates because of their usually very hydrophobic character. Metabolites, which are generally more hydrophilic than CYP substrates, are shifted from the membrane towards the water phase and may be ejected from the CYP active site via the solvent channel, which leads to the membrane/water interface [190] (see Fig. 8). It should be noted that the same access channels can convey inhibitors to the active site [196]. The positions of channels in the membrane may vary based on the CYP's conformation, the nature of the surrounding membrane lipids, and the presence of a ligand in the CYP active site. Additionally, given the dynamic nature of membrane-anchored CYPs (see 4.2. Access/egress channels), the precise positions of channels may change dynamically over time.

4.3. Mechanism of ligand passage to CYP active sites

The mechanism by which ligands pass from the external medium to the deeply buried CYP active site has been unclear for a long time. It is very challenging to track ligands' passage into the active site using current experimental techniques. Only indirect data are available, e.g., from X-ray crystallography structures with ligands in channels [24,176,197]. There is a general consensus that the CYP fold may undergo conformational changes that facilitate ligand accommodation during passage. This finding was supported by the X-ray structure of CYP3A4 bound to erythromycin, which showed significant remodeling of the CYP3A4 F/G-loop compared to the structure of ligand-free CYP3A4 [144]. The widely open structure of CYP2B4 [198] represented another experimental evidence of large plasticity of CYP2B subfamily in the region where helices A, C/D, H/I, and F/G are in contact [142]. The importance of this region for substrate channeling was confirmed by recent mutation and kinetics experiments [199]. The plasticity or malleability of CYPs has been explored first by spectroscopy under high hydrostatic pressure [160] and then, when X-ray data became available, by analyzing differences between various X-ray structures, as well as by NMR spectroscopy, hydrogen–deuterium exchange mass spectrometry (DMXS), and other spectroscopic methods [116,117,200]. The lack of direct experimental observations has prompted theoretical calculations, which permit direct monitoring of a ligand's passage to the buried CYP active site. Since the pioneering works by Garcia [201] on the passage of water to the active site, and the ligand permeation studies of Wade and coworkers, who focused on the egress of camphor from the P450cam active site [192,193], many other systems have been studied and many specialized techniques have been developed to tackle this problem. The following section focuses on recent progress in this field and briefly introduces some important techniques.

It should be noted that monitoring ligand passage to the CYP active site is quite a complex task even in computational studies. The first challenge arises from the possibility that the principal pathway for a given species in the in-to-out direction need not be the same as that in the out-to-in direction. In addition, ligand passage may induce local conformational changes that somewhat resemble peristaltic wave motion [10,190] and the degree of such conformational changes may depend on size of the ligand. Also the opening of new access channels can be induced by presence of the ligand [202]. This implies that algorithms for simulating this process must be robust and flexible enough to cover all these issues and provide convergent results. Advanced computational methods that extend classical MD simulations and other techniques are briefly reviewed below, focusing on their predictive power and achieved results.

4.3.1. RAMD simulations

The random accelerated molecular dynamics method (RAMD, originally also known as random expulsion MD) pushes the ligand from the active site through the channel by applying a randomly oriented artificial force on its center of mass until it reaches the channel mouth opening [192]. RAMD can be used to identify previously unknown channels, and by performing multiple simulations, a set of different channels can be observed. Within tens of ps, Lüdemann et al. were able to identify several pathways from the P450cam active site [192]. Using the same approach for the rabbit CYP2C5 enzyme, two potential mechanisms for the passage of substrates or products through the access or egress channels were identified [194]. Either substrates and products enter and leave the CYP2C5 active site via the same channel or alternatively, their access and egress may be one-way, with lipophilic substrates entering via channel 2a and the more hydrophilic products leaving via channel 2c. A study on the passage of the substrate coumarin into the active site of CYP2A6 [203] indicated that channels 2a, 2c, 3, 6, and the solvent channel are the most important channels in this process. Channel 2c was proposed to be the major access path to the CYP2A6 active site, and possibly also for the whole CYP2 family, which is consistent with the conclusions of previous studies (that used different approaches) on mammalian CYPs such as CYP2B1 [204], CYP2B4 [198], CYP2C8 [205], and CYP2C9 [93], as well as the results of another RAMD study examining CYP2E1 [206]. All the RAMD studies mentioned here indicated that the ligand's passage through the channel was accompanied by the disruption of some hydrogen bonds in the channels and usually also by rotations of gating residues.

The advantage of RAMD is that it requires no prior knowledge of the structure or dynamics of the access and egress channels. Also, it often induces ligand permeation within several tens of ps and is therefore very effective for detecting channels. On the other hand, the speed of the permeation is artificially high, and one must be careful about observations of non-equilibrated structures. Although RAMD does not provide direct thermodynamic data, the probability of a ligand permeating through a given channel is proportional to the number of observations of the ligand permeating each channel. RAMD can also serve as a first guess for other methods that provide direct thermodynamic data, such as steered molecular dynamics [193,194,203,206].

4.3.2. SMD

Steered molecular dynamics (SMD) [207] applies an artificial force to pull the ligand through the channel and then computes the resulting rupture force. It requires a definition of the direction of the applied force, and in most studies it benefits from previous RAMD results [193,194,203,206]. SMD was used to study the expulsion of ligands from the active site, which happens within several hundreds of ps or ns during simulations, and can be also used to estimate the potential of mean force along the channel [193,203,206]. Among other things, it has been used to study the expulsion of metyrapone from CYP3A4 [208], coumarin from CYP2A6 [203], testosterone from CYP2B1 [204,209], indazole from CYP2E1 [206], temazepam and testosterone-6βOH from CYP3A4 [210], and several other ligands through the channels of CYP101A1 or CYP102A1 [193]. SMD was also used to describe the mechanism of ligand egress and to explain the results of site-directed mutagenesis experiments [209] that modified the opening of channels in whole CYPs [204,206,208,209]. Several mechanisms of channel gating have been proposed, such as the disruption of aliphatic contacts or hydrogen bonds [210], but most SMD studies identified

phenylalanines as gating residues that primarily interact with ligands by π–π stacking [203,206,208,210]. It should be noted here that no one channel appeared to be consistently preferred; several different channels were identified as being preferred in different CYP isoforms.

An alternative approach based on SMD that can account for enzyme flexibility is known as IterTunnel and was used by Kingley and Lill to study CYP2B6 [202]. IterTunnel uses an iterative process that combines several tools. First, channels are identified using MolAxis [211]. Then, SMD is performed in the direction of the mouths of chosen channels, and after a chosen time, the simulation is stopped, and the channels are recalculated. The SMD direction is then reevaluated to reflect the conformational changes induced by pulling the ligand. Kingsley and Lill [202] also performed umbrella sampling along the ligand's path using WHAM [183], calculated free energy profiles for passage along each channel. Ligand binding was identified as a downhill process in all channels, and channel opening was observed as a consequence of ligand-induced conformational changes.

4.3.3. BE-META

The conformational changes caused by the presence of a ligand, together with the corresponding free energy profile, can be evaluated by methods such as bias-exchange metadynamics (BE-META) [212,213], which is a recent variant of metadynamics (META) [214]. META increases the sampling rate by adding a biasing potential to visited states of a predefined collective variable (such as the position along the path of an enzyme channel). The added biasing potential can be used to compute free energy profiles and the heights of free energy barriers. It also enables control over the simulation's convergence and should provide reliable thermodynamic data. BE-META allows the simultaneous biasing of multiple variables (such as channel radius and drug hydration), each in separate replicas, and exchanges the replicas regularly. It has been used to calculate free energy profiles for the permeation of the caffeine metabolite 1,3,7-trimethyluric acid (TMU) through the channels of CYP3A4 [190] (Fig. 9). The solvent channel was found to be the most favorable (i.e., to have the lowest energy pathway) for the molecule's ejection from the enzyme. The channels' flexibility was also analyzed and identified as the crucial property governing ligand permeation. Despite the relatively small size of the analyzed molecule (TMU), significant “peristaltic wave” of concerted side-chain motions allowing molecule to pass through the access/egress channel [10,215]. Unsurprisingly, pathways that required passage along rigid channels were associated with higher energy barriers. The highest energy point on the substrate's path corresponded to a configuration with the ligand on the surface of CYP3A4, and the movement of the ligand towards the active site was a downhill process in thermodynamic terms, confirming the conclusions of Kingsley and Lill [202]. This may indicate that substrates can enter the active site via various channels, but products probably leave via the most energetically favorable channel, which was the solvent channel for the particular case of TMU in CYP3A4. Many other substrate/product–CYP complexes will have to be explored to fully understand the general characteristics of this process; the BE-META method with the DMSDDrug collective variable seems to be well suited for such studies [190]. A recent study on testosterone binding from POPC bilayer to the active site of membrane-anchored CYP3A4, which employed a combination of various biased MD techniques, complemented the picture sketched by these studies. It was confirmed that the substrate (testosterone) binding from the membrane to the active site is a downhill process and that G'-helix could facilitate binding of amphiphilic/lipophilic ligands from the membrane interior [216], as suggested earlier [101].

4.3.4. Best practices in channel MD studies

Based on the above discussion, we can briefly outline an effective approach to a channel permeation study. To quickly identify channels, we can apply geometrical methods [185–187] to a single structure or structure ensemble [188,190], or perform short MD simulations, such as multiple RAMD simulations [192]. The identified channels can then be investigated by SMD. However, as in RAMD, the process of ligand permeation in SMD simulations is usually unrealistically quick, so the enzyme structures may not relax properly (Table S2). Both SMD and RAMD can only be used to model ligand expulsion and are not suitable for identifying channel mouths on the protein surface from outside. SMD can be used to estimate the free energy barriers associated with specific ligand transport paths. However, to ensure converged results (i.e., without any detectable trend in the observed variable upon further extension of simulation time), structures obtained by SMD can be used in a second biased simulation using a technique such as umbrella sampling with WHAM algorithm to reach free energy profile along the channel path. It should be noted that SMD assumes a fixed direction of ligand movement and cannot adapt to conformational changes. IterTunnel [202] or BE-META using DMSDDrug metric [190] can be used to study passage of ligand within flexible channels, but at a higher

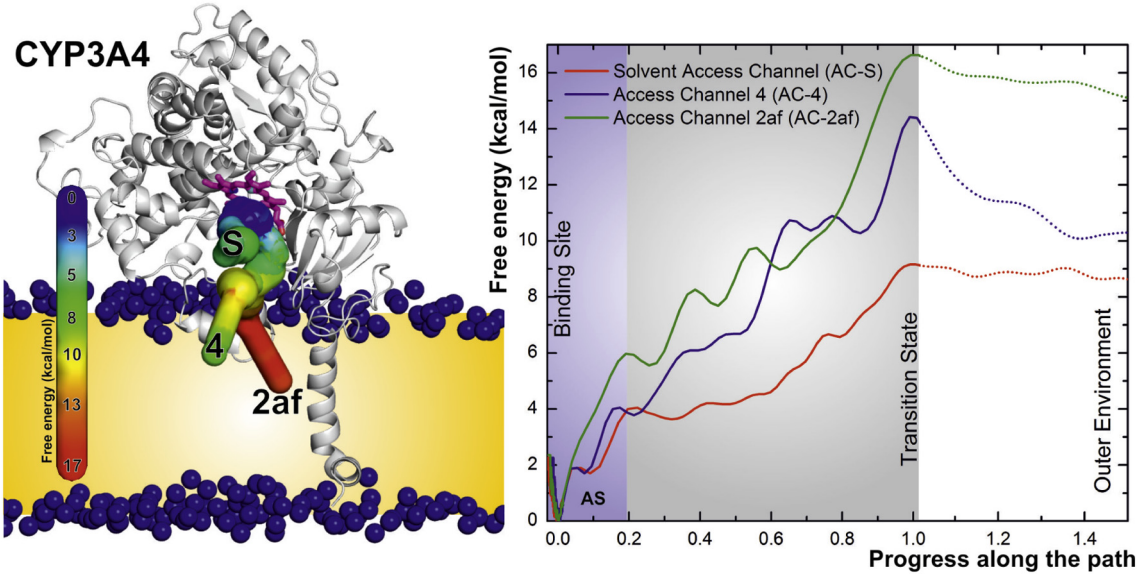

Fig. 9. 1,3,7-trimethyluric acid (TMU) can exit the CYP3A4 active site via channels 2af and 4 as well as the solvent channel. In the left panel, the channels are colored according to their free energies of TMU permeation. The right panel depicts the free energy profiles of TMU penetration along the channels. Data adapted from the literature [190].

computational cost. While IterTunnel provides results describing only a ligand expulsion, converged BE-META (or WHAM) free energy profiles represent systems at thermodynamic equilibrium and therefore BE-META can be also used to study ligand access.

The methods and studies discussed above have shed important light on substrate binding and product release by CYPs. The studies analyzed many CYP isoforms and revealed significant differences between the passage of substrates and products through the various channels, as well as the variation in the relative importance of different channels for different ligands and different CYP isoforms. Despite their differences, free energy calculations performed using various methods have consistently indicated that ligand binding is an energetically downhill process without a significant barrier [190,202]. Furthermore, phenylalanines were identified as typical gate-keeping residues [203,206,208,210]. Although the availability of computer power has increased immensely, and computational methods are becoming increasingly sophisticated, much remains to be done to clarify the passage of ligands through enzyme channels in general (Fig. 9).

4.4. Membrane effect on the ligand passage

The membrane may affect opening/closing of active site access and egress channels of CYPs. MD simulations showed that the membrane-bound CYPs had fewer open channels than the same CYPs simulated in water and this observation was attributed to an effect of the more viscous membrane environment [39,101,102,217]. It should be, however, noted that the so far presented MD simulations did not explicitly analyze the role of lateral membrane pressure on the behavior of CYPs. The channels with openings localized in the membrane interior were more widely open with respect to the same channels of CYPs simulated in the water environment. This applied particularly to channels passing along F/G-loop and also for the water channel on the proximal side. The CYP structures, which had many and widely open access channels in water (e.g., CYP3A4), retained this structural feature also in the membrane environment and vice versa [10]. This implies that the membrane affected all CYPs in the same way and the differences among individual isoforms remained intact in both environments. The membrane environment may contribute to an easier access of substrates from the membrane [39,217]. In addition, some lipids can induce opening of certain membrane-facing channels by allosteric occupation of another channel [122].

MD simulations show that the lipid membrane composition also plays a role in the opening/closing of access channels. The presence of cholesterol (at concentration comparable with cholesterol level in ER) opened membrane-facing channels in CYP3A4, but higher concentrations of cholesterol (similar to plasma membrane levels) lead to closing of membrane-facing channels and to openings of new channels leading to the proximal side [103]. The nature of lipid head groups (namely their charge) may also change the affinity of some substrates to the CYPs, e.g., lower affinity of cholesterol to CYP27A1 was observed in presence of negatively charged phosphatidylglycerol lipids [194]. In summary, the so far presented data are fragmental and come mostly from MD simulations. Nonetheless, they indicate a nontrivial role of membrane environment on activities of CYPs, which deserves more detailed studies in future.

5. Interactions of CYPs with redox partners on membranes

The biotransformation processes catalyzed by all mammalian CYPs depend on a supply of redox equivalents in the form of electrons from various redox partners. CYPs require consecutively two electrons, one by one in two very precise and synchronized steps, to catalyze the monooxygenation reaction [218]. In the microsomal electron transport chain, enzymes cytochrome P450 reductase (CPR) and cytochrome b_5 (b_5) function as electron donors to CYPs, whereas in mitochondria, electron transport is mediated via the ferredoxin redox system [219,220]. It should be noted that b_5 is not an obligatory redox partner of mammalian CYPs. In microsomal CYPs, both CYPs and their redox partners are membrane-attached proteins located on the cytosolic side of the ER at an approximate CYP:CPR ratio of 3–15:1 [221–223]. Similarly, there is an elevated concentration of cytochrome b_5 in human liver microsomes, which have a b_5:CPR ratio of 4–40:1 [224]. However, CYPs may also interact with other membrane-anchored macromolecules such as microsomal epoxide hydrolase, as suggested by FRET experiments [225]. CPR also supply electrons to other proteins, such as heme oxygenase, fatty acid elongases, and squalene epoxidase [226–229].

Cytochrome b_5 is a small (17 kDa) membrane-bound hemoprotein that serves as an intermediate transporter in the CYP electron transport chain. It can be reduced by either CPR or cytochrome b_5 reductase, but due to its low redox potential (+20 mV), it can only donate the second electron to CYPs [230,231]. The b_5 domain is rich in negative charge because it has several conserved residues with carboxylic acid side chains (23 of its 134 residues are glutamates or aspartates) that may serve as charge-pairing residues with its redox partners. It also has a C-terminal transmembrane anchor that is unresolved in all available crystal structures [232,233]. NMR structures show large fluctuations in the linker of the anchor helix, which enables flexible binding of b_5 to any other protein [234]. On the other hand, those fluctuations may be caused by the fact that NMR structure (PDB ID: 2I96 [234]) was determined in solution with no membrane present. Moreover, the binding of the b_5 redox partner seems to differ among various CYPs [235].

CPR is a diflavin reductase carrying both flavin adenine dinucleotide (FAD) and flavin mononucleotide (FMN) cofactors bound in distinct domains. These cofactors serve as mediators of reducing equivalents delivered by the reduced form of nicotinamide adenine dinucleotide phosphate (NADPH) [236]. Depending on the phase of the redox cycle, CPR can exist in either a closed or an open conformation [237–239] (Fig. 10). FRET studies have verified the existence of these distinct conformations, and found them to be based on the redox state of CPR [240–242]. However, it was shown that the corresponding conformational changes are small in the absence of CYP [243]. Recent solution SAXS and NMR data pointed out on very fast equilibrium between rigid, closed (locked state) and highly flexible open (unlocked state) conformations of the oxidized CPR [244]. For the sake of completeness it should be noted that the interaction of CPR with ER membrane and CYPs, and therefore its ability to sufficiently reduce CYPs, also correlates with its redox states [245,246].

Crystal structures of CPR proteins from various mammalian species in the closed conformation [247–252] (for a full list, see Supplementary Information Table S4) suggest that the compact structures favor intraprotein electron transfer from NADPH to the flavin cofactors (Fig. 11). Flavin cofactors FAD and FMN are in close contact (4 Å). The closed conformation was stable in a 10-ns-long solution-phase MD simulation of a truncated CPR model that lacked the transmembrane anchor [253]. Our MD simulations using the complete CPR protein attached to a DOPC membrane (see Supplementary Information for further information) showed that the closed conformation was stable over 700 ns with no spontaneous tendency to transition into the open conformation.

Conversely, a yeast-human chimeric CPR structure crystalized in the open conformation (PDB ID: 3FJO) [254] with an exposed FMN binding domain. This structure may be representative of CPR proteins ready for the docking of CYP (Fig. 12). In contrast to the compact closed form, the individual domains leave the flavin cofactors 86 Å apart in the open conformation. The experimentally resolved open structure seems to be stabilized by crystal contacts: multiple independent MD simulations of the monomeric open structure have resulted in the spontaneous closing of the structure on a 10-ns time scale. The open structure was only stabilized in the presence of CYP3A4 (see below).

An engineered CPR derivative with a deletion of four amino acids (^{236}TGEE^{239}) in the hinge region connecting FMN and the linker

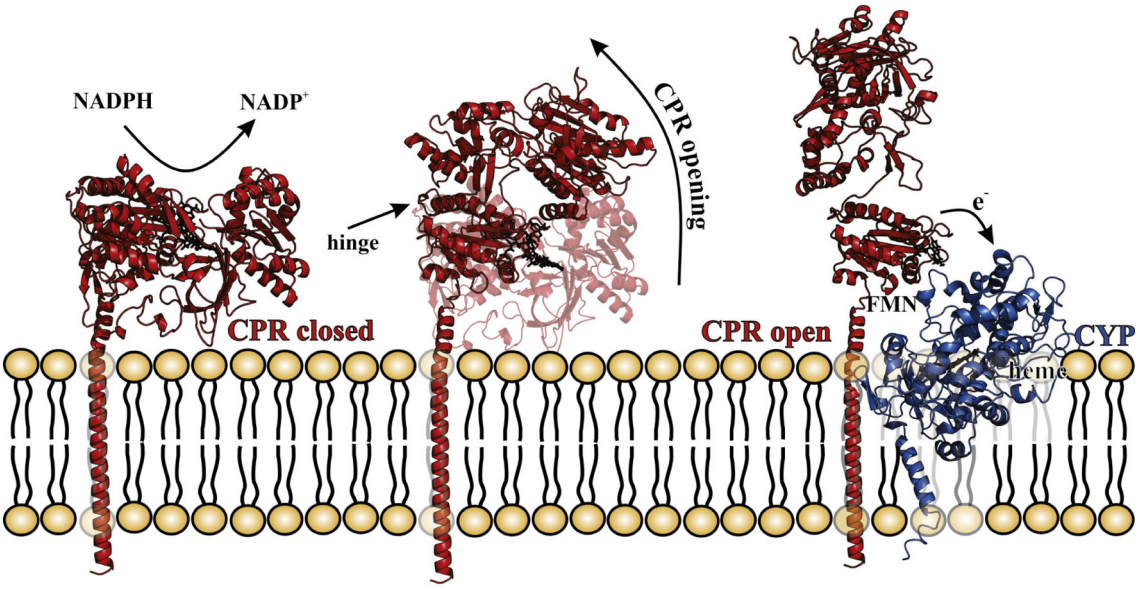

Fig. 10. Opening of CPR upon reduction and interaction with CYP. Upon the reduction of flavins within CPR by NADPH equivalents, the protein undergoes a small degree of opening; the open conformation is stabilized by binding to CYP, enabling the transfer of electrons from the exposed FMN to CYP's heme.

domain (Fig. 12) also crystalized in an extended conformation [255,256] (see Table S4 in Supplementary Information). This mutant was capable of reducing CYP2B4 [255]. However, its extended structure shows a displacement of the FMN and FAD cofactors (23 Å) that precludes interflavin electron transfer. MD simulations indicated that this conformation is stable in solution for 10 ns, or for 2 ns in membrane-attached form. The MD simulations also identified a hinge region as being essential for the conformational transition because it enables domain movement from closed to the open conformation [253]. A further investigation of the CPR transition process using metadynamics revealed that the amino acids ^{237}GEE^{239} showed the greatest collective movement (see Fig. 11). Interestingly, these amino acids are also unresolved in most crystal structures of CPR, supporting the hypothesized importance of hinge region flexibility for domain movement. Recent study also pointed out a role of ionic strength properties of this region in electron transfer to cytochrome *c* [257].

As mentioned above, CPR is attached to the membrane via an N-terminal transmembrane anchor (Fig. 10) that is integral to CPR–CYP electron mediating systems [258]. AFM experiments indicated that the height of the CPR globular domains is 5.6 ± 2.2 nm above the membrane [259]. This finding agrees with the closed conformation's height of 5.6 ± 0.4 nm in our CPR–membrane model. Whereas the FMN domain is at the same height as FAD domain in the structure of CPR alone on the membrane, further simulations showed that in the complex with CYP, the FAD domain is further from the membrane. The FMN domain remains at the same height, attached to the proximal side of CYP; this

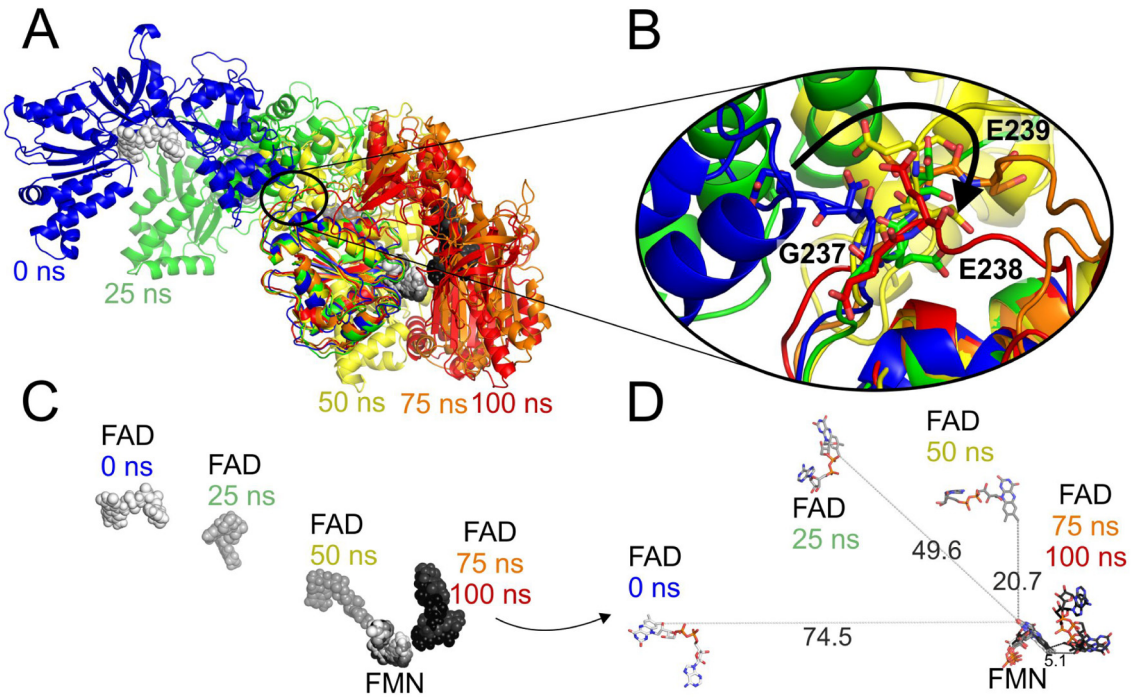

Fig. 11. CPR closing movement from open to closed structure. Overall domain movement (A) is guided on flexible hinge region with the largest collective motion at residues ^{237}GEE^{239} (B). FAD and FMN cofactors are closing in mainly within 75 ns (C), whereas the distance between cofactors is shortening from 75 Å to final 5 Å (D).

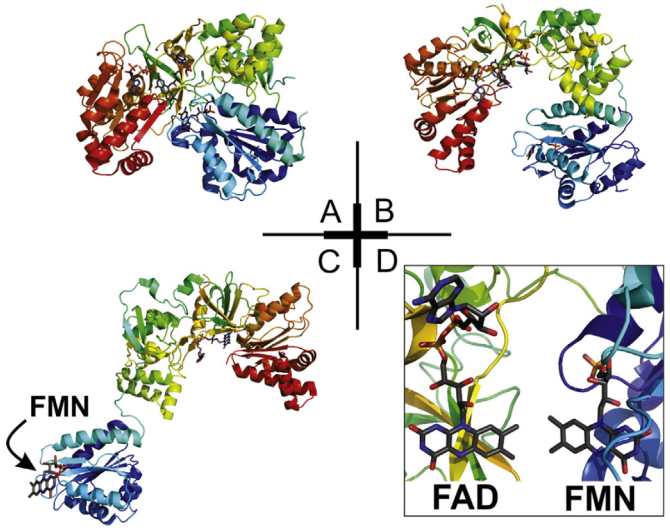

Fig. 12. Crystal structures of CPR in different conformations. The closed conformation (panel A) is the most compact structure of CPR (PDB ID: 3QE2; [251]). This conformation enables intraprotein electron transfer between the flavin (FAD and FMN) cofactors, which are held in close proximity (panel D). On the other hand, structures of CPRs in the extended (panel C; PDB ID: 3ES9; [255]) and open (panel D; PDB ID: 3FJO; [254]) conformations have the FMN cofactor exposed and ready for interaction with CYP. FMN domains are shown in blue in all structures.

was observed for both CYP51 [260] and CYP3A4 (this work, Fig. 13). Equilibration of these atomistic models using MD simulations enabled the identification of amino acids E270–P275, I307–R313, and N467 from the FAD domain and W549–G554 from the NADPH binding domain as points of contact with the membrane.

CYP forms membrane-bound protein–protein complexes with its redox partners. Its association with its redox partners is thought to be driven by electrostatic interactions between the positively charged amino acids of the CYP proximal side and the negatively charged residues of the FMN domain of CPR (Fig. 12) [261–263]. Site-directed mutagenesis studies mainly targeting positively charged residues on the proximal side of CYPs showed that these mutations significantly weakened the CYP–CPR interaction (see Table S5) [264–272]. The positively charged residues on the proximal side that interact with CPR are structurally conserved over the diverse CYP family, and (with the exception of R422 and R443) also play roles in binding to b_5. This implies that the CYP interaction sites for CPR and b_5 are similar but not fully identical [262]. It should be noted that CPR allele mutations can influence the activity of individual CYPs, which can lead to disordered steroidogenesis and/or Antley–Bixler syndrome (ABS) [273,274]. The ABS-associated mutations R454H in the FAD domain and A284P in the linker domain are abundant in Japanese and Caucasian populations, respectively [275]. Some CPR variants were shown to have different effects in specific CYPs – for example, CPR polymorphism A500V (in the FAD domain) reduces the activity of CYP3A4 and CYP17 but not CYP21, CYP1A2, or CYP2C19 [275–279]. In structural terms, many ABS-associated mutations lie in cofactor-binding regions, such as R454H, which forms hydrogen bonds with the pyrophosphate group of the FAD cofactor. The same is true for the mutation of Y178, which faces the isoalloxazine ring of FMN, into aspartic acid, and mutation G536R near the NADPH cofactor [275,280].

The key parameter for interprotein electron transport is mutual distance of individual cofactors. The FMN–heme distance was about 18.3 Å in a crystal structure of the complex between the heme- and FMN-binding domains of bacterial CYP102A1 [281]. A similar distance was observed in our model of the CPR–CYP3A4 complex in a DOPC membrane. The initial model was constructed by docking of CYP3A4 into the open conformation of CPR on a membrane and then relaxing the resulting structure in a 400-ns MD simulation (Fig. 14). The distance between the reduced FMN and the heme fluctuated around 21.7 ± 0.5 Å over the last 100 ns of the simulation, in reasonably good agreement with the distance observed in the X-ray structure of CYP102A1 with the FMN-binding domain. On the other hand, this distance is still larger than the optimal distance for interprotein electron transfer of 14 A or less [282]. Multiple CPR amino acids have been proposed to interact with CYPs (Table S6) [253,255,283], but a recent NMR experiment indicated that CPR primarily interacts with CYP via its ^{87}QTGT^{90} region (Table S6) [283]. Our model of the CPR–CYP3A4 complex also has these residues in contact with CYP. The loops ^{140}YGEGD^{144} in CPR and ^{441}NCIGMR^{446} in CYP3A4 may also be important for electron transport (Fig. 14). In contrast, Oostenbrink et al. concluded that the most likely electron transfer pathway involves a different loop residue in CPR (Y178) but a similar set of residues in CYP2D6 (^{440}RRAC^{443}) [253]. The amino acid residues C442, M445, and R446 from hypothetical model of Adx-CYP3A4 complex were previously proposed to be involved in the interaction with its redox partner [284]. Moreover, the R446A side chain mutation in CYP 2B4, which is located in the same region as R446 in CYP3A4, weakened the interaction with CPR [267]. The formation of slightly different complexes with

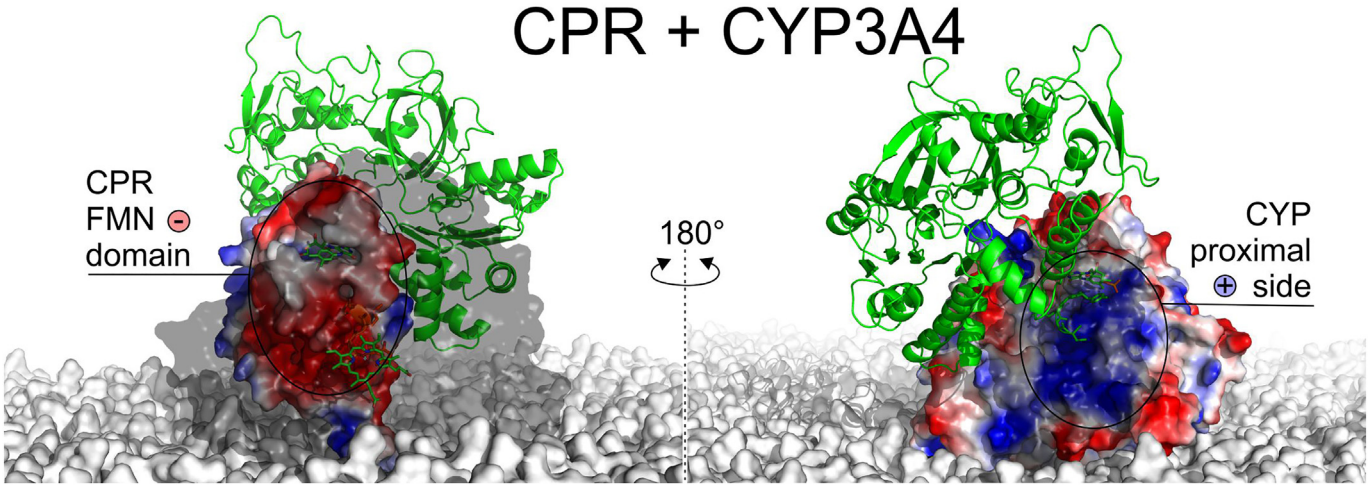

Fig. 13. Electrostatic potential surfaces at the site of interaction between the FMN domain (left) and the proximal surface of CYP3A4 (right). The FMN domain is rich in conserved negatively charged residues, whereas the CYP proximal side is mostly positive. The opposing charges on the meeting surfaces of the redox partners suggest that process of complex formation and interaction is driven by strong electrostatic forces. FMN domain and CYP are shown in surface representation with domain closer to reader rendered transparent to visualize interaction interface of the domain behind. FMN and heme are shown with sticks. Non-interacting NADPH-binding and FAD domains of CPR are shown in cartoon representation.

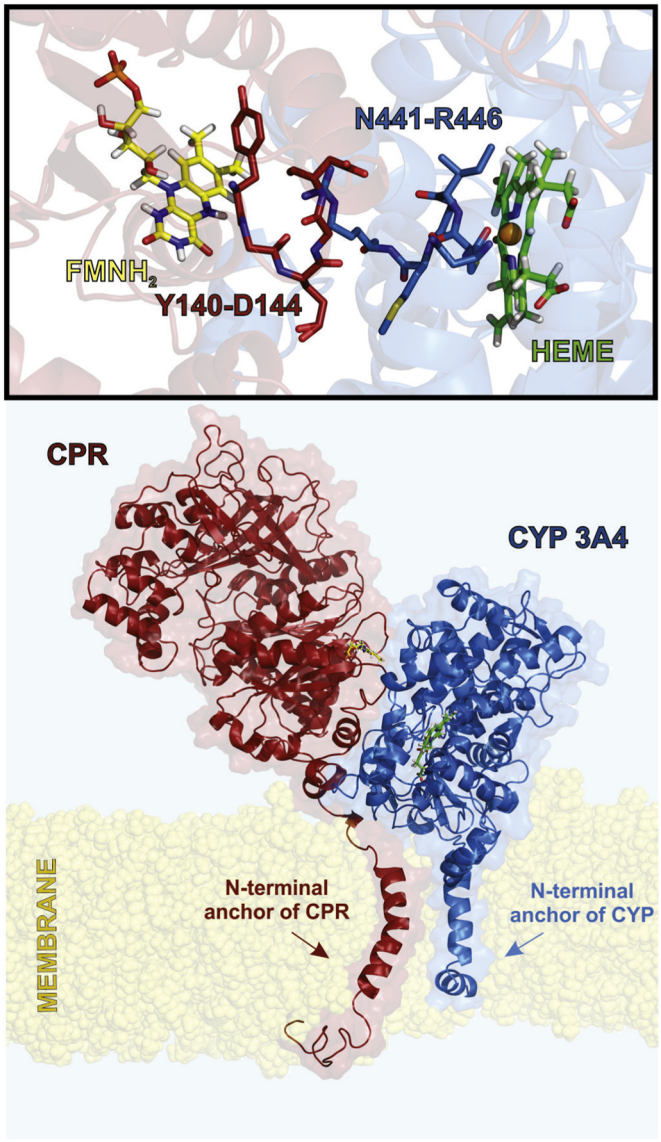

Fig. 14. Structure of the human CPR–CYP3A4 complex embedded in a membrane after a 400 ns MD simulation. The complex was stable during the simulation, and the interaction sites were consistent with experimental findings. The $FMNH_2$ and heme cofactors were located in close proximity, between residues possibly involved in electron transfer. Residues involved in cofactor binding include the Y140–D144 loop of CPR and N441–R446 in CYP3A4 (upper panel).

different CYPs is consistent with the promiscuous character of CPR.

There are some notable differences between the protein–protein complexes of CYPs with b_5 and CPR, and the nature of these differences depends on the CYP isoform under consideration. The rate of CYP substrate metabolism is elevated at low molar ratios of b_5 (with respect to CPR) but reduced at higher levels [231]. The interactions between all three partners can be also affected by the membrane environment; membranes with more negatively charged lipids induce stronger interactions between CYP2B4 and b_5 [141]. Membrane domain localization was found to stimulate the catalytic activity of CYP1A2 by promoting co-localization of CPR and CYP1A2 in ordered microdomains [84]. In sum, the interactions between CYP and its redox partners are mediated by the membrane environment, which directs the formation of protein–protein complexes and also affects their cooperation.

6. Perspectives

This review summarized the current state of knowledge regarding the behavior of CYPs in membranes. Advances in experimental and computational methods have provided important additional information on this subject and potential mechanisms of substrate binding by CYPs. On the other hand, many important questions remain to be answered. More computational studies on substrate/product binding/unbinding to the active sites of membrane-bound CYPs are needed to generalize the current preliminary picture of the mechanism of substrate binding and the role of membrane environment. Additionally, the roles of UDP-glucuronosyltransferases in consecutive steps of xenobiotic biotransformation, their co-localization, and the nature of their communication with CYPs all remain unclear. Finally, despite recent advances in NMR methods, many details of the interactions of redox partners with CYP are unknown. We are certain that future progress in H/D exchange methods, NMR and EPR spectroscopy as well as cryo-EM microscopy, and MD simulations will provide very important insights into the structural details of biotransformation of chemicals in their native environment.

7. Conclusions

Over the last few decades, the perception of CYPs on membranes has changed radically thanks to advances in experimental techniques, with X-ray crystallography playing a particularly prominent role. The early model of CYPs as transmembrane enzymes [285] has been replaced with a new model in which the CYP catalytic domain is partially immersed in the membrane and anchored to it via the N-terminal helix, as first suggested by Williams and coworkers [90]. Also the interaction of the CYP with the membrane was earlier expected to be rather rigid, and assumed the heme plane to be perpendicular or parallel to the membrane plane [28]. However, concerted efforts involving both experimental and computational techniques showed that the heme is tilted with respect to the membrane surface and that the binding and positioning of CYPs on membranes is very dynamic. The catalytic domains also interact with the membrane specifically via F/G- and B/C-loops, which are extended and more hydrophobic for membrane-bound CYPs with respect to the bacterial soluble CYPs [286]. The newer models also suggested a mechanism by which a substrate may bind to the CYP active site after entering via either the cytosol or the membrane interior, whereas in bacterial CYPs the access and egress seems to be achieved by the same channel [194]. Because amphiphilic compounds may accumulate in membranes or at the membrane/water interface, there was presumably a strong evolutionary pressure driving the colocation of biotransformation enzymes (i.e., CYPs) and their potential substrates. Membranes also house CYPs' redox partners and other enzymes that contribute to the consecutive steps of xenobiotic biotransformation (UDP-glucuronosyltransferases), which makes membranes' active playgrounds responsible for the colocation and cooperation of processes involved in the biotransformation of xenobiotics and other compounds.

Abbreviations

ABS	Antley–Bixler syndrome
BE-META	bias-exchange metadynamics
b_5	cytochrome b_5
CG	coarse grain
CPR	cytochrome P450 reductase
CYP/CYPs	cytochrome P450
DAPC	1,2-diarachidonoyl-*sn*-glycero-3-phosphocholine
DMPC	1,2-dimyristoyl-*sn*-glycero-3-phosphocholine
DMXS	hydrogen–deuterium exchange mass spectrometry
DOPC	1,2-dioleoyl-*sn*-glycero-3-phosphocholine
DOPE	1,2-dioleoyl-*sn*-glycero-3-phosphoethanolamine
DOPG	1,2-dioleoyl-*sn*-glycero-3-[phospho-rac-(3-lysyl(1-glycerol))]
DOPS	1,2-dioleoyl-*sn*-glycero-3-phosphoserine
DPPC	1,2-dipalmitoyl-*sn*-glycero-3-phosphocholine
DPPE	1,2-dipalmitoyl-*sn*-glycero-3-phosphoethanolamine

DSPC	1,2-distearoyl-*sn*-glycero-3-phosphocholine
EPR	electron paramagnetic resonance
ER	endoplasmic reticulum
FAD	flavinadenindinucleotide
FMN	flavinmononucleotide
FRET	Foerster resonance energy transfer
HMMM	highly mobile membrane mimetic
MD	molecular dynamics
META	metadynamics
NADPH	nicotinamide adenine dinucleotide phosphate
NMR	nuclear magnetic resonance
PA	phosphatidic acid
PC	phosphatidylcholine
PE	phosphatidylethanolamine
PG	phosphatidylglycerol
PI	phosphatidylinositol
POPS	1-palmitoyl-2-oleoyl-*sn*-glycero-3-phospho-L-serine
PS	phosphatidylserin
RAMD	random accelerated molecular dynamics
SAXS	small-angle X-ray scattering
SMD	steered molecular dynamics
SOPC	1-stearoyl-2-oleoyl-*sn*-glycero-3-phosphocholine
TMU	1,3,7-trimethyluric acid
WHAM	weighted histogram analysis method

Acknowledgements

This work was supported by the Czech Grant Agency [project P208/12/G016]. V.B., V.N. and M.Š. acknowledge support from a student project of Palacký University Olomouc IGA_PrF_2018_032. The authors gratefully acknowledge support from the Ministry of Education, Youth and Sports of the Czech Republic [projects LO1305; CZ.02.2.69/0.0/0.0/16 (Toxicology)].

Appendix A. Supplementary data

Supplementary data to this article can be found online at https://doi.org/10.1016/j.jinorgbio.2018.03.002.

References

[1] P.R. Ortiz de Montellano, Cytochrome P450: Structure, Mechanism and Biochemistry, third ed., Kluwer Academic/Plenum Publishers, New York, 2005, http://dx.doi.org/10.1016/0891-5849(96)83807-X.
[2] P. Anzenbacher, E. Anzenbacherová, Cytochromes P450 and metabolism of xenobiotics, Cell. Mol. Life Sci. 58 (2001) 737–747, http://dx.doi.org/10.1007/PL00000897.
[3] D.R. Nelson, Cytochrome P450 diversity in the tree of life, Biochim. Biophys. Acta, Proteins Proteomics 1866 (2018) 141–154, http://dx.doi.org/10.1016/j.bbapap.2017.05.003.
[4] F.P. Guengerich, T.L. Macdonald, Chemical mechanisms of catalysis by cytochromes P-450: a unified view, Acc. Chem. Res. 17 (1984) 9–16, http://dx.doi.org/10.1021/ar00097a002.
[5] A.W. Munro, H.M. Girvan, A.E. Mason, A.J. Dunford, K.J. McLean, What makes a P450 tick? Trends Biochem. Sci. 38 (2013) 140–150, http://dx.doi.org/10.1016/j.tibs.2012.11.006.
[6] F.P. Guengerich, Mechanisms of cytochrome P450 substrate oxidation: miniReview, J. Biochem. Mol. Toxicol. 21 (2007) 163–168, http://dx.doi.org/10.1002/jbt.20174.
[7] U.M. Zanger, M. Schwab, Cytochrome P450 enzymes in drug metabolism: regulation of gene expression, enzyme activities, and impact of genetic variation, Pharmacol. Ther. 138 (2013) 103–141, http://dx.doi.org/10.1016/j.pharmthera.2012.12.007.
[8] M. Ingelman-Sundberg, S.C. Sim, A. Gomez, C. Rodriguez-Antona, Influence of cytochrome P450 polymorphisms on drug therapies: pharmacogenetic, pharmacoepigenetic and clinical aspects, Pharmacol. Ther. 116 (2007) 496–526, http://dx.doi.org/10.1016/j.pharmthera.2007.09.004.
[9] P. Anzenbacher, U.M. Zanger, Metabolism of Drugs and Other Xenobiotics, Wiley-VCH Verlag GmbH & Co. KGaA, Weinheim, Germany, 2012, http://dx.doi.org/10.1002/9783527630905.
[10] K. Berka, M. Paloncýová, P. Anzenbacher, M. Otyepka, Behavior of human cytochromes P450 on lipid membranes, J. Phys. Chem. B 117 (2013) 11556–11564, http://dx.doi.org/10.1021/jp4059559.
[11] K.P. Conner, C.M. Woods, W.M. Atkins, Interactions of cytochrome P450s with their ligands, Arch. Biochem. Biophys. 507 (2011) 56–65, http://dx.doi.org/10.1016/j.abb.2010.10.006.
[12] S. Rendic, F.P. Guengerich, Survey of human oxidoreductases and cytochrome P450 enzymes involved in the metabolism of xenobiotic and natural chemicals, Chem. Res. Toxicol. 28 (2015) 38–42, http://dx.doi.org/10.1021/tx500444e.
[13] U.M. Zanger, M. Turpeinen, K. Klein, M. Schwab, Functional pharmacogenetics/genomics of human cytochromes P450 involved in drug biotransformation, Anal. Bioanal. Chem. 392 (2008) 1093–1108, http://dx.doi.org/10.1007/s00216-008-2291-6.
[14] I.F. Sevrioukova, T.L. Poulos, Understanding the mechanism of cytochrome P450 3A4: recent advances and remaining problems, Dalton Trans. 42 (2013) 3116–3126, http://dx.doi.org/10.1039/c2dt31833d.
[15] M. Klingenberg, Pigments of rat liver microsomes, Arch. Biochem. Biophys. 75 (1958) 376–386, http://dx.doi.org/10.1016/0003-9861(58)90436-3.
[16] D. Garfinkel, Studies on pig liver microsomes. I. Enzymic and pigment composition of different microsomal fractions, Arch. Biochem. Biophys. 77 (1958) 493–509 http://www.ncbi.nlm.nih.gov/pubmed/13584011.
[17] T. Omura, R. Sato, A new cytochrome in liver microsomes, J. Biol. Chem. 237 (1962) PC1375–PC1376.
[18] T. Omura, R. Sato, The carbon monoxide-biding pigment of liver microsomes: I. Evidence for its hemoprotein nature, J. Biol. Chem. 239 (1964) 2370–2378.
[19] M. Otyepka, J. Skopalík, E. Anzenbacherová, P. Anzenbacher, What common structural features and variations of mammalian P450s are known to date? Biochim. Biophys. Acta, Gen. Subj. 1770 (2007) 376–389, http://dx.doi.org/10.1016/j.bbagen.2006.09.013.
[20] F.P. Guengerich, M.R. Waterman, M. Egli, Recent structural insights into cytochrome P450 function, Trends Pharmacol. Sci. 37 (2016) 625–640, http://dx.doi.org/10.1016/j.tips.2016.05.006.
[21] P.W. Rose, B. Beran, C. Bi, W.F. Bluhm, D. Dimitropoulos, D.S. Goodsell, A. Prlic, M. Quesada, G.B. Quinn, J.D. Westbrook, J. Young, B. Yukich, C. Zardecki, H.M. Berman, P.E. Bourne, The RCSB Protein Data Bank: redesigned web site and web services, Nucleic Acids Res. 39 (2011) D392–D401, http://dx.doi.org/10.1093/nar/gkq1021.
[22] K. Yamamoto, U.H. Dürr, J. Xu, S.-C. Im, L. Waskell, A. Ramamoorthy, Dynamic interaction between membrane-bound full-length cytochrome P450 and cytochrome b5 observed by solid-state NMR spectroscopy, Sci. Rep. 3 (2013) 1–5, http://dx.doi.org/10.1038/srrep02538.
[23] K. Yamamoto, M.A. Caporini, S.-C. Im, L. Waskell, A. Ramamoorthy, Cellular solid-state NMR investigation of a membrane protein using dynamic nuclear polarization, Biochim. Biophys. Acta Biomembr. 1848 ((2015) 342–349, http://dx.doi.org/10.1016/j.bbamem.2014.07.008.
[24] S.C. Gay, A.G. Roberts, J.R. Halpert, Structural features of cytochromes P450 and ligands that affect drug metabolism as revealed by X-ray crystallography and NMR, Future Med. Chem. 2 (2010) 1451–1468, http://dx.doi.org/10.4155/fmc.10.229.
[25] V.L. Tsuprun, K.N. Myasoedova, P. Berndt, O.N. Sograf, E.V. Orlova, V.Y. Chernyak, A.I. Archakov, V.P. Skulachev, Quaternary structure of the liver microsomal cytochrome P-450, FEBS Lett. 205 (1986) 35–40, http://dx.doi.org/10.1016/0014-5793(86)80861-4.
[26] T.H. Bayburt, S.G. Sligar, Single-molecule height measurements on microsomal cytochrome P450 in nanometer-scale phospholipid bilayer disks, Proc. Natl. Acad. Sci. 99 (2002) 6725–6730, http://dx.doi.org/10.1073/pnas.062565599.
[27] M.R. Nussio, N.H. Voelcker, J.O. Miners, B.C. Lewis, M.J. Sykes, J.G. Shapter, AFM study of the interaction of cytochrome P450 2C9 with phospholipid bilayers, Chem. Phys. Lipids 163 (2010) 182–189, http://dx.doi.org/10.1016/j.chemphyslip.2009.11.003.
[28] S.D. Black, Membrane topology of the mammalian P450 cytochromes, FASEB J. 6 (1992) 680–685.
[29] C. von Wachenfeldt, E.F. Johnson, Structures of Eukaryotic Cytochrome P450 Enzymes, Springer US, Boston, MA, 1995, http://dx.doi.org/10.1007/978-1-4757-2391-5_6.
[30] E. Langenfeld, U.M. Zanger, K. Jung, H.E. Meyer, K. Marcus, Mass spectrometry-based absolute quantification of microsomal cytochrome P450 2D6 in human liver, Proteomics 9 (2009) 2313–2323, http://dx.doi.org/10.1002/pmic.200800680.
[31] G. Redlich, U.M. Zanger, S. Riedmaier, N. Bache, A.B.M. Giessing, M. Eisenacher, C. Stephan, H.E. Meyer, O.N. Jensen, K. Marcus, Distinction between human cytochrome P450 (CYP) isoforms and identification of new phosphorylation sites by mass spectrometry, J. Proteome Res. 7 (2008) 4678–4688, http://dx.doi.org/10.1021/pr800231w.
[32] K. Nithipatikom, A.J. Grall, B.B. Holmes, D.R. Harder, J.R. Falck, W.B. Campbell, Liquid chromatographic-electrospray ionization-mass spectrometric analysis of cytochrome P450 metabolites of arachidonic acid, Anal. Biochem. 298 (2001) 327–336, http://dx.doi.org/10.1006/abio.2001.5395.
[33] I.A. Pikuleva, N. Mast, W.-L. Liao, I.V. Turko, Studies of membrane topology of mitochondrial cholesterol hydroxylases CYPs 27A1 and 11A1, Lipids 43 (2008) 1127–1132, http://dx.doi.org/10.1007/s11745-008-3234-x.
[34] N. Mast, W.-L. Liao, I.A. Pikuleva, I.V. Turko, Combined use of mass spectrometry and heterologous expression for identification of membrane-interacting peptides in cytochrome P450 46A1 and NADPH-cytochrome P450 oxidoreductase, Arch. Biochem. Biophys. 483 (2009) 81–89, http://dx.doi.org/10.1016/j.abb.2009.01.002.
[35] C. Ozalp, E. Szczesna-Skorupa, B. Kemper, Identification of membrane-contacting loops of the catalytic domain of cytochrome P450 2C2 by tryptophan fluorescence ccanning, Biochemistry 45 (2006) 4629–4637, http://dx.doi.org/10.1021/

bi051372t.
[36] J.L. Baylon, I.L. Lenov, S.G. Sligar, E. Tajkhorshid, Characterizing the membrane-bound state of cytochrome P450 3A4: structure, depth of insertion, and orientation, J. Am. Chem. Soc. 135 (2013) 8542–8551, http://dx.doi.org/10.1021/ja4003525.
[37] G. Hu, E.F. Johnson, B. Kemper, CYP2C8 exists as a dimer in natural membranes, Drug Metab. Dispos. 38 (2010) 1976–1983, http://dx.doi.org/10.1124/dmd.110.034942.
[38] S. Shaik, D. Kumar, S.P. de Visser, A. Altun, W. Thiel, Theoretical perspective on the structure and mechanism of cytochrome P450 enzymes, Chem. Rev. 105 (2005) 2279–2328, http://dx.doi.org/10.1021/cr030722j.
[39] J. Sgrignani, A. Magistrato, Influence of the membrane lipophilic environment on the structure and on the substrate access/egress routes of the human aromatase enzyme. A computational study, J. Chem. Inf. Model. 52 (2012) 1595–1606, http://dx.doi.org/10.1021/ci300151h.
[40] J. Park, L. Czapla, R.E. Amaro, Molecular simulations of aromatase reveal new insights into the mechanism of ligand binding, J. Chem. Inf. Model. 53 (2013) 2047–2056, http://dx.doi.org/10.1021/ci400225w.
[41] G.D. Szklarz, J.R. Halpert, Use of homology modeling in conjunction with site-directed mutagenesis for analysis of structure-function relationships of mammalian cytochromes P450, Life Sci. 61 (1997) 2507–2520, http://dx.doi.org/10.1016/S0024-3205(97)00717-0.
[42] D.F. Lewis, M. Dickins, P.J. Eddershaw, M.H. Tarbit, P.S. Goldfarb, Cytochrome P450 substrate specificities, substrate structural templates and enzyme active site geometries, Drug Metabol. Drug Interact. 15 (1999) 1–49.
[43] R. Dai, M.R. Pincus, F.K. Friedman, Molecular modeling of mammalian cytochrome P450s, Cell. Mol. Life Sci. 57 (2000) 487–499, http://dx.doi.org/10.1007/PL00000709.
[44] D.R. Nelson, L. Koymans, T. Kamataki, J.J. Stegeman, R. Feyereisen, D.J. Waxman, M.R. Waterman, O. Gotoh, M.J. Coon, R.W. Estabrook, I.C. Gunsalus, D.W. Nebert, P450 superfamily: update on new sequences, gene mapping, accession numbers and nomenclature, Pharmacogenetics 6 (1996) 1–42, http://dx.doi.org/10.1097/00008571-199602000-00002.
[45] T.L. Poulos, B.C. Finzel, A.J. Howard, High-resolution crystal structure of cytochrome P450cam, J. Mol. Biol. 195 (1987) 687–700, http://dx.doi.org/10.1016/0022-2836(87)90190-2.
[46] V. Cojocaru, P.J. Winn, R.C. Wade, The ins and outs of cytochrome P450s, Biochim. Biophys. Acta, Gen. Subj. 1770 (2007) 390–401, http://dx.doi.org/10.1016/j.bbagen.2006.07.005.
[47] R.C. Wade, P.J. Winn, I. Schlichting, Sudarko, A survey of active site access channels in cytochromes P450, J. Inorg. Biochem. 98 (2004) 1175–1182, http://dx.doi.org/10.1016/j.jinorgbio.2004.02.007.
[48] J. Mestres, Structure conservation in cytochromes P450, Proteins: Struct., Funct., Bioinf. 58 (2004) 596–609, http://dx.doi.org/10.1002/prot.20354.
[49] G. van Meer, D.R. Voelker, G.W. Feigenson, Membrane lipids: where they are and how they behave, Nat. Rev. Mol. Cell Biol. 9 (2008) 112–124, http://dx.doi.org/10.1038/nrm2330.
[50] B. Alberts, A. Johnson, J. Lewis, M. Raff, K. Roberts, P. Walter, Molecular Biology of the Cell, fifth ed., Garland Science, New York, 2008.
[51] J. Zidar, F. Merzel, M. Hodošček, K. Rebolj, K. Sepčić, P. Maček, D. Janežič, Liquid-ordered phase formation in cholesterol/sphingomyelin bilayers: all-atom molecular dynamics simulations, J. Phys. Chem. B 113 (2009) 15795–15802, http://dx.doi.org/10.1021/jp907138h.
[52] P. Niemelä, M.T. Hyvönen, I. Vattulainen, Structure and dynamics of sphingomyelin bilayer: insight gained through systematic comparison to phosphatidylcholine, Biophys. J. 87 (2004) 2976–2989, http://dx.doi.org/10.1529/biophysj.104.048702.
[53] G.F. Gibbons, The role of cytochrome P450 in the regulation of cholesterol biosynthesis, Lipids 37 (2002) 1163–1170, http://dx.doi.org/10.1007/s11745-002-1016-x.
[54] R.M. Epand, Cholesterol and the interaction of proteins with membrane domains, Prog. Lipid Res. 45 (2006) 279–294, http://dx.doi.org/10.1016/j.plipres.2006.02.001.
[55] J. Fantini, Interaction of proteins with lipid rafts through glycolipid-binding domains: biochemical background and potential therapeutic applications, Curr. Med. Chem. 14 (2007) 2911–2917, http://dx.doi.org/10.2174/092986707782360033.
[56] T. Róg, M. Pasenkiewicz-Gierula, I. Vattulainen, M. Karttunen, Ordering effects of cholesterol and its analogues, Biochim. Biophys. Acta Biomembr. 1788 (2009) 97–121, http://dx.doi.org/10.1016/j.bbamem.2008.08.022.
[57] T.X. Xiang, B.D. Anderson, Permeability of acetic acid across gel and liquid-crystalline lipid bilayers conforms to free-surface-area theory, Biophys. J. 72 (1997) 223–237, http://dx.doi.org/10.1016/S0006-3495(97)78661-2.
[58] E. Sackmann, Biological Membranes Architecture and Function, Elsevier, Amsterdam, 1995, http://dx.doi.org/10.1016/S1383-8121(06)80018-7.
[59] M. Panchal, J. Loeper, J.-C. Cossec, C. Perruchini, A. Lazar, D. Pompon, C. Duyckaerts, Enrichment of cholesterol in microdissected Alzheimer's disease senile plaques as assessed by mass spectrometry, J. Lipid Res. 51 (2010) 598–605, http://dx.doi.org/10.1194/jlr.M001859.
[60] G. van Meer, A.I.P.M. de Kroon, Lipid map of the mammalian cell, J. Cell Sci. 124 (2011) 5–8, http://dx.doi.org/10.1242/jcs.071233.
[61] S. Balaz, Modeling kinetics of subcellular disposition of chemicals, Chem. Rev. 109 (2009) 1793–1899, http://dx.doi.org/10.1021/cr030440j.
[62] S. Nagar, K. Korzekwa, Commentary: nonspecific protein binding versus membrane partitioning: it is not just semantics, Drug Metab. Dispos. 40 (2012) 1649–1652, http://dx.doi.org/10.1124/dmd.112.046599.
[63] D.B. Kell, S.G. Oliver, How drugs get into cells: tested and testable predictions to help discriminate between transporter-mediated uptake and lipoidal bilayer diffusion, Front. Pharmacol. 5 (2014) 1–32, http://dx.doi.org/10.3389/fphar.2014.00231.
[64] D. Smith, P. Artursson, A. Avdeef, L. Di, G.F. Ecker, B. Faller, J.B. Houston, M. Kansy, E.H. Kerns, S.D. Krämer, H. Lennernäs, H. van de Waterbeemd, K. Sugano, B. Testa, Passive lipoidal diffusion and carrier-mediated cell pptake are both important mechanisms of membrane permeation in drug disposition, Mol. Pharm. 11 (2014) 1727–1738, http://dx.doi.org/10.1021/mp400713v.
[65] F. Di Meo, G. Fabre, K. Berka, T. Ossman, B. Chantemargue, M. Paloncýová, P. Marquet, M. Otyepka, P. Trouillas, In silico pharmacology: drug membrane partitioning and crossing, Pharmacol. Res. 111 (2016) 471–486, http://dx.doi.org/10.1016/j.phrs.2016.06.030.
[66] R.C. Bean, W.C. Shepherd, H. Chan, Permeability of lipid bilayer membranes to organic solutes, J. Gen. Physiol. 52 (1968) 495–508, http://dx.doi.org/10.1085/jgp.52.3.495.
[67] M.B. Yatvin, J.N. Weinstein, W.H. Dennis, R. Blumenthal, Design of liposomes for enhanced local release of drugs by hyperthermia, Science 202 (1978) 1290–1293, http://dx.doi.org/10.1126/science.364652.
[68] J.R. Lakowicz, Fluorescence spectroscopic investigations of the dynamic properties of proteins, membranes and nucleic acids, J. Biochem. Biophys. Methods 2 (1980) 91–119, http://dx.doi.org/10.1016/0165-022X(80)90077-9.
[69] C.L. Wennberg, D. van der Spoel, J.S. Hub, Large influence of cholesterol on solute partitioning into lipid membranes, J. Am. Chem. Soc. 134 (2012) 5351–5361, http://dx.doi.org/10.1021/ja211929h.
[70] M. Paloncýová, R. DeVane, B. Murch, K. Berka, M. Otyepka, Amphiphilic drug-like molecules accumulate in a membrane below the head group region, J. Phys. Chem. B 118 (2014) 1030–1039, http://dx.doi.org/10.1021/jp4112052.
[71] M. Paloncýová, K. Berka, M. Otyepka, Molecular insight into affinities of drugs and their metabolites to lipid bilayers, J. Phys. Chem. B 117 (2013) 2403–2410, http://dx.doi.org/10.1021/jp311802x.
[72] M.J. Headlam, M.C.J. Wilce, R.C. Tuckey, The F–G loop region of cytochrome P450scc (CYP11A1) interacts with the phospholipid membrane, Biochim. Biophys. Acta Biomembr. 1617 (2003) 96–108, http://dx.doi.org/10.1016/j.bbamem.2003.09.007.
[73] J. Loeper, A. Le Berre, D. Pompon, Topology inversion of CYP2D6 in the endoplasmic reticulum is not required for plasma membrane transport, Mol. Pharmacol. 53 (1998) 408–414 http://www.ncbi.nlm.nih.gov/pubmed/9495805.
[74] J. Loeper, B. Louérat-Oriou, C. Duport, D. Pompon, Yeast expressed cytochrome P450 2D6 (CYP2D6) exposed on the external face of plasma membrane is functionally competent, Mol. Pharmacol. 54 (1998) 8–13.
[75] G.E. Tarr, S.D. Black, V.S. Fujita, M.J. Coon, Complete amino acid sequence and predicted membrane topology of phenobarbital-induced cytochrome P-450 (isozyme 2) from rabbit liver microsomes, PNAS 80 (1983) 6552–6556.
[76] J. Hudeček, P. Anzenbacher, Secondary structure prediction of liver microsomal cytochrome P-450; proposed model of spatial arrangement in a membrane, Biochim. Biophys. Acta Protein Struct. Mol. Enzymol. 955 (1988) 361–370, http://dx.doi.org/10.1016/0167-4838(88)90216-6.
[77] E. Szczesna-Skorupa, B. Kemper, NH2-terminal substitutions of basic amino acids induce translocation across the microsomal membrane and glycosylation of rabbit cytochrome P450IIC2, J. Cell Biol. 108 (1989) 1237–1243, http://dx.doi.org/10.1083/jcb.108.4.1237.
[78] S. Monier, P. Van Luc, G. Kreibich, D.D. Sabatini, M. Adesnik, Signals for the incorporation and orientation of cytochrome P450 in the endoplasmic reticulum membrane, J. Cell Biol. 107 (1988) 457–470.
[79] C. Cullin, Two distinct sequences control the targeting and anchoring of the mouse P450 1A1 into the yeast endoplasmic reticulum membrane, Biochem. Biophys. Res. Commun. 184 (1992) 1490–1495, http://dx.doi.org/10.1016/S0006-291X(05)80051-8.
[80] G. Vergères, K.H. Winterhalter, C. Richter, Localization of the N-terminal methionine of rat liver cytochrome P-450 in the lumen of the endoplasmic reticulum, Biochim. Biophys. Acta Biomembr. 1063 (1991) 235–241, http://dx.doi.org/10.1016/0005-2736(91)90376-J.
[81] S. High, B. Dobberstein, Mechanisms that determine the transmembrane disposition of proteins, Curr. Opin. Cell Biol. 4 (1992) 581–586, http://dx.doi.org/10.1016/0955-0674(92)90075-N.
[82] N.G. Avadhani, M.C. Sangar, S. Bansal, P. Bajpai, Bimodal targeting of cytochrome P450s to endoplasmic reticulum and mitochondria: the concept of chimeric signals, FEBS J. 278 (2011) 4218–4229, http://dx.doi.org/10.1111/j.1742-4658.2011.08356.x.
[83] H.H. Jang, D.H. Kim, T. Ahn, C.H. Yun, Functional and conformational modulation of human cytochrome P450 1B1 by anionic phospholipids, Arch. Biochem. Biophys. 493 (2010) 143–150, http://dx.doi.org/10.1016/j.abb.2009.10.012.
[84] J.W. Park, J.R. Reed, W.L. Backes, The localization of cytochrome P450s CYP1A1 and CYP1A2 into different lipid microdomains is governed by their N-terminal and internal protein regions, J. Biol. Chem. 290 (2015) 29449–29460, http://dx.doi.org/10.1074/jbc.M115.687103.
[85] M. Subramanian, H. Tam, H. Zheng, T.S. Tracy, CYP2C9-CYP3A4 protein-protein interactions: role of the hydrophobic N terminus, Drug Metab. Dispos. 38 (2010) 1003–1009, http://dx.doi.org/10.1124/dmd.109.030155.
[86] D.A. Gideon, R. Kumari, A.M. Lynn, K.M. Manoj, What is the functional role of N-terminal transmembrane helices in the metabolism mediated by liver microsomal cytochrome P450 and its reductase? Cell Biochem. Biophys. 63 (2012) 35–45, http://dx.doi.org/10.1007/s12013-012-9339-0.
[87] M. Sakaguchi, R. Tomiyoshi, T. Kuroiwa, K. Mihara, T. Omura, Functions of signal and signal-anchor sequences are determined by the balance between the hydrophobic segment and the N-terminal charge, Proc. Natl. Acad. Sci. 89 (1992) 16–19,

http://dx.doi.org/10.1073/pnas.89.1.16.
[88] T. Omura, Mitochondrial P450s, Chem. Biol. Interact. 163 (2006) 86–93, http://dx.doi.org/10.1016/j.cbi.2006.06.008.
[89] R.N. DuBois, E.R. Simpson, J. Tuckey, J.D. Lambeth, M.R. Waterman, Evidence for a higher molecular weight precursor of cholesterol side-chain-cleavage cytochrome P-450 and induction of mitochondrial and cytosolic proteins by corticotropin in adult bovine adrenal cells, Proc. Natl. Acad. Sci. 78 (1981) 1028–1032, http://dx.doi.org/10.1073/pnas.78.2.1028.
[90] P.A. Williams, J. Cosme, V. Sridhar, E.F. Johnson, D.E. McRee, Mammalian microsomal cytochrome P450 monooxygenase: structural adaptations for membrane binding and functional diversity, Mol. Cell 5 (2000) 121–131, http://dx.doi.org/10.1016/S1097-2765(00)80408-6.
[91] S.J. Pernecky, J.R. Larson, R.M. Philpot, M.J. Coon, Expression of truncated forms of liver microsomal P450 cytochromes 2B4 and 2E1 in Escherichia coli: influence of NH2-terminal region on localization in cytosol and membranes, Proc. Natl. Acad. Sci. U. S. A. 90 (1993) 2651–2655.
[92] A.C. Kempf, U.M. Zanger, U.a. Meyer, Truncated human P450 2D6P: expression in Escherichia coli, Ni2+-chelate affinity purification, and characterization of solubility and aggregation, Arch. Biochem. Biophys. 321 (1995) 277–288, http://dx.doi.org/10.1006/abbi.1995.1396.
[93] P.A. Williams, J. Cosme, A. Ward, H.C. Angove, D. Matak Vinković, H. Jhoti, Crystal structure of human cytochrome P450 2C9 with bound warfarin, Nature 424 (2003) 464–468, http://dx.doi.org/10.1038/nature01862.
[94] M.R. Wester, J.K. Yano, G.A. Schoch, C. Yang, K.J. Griffin, C.D. Stout, E.F. Johnson, The structure of human cytochrome P450 2C9 complexed with flurbiprofen at 2.0-Å sesolution, J. Biol. Chem. 279 (2004) 35630–35637, http://dx.doi.org/10.1074/jbc.M405427200.
[95] S. Kumar, Engineering cytochrome P450 biocatalysts for biotechnology, medicine and bioremediation, Expert Opin. Drug Metab. Toxicol. 6 (2010) 115–131, http://dx.doi.org/10.1517/17425250903431040.
[96] B.C. Monk, T.M. Tomasiak, M.V. Keniya, F.U. Huschmann, J.D.A. Tyndall, J.D. O'Connell, R.D. Cannon, J.G. McDonald, A. Rodriguez, J.S. Finer-Moore, R.M. Stroud, Architecture of a single membrane spanning cytochrome P450 suggests constraints that orient the catalytic domain relative to a bilayer, Proc. Natl. Acad. Sci. 111 (2014) 3865–3870, http://dx.doi.org/10.1073/pnas.1324245111.
[97] J.D.A. Tyndall, M. Sabherwal, A.A. Sagatova, M.V. Keniya, J. Negroni, R.K. Wilson, M.A. Woods, K. Tietjen, B.C. Monk, Structural and functional elucidation of yeast lanosterol 14α-demethylase in complex with agrochemical antifungals, PLoS One 11 (2016) e0167485, , http://dx.doi.org/10.1371/journal.pone.0167485.
[98] B.C. Monk, M. Sabherwal, J.D.A. Tyndall, PDB ID 5UL0; Structure of Pre-Clinical Drug VT-1161 with *Saccharomyces Cerevisiae* Lanosterol 14alpha Demthylase, https://www.rcsb.org/structure/5ul0.
[99] J. Skopalík, P. Anzenbacher, M. Otyepka, Flexibility of human cytochromes P450: molecular dynamics reveals differences between CYPs 3A4, 2C9, and 2A6, which correlate with their substrate preferences, J. Phys. Chem. B 112 (2008) 8165–8173, http://dx.doi.org/10.1021/jp800311c.
[100] J.K. Yano, M.R. Wester, G.A. Schoch, K.J. Griffin, C.D. Stout, E.F. Johnson, The structure of human microsomal cytochrome P450 3A4 determined by X-ray crystallography to 2.05 Å resolution, J. Biol. Chem. 279 (2004) 38091–38094, http://dx.doi.org/10.1074/jbc.C400293200.
[101] K. Berka, T. Hendrychová, P. Anzenbacher, M. Otyepka, Membrane position of ibuprofen agrees with suggested access path entrance to cytochrome P450 2C9 active site, J. Phys. Chem. A 115 (2011) 11248–11255, http://dx.doi.org/10.1021/jp204488j.
[102] V. Cojocaru, K. Balali-Mood, M.S.P. Sansom, R.C. Wade, Structure and dynamics of the membrane-bound cytochrome P450 2C9, PLoS Comput. Biol. 7 (2011) e1002152, , http://dx.doi.org/10.1371/journal.pcbi.1002152.
[103] D.R. McDougle, J.L. Baylon, D.D. Meling, A. Kambalyal, Y.V. Grinkova, J. Hammernik, E. Tajkhorshid, A. Das, Incorporation of charged residues in the CYP2J2 F-G loop disrupts CYP2J2–lipid bilayer interactions, Biochim. Biophys. Acta Biomembr. 1848 (2015) 2460–2470, http://dx.doi.org/10.1016/j.bbamem.2015.07.015.
[104] A.A. Sagatova, M.V. Keniya, R.K. Wilson, B.C. Monk, J.D.A. Tyndall, Structural insights into binding of the antifungal drug fluconazole to Saccharomyces cerevisiae lanosterol 14α-demethylase, Antimicrob. Agents Chemother. 59 (2015) 4982–4989, http://dx.doi.org/10.1128/AAC.00925-15.
[105] N. Skar-Gislinge, S.A. Kynde, I.G. Denisov, X. Ye, I. Lenov, S.G. Sligar, L. Arleth, Small-angle scattering determination of the shape and localization of human cytochrome P450 embedded in a phospholipid nanodisc environment, Acta Crystallogr., Sect. D: Biol. Crystallogr. 71 (2015) 2412–2421, http://dx.doi.org/10.1107/S1399004715018702.
[106] H.-C. Yang, C.-H. Yang, M.Y. Huang, J.-F. Lu, J.-S. Wang, Y.-Q. Yeh, U.-S. Jeng, Homology modeling and molecular dynamics simulation combined with X-ray solution scattering defining protein structures of thromboxane and prostacyclin synthases, J. Phys. Chem. B 121 (2017) 11229–11240, http://dx.doi.org/10.1021/acs.jpcb.7b08299.
[107] V. Navrátilová, M. Paloncýová, M. Kajšová, K. Berka, M. Otyepka, Effect of cholesterol on the structure of membrane-attached cytochrome P450 3A4, J. Chem. Inf. Model. 55 (2015) 628–635, http://dx.doi.org/10.1021/ci500645k.
[108] V. Navrátilová, M. Paloncýová, K. Berka, M. Otyepka, Effect of lipid charge on membrane immersion of cytochrome P450 3A4, J. Phys. Chem. B 120 (2016) 11205–11213, http://dx.doi.org/10.1021/acs.jpcb.6b10108.
[109] Y.-L. Cui, Q. Xue, Q.-C. Zheng, J.-L. Zhang, C.-P. Kong, J.-R. Fan, H.-X. Zhang, Structural features and dynamic investigations of the membrane-bound cytochrome P450 17A1, Biochim. Biophys. Acta Biomembr. 1848 (2015) 2013–2021, http://dx.doi.org/10.1016/j.bbamem.2015.05.017.
[110] X. Yu, V. Cojocaru, G. Mustafa, O.M. Salo-Ahen, G.I. Lepesheva, R.C. Wade, Dynamics of CYP51: implications for function and inhibitor design, J. Mol. Recognit. 28 (2015) 59–73, http://dx.doi.org/10.1002/jmr.2412.
[111] Y. Ohta, S. Kawato, H. Tagashira, S. Takemori, S. Kominami, Dynamic structures of adrenocortical cytochrome P-450 in proteoliposomes and microsomes: protein rotation study, Biochemistry 31 (1992) 12680–12687, http://dx.doi.org/10.1021/bi00165a019.
[112] R.J. Edwards, B.P. Murray, A.M. Singleton, A.R. Boobis, Orientation of cytochromes P450 in the endoplasmic reticulum, Biochemistry 30 (1991) 71–76, http://dx.doi.org/10.1021/bi00215a011.
[113] S. Kawato, J. Gut, R.J. Cherry, K.H. Winterhalter, C. Richter, Rotation of Cytochrome P-450, J. Biol. Chem. 257 (1982) 7023–7029.
[114] E.E. Scott, C.R. Wolf, M. Otyepka, S.C. Humphreys, J.R. Reed, C.J. Henderson, L.A. McLaughlin, M. Paloncyova, V. Navratilova, K. Berka, P. Anzenbacher, U.P. Dahal, C. Barnaba, J.A. Brozik, J.P. Jones, D.F. Estrada, J.S. Laurence, J.W. Park, W.L. Backes, The role of protein-protein and protein-membrane interactions on P450 function, Drug Metab. Dispos. 44 (2016) 576–590, http://dx.doi.org/10.1124/dmd.115.068569.
[115] P.C. Nair, R.A. McKinnon, J.O. Miners, Cytochrome P450 structure–function: insights from molecular dynamics simulations, Drug Metab. Rev. 48 (2016) 434–452, http://dx.doi.org/10.1080/03602532.2016.1178771.
[116] T.C. Pochapsky, S. Kazanis, M. Dang, Conformational plasticity and structure/function relationships in cytochromes P450, Antioxid. Redox Signal. 13 (2010) 1273–1296, http://dx.doi.org/10.1089/ars.2010.3109.
[117] M. Otyepka, K. Berka, P. Anzenbacher, Is there a relationship between the substrate preferences and structural flexibility of cytochromes P450? Curr. Drug Metab. 13 (2012) 130–142, http://dx.doi.org/10.2174/138920012798918372.
[118] T. Hendrychová, E. Anzenbacherová, J. Hudeček, J. Skopalík, R. Lange, P. Hildebrandt, M. Otyepka, P. Anzenbacher, Flexibility of human cytochrome P450 enzymes: molecular dynamics and spectroscopy reveal important function-related variations, Biochim. Biophys. Acta, Proteins Proteomics 1814 (2011) 58–68, http://dx.doi.org/10.1016/j.bbapap.2010.07.017.
[119] K. Berka, E. Anzenbacherová, T. Hendrychová, R. Lange, V. Mašek, P. Anzenbacher, M. Otyepka, Binding of quinidine radically increases the stability and decreases the flexibility of the cytochrome P450 2D6 active site, J. Inorg. Biochem. 110 (2012) 46–50, http://dx.doi.org/10.1016/j.jinorgbio.2012.02.010.
[120] S.J. Marrink, H.J. Risselada, S. Yefimov, D.P. Tieleman, A.H. de Vries, The MARTINI force field: coarse grained model for biomolecular simulations, J. Phys. Chem. B 111 (2007) 7812–7824, http://dx.doi.org/10.1021/jp071097f.
[121] R. Lonsdale, S.L. Rouse, M.S.P. Sansom, A.J. Mulholland, A multiscale approach to modelling drug metabolism by membrane-bound cytochrome P450 enzymes, PLoS Comput. Biol. 10 (2014) e1003714, , http://dx.doi.org/10.1371/journal.pcbi.1003714.
[122] P. Jeřábek, J. Florián, V. Martínek, Lipid molecules can induce an opening of membrane-facing tunnels in cytochrome P450 1A2, Phys. Chem. Chem. Phys. 18 (2016) 30344–30356, http://dx.doi.org/10.1039/C6CP03692A.
[123] P. Jeřábek, J. Florián, V. Martínek, Membrane-anchored cytochrome P450 1A2–cytochrome b 5 complex features an X-shaped contact between antiparallel transmembrane helices, Chem. Res. Toxicol. 29 (2016) 626–636, http://dx.doi.org/10.1021/acs.chemrestox.5b00349.
[124] L.J. Pike, The challenge of lipid rafts, J. Lipid Res. 50 (2009) S323–S328, http://dx.doi.org/10.1194/jlr.R800040-JLR200.
[125] E.E. Prieschl, T. Baumruker, Sphingolipids: second messengers, mediators and raft constituents in signaling, Immunol. Today 21 (2000) 555–560, http://dx.doi.org/10.1016/S0167-5699(00)01725-4.
[126] J.P. Incardona, S. Eaton, Cholesterol in signal transduction, Curr. Opin. Cell Biol. 12 (2000) 193–203, http://dx.doi.org/10.1016/S0955-0674(99)00076-9.
[127] T.V. Kurzchalia, R.G. Parton, Membrane microdomains and caveolae, Curr. Opin. Cell Biol. 11 (1999) 424–431, http://dx.doi.org/10.1016/S0955-0674(99)80061-1.
[128] K. Jacobson, C. Dietrich, Looking at lipid rafts? Trends Cell Biol. 9 (1999) 87–91, http://dx.doi.org/10.1016/S0962-8924(98)01495-0.
[129] D.A. Brown, E. London, Functions of lipid rafts in biological membranes, Annu. Rev. Cell Dev. Biol. 14 (1998) 111–136, http://dx.doi.org/10.1146/annurev.cellbio.14.1.111.
[130] L.M. Brignac-Huber, J.R. Reed, M.K. Eyer, W.L. Backes, Relationship between CYP1A2 localization and lipid microdomain formation as a function of lipid composition, Drug Metab. Dispos. 41 (2013) 1896–1905, http://dx.doi.org/10.1124/dmd.113.053611.
[131] J.W. Park, J.R. Reed, L.M. Brignac-Huber, W.L. Backes, Cytochrome P450 system proteins reside in different regions of the endoplasmic reticulum, Biochem. J. 464 (2014) 241–249, http://dx.doi.org/10.1042/BJ20140787.
[132] J.R. Reed, W.L. Backes, Formation of P450·P450 complexes and their effect on P450 function, Pharmacol. Ther. 133 (2012) 299–310, http://dx.doi.org/10.1016/j.pharmthera.2011.11.009.
[133] W.D. McClary, J.P. Sumida, M. Scian, L. Paço, W.M. Atkins, Membrane fluidity modulates thermal stability and ligand binding of cytochrome P4503A4 in lipid nanodiscs, Biochemistry 55 (2016) 6258–6268, http://dx.doi.org/10.1021/acs.biochem.6b00715.
[134] K. Bodin, U. Andersson, E. Rystedt, E. Ellis, M. Norlin, I. Pikuleva, G. Eggertsen, I. Björkhem, U. Diczfalusy, Metabolism of 4β-hydroxycholesterol in humans, J. Biol. Chem. 277 (2002) 31534–31540, http://dx.doi.org/10.1074/jbc.M201712200.
[135] R. Shinkyo, F.P. Guengerich, Inhibition of human cytochrome P450 3A4 by cholesterol, J. Biol. Chem. 286 (2011) 18426–18433, http://dx.doi.org/10.1074/jbc.

M111.240457.
[136] T. Ahn, F.P. Guengerich, C.-H. Yun, Membrane insertion of cytochrome P450 1A2 promoted by anionic phospholipids, Biochemistry 37 (1998) 12860–12866, http://dx.doi.org/10.1021/bi980804f.
[137] K.-H. Kim, T. Ahn, C.-H. Yun, Membrane properties induced by anionic phospholipids and phosphatidylethanolamine are critical for the membrane binding and catalytic activity of human cytochrome P450 3A4, Biochemistry 42 (2003) 15377–15387, http://dx.doi.org/10.1021/bi035280k.
[138] C. Barnaba, K. Gentry, N. Sumangala, A. Ramamoorthy, The catalytic function of cytochrome P450 is entwined with its membrane-bound nature, F1000Research. 6 (2017) 662, http://dx.doi.org/10.12688/f1000research.11015.1.
[139] T. Laursen, K. Jensen, B.L. Møller, Conformational changes of the NADPH-dependent cytochrome P450 reductase in the course of electron transfer to cytochromes P450, Biochim. Biophys. Acta, Proteins Proteomics 1814 (2011) 132–138, http://dx.doi.org/10.1016/j.bbapap.2010.07.003.
[140] M. Ingelman-Sundberg, A.-L. Hagbjörk, Y.-F. Ueng, H. Yamazaki, F.P. Guengerich, High rates of substrate hydroxylation by human cytochrome P450 3A4 in reconstituted membranous vesicles: influence of membrane charge, Biochem. Biophys. Res. Commun. 221 (1996) 318–322, http://dx.doi.org/10.1006/bbrc.1996.0593.
[141] T. Ravula, C. Barnaba, M. Mahajan, G.M. Anantharamaiah, S.-C. Im, L. Waskell, A. Ramamoorthy, Membrane environment drives cytochrome P450's spin transition and its interaction with cytochrome b 5, Chem. Commun. 53 (2017) 12798–12801, http://dx.doi.org/10.1039/c7cc07520k.
[142] P. Ross Wilderman, J.R. Halpert, Plasticity of CYP2B enzymes: structural and solution biophysical methods, Curr. Drug Metab. 13 (2012) 167–176, http://dx.doi.org/10.2174/138920012798918417.
[143] J. Hritz, A. de Ruiter, C. Oostenbrink, Impact of plasticity and flexibility on docking results for cytochrome P450 2D6: a combined approach of molecular dynamics and ligand docking, J. Med. Chem. 51 (2008) 7469–7477, http://dx.doi.org/10.1021/jm801005m.
[144] M. Ekroos, T. Sjogren, Structural basis for ligand promiscuity in cytochrome P450 3A4, Proc. Natl. Acad. Sci. 103 (2006) 13682–13687, http://dx.doi.org/10.1073/pnas.0603236103.
[145] C. Hayes, D. Ansbro, M. Kontoyianni, Elucidating substrate promiscuity in the human cytochrome 3A4, J. Chem. Inf. Model. 54 (2014) 857–869, http://dx.doi.org/10.1021/ci4006782.
[146] A. Babtie, N. Tokuriki, F. Hollfelder, What makes an enzyme promiscuous? Curr. Opin. Chem. Biol. 14 (2010) 200–207, http://dx.doi.org/10.1016/j.cbpa.2009.11.028.
[147] F.P. Guengerich, Common and uncommon cytochrome P450 reactions related to metabolism and chemical toxicity, Chem. Res. Toxicol. 14 (2001) 611–650, http://dx.doi.org/10.1021/tx0002583.
[148] F.P. Guengerich, Cytochrome P450: what have we learned and what are the future issues? Drug Metab. Rev. 36 (2004) 159–197, http://dx.doi.org/10.1081/DMR-120033996.
[149] I.F. Sevrioukova, T.L. Poulos, Current approaches for investigating and predicting cytochrome P450 3A4-ligand interactions, Adv. Exp. Med. Biol. 851 (2015) 83–105, http://dx.doi.org/10.1007/978-3-319-16009-2_3.
[150] J.W. Levy, J.H. Hartman, M.D. Perry, G.P. Miller, Structural basis for cooperative binding of azoles to CYP2E1 as interpreted through guided molecular dynamics simulations, J. Mol. Graph. Model. 56 (2015) 43–52, http://dx.doi.org/10.1016/j.jmgm.2014.11.013.
[151] P. Hlavica, Challenges in assignment of allosteric effects in cytochrome P450-catalyzed substrate oxidations to structural dynamics in the hemoprotein architecture, J. Inorg. Biochem. 167 (2017) 100–115, http://dx.doi.org/10.1016/j.jinorgbio.2016.11.025.
[152] B. Ma, M. Shatsky, H.J. Wolfson, R. Nussinov, Multiple diverse ligands binding at a single protein site: a matter of pre-existing populations, Protein Sci. 11 (2009) 184–197, http://dx.doi.org/10.1110/ps.21302.
[153] H.A. Carlson, Protein flexibility and drug design: how to hit a moving target, Curr. Opin. Chem. Biol. 6 (2002) 447–452, http://dx.doi.org/10.1016/S1367-5931(02)00341-1.
[154] S. Ekins, D.M. Stresser, J.A. Williams, In vitro and pharmacophore insights into CYP3A enzymes, Trends Pharmacol. Sci. 24 (2003) 161–166, http://dx.doi.org/10.1016/S0165-6147(03)00049-X.
[155] E.M. Isin, F.P. Guengerich, Substrate binding to cytochromes P450, Anal. Bioanal. Chem. 392 (2008) 1019–1030, http://dx.doi.org/10.1007/s00216-008-2244-0.
[156] Y. Ueng, T. Kuwabara, Y. Chun, F.P. Guengerich, Cooperativity in oxidations catalyzed by cytochrome P450 3A4, Biochemistry 36 (1997) 370–381, http://dx.doi.org/10.1021/bi962359z.
[157] M.D. Cameron, B. Wen, A.G. Roberts, W.M. Atkins, A.P. Campbell, S.D. Nelson, Cooperative binding of acetaminophen and caffeine within the P450 3A4 active site, Chem. Res. Toxicol. 20 (2007) 1434–1441, http://dx.doi.org/10.1021/tx7000702.
[158] J. Hudeček, E. Anzenbacherová, P. Anzenbacher, A.W. Munro, P. Hildebrandt, Structural similarities and differences of the heme pockets of various P450 isoforms as revealed by resonance Raman spectroscopy, Arch. Biochem. Biophys. 383 (2000) 70–78, http://dx.doi.org/10.1006/abbi.2000.2034.
[159] P.J. Mak, I.G. Denisov, Y.V. Grinkova, S.G. Sligar, J.R. Kincaid, Defining CYP3A4 structural responses to substrate binding. Raman spectroscopic studies of a nanodisc-incorporated mammalian cytochrome P450, J. Am. Chem. Soc. 133 (2011) 1357–1366, http://dx.doi.org/10.1021/ja105869p.
[160] E. Anzenbacherová, N. Bec, P. Anzenbacher, J. Hudeček, P. Souček, C. Jung, A.W. Munro, R. Lange, Flexibility and stability of the structure of cytochromes P450 3A4 and BM-3, Eur. J. Biochem. 267 (2000) 2916–2920, http://dx.doi.org/10.1046/j.1432-1327.2000.01305.x.
[161] H. Fernando, D.R. Davydov, C.C. Chin, J.R. Halpert, Role of subunit interactions in P450 oligomers in the loss of homotropic cooperativity in the cytochrome P450 3A4 mutant L211F/D214E/F304W, Arch. Biochem. Biophys. 460 (2007) 129–140, http://dx.doi.org/10.1016/j.abb.2006.12.025.
[162] J.E. LeLean, N. Moon, W.R. Dunham, M.J. Coon, EPR spectrometry of cytochrome P450 2B4: effects of mutations and substrate binding, Biochem. Biophys. Res. Commun. 276 (2000) 762–766, http://dx.doi.org/10.1006/bbrc.2000.3539.
[163] A.G. Roberts, A.P. Campbell, W.M. Atkins, The thermodynamic landscape of testosterone binding to cytochrome P450 3A4: ligand binding and spin state equilibria, Biochemistry 44 (2005) 1353–1366, http://dx.doi.org/10.1021/bi0481390.
[164] A.G. Roberts, W.M. Atkins, Energetics of heterotropic cooperativity between α-naphthoflavone and testosterone binding to CYP3A4, Arch. Biochem. Biophys. 463 (2007) 89–101, http://dx.doi.org/10.1016/j.abb.2007.03.006.
[165] A. Luthra, I.G. Denisov, S.G. Sligar, Spectroscopic features of cytochrome P450 reaction intermediates, Arch. Biochem. Biophys. 507 (2011) 26–35, http://dx.doi.org/10.1016/j.abb.2010.12.008.
[166] M.D. Cameron, B. Wen, K.E. Allen, A.G. Roberts, J.T. Schuman, A.P. Campbell, K.L. Kunze, S.D. Nelson, Cooperative binding of midazolam with testosterone and α-naphthoflavone within the CYP3A4 active site: a NMR T1 paramagnetic relaxation study, Biochemistry 44 (2005) 14143–14151, http://dx.doi.org/10.1021/bi051689t.
[167] A.G. Roberts, J. Yang, J.R. Halpert, S.D. Nelson, K.T. Thummel, W.M. Atkins, The structural basis for homotropic and heterotropic cooperativity of midazolam metabolism by human cytochrome P450 3A4, Biochemistry 50 (2011) 10804–10818, http://dx.doi.org/10.1021/bi200924t.
[168] D. Basudhar, Y. Madrona, S. Kandel, J.N. Lampe, C.R. Nishida, P.R. Ortiz de Montellano, Analysis of cytochrome P450 CYP119 ligand-dependent conformational dynamics by two-dimensional NMR and X-ray crystallography, J. Biol. Chem. 290 (2015) 10000–10017, http://dx.doi.org/10.1074/jbc.M114.627935.
[169] H. Fernando, J.R. Halpert, D.R. Davydov, Resolution of multiple substrate binding sites in cytochrome P450 3A4: the stoichiometry of the enzyme−substrate complexes probed by FRET and job's titration, Biochemistry 45 (2006) 4199–4209, http://dx.doi.org/10.1021/bi052491b.
[170] H. Fernando, J.A.O. Rumfeldt, N.Y. Davydova, J.R. Halpert, D.R. Davydov, Multiple substrate-binding sites are retained in cytochrome P450 3A4 mutants with decreased cooperativity, Xenobiotica 41 (2011) 281–289, http://dx.doi.org/10.3109/00498254.2010.538748.
[171] E.F. Johnson, C.D. Stout, Structural diversity of human xenobiotic-metabolizing cytochrome P450 monooxygenases, Biochem. Biophys. Res. Commun. 338 (2005) 331–336, http://dx.doi.org/10.1016/j.bbrc.2005.08.190.
[172] I.F. Sevrioukova, T.L. Poulos, Structure and mechanism of the complex between cytochrome P4503A4 and ritonavir, Proc. Natl. Acad. Sci. 107 (2010) 18422–18427, http://dx.doi.org/10.1073/pnas.1010693107.
[173] I.F. Sevrioukova, T.L. Poulos, Structural and mechanistic insights into the interaction of cytochrome P4503A4 with bromoergocryptine, a type I ligand, J. Biol. Chem. 287 (2012) 3510–3517, http://dx.doi.org/10.1074/jbc.M111.317081.
[174] I.F. Sevrioukova, T.L. Poulos, Interaction of human cytochrome P4503A4 with ritonavir analogs, Arch. Biochem. Biophys. 520 (2012) 108–116, http://dx.doi.org/10.1016/j.abb.2012.02.018.
[175] P.A. Williams, J. Cosme, D.M. Vinkovic, A. Ward, H.C. Angove, P.J. Day, C. Vonhrein, I.J. Tickle, H. Jhoti, Crystal structures of human cytochrome P450 3A4 bound to metyrapone and progesterone, Science 305 (2004) 683–686, http://dx.doi.org/10.1126/science.1099736.
[176] A. Wang, C.D. Stout, Q. Zhang, E.F. Johnson, Contributions of ionic interactions and protein dynamics to cytochrome P450 2D6 (CYP2D6) substrate and inhibitor binding, J. Biol. Chem. 290 (2015) 5092–5104, http://dx.doi.org/10.1074/jbc.M114.627661.
[177] H. Berman, K. Henrick, H. Nakamura, Announcing the worldwide Protein Data Bank, Nat. Struct. Biol. 10 (2003) 980, http://dx.doi.org/10.1038/nsb1203-980.
[178] M.J. Sykes, R.A. McKinnon, J.O. Miners, Prediction of metabolism by cytochrome P450 2C9: alignment and docking studies of a validated database of substrates, J. Med. Chem. 51 (2008) 780–791, http://dx.doi.org/10.1021/jm7009793.
[179] C. de Graaf, C. Oostenbrink, P.H.J. Keizers, T. van der Wijst, A. Jongejan, N.P.E. Vermeulen, Catalytic site prediction and virtual screening of cytochrome P450 2D6 substrates by consideration of water and rescoring in automated docking, J. Med. Chem. 49 (2006) 2417–2430, http://dx.doi.org/10.1021/jm0508538.
[180] H. Park, S. Lee, J. Suh, Structural and dynamical basis of broad substrate specificity, catalytic mechanism, and inhibition of cytochrome P450 3A4, J. Am. Chem. Soc. 127 (2005) 13634–13642, http://dx.doi.org/10.1021/ja053809q.
[181] D. Fishelovitch, C. Hazan, S. Shaik, H.J. Wolfson, R. Nussinov, Structural dynamics of the cooperative binding of organic molecules in the human cytochrome P450 3A4, J. Am. Chem. Soc. 129 (2007) 1602–1611, http://dx.doi.org/10.1021/ja066007j.
[182] Y.-L. Cui, R.-L. Wu, Molecular dynamics investigations of membrane-bound CYP2C19 polymorphisms reveal distinct mechanisms for peripheral variants by long-range effects on the enzymatic activity, Mol. BioSyst. 13 (2017) 1070–1079, http://dx.doi.org/10.1039/C6MB00827E.
[183] S. Kumar, J.M. Rosenberg, D. Bouzida, R.H. Swendsen, P.A. Kollman, The weighted histogram analysis method for free-energy calculations on biomolecules. I. The method, J. Comput. Chem. 13 (1992) 1011–1021, http://dx.doi.org/10.1002/jcc.540130812.
[184] Y. Yang, S.E. Wong, F.C. Lightstone, Understanding a substrate's product regioselectivity in a family of enzymes: a case study of acetaminophen binding in cytochrome P450s, PLoS One 9 (2014) e87058, , http://dx.doi.org/10.1371/journal.pone.0087058.

[185] D. Sehnal, R. Svobodová Vařeková, K. Berka, L. Pravda, V. Navrátilová, P. Banáš, C.-M. Ionescu, M. Otyepka, J. Koča, MOLE 2.0: advanced approach for analysis of biomacromolecular channels, Aust. J. Chem. 5 (2013) 39, http://dx.doi.org/10.1186/1758-2946-5-39.
[186] K. Berka, O. Hanák, D. Sehnal, P. Banáš, V. Navrátilová, D. Jaiswal, C.-M. Ionescu, R. Svobodová Vařeková, J. Koča, M. Otyepka, MOLEonline 2.0: interactive web-based analysis of biomacromolecular channels, Nucleic Acids Res. 40 (2012) W222–W227, http://dx.doi.org/10.1093/nar/gks363.
[187] M. Petřek, M. Otyepka, P. Banáš, P. Kosinová, J. Koča, J. Damborský, CAVER: a new tool to explore routes from protein clefts, pockets and cavities, BMC Bioinf. 7 (2006) 316, http://dx.doi.org/10.1186/1471-2105-7-316.
[188] L.J. Kingsley, M.A. Lill, Ensemble generation and the influence of protein flexibility on geometric tunnel prediction in cytochrome P450 enzymes, PLoS One 9 (2014) e99408, , http://dx.doi.org/10.1371/journal.pone.0099408.
[189] L. Pravda, D. Sehnal, R. Svobodová Vařeková, V. Navrátilová, D. Toušek, K. Berka, M. Otyepka, J. Koča, ChannelsDB: database of biomolecular tunnels and pores, Nucleic Acids Res. (2017) 1–7, http://dx.doi.org/10.1093/nar/gkx868.
[190] M. Paloncýová, V. Navrátilová, K. Berka, A. Laio, M. Otyepka, Role of enzyme flexibility in ligand access and egress to active site: bias-exchange metadynamics study of 1,3,7-trimethyluric acid in cytochrome P450 3A4, J. Chem. Theory Comput. 12 (2016) 2101–2109, http://dx.doi.org/10.1021/acs.jctc.6b00075.
[191] P.J. Winn, S.K. Ludemann, R. Gauges, V. Lounnas, R.C. Wade, S.K. Lüdemann, R. Gauges, V. Lounnas, R.C. Wade, Comparison of the dynamics of substrate access channels in three cytochrome P450s reveals different opening mechanisms and a novel functional role for a buried arginine, Proc. Natl. Acad. Sci. 99 (2002) 5361–5366, http://dx.doi.org/10.1073/pnas.082522999.
[192] S.K. Lüdemann, V. Lounnas, R.C. Wade, How do substrates enter and products exit the buried active site of cytochrome P450cam? 1. Random expulsion molecular dynamics investigation of ligand access channels and mechanisms, J. Mol. Biol. 303 (2000) 797–811, http://dx.doi.org/10.1006/jmbi.2000.4154.
[193] S.K. Lüdemann, V. Lounnas, R.C. Wade, How do substrates enter and products exit the buried active site of cytochrome P450cam? 2. Steered molecular dynamics and adiabatic mapping of substrate pathways, J. Mol. Biol. 303 (2000) 813–830, http://dx.doi.org/10.1006/jmbi.2000.4155.
[194] K. Schleinkofer, P.J. Winn Sudarko, S.K. Lüdemann, R.C. Wade, Do mammalian cytochrome P450s show multiple ligand access pathways and ligand channelling? EMBO Rep. 6 (2005) 584–589, http://dx.doi.org/10.1038/sj.embor.7400420.
[195] L. Ducassou, L. Dhers, G. Jonasson, N. Pietrancosta, J.-L. Boucher, D. Mansuy, F. André, Membrane-bound human orphan cytochrome P450 2U1: sequence singularities, construction of a full 3D model, and substrate docking, Biochimie 140 (2017) 166–175, http://dx.doi.org/10.1016/j.biochi.2017.07.007.
[196] G. Di Nardo, G. Cimicata, R. Baravalle, V. Dell'Angelo, A. Ciaramella, G. Catucci, P. Ugliengo, G. Gilardi, Working at the membrane interface: Ligand-induced changes in dynamic conformation and oligomeric structure in human aromatase, Biotechnol. Appl. Biochem. 65 (2017) 46–53, http://dx.doi.org/10.1002/bab.1613.
[197] M.B. Shah, H.H. Jang, P.R. Wilderman, D. Lee, S. Li, Q. Zhang, C.D. Stout, J.R. Halpert, Effect of detergent binding on cytochrome P450 2B4 structure as analyzed by X-ray crystallography and deuterium-exchange mass spectrometry, Biophys. Chem. 216 (2016) 1–8, http://dx.doi.org/10.1016/j.bpc.2016.05.007.
[198] E.E. Scott, Y.A. He, M.R. Wester, M.A. White, C.C. Chin, J.R. Halpert, E.F. Johnson, C.D. Stout, An open conformation of mammalian cytochrome P450 2B4 at 1.6-Å resolution, Proc. Natl. Acad. Sci. 100 (2003) 13196–13201, http://dx.doi.org/10.1073/pnas.2133986100.
[199] T. Lautier, P. Urban, J. Loeper, L. Jezequel, D. Pompon, G. Truan, Ordered chimerogenesis applied to CYP2B P450 enzymes, Biochim. Biophys. Acta, Gen. Subj. 1860 (2016) 1395–1403, http://dx.doi.org/10.1016/j.bbagen.2016.03.028.
[200] P.R. Wilderman, M.B. Shah, T. Liu, S. Li, S. Hsu, A.G. Roberts, D.R. Goodlett, Q. Zhang, V.L. Woods, C.D. Stout, J.R. Halpert, Plasticity of cytochrome P450 2B4 as investigated by hydrogen-deuterium exchange mass spectrometry and x-ray crystallography, J. Biol. Chem. 285 (2010) 38602–38611, http://dx.doi.org/10.1074/jbc.M110.180646.
[201] T.I. Oprea, G. Hummer, A.E. Garcia, Identification of a functional water channel in cytochrome P450 enzymes, 94 (1997) 2133–2138, http://dx.doi.org/10.1073/pnas.94.6.2133.
[202] L.J. Kingsley, M.A. Lill, Including ligand-induced protein flexibility into protein tunnel prediction, J. Comput. Chem. 35 (2014) 1748–1756, http://dx.doi.org/10.1002/jcc.23680.
[203] W. Li, J. Shen, G. Liu, Y. Tang, T. Hoshino, Exploring coumarin egress channels in human cytochrome p450 2a6 by random acceleration and steered molecular dynamics simulations, Proteins: Struct., Funct., Bioinf. 79 (2011) 271–281, http://dx.doi.org/10.1002/prot.22880.
[204] W. Li, H. Liu, E.E. Scott, F. Gräter, J.R. Halpert, X. Luo, J. Shen, H. Jiang, Possible pathway(s) of testosterone egress from the active site of cytochrome P450 2B1: a steered molecular dynamics simulation, Drug Metab. Dispos. 33 (2005) 910–919, http://dx.doi.org/10.1124/dmd.105.004200.
[205] G.A. Schoch, J.K. Yano, M.R. Wester, K.J. Griffin, C.D. Stout, E.F. Johnson, Structure of human microsomal cytochrome P450 2C8: evidence for a peripheral fatty acid binding site, J. Biol. Chem. 279 (2004) 9497–9503, http://dx.doi.org/10.1074/jbc.M312516200.
[206] Z. Shen, F. Cheng, Y. Xu, J. Fu, W. Xiao, J. Shen, G. Liu, W. Li, Y. Tang, Investigation of indazole unbinding pathways in CYP2E1 by molecular dynamics simulations, PLoS One 7 (2012) e33500, , http://dx.doi.org/10.1371/journal.pone.0033500.
[207] B. Israelewitz, M. Gao, K. Schulten, Steered molecular dynamics and mechanical functions of proteins, Curr. Opin. Struct. Biol. 11 (2001) 224–230, http://dx.doi.org/10.1016/S0959-440X(00)00194-9.
[208] W. Li, H. Liu, X. Luo, W. Zhu, Y. Tang, J.R. Halpert, H. Jiang, Possible pathway(s) of metyrapone egress from the active site of cytochrome P450 3A4: a molecular dynamics simulation, Drug Metab. Dispos. 35 (2007) 689–696, http://dx.doi.org/10.1124/dmd.106.014019.
[209] E.E. Scott, H. Liu, Y. Qun He, W. Li, J.R. Halpert, Mutagenesis and molecular dynamics suggest structural and functional roles for residues in the N-terminal portion of the cytochrome P450 2B1 I helix, Arch. Biochem. Biophys. 423 (2004) 266–276, http://dx.doi.org/10.1016/j.abb.2003.12.035.
[210] D. Fishelovitch, S. Shaik, H.J. Wolfson, R. Nussinov, Theoretical characterization of substrate access/exit channels in the human cytochrome P450 3A4 enzyme: involvement of phenylalanine residues in the gating mechanism, J. Phys. Chem. B 113 (2009) 13018–13025, http://dx.doi.org/10.1021/jp810386z.
[211] E. Yaffe, D. Fishelovitch, H.J. Wolfson, D. Halperin, R. Nussinov, MolAxis: efficient and accurate identification of channels in macromolecules, Proteins: Struct., Funct., Bioinf. 73 (2008) 72–86, http://dx.doi.org/10.1002/prot.22052.
[212] S. Piana, A. Laio, A bias-exchange approach to protein folding, J. Phys. Chem. B 111 (2007) 4553–4559, http://dx.doi.org/10.1021/jp067873l.
[213] D. Granata, C. Camilloni, M. Vendruscolo, A. Laio, Characterization of the free-energy landscapes of proteins by NMR-guided metadynamics, Proc. Natl. Acad. Sci. 110 (2013) 6817–6822, http://dx.doi.org/10.1073/pnas.1218350110.
[214] A. Laio, F.L. Gervasio, Metadynamics: a method to simulate rare events and reconstruct the free energy in biophysics, chemistry and material science, Rep. Prog. Phys. 71 (2008) 126601, , http://dx.doi.org/10.1088/0034-4885/71/12/126601.
[215] T. Hendrychová, K. Berka, V. Navrátilová, P. Anzenbacher, M. Otyepka, Dynamics and hydration of the active sites of mammalian cytochromes P450 probed by molecular dynamics simulations, Curr. Drug Metab. 13 (2012) 177–189, http://dx.doi.org/10.2174/138920012798918408.
[216] J.C. Hackett, Membrane-embedded substrate recognition by cytochrome P450 3A4, J. Biol. Chem. (2018), http://dx.doi.org/10.1074/jbc.RA117.000961 jbc.RA117.000961.
[217] W. Jiang, D. Ghosh, Motion and flexibility in human cytochrome P450 aromatase, PLoS One 7 (2012) e32565, , http://dx.doi.org/10.1371/journal.pone.0032565.
[218] I.G. Denisov, T.M. Makris, S.G. Sligar, I. Schlichting, Structure and chemistry of cytochrome P450, Chem. Rev. 105 (2005) 2253–2278, http://dx.doi.org/10.1021/cr0307143.
[219] K.J. McLean, D. Luciakova, J. Belcher, K.L. Tee, A.W. Munro, Biological diversity of cytochrome P450 redox partner systems, Adv. Exp. Med. Biol. 851 (2015) 299–317, http://dx.doi.org/10.1007/978-3-319-16009-2_11.
[220] F. Hannemann, A. Bichet, K.M. Ewen, R. Bernhardt, Cytochrome P450 systems-biological variations of electron transport chains, Biochim. Biophys. Acta, Gen. Subj. 1770 (2007) 330–344, http://dx.doi.org/10.1016/j.bbagen.2006.07.017.
[221] E.A. Shephard, I.R. Phillips, R.M. Bayney, S.F. Pike, B.R. Rabin, Quantification of NADPH: cytochrome P -450 reductase in liver microsomes by a specific radioimmunoassay technique, Biochem. J. 211 (1983) 333–340, http://dx.doi.org/10.1042/bj2110333.
[222] M.F. Paine, M. Khalighi, J.M. Fisher, D.D. Shen, K.L. Kunze, C.L. Marsh, J.D. Perkins, K.E. Thummel, Characterization of interintestinal and intraintestinal variations in human CYP3A-dependent metabolism, J. Pharmacol. Exp. Ther. 283 (1997) 1552–1562.
[223] K. Venkatakrishnan, L.L. von Moltke, M.H. Court, J.S. Harmatz, C.L. Crespi, D.J. Greenblatt, Comparison between cytochrome P450 (CYP) content and relative activity approaches to scaling from CDNA-expressed CYPs to human liver microsomes: ratios of accessory proteins as sources of discrepancies between the approaches, Drug Metab. Dispos. 28 (2000) 1493–1504.
[224] L. Gan, L.L. von Moltke, L.A. Trepanier, J.S. Harmatz, D.J. Greenblatt, M.H. Court, Role of NADPH-cytochrome P450 reductase and cytochrome-b5/NADH-b5 reductase in variability of CYP3A activity in human liver microsomes, Drug Metab. Dispos. 37 (2009) 90–96, http://dx.doi.org/10.1124/dmd.108.023424.
[225] A.C. Orjuela Leon, A. Marwosky, M. Arand, Evidence for a complex formation between CYP2J5 and mEH in living cells by FRET analysis of membrane protein interaction in the endoplasmic reticulum (FAMPIR), Arch. Toxicol. 91 (2017) 3561–3570, http://dx.doi.org/10.1007/s00204-017-2072-0.
[226] B.A. Schacter, E.B. Nelson, H.S. Marver, B.S. Masters, Immunochemical evidence for an association of heme oxygenase with the microsomal electron transport system, J. Biol. Chem. 247 (1972) 3601–3607.
[227] M. Nagao, T. Ishibashi, T. Okayasu, Y. Imai, Possible involvement of NADPH-cytochrome P450 reductase and cytochrome b5 on beta-ketostearoyl-CoA reduction in microsomal fatty acid chain elongation supported by NADPH, FEBS Lett. 155 (1983) 11–14, http://dx.doi.org/10.1016/0014-5793(83)80198-7.
[228] T.D. Porter, New insights into the role of cytochrome P450 reductase (POR) in microsomal redox biology, Acta Pharm. Sin. B 2 (2012) 102–106, http://dx.doi.org/10.1016/j.apsb.2012.02.002.
[229] O. Teruo, O. Shigeru, H. Fumihiko, I. Yoh, Involvement of NADPH-cytochrome c reductase in the rat liver squalene epoxidase system, Biochim. Biophys. Acta (BBA) - Mol. Basis Dis. 486 (1977) 401–407, http://dx.doi.org/10.1016/0005-2760(77)90089-3.
[230] F. Velick, The oxidation-reduction stoichiometry and potential of microsomal cytochrome, J. Biol. Chem. 221 (1955) 265–276.
[231] S.-C. Im, L. Waskell, The interaction of microsomal cytochrome P450 2B4 with its redox partners, cytochrome P450 reductase and cytochrome b5, Arch. Biochem. Biophys. 507 (2011) 144–153, http://dx.doi.org/10.1016/j.abb.2010.10.023.
[232] J.B. Schenkman, I. Jansson, The many roles of cytochrome b5, Pharmacol. Ther. 97 (2003) 139–152, http://dx.doi.org/10.1016/S0163-7258(02)00327-3.
[233] B. Bösterlings, J.R. Trudell, Association of cytochrome b5 and cytochrome P-450 reductase with cytochrome P-450 in the membrane of reconstituted vesicles, J.

Biol. Chem. 257 (1982) 4783–4787.
[234] M. Nunez-Quintana, G. Truan, C. Van Heijenoort, PDB ID 2I96; Solution structure of the oxidized microsomal human cytochrome b5, https://www.rcsb.org/pdb/explore.do?structureId=2i96.
[235] A.G. Bart, E.E. Scott, Structural and functional effects of cytochrome b5 interactions with human cytochrome P450 enzymes, J. Biol. Chem. 292 (2017) 20818–20833, http://dx.doi.org/10.1074/jbc.RA117.000220.
[236] M.B. Murataliev, R. Feyereisen, F.A. Walker, Electron transfer by diflavin reductases, Biochim. Biophys. Acta, Proteins Proteomics 1698 (2004) 1–26, http://dx.doi.org/10.1016/j.bbapap.2003.10.003.
[237] W.-C. Huang, J. Ellis, P.C. Moody, E.L. Raven, G.C. Roberts, Redox-linked domain movements in the catalytic cycle of cytochrome P450 reductase, Structure 21 (2013) 1581–1589, http://dx.doi.org/10.1016/j.str.2013.06.022.
[238] S.L. Freeman, A. Martel, E.L. Raven, G.C.K. Roberts, Orchestrated domain movement in catalysis by cytochrome P450 reductase, Sci. Rep. 7 (2017) 9741, , http://dx.doi.org/10.1038/s41598-017-09840-8.
[239] T. Laursen, A. Singha, N. Rantzau, M. Tutkus, J. Borch, P. Hedegård, D. Stamou, B.L. Møller, N.S. Hatzakis, Single molecule activity measurements of cytochrome P450 oxidoreductase reveal the existence of two discrete functional states, ACS Chem. Biol. 9 (2014) 630–634, http://dx.doi.org/10.1021/cb400708v.
[240] C.R. Pudney, B. Khara, L.O. Johannissen, N.S. Scrutton, Coupled motions direct electrons along human microsomal P450 chains, PLoS Biol. 9 (2011) e1001222, , http://dx.doi.org/10.1371/journal.pbio.1001222.
[241] T.M. Hedison, S. Hay, N.S. Scrutton, Real-time analysis of conformational control in electron transfer reactions of human cytochrome P450 reductase with cytochrome c, FEBS J. 282 (2015) 4357–4375, http://dx.doi.org/10.1111/febs.13501.
[242] A.R. Galiakhmetov, E.A. Kovrigina, C. Xia, J.-J.P. Kim, E.L. Kovrigin, Application of methyl-TROSY to a large paramagnetic membrane protein without perdeuteration: 13C-MMTS-labeled NADPH-cytochrome P450 oxidoreductase, J. Biomol. NMR (2017), http://dx.doi.org/10.1007/s10858-017-0152-3.
[243] E.A. Kovrigina, B. Pattengale, C. Xia, A.R. Galiakhmetov, J. Huang, J.-J.P. Kim, E.L. Kovrigin, Conformational states of cytochrome P450 oxidoreductase evaluated by Förster resonance energy transfer using ultrafast transient absorption spectroscopy, Biochemistry 55 (2016) 5973–5976, http://dx.doi.org/10.1021/acs.biochem.6b00623.
[244] O. Frances, F. Fatemi, D. Pompon, E. Guittet, C. Sizun, J. Pérez, E. Lescop, G. Truan, A well-balanced preexisting equilibrium governs electron flux efficiency of a multidomain diflavin reductase, Biophys. J. 108 (2015) 1527–1536, http://dx.doi.org/10.1016/j.bpj.2015.01.032.
[245] C. Barnaba, E. Taylor, J.A. Brozik, Dissociation constants of cytochrome P450 2C9/cytochrome P450 reductase complexes in a lipid bilayer membrane depend on NADPH: a single protein tracking study, J. Am. Chem. Soc. 139 (2017) 17923–17934, http://dx.doi.org/10.1021/jacs.7b08750.
[246] C. Barnaba, M.J. Martinez, E. Taylor, A.O. Barden, J.A. Brozik, Single-protein tracking reveals that NADPH mediates the insertion of cytochrome P450 reductase into a biomimetic of the endoplasmic reticulum, J. Am. Chem. Soc. 139 (2017) 5420–5430, http://dx.doi.org/10.1021/jacs.7b00663.
[247] P. Hubbard, A.L. Shen, R. Paschke, C.B. Kasper, J.J. Kim, NADPH-Cytochrome P450 oxidoreductase: structural basis for hydride and electron transfer, J. Biol. Chem. 276 (2001) 29163–29170, http://dx.doi.org/10.1074/jbc.M101731200.
[248] F. Rwere, C. Xia, S. Im, M.M. Haque, D.J. Stuehr, L. Waskell, J.-J.P. Kim, Mutants of cytochrome P450 reductase lacking either Gly-141 or Gly-143 destabilize its FMN semiquinone, J. Biol. Chem. 291 (2016) 14639–14661, http://dx.doi.org/10.1074/jbc.M116.724625.
[249] K.M. McCammon, S.P. Panda, C. Xia, J.J. Kim, D. Moutinho, M. Kranendonk, R.J. Auchus, E.M. Lafer, D. Ghosh, P. Martásek, R. Kar, B.S. Masters, L.J. Roman, Instability of the human cytochrome P450 reductase A287P variant is the major contributor to its Antley-Bixler syndrome-like phenotype, J. Biol. Chem. 291 (2016) 20487–20502, http://dx.doi.org/10.1074/jbc.M116.716019.
[250] C. Xia, D. Hamdane, A.L. Shen, V. Choi, C.B. Kasper, N.M. Pearl, H. Zhang, S.C. Im, L. Waskell, J.-J. Kim, Conformational changes of NADPH-cytochrome P450 oxidoreductase are essential for catalysis and cofactor binding, J. Biol. Chem. 286 (2011) 16246–16260, http://dx.doi.org/10.1074/jbc.M111.230532.
[251] C. Xia, S.P. Panda, C.C. Marohnic, P. Martásek, B.S. Masters, J.J. Kim, Structural basis for human NADPH-cytochrome P450 oxidoreductase deficiency, Proc. Natl. Acad. Sci. 108 (2011) 13486–13491, http://dx.doi.org/10.1073/pnas.1106632108.
[252] M. Wang, D.L. Roberts, R. Paschke, T.M. Shea, B.S. Masters, J.-J.P. Kim, Three-dimensional structure of NADPH-cytochrome P450 reductase: prototype for FMN- and FAD-containing enzymes, Proc. Natl. Acad. Sci. U. S. A. 94 (1997) 8411–8416.
[253] A. Sündermann, C. Oostenbrink, Molecular dynamics simulations give insight into the conformational change, complex formation, and electron transfer pathway for cytochrome P450 reductase, Protein Sci. 22 (2013) 1183–1195, http://dx.doi.org/10.1002/pro.2307.
[254] L. Aigrain, D. Pompon, S. Moréra, G. Truan, Structure of the open conformation of a functional chimeric NADPH cytochrome P450 reductase, EMBO Rep. 10 (2009) 742–747, http://dx.doi.org/10.1038/embor.2009.82.
[255] D. Hamdane, C. Xia, S.-C. Im, H. Zhang, J.-J.P. Kim, L. Waskell, Structure and function of an NADPH-cytochrome P450 oxidoreductase in an open conformation capable of reducing cytochrome P450, J. Biol. Chem. 284 (2009) 11374–11384, http://dx.doi.org/10.1074/jbc.M807868200.
[256] M. Sugishima, H. Sato, Y. Higashimoto, J. Harada, K. Wada, K. Fukuyama, M. Noguchi, Structural basis for the electron transfer from an open form of NADPH-cytochrome P450 oxidoreductase to heme oxygenase, Proc. Natl. Acad. Sci. 111 (2014) 2524–2529, http://dx.doi.org/10.1073/pnas.1322034111.
[257] D. Campelo, T. Lautier, P. Urban, F. Esteves, S. Bozonnet, G. Truan, M. Kranendonk, The hinge segment of human NADPH-cytochrome P450 reductase in conformational switching: the critical role of ionic strength, Front. Pharmacol. 8 (2017), http://dx.doi.org/10.3389/fphar.2017.00755.
[258] K.-C. Liu, J.M.X. Hughes, S. Hay, N.S. Scrutton, Liver microsomal lipid enhances the activity and redox coupling of colocalized cytochrome P450 reductase-cytochrome P450 3A4 in nanodiscs, FEBS J. 284 (2017) 2302–2319, http://dx.doi.org/10.1111/febs.14129.
[259] T.H. Bayburt, J.W. Carlson, S.G. Sligar, Single molecule height measurements on a membrane protein in nanometer-scale phospholipid bilayer disks, Langmuir 16 (2000) 5993–5997, http://dx.doi.org/10.1021/la991449c.
[260] X. Yu, D.B. Kokh, P. Nandekar, G. Mustafa, S. Richter, R.C. Wade, Dynathor: Dynamics of the complex of cytochrome P450 and cytochrome P450 reductase in a phospholipid bilayer, High Perform. Comput. Sci. 15 Springer International Publishing, 2016, pp. 255–264, , http://dx.doi.org/10.1007/978-3-642-04665-0.
[261] S.G. Nadler, H.W. Strobel, Role of electrostatic interactions in the reaction of NADPH-cytochrome P-450 reductase with cytochromes P-450, Arch. Biochem. Biophys. 261 (1988) 418–429, http://dx.doi.org/10.1016/0003-9861(88)90358-X.
[262] H. Zhang, S.-C. Im, L. Waskell, Cytochrome b5 increases the rate of product formation by cytochrome P450 2B4 and competes with cytochrome P450 reductase for a binding site on cytochrome P450 2B4, J. Biol. Chem. 282 (2007) 29766–29776, http://dx.doi.org/10.1074/jbc.M703845200.
[263] A.L. Shen, C.B. Kasper, Role of acidic residues in the interaction of NADPH-cytochrome P450 oxidoreductase with cytochrome P450 and cytochrome c, J. Biol. Chem. 270 (1995) 27475–27480, http://dx.doi.org/10.1074/jbc.270.46.27475.
[264] T. Shimizu, T. Tateishi, M. Hatano, Y. Fujii-Kuriyama, Probing the role of lysines and arginines in the catalytic function of cytochrome-P450d by site-directed mutagenesis - interaction with NADPH- Cytochrome-P450 reductase, J. Biol. Chem. 266 (1991) 3372–3375.
[265] S.J. Shen, H.W. Strobel, Role of lysine and arginine residues of cytochrome P450 in the interaction between cytochrome P4502B1 and NADPH-cytochrome P450 reductase, Arch. Biochem. Biophys. 304 (1993) 257–265, http://dx.doi.org/10.1006/abbi.1993.1347.
[266] S.G. Nadler, H.W. Strobel, Identification and characterization of an NADPH-cytochrome P450 reductase derived peptide involved in binding to cytochrome P450, Arch. Biochem. Biophys. 290 (1991) 277–284, http://dx.doi.org/10.1016/0003-9861(91)90542-Q.
[267] A. Bridges, L. Gruenke, Y.-T. Chang, I.A. Vakser, G. Loew, L. Waskell, Identification of the binding site on cytochrome P450 2B4 for cytochrome b5 and cytochrome P450 reductase, J. Biol. Chem. 273 (1998) 17036–17049, http://dx.doi.org/10.1074/jbc.273.27.17036.
[268] M. Lehnerer, J. Schulze, S.J. Pernecky, D.F. Lewis, M. Eulitz, P. Hlavica, Influence of mutation of the amino-terminal signal anchor sequence of cytochrome P450 2B4 on the enzyme structure and electron transfer processes, J. Biochem. 124 (1998) 396–403.
[269] M. Lehnerer, J. Schulze, K. Achterhold, D.F. Lewis, P. Hlavica, Identification of key residues in rabbit liver microsomal cytochrome P450 2B4: importance in interactions with NADPH-cytochrome P450 reductase, J. Biochem. 127 (2000) 163–169.
[270] C. Kenaan, H. Zhang, E.V. Shea, P.F. Hollenberg, Uncovering the role of hydrophobic residues in cytochrome P450 – cytochrome P450 reductase interactions, Biochemistry 50 (2011) 3957–3967, http://dx.doi.org/10.1021/bi1020748.
[271] L. Nikfarjam, S. Izumi, T. Yamazaki, S. Kominami, The interaction of cytochrome P450 17α with NADPH-cytochrome P450 reductase, investigated using chemical modification and MALDI-TOF mass spectrometry, Biochim. Biophys. Acta, Proteins Proteomics 1764 (2006) 1126–1131, http://dx.doi.org/10.1016/j.bbapap.2006.04.003.
[272] H.L. Lin, C. Kenaan, H. Zhang, P.F. Hollenberg, Reaction of human cytochrome P450 3A4 with peroxynitrite: Nitrotyrosine formation on the proximal side impairs its interaction with NADPH-cytochrome P450 reductase, Chem. Res. Toxicol. 25 (2012) 2642–2653, http://dx.doi.org/10.1021/tx3002753.
[273] A.V. Pandey, C.E. Flück, NADPH P450 oxidoreductase: structure, function, and pathology of diseases, Pharmacol. Ther. 138 (2013) 229–254, http://dx.doi.org/10.1016/j.pharmthera.2013.01.010.
[274] C.E. Flück, T. Tajima, A.V. Pandey, W. Arlt, K. Okuhara, C.F. Verge, E.W. Jabs, B.B. Mendonça, K. Fujieda, W.L. Miller, Mutant P450 oxidoreductase causes disordered steroidogenesis with and without Antley-Bixler syndrome, Nat. Genet. 36 (2004) 228–230, http://dx.doi.org/10.1038/ng1300.
[275] N. Huang, A.V. Pandey, V. Agrawal, W. Reardon, P.D. Lapunzina, D. Mowat, E.W. Jabs, G. Van Vliet, J. Sack, C.E. Flück, W.L. Miller, Diversity and function of mutations in P450 oxidoreductase in patients with Antley-Bixler syndrome and disordered steroidogenesis, Am. J. Hum. Genet. 76 (2005) 729–749, http://dx.doi.org/10.1086/429417.
[276] D. Sandee, K. Morrissey, V. Agrawal, H.K. Tam, M. a Kramer, T.S. Tracy, K.M. Giacomini, W.L. Miller, Effects of genetic variants of human P450 oxidoreductase on catalysis by CYP2D6 in vitro, Pharmacogenet. Genomics 20 (2010) 677–686, http://dx.doi.org/10.1097/FPC.0b013e32833f4f9b.
[277] L.G. Gomes, N. Huang, V. Agrawal, B.B. Mendonça, T.A.S.S. Bachega, W.L. Miller, The common P450 oxidoreductase variant A503V is not a modifier gene for 21-hydroxylase deficiency, J. Clin. Endocrinol. Metab. 93 (2008) 2913–2916, http://dx.doi.org/10.1210/jc.2008-0304.
[278] V. Agrawal, N. Huang, W.L. Miller, Pharmacogenetics of P450 oxidoreductase: effect of sequence variants on activities of CYP1A2 and CYP2C19, Pharmacogenet. Genomics 18 (2008) 569–576, http://dx.doi.org/10.1097/FPC.0b013e32830054ac.
[279] V. Agrawal, J.H. Choi, K.M. Giacomini, W.L. Miller, Substrate-specific modulation

of CYP3A4 activity by genetic variants of cytochrome P450 oxidoreductase, Pharmacogenet. Genomics 20 (2010) 611–618, http://dx.doi.org/10.1097/FPC.0b013e32833e0cb5.
[280] C.C. Marohnic, S.P. Panda, K. McCammon, J. Rueff, B.S. Masters, M. Kranendonk, Human cytochrome P450 oxidoreductase deficiency caused by the Y181D mutation: molecular consequences and rescue of defect, Drug Metab. Dispos. 38 (2010) 332–340, http://dx.doi.org/10.1124/dmd.109.030445.
[281] I.F. Sevrioukova, H. Li, H. Zhang, J.A. Peterson, T.L. Poulos, Structure of a cytochrome P450-redox partner electron-transfer complex, Proc. Natl. Acad. Sci. 96 (1999) 1863–1868, http://dx.doi.org/10.1073/pnas.96.5.1863.
[282] C.C. Page, C.C. Moser, P.L. Dutton, Mechanism for electron transfer within and between proteins, Curr. Opin. Chem. Biol. 7 (2003) 551–556, http://dx.doi.org/10.1016/j.cbpa.2003.08.005.
[283] D.F. Estrada, J.S. Laurence, E.E. Scott, Cytochrome P450 17A1 interactions with the FMN domain of its reductase as characterized by NMR, J. Biol. Chem. 291 (2016) 3990–4003, http://dx.doi.org/10.1074/jbc.M115.677294.
[284] J. Liu, G.J. Tawa, A. Wallqvist, Identifying cytochrome P450 functional networks and their allosteric regulatory elements, PLoS One 8 (2013) e81980, , http://dx.doi.org/10.1371/journal.pone.0081980.
[285] D.R. Nelson, H.W. Strobel, On the membrane topology of vertebrate cytochrome P-450 proteins, J. Biol. Chem. 263 (1988) 6038–6050 http://www.ncbi.nlm.nih.gov/pubmed/2834360.
[286] I.G. Denisov, A.Y. Shih, S.G. Sligar, Structural differences between soluble and membrane bound cytochrome P450s, J. Inorg. Biochem. 108 (2012) 150–158, http://dx.doi.org/10.1016/j.jinorgbio.2011.11.026.